

**ADVERTIMENT.** L'accés als continguts d'aquesta tesi doctoral i la seva utilització ha de respectar els drets de la persona autora. Pot ser utilitzada per a consulta o estudi personal, així com en activitats o materials d'investigació i docència en els termes establerts a l'art. 32 del Text Refós de la Llei de Propietat Intel·lectual (RDL 1/1996). Per altres utilitzacions es requereix l'autorització prèvia i expressa de la persona autora. En qualsevol cas, en la utilització dels seus continguts caldrà indicar de forma clara el nom i cognoms de la persona autora i el títol de la tesi doctoral. No s'autoritza la seva reproducció o altres formes d'explotació efectuades amb finalitats de lucre ni la seva comunicació pública des d'un lloc aliè al servei TDX. Tampoc s'autoritza la presentació del seu contingut en una finestra o marc aliè a TDX (framing). Aquesta reserva de drets afecta tant als continguts de la tesi com als seus resums i índexs.

**ADVERTENCIA.** El acceso a los contenidos de esta tesis doctoral y su utilización debe respetar los derechos de la persona autora. Puede ser utilizada para consulta o estudio personal, así como en actividades o materiales de investigación y docencia en los términos establecidos en el art. 32 del Texto Refundido de la Ley de Propiedad Intelectual (RDL 1/1996). Para otros usos se requiere la autorización previa y expresa de la persona autora. En cualquier caso, en la utilización de sus contenidos se deberá indicar de forma clara el nombre y apellidos de la persona autora y el título de la tesis doctoral. No se autoriza su reproducción u otras formas de explotación efectuadas con fines lucrativos ni su comunicación pública desde un sitio ajeno al servicio TDR. Tampoco se autoriza la presentación de su contenido en una ventana o marco ajeno a TDR (framing). Esta reserva de derechos afecta tanto al contenido de la tesis como a sus resúmenes e índices.

**WARNING.** Access to the contents of this doctoral thesis and its use must respect the rights of the author. It can be used for reference or private study, as well as research and learning activities or materials in the terms established by the 32nd article of the Spanish Consolidated Copyright Act (RDL 1/1996). Express and previous authorization of the author is required for any other uses. In any case, when using its content, full name of the author and title of the thesis must be clearly indicated. Reproduction or other forms of for profit use or public communication from outside TDX service is not allowed. Presentation of its content in a window or frame external to TDX (framing) is not authorized either. These rights affect both the content of the thesis and its abstracts and indexes.



Universitat Politècnica de Catalunya  
Departament d'Arquitectura de Computadors

# Cross-Layer Optimization for Optical Networks

Ph.D. Dissertation  
Marianna Angelou

**Advisors:**

Prof. Ioannis Tomkos  
Prof. Davide Careglio  
Prof. Salvatore Spadaro

February 2012







# Acknowledgements

“It was the best of times...It was the worst of times...”<sup>1</sup> It is strange how when a difficult yet exciting period of time in your life ends you struggle to remember all the things that made it difficult. Instead you are left with a bittersweet feeling that you hope will fade away with time. Certainly though, it has been a period I will always cherish because it made me a better person (and slightly more crazy). I always thought I should write this part of the dissertation on a day I would be relaxed and detached so as to avoid being too emotional. But I can't help it. So here it goes...

I cannot but start with Prof. Ioannis Tomkos, the person who gave me this amazing opportunity. I am grateful for the knowledge and experience I gained, the people I met, the places I visited and of course the realization of my PhD. I would also like to thank Prof. Josep Sole Pareta for all the kind help and support. Special thanks go to Prof. Davide Careglio and Prof. Salvatore Spadaro for standing next to me as excellent advisors but also good friends.

During the course of this PhD I had the luck and privilege to know and work with some amazing people and brilliant scientists. First and foremost in my work family I would like to thank Prof. Dimitrios Klonidis for always being available; as a teacher, a colleague and above all a friend. I will never forget my big brother Dr. Siamak Azodolmolky for the valuable help and guidance in all matters and for always staying positive. Dr. Yvan Pointurier for helping me to complete a valuable piece in my research work. My dear friends Ms. Maria Spyropoulou and Dr. Ioannis Papagiannakis for instantly welcoming me in the group and making me feel one of their own. My officemate Dr. Konstantinos Kanonakis for all the fun breaks during the day and the hundreds of “koulouria” he brought me in the morning. Dr. Panagiotis Zakynthinos for believing in me and teaching me a thing or two about ber measurements. I would also like to thank my newest work siblings, Dr. Christoforos Kachris and Dr. Eleni Palkopoulou.

Finally I cannot but be eternally grateful to my real family, my mother, my father, Paris, Katerina and of course Theodore whose name should be there in the front page next to mine. This is for you.

Marianna Angelou  
Athens, February 29, 2012

---

<sup>1</sup> Charles Dickens, “A tale of two cities”



# Table of Contents

List of Figures .....	viii
List of Tables.....	xi
Abstract .....	1
1. Introduction.....	3
1.1. Evolution of Core Optical Networks .....	3
1.2. Motivation .....	4
1.3. Dynamic Impairment-Aware Networking.....	5
1.4. Concurrent Research Challenges .....	7
1.5. Contributions and Thesis Structure .....	11
1.6. References .....	13
2. Dynamic Impairment-Aware Single Line-Rate Networks .....	15
2.1. Network Planning and Operation .....	15
2.2. Dynamic Impairment-Aware Architecture .....	18
2.3. Network Planning and Operation Tool .....	18
2.4. Cross-Layer Optimization Modules.....	19
2.5. Control Plane .....	21
2.6. Chapter Summary .....	23
2.7. References .....	23
3. Physical-Layer Awareness in Dynamic Single Line-Rate Networks .....	25
3.1. The Q-Tool .....	25
3.2. Physical-layer Modelling in 10Gb/s OOK systems .....	26
3.3. QoT development approach.....	34
3.4. Physical-Layer Awareness in Network Planning and Operation.....	37
3.5. Monitor Placement.....	39
3.6. Experimental Evaluation of IA-RWA Processes using the Q-Tool.....	39
3.7. Chapter Summary .....	42
3.8. References .....	43
4. Optimized Monitor Placement for Accurate QoT Assessment in Core Optical Networks	45
4.1. Modelling and Problem Formulation.....	46
4.2. Monitor Placement Algorithms .....	49
4.3. Numerical Results .....	51
4.4. Monitor Placement in the presence of Dynamic Traffic.....	58
4.5. Chapter Summary .....	59
4.6. References .....	59
5. Resource Optimization in Dynamic Single Line-Rate Networks .....	63
5.1. Node Architectures .....	64
5.2. Methodology .....	66
5.3. Cost Modelling .....	69
5.4. Results.....	71
5.5. Chapter Summary .....	74
5.6. References .....	75
6. Flexible Optical Networks.....	77
6.1. Advanced Modulation Formats .....	80



6.2.	Fixed and Flexible Spectrum Grid .....	82
6.3.	Single-carrier Solutions .....	84
6.4.	Multi-carrier Solutions .....	85
6.5.	Software-Defined Optics.....	89
6.6.	Experimental Investigation of a Multi-carrier Spectrum-flexible System .....	91
6.7.	Chapter Summary .....	96
6.8.	References .....	96
7.	Resource Optimization in Mixed Line-Rate and Flexible Networks .....	101
7.1.	Methodology .....	102
7.2.	Spectrum Allocation in Fixed-Grid and Flex-Grid Networks .....	106
7.3.	Cost Efficiency.....	107
7.4.	Energy Efficiency.....	110
7.5.	Chapter Summary .....	112
7.6.	References .....	113
8.	Conclusions and Future Work .....	115
Appendix A: Network Topologies.....		121
A.1	Deutsche Telekom's Backbone Network.....	121
A.2	Telekomunikacja Polska (TP SA) Network .....	125
A.3	Pan-European Topology based on the GÉANT2 Network .....	129
Appendix B: List of Acronyms.....		133
B.1	List of Acronyms .....	133
Appendix C: Contributions .....		135
C.1	Journal Publications .....	135
C.2	Conference Publications .....	136
C.3	Book Chapters.....	138
C.4	Publications Under Review .....	138

# List of Figures

Figure 1-1: Evolution of Optical Networks .....	3
Figure 1-2: Current and Dynamic Impairment-Aware core optical networks .....	6
Figure 1-3: The Energy-Driven Optical Network .....	8
Figure 1-4: Mixed 10G/40G/100G transmission with multiple modulation formats .....	9
Figure 1-5: High-capacity fully flexible optical network.....	11
Figure 1-6: Thesis Structure and Contributions .....	12
Figure 2-1: Lightpaths established in a typical WDM network. ....	16
Figure 2-2: Planning and Operational Phases of a WDM core network. In the planning phase the traffic is considered static and the routing is handled by an Offline IA-RWA algorithm, whereas in the operational phase demands arrive and depart at random time instants. Specially designed Online (Dynamic) IA-RWA algorithms compute the route and wavelength of each demand on a one-by-one basis as they arrive. ....	17
Figure 2-3: Anatomy of DICONET Network Planning and Operation Tool.....	19
Figure 2-4: (a) Offline IA-RWA Blocking Ratio and running times as a function of the available wavelengths $W$ (b) Online IA-RWA - Blocking ratio and average execution time per connection in seconds presented as a function of the network load, for a fixed number of wavelengths ( $W=20$ ). ....	21
Figure 2-5: Qualitative assessment of the various control plane options .....	23
Figure 3-1: The Q-tool building blocks and flow. ....	26
Figure 3-2: The distorted eye diagram. ....	27
Figure 3-3: Q-factor value vs. lightpath length ( $Q_{\text{Threshold}}=15.5$ dB). ....	34
Figure 3-4: A Network Planning and Operation Tool with the Q-Tool.....	38
Figure 3-5: Distributed and Centralized Control Plane Integration Schemes. ....	39
Figure 3-6: The experimental test-bed. ....	40
Figure 3-7: (a) OR yields longer connection setup times that tend to improve for more loaded traffic scenarios, (b) MP leads to higher blocking ratios than OR that makes optimal impairment-aware decisions.....	41
Figure 4-1: Two nodes with nodal degree of 3 are connected with a pair of unidirectional links. Monitors may be placed at the drop points of the nodes, yielding 6 possible monitor locations. ....	47
Figure 4-2: It is possible to use monitoring measurements collected from a subset of all the network lightpaths (LP1, LP2, LP3, LP4) to estimate accurately the corresponding end-to-end metric (e.g. OSNR) of a lightpath that is not monitored (LP5) using the “network kriging” estimation framework [2], [17], [23]. Placing monitoring devices at the termination points of LP1, LP2, LP3 and LP4 would allow the operator to also estimate the QoT of LP5 using only partial network information.....	48
Figure 4-3: The Deutsche Telekom backbone network is shown with 20 monitored locations resulting from the PM placement. ....	52
Figure 4-4: Comparison of the placement techniques for the Deutsche Telekom (DT) network. The averaged relative root mean square error was computed for all placements methods applied in the DT backbone network for traffic load equal to 2, i.e. 2 connections on average per pair of nodes. With the PM heuristic, 15 monitors out of the possible 46 locations are enough to yield an estimation error for OSNR below 1%. ....	53
Figure 4-5: Fraction of the energy (“energy ratio”) of the unobserved lightpaths that lies in the space spanned by the observed lightpaths for the DT Topology with a load of 2. The	

energy ratio is higher when more information about the unobserved lightpaths through the observation of other lightpaths with the deployed monitors. ....	54
Figure 4-6: Comparison of optimum solutions against the solutions retrieved by the 3 heuristics for the DT topology; the resulting error is the average of 50 randomly generated traffic matrices of load equal to 1. ....	54
Figure 4-7: PM and optimum relative RMSE error results for each of the 50 traffic matrices, when 5 monitored locations are assumed. ....	54
Figure 4-8: Averaged relative RMSE of all placements methods applied on the Polish Telecom topology. The traffic load is equal to 2. ....	55
Figure 4-9: Relative RMSE for the PM monitor placement method with respect to the number of available monitors and increasing traffic load in the TP topology. PM is not affected by the traffic load and achieves estimation error below 1% for $m = 20$ deployed monitors. ....	56
Figure 4-10: Relative RMSE for the QR monitor placement method with respect to the number of available monitors and increasing traffic load in the TP topology. ....	56
Figure 4-11: Averaged relative root mean square error of all placements methods applied on the GEANT2 topology (load 0.5). ....	57
Figure 4-12: Averaged relative root mean square error of all placements methods applied on the GEANT2 topology (load 1). PM achieves estimation error below 1% for $m = 25$ monitored locations out of 104 available. ....	57
Figure 4-13: Example of monitor placement in the presence of varying incremental traffic. 20 fixed equipped locations computed by the PM algorithm for a traffic matrix of load 1 is studied as “chunks” of traffic are added to the already established lightpaths. Without installing additional monitors the estimation error becomes larger than 1% for a traffic load larger than 2. It was observed by inspection that only 3 (out of 20 possible) monitors displacements are sufficient to decrease the estimation error back to less than 1%. ....	58
Figure 5-1: The flow of the techno-economic analysis process. ....	67
Figure 5-2: Flow chart of offline Rahyab algorithm. ....	68
Figure 5-3: Total CapEx of IA vs. IUA with R-OXC6. ....	71
Figure 5-4: Total CapEx of IA vs. IUA with R-OXC4. ....	71
Figure 5-5: Cost difference between the different node architectures with load 0.8. ....	72
Figure 5-6: Cost difference between the different node architectures with load 1.1. ....	73
Figure 5-7: Network related OpEx of IA vs. IUA with R-OXC6. ....	73
Figure 5-8: Network related OpEx of IA vs. IUA for the different node architectures with load 1.1. ....	74
Figure 6-1: Fixed Optical Network with mixed line rates of 10Gb/s, 40Gb/s and 100 Gb/s – optical connections fit in fixed spectrum slots and get switched at specific center frequencies and optical bandwidths utilizing a standard DWDM system. ....	78
Figure 6-2: Flexible optical network concept – optical connections have flexible bandwidth and adaptive line-rate and modulation format; optical nodes are also bandwidth agnostic. ....	79
Figure 6-3: Constellations that use only the real part of the field and carry 1 bit per symbol. ....	80
Figure 6-4: Constellations that use both quadratures of the field and carry multiple bits per symbol. ....	80
Figure 6-5: The cases of Fixed-Grid, Flex-Grid and Grid-less. ....	82
Figure 6-6: Single-carrier adaptive transmitter – Structure and characteristics of the PDM-xPSK transmitter [41]. ....	85

Figure 6-7: Example of a terabit superchannel made up of 10x100Gb/s subcarriers, generated with a multi-carrier transmission technique. ....	85
Figure 6-8: Generic design of a Co-OFDM transmitter and signal output. Co-OFDM signals consist of sinc-shaped subcarriers in the frequency domain and rectangular pulses in the time domain. ....	86
Figure 6-9: Generic design of a Nyquist-WDM transmitter and signal output. Nyquist-WDM superchannels consist of rectangular-shaped subcarriers in the frequency domain and sinc pulses in the time domain. ....	87
Figure 6-10: Generic design of a multi-band OFDM transmitter and signal output. Multi-band OFDM superchannels consist of RF generated OFDM channels with almost rectangular-shaped spectra separated by a small guard band. ....	88
Figure 6-11: Experimental set-up for the study of spectrum allocation scenarios within a BOI of a superchannel. ....	93
Figure 7-1: Spectrum utilization and spectrum gain (in 50GHz slots ) of the SF network as opposed to a SLR 100 Gb/s system for different traffic loads. ....	103
Figure 7-2: Percentage of additional cost of the SF transponder over the cost of the 100 Gb/s transponder as a function of the cost of the 50 GHz slot, for different traffic loads and 50% SF-WSS extra cost. ....	104
Figure 7-3: Percentage of additional cost of the SF transponder over the cost of the 100 Gb/s transponder as a function of the cost of the 50 GHz slot, for different SF-WSS extra cost percentages and for load=1. ....	104
Figure 7-4: Percentage of additional cost of the SF transponder over the cost of the 100 Gb/s transponder as a function of the cost of the 50 GHz slot, for different SF-WSS extra cost percentages and for load=5. ....	105
Figure 7-5: Percentage of additional cost of the SF transponder over the cost of the 100 Gb/s transponder as a function of the cost of the 50 GHz slot, for different SF-WSS extra cost percentages and for load=10. ....	105
Figure 7-6: Percentage of total network cost saving as a function of the cost of the 50 GHz slot, for different SF-WSS and different SF-transponder values. ....	105
Figure 7-7: Spectrum utilization for all solutions and different traffic loads. ....	107
Figure 7-8: Required number of transponders for all solutions to serve the different traffic matrices (in absolute numbers). ....	108
Figure 7-9: Relative transponder cost for the fixed-grid networking solutions. ....	108
Figure 7-10: Number of allocated 10Gb/s, 40 Gb/s, 100 Gb/s, 400 Gb/s transponders for each traffic scenario for an MLR network with transponder cost optimization. ....	108
Figure 7-11: Number of allocated 10Gb/s, 40 Gb/s, 100 Gb/s, 400 Gb/s transponders for each traffic scenario for an MLR network with wavelength optimization. ....	108
Figure 7-12: Allowable additional cost for E-OFDM transponder compared to SLR 100G from spectrum savings for different traffic loads. ....	109
Figure 7-13: Allowable additional cost for O-OFDM transponder compared to SLR 100G from spectrum savings for different traffic loads. ....	110
Figure 7-14: Energy Efficiency achieved for all solutions and different traffic loads. ....	111
Figure 7-15: Power consumption of transponder in MLR, E-OFDM and O-OFDM solutions. ....	112

## List of Tables

Table 4-1: Pseudo-Monitoring (PM) monitor placement algorithm.....	50
Table 4-2: Network Topologies Specifications .....	52
Table 5-1: Types of R-OXC's .....	66
Table 5-2: Component CapEx.....	69
Table 5-3: Network-related OpEx.....	70
Table 6-1: Parameters in single-carrier modulation with variable bit and subcarrier [27] ....	81
Table 6-2: Parameters in multi-carrier modulation with variable bit and subcarrier [27]. ....	82
Table 6-3: Comparison between N-WDM and MB-OFDM.....	89
Table 6-4: Investigated scenarios and data obtained from the analysis of the results .....	94
Table 7-1: Reach of fixed-grid signals.....	106
Table 7-2: Reach of O-OFDM channels .....	107
Table 7-3: Power Consumption of Fixed-Grid Transponders.....	111

# Abstract

Network planning and operation in core optical networks require processes that lead to a cost-effective network able to effectively accommodate the given traffic demands. Cross-layer techniques that exploit information coming from the transport plane to serve either the network planning or the operation phases have been proposed to achieve optimal resource utilization and network performance.

Dynamic impairment-aware networking refers to a solution that utilizes the dynamicity as well as the valuable physical-layer information of a reconfigurable WDM network to provide a smooth transition from the quasi-static networking of today to an intelligent reconfigurable and physical impairment-aware architecture. The concept of physical layer awareness allows intelligent techniques to offer optimal planning, dynamic configuration and management of the network while ensuring strong quality of transmission (QoT). A physical-layer performance estimating tool called Q-tool, has been designed and developed to deliver fast and accurate QoT assessments in dynamic single line-rate WDM networks employing 10 Gb/s OOK systems. The Q-tool was developed so as to feed with QoT evaluations the various cross-layer modules including offline RWA, monitor placement, regenerator placement, online RWA and failure handling. The significance of the physical-layer awareness and the role of Q-tool in the online routing strategy have been experimentally investigated using an impairment-enabled control-plane testbed. A cross-layer module that utilizes physical layer information to optimize the planning phase of single line-rate networks has been also developed; a monitor placement scheme was designed that takes into account partial monitoring information coming from the physical layer to decide the optimum number and locations of the optical monitoring devices. A techno-economic analysis was also conducted to explore the cost implications stemming from the resource optimization of a dynamic single line-rate network. Impairment aware and impairment-unaware algorithms along with the developed QoT tool were used to compare the planning solutions in terms of CapEx and OpEx.

The challenges arising in the core networks of the next generation have also been addressed. Flexible optical networking has been introduced by the research community as a way to offer efficient utilization of the available optical resources while offering ultra-high speed rates. As opposed to the rate-specific and fixed-grid solution of a mixed line-rate (MLR) network, flexible networks are bandwidth agnostic and have the ability to adapt on-demand the delivered bit-rate. Yet, the increased level of flexibility imposes complex requirements; during network operation traffic is changing with time, leaving windows of spectrum of variable size unused. Moreover, interference from the neighbouring channels has to be taken into account and sufficient guard-bands ought to be considered. In such context the physical layer requirements for a spectrum-flexible optical superchannel were experimentally investigated by implementing a set of networking scenarios. The importance of the result is that it can act as input for cognitive algorithms that will enable a novel networking paradigm. Finally next generation core networks were evaluated from a cost, spectral and energy perspective so as to give a comprehensive view of the potential of the proposed technologies. The resource optimization achieved by flexible networks has been compared to single and mixed line-rate networks under the prism of cost and energy efficiency. It was shown that the capability of flexible networks to allocate efficiently the available spectrum, counterbalances the additional capital expenditures that are required to migrate to a multi-carrier system. In addition flexible networks achieve low energy per bit as they use just the amount of network resources needed for the given input traffic.



# Chapter 1

## 1. Introduction

### 1.1. Evolution of Core Optical Networks

After the establishment of the first fiber-based telecom networks in the 1980s, it was the emergence of *Wavelength Division Multiplexing* (WDM) a decade later that enabled optical networks to satisfy the increasing capacity requirements. Until then the spectral efficiency of intensity-modulated fiber-optic communication systems was limited to  $10^{-6}$ - $10^{-7}$  bits/s/Hz and multiplexing multiple optical channels onto a single optical fiber allowed a giant leap forward to  $10^{-2}$ - $10^{-1}$  bits/s/Hz [1].

In these early steps of WDM networks though, each optical channel had to be converted to the electrical domain and then back to the optical at every node even if the optical channel was not destined for that node. Networks with optical signals undergoing optical-electronic-optical (O/E/O) regeneration at every switching or routing node are commonly referred to as opaque (Figure 1-1 (a)). More recently, the idea of avoiding all these costly O/E/O conversions triggered the development of *Optical Add-Drop Multiplexers* (OADMs). The realisation of these network components marked a new era in optical networking as they enabled an optical signal to enter or leave a node without affecting the transit traffic while always remaining in the optical domain. *Transparent* networks, where the signal propagates all-optically from source to destination throughout the network (Figure 1-1 (c)), were then proposed as the means to totally eliminate the regeneration-related costs of opaque networks [2]. The evolution of optical networks from opaque to transparent was driven and justified by the provision of ultra-high bandwidth, Quality of Service (QoS) guarantee and scalability. Yet this transition proved to be also particularly cost-effective. The cost savings of a transparent network design over an opaque network may be up to 50% [3]. The OpEx savings in the all-optical core networks mostly due to the minimised power needs of photonics [4], along with the CapEx savings stemming from the elimination of the costly optoelectronic interfaces, render transparency highly correlated with the deployment of an economically viable network.

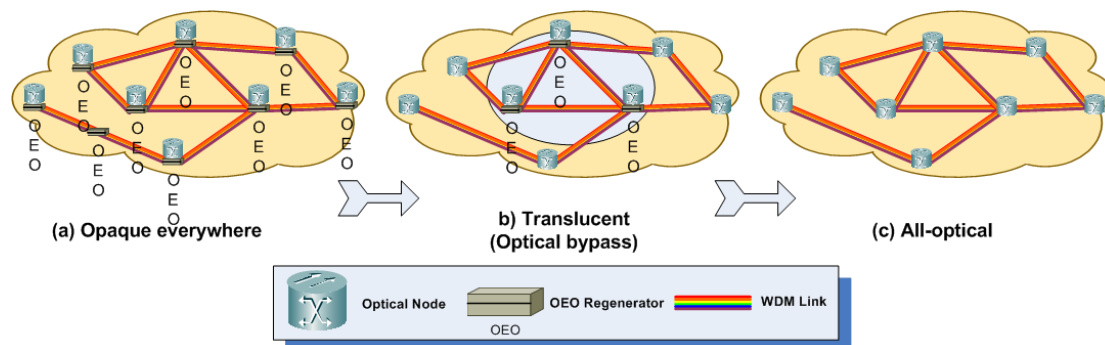


Figure 1-1: Evolution of Optical Networks



Nonetheless error free detection of the optical signal can be achieved for a finite distance, as the physical layer impairments accumulate degrading the quality of transmission (QoT) [5]. Thus in large scale networks a small number of regeneration sites is still required to maintain the acceptable signal quality. These semi-transparent or *translucent* architectures (Figure 1-1 (b)) were proposed as a compromise between opaque and transparent networks.

Further to the introduction of the OADMs that triggered the vision of transparency, *reconfigurable* optical add/drop and switching equipment was implemented to achieve a higher degree of flexibility. The early OADMs were capable only of a fixed configuration that allowed only predetermined wavelengths to enter or leave a node on predetermined network ports. In case the routing had to be changed due to a change in traffic, personnel had to travel on-site and configure the equipment manually. Reconfigurable OADMs (ROADMs) and Optical Cross-Connects (OXC) enabled networks to adapt remotely and on-demand to the potential traffic changes eliminating the associated operational costs. ROADMS are rapidly adopted due to their inherent ability to support the dynamic traffic evolution in a flexible and economic manner [6]. Reconfigurable optical networks present a clear business case since the operators do not have to overprovision their network with equipment meant to serve future variations in traffic.

All in all the optical networks of the point-to-point optical links evolved to an architecture with *higher spectral efficiency and dynamic transparency*, where the WDM channels flow optically end-to-end and get routed dynamically. Advancements in photonic technology encourage current operating networks to invest on the reconfigurable equipment and realise commercially a fully-flexible and robust optical network.

## 1.2. Motivation

In old voice-centric telecom networks, planning and operation phases little resembled the equivalent functions of today's data-centric telecom networks. Nowadays the indisputable growth of data traffic with dynamic usage patterns generated by novel capacity-demanding applications drives the developments in communications worldwide. Core optical networks, occupying a fundamental piece in the Internet puzzle, evolved to networks that span over thousands of kilometres of fiber, carry high-capacity traffic and switch connections all-optically. In this context, telecom operators seek for a cost-effective core optical network that satisfies the new traffic conditions. During network design, operators need to employ methods that minimise the total cost of ownership and the network-related operational expenses while ensuring scalability, dynamicity and adaptation to future demands. In this context though, new and more complicated implications were introduced in order to commercially realize an optical network that is fully-dynamic, robust and cost-effective.

Therefore, the vision of high end-to-end all-optical connectivity, reliability and dynamicity has to be addressed under the prism of capital and operational cost. The authors in [7] have proposed and developed a comprehensive networking solution that tackles the aforementioned challenges. This networking solution is realised through a set of *resource-optimization* algorithms that introduce also a business opportunity for the network operators. Intelligent routing and wavelength assignment, optimized component placement, failure localisation and resilience, all integrated in a unified control plane, provide the network with an extended level of optimization.

Transponders, performance and impairment monitors, regenerators, are all costly equipment whose associated capital and operational cost, justifies the need for resource-

optimization. Nonetheless, apart from the careful network planning which is directly linked to cost, it is crucial to fortify the network with the ability to locate failures and restore the affected traffic, ensuring always smooth operation. QoS guarantee is an important revenue-generating feature and an essential building block of the overall networking solution.

Further to the educated resource utilization and failure management, recently operators have come up against another challenge that enforces an additional level of optimization in the network. The constantly-increasing traffic demand has introduced the need to tackle the excessive power-consumption issue. The environmental implications of the exponential increase of the IP traffic impose an immediate need to minimize the ICT *carbon footprint* generated from the consumption of fossil fuels. It is estimated that the ICT industry is responsible for 2-2.5% of the global Green House Gas (GHG) emissions, a percentage that is expected to grow rapidly in coming years [8]. Concentrating on the optical core segment of the telecom networks, new design rules and techniques are necessary in order to minimize the energy-consumption and allow the operators to deploy the future green sustainable networks.

To achieve optimal resource utilization and network performance, cross-layer techniques have been introduced and identified by the research community as an efficient solution [9]. Regardless of the underlay infrastructure (wireless/wireline) the notion of *cross-layer optimization* implies the utilization of knowledge coming from one communication layer by another communication layer to improve the performance of the network. In other words the typical communication stack escapes from its strict horizontal boundaries and layers cooperate with each other to bring a higher degree of intelligence and functionality. For the purposes of the research conducted in the framework of this PhD, the cross-layer optimization methods focus on the exploitation of information coming from the transport plane to feed the control and management planes.

### 1.3. Dynamic Impairment-Aware Networking

The state-of-the-art core network is the result of a technological and socioeconomic evolution that transformed optical networks from opaque to translucent or transparent in an effort to satisfy the ever-growing demand for bandwidth, yet with improved economics. The dynamic traffic patterns that came along with the rapid traffic increase though, led to the need for and the fast adoption of reconfigurable networking equipment that allow the operators to adapt dynamically their network to the new conditions. This concept along with the impairment-aware network planning and operation reside in the core of the dynamic impairment-aware networking solution [7] which takes advantage of the optical signal performance to allocate efficiently and therefore cost-effectively the available resources. Figure 1-2, shows the evolution step in optical networking from a physical layer unaware, quasi-static and costly status to an optimised network in terms of resource allocation and utilization, achieved with the introduction of physical layer awareness.

The dynamic impairment-aware solution [7], [10] is realized through a set of physical-layer-aware modules that serve both the planning and operation phases of an optical network. Network planning entails all the activities that are required to accommodate an initial traffic matrix with optimal resource provisioning. The well-known problem of Routing and Wavelength Assignment (RWA) constrained by the performance of the optical signal has received great attention from the research community [11]. Impairment-Aware RWA (IA-RWA) refers to the process which given a set of matrix demands assigns a route and a

wavelength to each of the demands always taking into account the physical impairments that degrade the quality of transmission.

The authors in [12] studied and classified more than 100 publications dealing with impairment-aware routing. During the planning phase, such an algorithm computes the routes and allocates the available resources (i.e. in this case the optical channels) for a static traffic in order to find the optimal strategy to accommodate it. This “offline” operation takes place before a network actually starts to operate. In [13] such an algorithm is proposed that returns an offline RWA solution for transparent networks where no regeneration is assumed. [14] on the other hand, proposes an RWA algorithm suitable for translucent networks where regenerators are necessary in certain nodes to serve the traffic demands. Both algorithms utilize a QoT estimator to assess the impact of the physical layer, thus ensuring the feasibility and reliability of the computed solution. In addition to the RWA process operators may have other cross-layer optimization tools to support the planning phase. Regenerator [15] and monitor placement [16] refer to the modules developed to make educated decisions on the number and location of the regenerating and monitoring equipment required in the network, by considering again the physical layer performance.

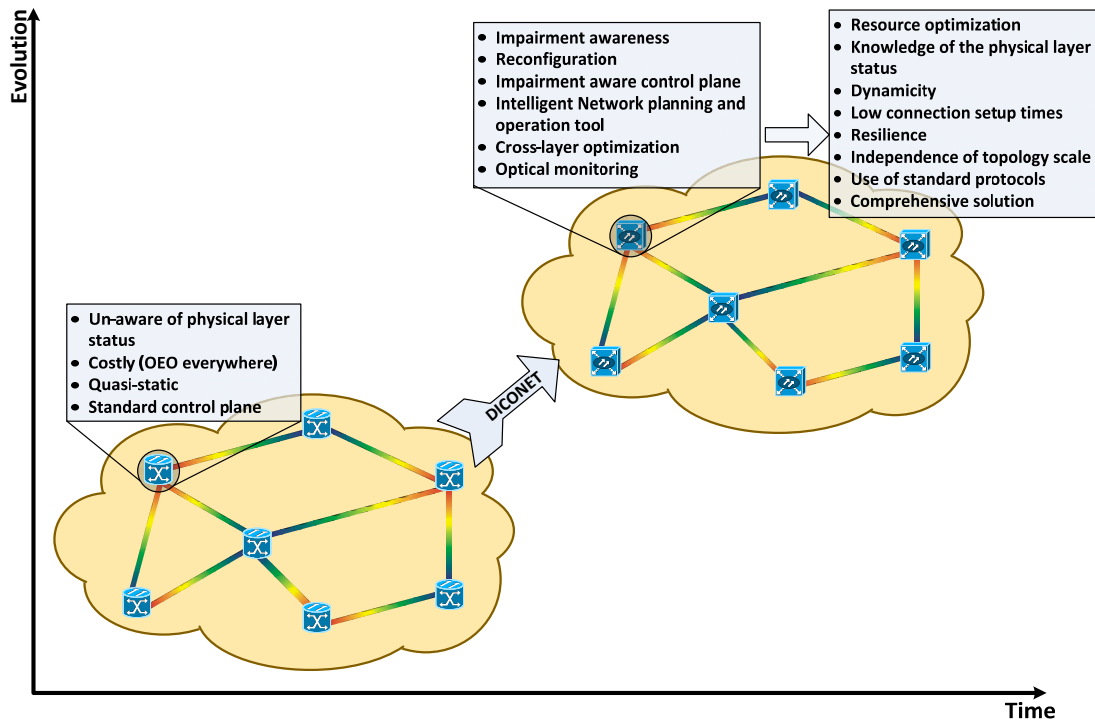


Figure 1-2: Current and Dynamic Impairment-Aware core optical networks

After the offline planning has been applied and the deployed network starts to operate, traffic demands may be requested or dropped in a dynamic fashion. “Online” IA-RWA algorithms [17], [18] specially designed for the operation phase, process the new demands upon their arrival and once at a time, taking into consideration the current state of the network. Therefore a new demand is served constrained by the traffic and physical layer characteristics present at the time of the arrival and as a consequence a sub-optimal path may be computed. Another important building block of the overall networking solution is responsible for monitoring the network for potential failures and locating the exact link that needs to be recovered. Upon a failure and after this failure is located [19], the network

utilizes its reaction mechanisms and restores all affected traffic. The result is a robust and reliable core network with guaranteed QoS.

The dynamic impairment-aware network is supported by an impairment-enabled control plane that integrates the aforementioned functions [10]. Through properly developed Generalized Multi-Protocol Label Switching (GMPLS) protocol extensions, the control plane supports the overall networking solution and allows the different building blocks to cooperate and run in an orchestrated manner. The idea of enhancing the control plane with QoT awareness as a way to facilitate the realization of the solution has also attracted the attention of the research community [20]. The work in [21] demonstrated interworking between the control and management plane taking into account the physical layer impairments to support the planning and operation of transparent networks, utilizing a centralized integration scheme. The authors in [22] investigated experimentally a distributed impairment-enabled GMPLS integration scheme that targets translucent networks. In [10] the authors experimentally tested and compared distributed and centralized integration schemes with integrated real-time QoT estimation for transparent and translucent networks.

On the whole the concept of physical impairment awareness utilizes intelligent techniques to offer optimal planning, dynamic configuration and management of optical signal with acceptable QoT. Static and dynamic routing and wavelength assignment, performance and impairment monitoring, failure localization and handling work in conjunction with the control and management plane. In turn, the information stemming from the data plane which is valuable to the various modules is disseminated to the nodes of the network through properly enhanced control plane extensions.

## 1.4. Concurrent Research Challenges

The multi-plane solution discussed in the previous section was proposed by the research community to cope with the challenges associated with core optical networks that deliver connections at a single line-rate, either 10 Gb/s or 40 Gb/s. This section summarizes the main challenges that arise and need to be addressed in the core networks of the next generation, focusing on the excessive power-consumption, the heterogeneity of the traffic and the ever-growing need for transmission capacity. First, an energy-driven planning framework is proposed that consists of promising research efforts to achieve the “greening” of optical networks. Then, the heterogeneous nature of the traffic that is rapidly transforming today’s optical networks is visited. To this end the planning issues of networks that accommodate mixed-line rates of 10 Gb/s, 40 Gb/s and 100 Gb/s are discussed. The unprecedented data traffic growth though, drives future optical networks even beyond 100 Gb/s. Multi-carrier systems based on Optical Orthogonal Frequency Division Multiplexing (O-OFDM) are identified as a promising solution due to the intrinsic characteristics of spectrum efficiency and scalability, imposing though new networking constraints.

### Energy-Driven Optical Network

Focusing on the planning issues of the future optical networks, it has become apparent that *energy-efficiency* is the new design constraint that operators have to consider in addition to the typical resource optimization which targets cost-effectiveness. Energy-efficiency refers to the techniques or technologies designed or developed to reduce energy consumption without compromising the performance. Nevertheless, improving the energy-efficiency of a piece of equipment does not necessarily result into reduction of the carbon emissions. The energy consumption of the equipment may or may not generate CO<sub>2</sub>, depending on the

energy source that powers them up. In this context, a complimentary solution to the reduction of the ICT carbon footprint is identified in *energy-awareness*. Energy-aware is characterized a technology that adjusts its behaviour or performance according to the energy source that supplies the network (renewable or fossil) and its components. Therefore, an energy-aware network may be extremely energy-inefficient, but still contribute little to the ICT carbon footprint. Energy-efficiency and energy-awareness may be achieved in the next-generation optical networks through a multi-level *energy-driven* framework of design solutions and optimization schemes. Figure 1-3 illustrates an energy-driven optical IP network that incorporates “greening” techniques in multiple levels, cooperating in an orchestrated manner.

Although optics may not be a novel “green” solution per se, optical technologies seem to be omnipresent and indispensable in the effort to tackle the energy wastage problem. From an architectural point of view, it is foreseen that IP networks will eventually remove the intermediate layers to eliminate the corresponding underutilized equipment and push some of the network functionality down to the energy-efficient WDM layer. In the transport plane, legacy technology is replaced by advanced optical transmission techniques [23] that manage to transmit data to constantly longer distances with moderate power budgets while still achieving low bit-error rates (BER). At the same time technology advancements in photonics allow traditional electronic operations such as switching to be moved to the optical domain. It has been shown [24] that power consumption of electronic routers grows almost linearly with the increased capacity, imposing a critical limitation to the future networks. So the green IP-over-WDM network will carry high-capacity optoelectronic routers that demonstrate significant improvement in power consumption and performance [25]. Nevertheless the electronic counterpart of these routers still contributes massively to the total power consumed in the IP-over-WDM network. Therefore minimizing the number of potential IP hops can bring significant power savings. To this end, under the concept of lightpath bypass [26] all traffic bypasses intermediate IP routers and the communication between two IP routers is performed directly over a lightpath. It has been found [26] that the power saving in IP-over-WDM with intelligent optical nodes that employ the lightpath bypass technique ranges from 25% to 45%.

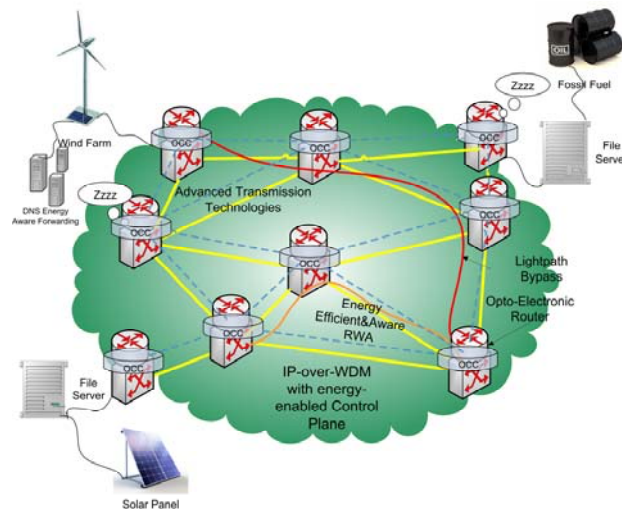


**Figure 1-3:** The Energy-Driven Optical Network

In the context of the energy-driven network planning, the well known problem of Routing and Wavelength Assignment (RWA) is addressed under the power-consumption

constraint. An energy-efficient RWA algorithm [27] typically tends to reuse the same network link along a path as much as possible so as to make maximum use of the components that are already “on”. Nevertheless, it is anticipated that gradually the telecom networks and particularly the power-demanding Content Delivery Networks will be supplied by renewable energy sources. The RWA proposed here is not only energy-efficient but also energy-aware by considering the type of energy source that supplies a node and trying to avoid the ones that consume fossil fuel. An *energy-enabled control plane* will support the *Energy Efficient & Aware RWA* during operation (online RWA). The properly enhanced control plane distributes energy-related parameters including the energy source and the power consumption specifications of the network elements, imposing the energy-awareness feature in various operations of the network, such as Domain Name System and URL energy-aware forwarding. Moreover the energy-enabled control plane will be able to exchange information about the power state of the network nodes, either “on”, “off” or on *sleep mode*. Putting network components in a low-energy consumption has been introduced and studied [28] as an effective way to save energy. To enable this functionality the legacy equipment needs to be upgraded at hardware and software level, satisfying the need for solutions that do not incur major capital expenses.

In essence the energy-driven optical network is not only the result of a careful architecture selection and adoption of advanced technologies. It is an intelligent system that utilizes its intrinsic characteristics, like the power consumption and the energy source of a device, to bring an additional level of optimization in the planning phase. The valuable energy-related information is then utilized to even optimize the operation phase with novel methods, such as energy-efficient traffic engineering [29] and energy-efficient IPTV networks [30].

### Mixed Line-Rate Optical Networks

The continuous growth of the Internet traffic driven by the bandwidth-intensive new multimedia applications is expected to render telecom networks particularly *heterogeneous*. To satisfy the increased demand in capacity, current commercial networks will not leap to the 100 Gb/s era overnight. Transforming a core network to provide 100 Gb/s everywhere entails a significant capital investment. Besides, not all traffic demands require such high bit rates and operators are seeking for networks that are not wasting resources but are cost-effective and therefore versatile. In this framework existing 10 Gb/s OOK optical networks may upgrade their infrastructure gradually migrating to higher line rates that coexist with the old 10 Gb/s channels (Figure 1-4). The research community has identified this need and heterogeneous networks that accommodate mixed 10/40/100 Gb/s traffic has attracted attention [31]. In [32] a field experiment demonstrated the feasibility of such a mixed-rate transmission system over 1000km of fiber. To support though the high bit rates of 40 Gb/s and 100 Gb/s proper advanced modulation formats need to be employed so as to improve the un-regenerated bandwidth-distance product accordingly. The channels of 40 and 100 Gb/s are typically phase-modulated and therefore more prone to the cross-phase modulation (XPM) induced by the 10G channels. This effect may be mitigated though by either proper dispersion management or carefully selecting the power levels of the 10G channels.

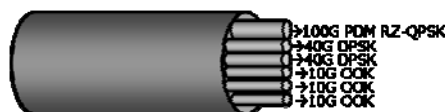


Figure 1-4: Mixed 10G/40G/100G transmission with multiple modulation formats

Nevertheless the emerging heterogeneous networks are introducing a new type of challenge in network design. So far the resources at hand during the design phase were limited to the channels available while the rate and the modulation format were fixed. The new network paradigm introduces an additional level of flexibility also interpreted as additional complexity. To serve a given traffic demand, the network manager has to make an educated decision about the route, the channel, the bit-rate and the modulation format. The authors in [33] addressed this problem using an Integer Linear Programming (ILP) formulation to determine a minimum-cost solution for the resources required to design the heterogeneous network. The solution returned defines the number of the required transponders of the various bit-rates and formats that satisfy a given traffic matrix, always choosing the combination of route-channel-rate-format that achieves the longest reach.

The heterogeneity underlines the need for novel routing algorithms for the next-generation optical networks. As opposed to the common RWA process that is restricted to the typical lightpath computation the new *Routing Wavelength Bit-Rate and Format Assignment (RWBFA) algorithms* tries to solve an even more complex problem. Constrained by the Quality of Transmission (QoT), the wavelength-continuity and the network transparency these algorithms compute the optimum routes and assign to them the optimum available resources. Yet, to estimate the QoT of a lightpath and its neighbors that run on mixed rates and multiple modulation formats *new physical models* need to be considered and studied. The QoT metrics calculation formulas, such as the BER/Q-factor for the advanced modulation formats ought to be properly tailored. The models that quantify the impact of the cross-channel physical impairments on the phase-modulated channels (e.g. XPM) and the self-channel impairments on the high bit-rate signals (e.g. PMD) are important issues under these heterogeneous conditions.

In view though of the diverse online traffic (operation phase), it is foreseen that the RWBFA algorithms have also to account for the dynamic variations in bandwidth demand. However, there is a strong precondition to meet in order to achieve this dynamicity. Fully tunable transmission systems with multi-format and multi-bit-rate functionality are required to allocate in a customized and online fashion the resources (route, channels, rate and format) according to the current traffic conditions.

### **100G and Beyond**

In order to facilitate the advent of the future 100G Ethernet channels, 100-Gb/s-class technologies are necessary to be established. Recent 100-Gb/s-based experiments with multilevel modulation formats (M-QAM and M-PSK), polarization-division multiplexing (PDM) and digital coherent detection have demonstrated performance that exceeds expectations both in spectral efficiency and the bandwidth-distance product. The authors in [34] demonstrated a bandwidth-capacity product of 13.5 Tb/s x 6,248 km utilizing a PDM coherent optical OFDM transmission system. Indeed OFDM has enabled record-breaking setups due to its inherent ability to offer particularly high bit-rates combining a large number of low-rate subcarriers in the most flexible and scalable manner.

Optical networks today operate under added complexity and cost due to the rigid wavelength granularity of the systems currently deployed. Operators provide connections with capacity that fulfils the highest (worst case) demand (over-provisioning), while these connections remain underutilised for most of the time. In contrast with this, OFDM introduces significantly high *spectrum-efficiency* providing a fractional bandwidth feature. In

effect, it enables a new network architecture (Figure 1-5) where any two nodes can be connected with the amount of bandwidth required, either providing a sub-wavelength service or super-channel connectivity. In addition the OFDM-based systems can easily modify the properties of a given connection, i.e. bit-rate, modulation format, with digital signal processing and therefore adapt to dynamic network conditions without the restriction of a fixed hardware system. Optical OFDM will likely become a major building block of the 100G networks and beyond, offering unmatched spectrum-efficiency, scalability and cost-effectiveness.

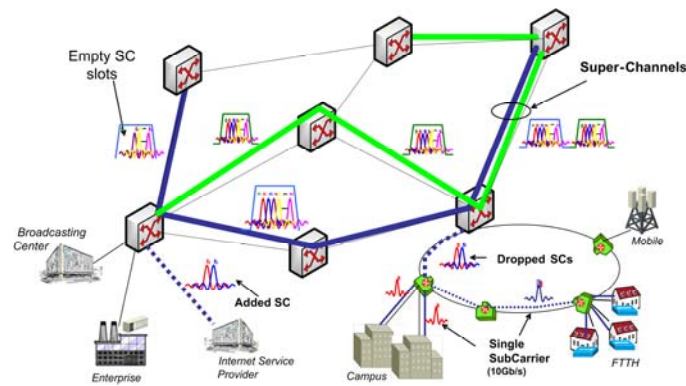


Figure 1-5: High-capacity fully flexible optical network

In this context, due to the finer granularity of an OFDM-based network compared to a traditional WDM network just enough bandwidth can be allocated to a given traffic demand presenting new constraints in network planning [34]. Traditional RWA algorithms are no longer applicable or require significant tailoring work to satisfy the new challenges. Bandwidth allocation is not fixed but varies with the different traffic demands. Therefore the RWA problem transforms to a Routing and *Spectrum Allocation* problem where every connection request is assigned a spectrum fraction. Novel algorithms are required to handle this issue that along with the wavelength-continuity constraint will have to operate under the *spectrum-continuity* constraint. To serve a given traffic matrix, the developed algorithms will have to properly allocate the spectrum avoiding any overlapping and at the same time minimizing the total spectrum utilized.

## 1.5. Contributions and Thesis Structure

The research work conducted in the course of this PhD followed the evolution path of core optical networks imposed by the research trends and technology advancements that have taken place with time (Figure 1-6). It addresses *dynamic single-line rate* networks as well as the more recent solutions that have been proposed for the *next generation networks that bear truly adaptive features* in terms of the offered capacity and resource allocation. The contributions have been focused on optimization of core networks along two dimensions. First, *optimization aimed at performance improvement* of the overall network in a cross-layer fashion by introducing physical layer awareness at the higher layers of the multiplane network. Then, the *resource optimization* that resulted from introducing the physical layer information in the network planning and operation phases was studied under the prism of cost and energy efficiency.



## Thesis Structure

Following the introductory chapter, the remainder is structured as follows: Chapter 2 introduces the topics of network planning and operation in the context of dynamic and impairment aware networks and presents the main benefits of the DICONET architecture that addresses such networks. Chapter 3 discusses the concept of physical layer awareness and presents the development of a physical layer performance estimating tool along with its applications. Chapter 4 reports on a novel monitor placement scheme that finds the optimum locations of optical monitoring devices while minimizing the total required number. The topic of Chapter 5 is a techno-economic analysis conducted in the framework of dynamic single line-rate networks to explore the cost implications stemming from resource optimization. Chapter 6 presents the concept and technologies of next generation core networks that carry ultra high bit-rates yet with an increased level of flexibility on the utilization of resources. In addition it reports on the experimental investigation of various flexible superchannel scenarios meant to work as the basis for a novel cognitive networking paradigm. Chapter 7 describes a comprehensive analysis that seeks to assess various technologies for the core networks of next generation with respect to cost and energy efficiency. The main conclusions of the research work are discussed in Chapter 8 along with the future research activities that will follow this work.

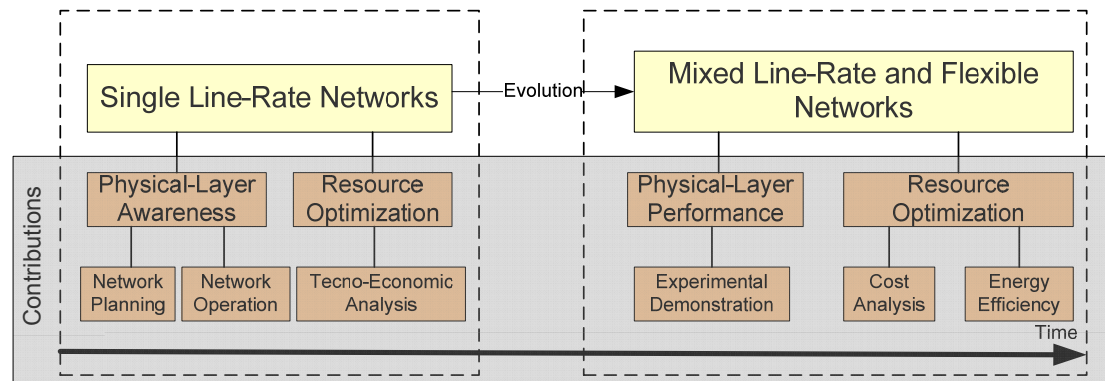


Figure 1-6: Thesis Structure and Contributions

## Contributions

In brief, the contributions presented in this dissertation include the following works:

- ✓ **Single Line-Rate Networks**
  - Design and development of a physical-layer performance estimating tool that applies the concept of impairment awareness to the network planning and operation processes (Chapter 3).
  - Design and development of an optimized monitor placement scheme for resource optimization and accurate QoT assessment during network operation (Chapter 4).
  - Techno-economic study that investigates the benefits of dynamic and impairment-aware network planning compared to a network that does not consider the quality of transmission (Chapter 5).
- ✓ **Mixed Line-Rate and Flexible Networks**
  - Experimental investigation of the physical layer performance parameters for a spectrum-flexible optical *superchannel* to act as input

- for the implementation of the new paradigm of flexible optical networks (Chapter 6).
- Resource optimization study for the evaluation of solutions for the realization of the next generation core networks from a spectral, cost and energy efficiency perspective (Chapter 7).

## 1.6. References

- [1] K. Nosu and K. Iwashita, "Coherent FDM transmission techniques," in Optical Fiber Communication, 1987 OSA Technical Digest Series (Optical Society of America, 1987), paper TUG2.
- [2] A. Saleh, "Transparent optical networking in backbone networks," in Optical Fiber Communication Conference, OSA Technical Digest Series (Optical Society of America, 2000), paper ThD7.
- [3] M. Gunkel, R. Leppla, M. Wade, A. Lord, D.A. Schupke, G. Lehmann, C. Fürst, S. Bodamer, B. Bollenz, H. Haunstein, H. Nakajima, J. Martensson, "A Cost Model for the WDM Layer", Photonics in Switching Conference PS' 2006.
- [4] A. Lord, C. Engineer, "OPEX savings of all-optical core networks", ECOC '09, vol., no., pp.1-2, 20-24 Sept. 2009.
- [5] R. Cardillo, V. Curri, M. Mellia, "Considering Transmission Impairments in Wavelength Routed Networks", OFC/NFOEC 2006, paper OFG6.
- [6] M. Ruffini, D. Kilper, D. O'Mahony, and L. Doyle, "Cost Study of Dynamically Transparent Networks", OFC/NFOEC 2008, paper OMG2.
- [7] Siamak Azodolmolky, Dimitrios Klonidis, Ioannis Tomkos, Yabin Ye, Chava Vijaya Saradhi, Elio Salvadori, Matthias Gunkel, Kostas Manousakis, Kyriakos Vlachos, and Emmanouel (Manos) Varvarigos, Reza Nejabati, Dimitra Simeonidou, Michael Eiselt, Jaume Comellas, Josep Solé-Pareta, Christian Simonneau, Dominique Bayart, Dimitri Staessens, Didier Colle, Mario Pickavet, "A Dynamic Impairment Aware Networking Solution for Transparent Mesh Optical Networks," IEEE Communications Magazine, May 2009.
- [8] ITU and Climate Change, <http://www.itu.int/themes/climate/>
- [9] I. Tomkos, "Dynamically Reconfigurable Transparent Optical Networking Based on Cross-Layer Optimization", ONDM 2007, vol.1, pp.327, Rome, Italy, July 2007.
- [10] F. Agraz, S. Azodolmolky, **M. Angelou**, J. Perelló, L. Velasco, S. Spadaro, A. Francescon, C. V. Saradhi, Y. Pointurier, P. Kokkinos, E. Varvarigos, M. Gunkel, and I. Tomkos, "Experimental Demonstration of Centralized and Distributed Impairment-Aware Control Plane Schemes for Dynamic Transparent Optical Networks," OFC/NFOEC 2010, paper PDPD5.
- [11] C.V Saradhi and S. Subramaniam, "Physical layer impairment aware routing (PLIAR) in WDM optical networks: issues and challenges," Communications Surveys & Tutorials, IEEE, vol.11, no.4, pp.109 -130, Fourth Quarter 2009.
- [12] S. Azodolmolky, M. Klinkowski, E. Marín Tordera, D. Careglio, J. Solé-Pareta, and I. Tomkos, "A Survey on Physical Layer Impairments Aware Routing and Wavelength Assignment Algorithms in Optical Networks," Computer Networks (Elsevier), vol. 53, no. 7, pp. 926-944, May 2009.
- [13] Siamak Azodolmolky, Yvan Pointurier, **Marianna Angelou**, Josep Solé-Pareta, and Ioannis Tomkos, "An Offline Impairment Aware RWA Algorithm with Dedicated Path Protection Consideration," OFC/NFOEC 2009, OWI1, San Diego, California, USA, 22-26 March 2009.
- [14] K. Manousakis, K. Christodoulouopoulos, E. Kamitsas, I. Tomkos, and E. A. Varvarigos, "Offline impairment-aware routing and wavelength assignment algorithms in translucent WDM optical networks," J. Lightw. Technol., vol. 27, no. 12, pp. 1866-1877, Jun. 2009.
- [15] M. Youssef, S. A. Zahr, and M. Gagnaire, "Cross optimization for RWA and regenerator placement in translucent WDM networks," in Proc. IFIP ONDM, Feb. 2010, pp. 1-6.
- [16] M. Youssef, S. Al Zahr, and M. Gagnaire. "Traffic-Driven vs Topology-Driven Strategies for Regeneration Sites Placement", in Proc. of the IEEE ICC Conference, Cape Town, South Africa, May 2010.

- [17] P. Kokkinos, K. Christodoulopoulos, K. Manousakis, and E. Varvarigos, "Multi-parametric online RWA based on impairment generating sources", in Proc. IEEE GLOBECOM, 2009, pp. 1-7.
- [18] Siamak Azodolmolky, Yvan Pointurier, **Marianna Angelou**, Josep Solé-Pareta, and Ioannis Tomkos, "Routing and Wavelength Assignment for Transparent Optical Networks with QoT Estimation Inaccuracies," OFC/NFOEC 2010, OMM4, San Diego, California, USA, 21-25 March 2010.
- [19] E. A. Doumith, S. Al Zahr, M. Gagnaire, "Monitoring-Tree: An Innovative Technique for Failure Localization in WDM Translucent Networks" in Proc. GLOBECOM 2010, vol., no., pp.1-6, 6-10 Dec. 2010.
- [20] Filippo Cugini, N. Sambo, N. Andriolli, A. Giorgetti, L. Valcarengi, P. Castoldi, E. Le Rouzic, and J. Poirrier, "Enhancing GMPLS Signaling Protocol for Encompassing Quality of Transmission (QoT) in All-Optical Networks," J. Lightwave Technol. 26, 3318-3328 (2008).
- [21] T. Tsuritani, M. Miyazawa, S. Kashihara, and T. Otani, "Optical path computation element interworking with network management system for transparent mesh networks," in Proc. IEEE/OSA OFC/NFOEC, NWF5, Mar. 2008.
- [22] R. Martinez, R. Casellas, R. Muñoz, T. Tsuritani, and T. Otani, "Experimental GMPLS routing for dynamic provisioning in translucent wavelength switched optical networks," in Proc. IEEE/OSA OFC/NFOEC, NTuB4, Mar. 2009.
- [23] M. Cvijetic: Advanced Technologies for Next-Generation Fiber Networks, in Proc. OFC/NFOEC 2010, San Diego, USA, March 2010, paper OWY1.
- [24] E. Bonetto, L. Chiaraviglio, D. Cuda, G. A. Gavilanes Castillo, F. Neri, "Optical Technologies Can Improve the Energy Efficiency of Networks", in Proc. ECOC 2009, Vienna, Austria, September 2009.
- [25] J. Gripp, M. Duell, J. E. Simsarian, A. Bhardwaj, P. Bernasconi, O. Laznicka, and M. Zirngibl, Optical Switch Fabrics for Ultra-High-Capacity IP Routers, J. Lightwave Technol. 21, 2839- (2003).
- [26] G. Shen, R. S. Tucker, "Energy-Minimized Design for IP Over WDM networks", IEEE J. Opt. Commun. Netw. Vol.1, No.1, June 2009.
- [27] Yong Wu, L. Chiaraviglio, M. Mellia, F. Neri, "Power Aware Routing and Wavelength Assignment in Optical Networks", in Proc. ECOC 2009, Vienna, Austria, September 2009.
- [28] M. Gupta and S. Singh, "Greening of the Internet", in Proc. ACM SIGCOMM, Karlsruhe, Germany, Aug. 2003.
- [29] B. Puype, D. Colle, M. Pickavet, P. Demeester, "Energy Efficient Multilayer Traffic Engineering", in Proc. ECOC 2009, Vienna, Austria, September 2009.
- [30] J. Baliga, R. Ayre, K. Hinton, and R. S. Tucker, "Architectures for Energy-Efficient IPTV Networks", in Proc. OFC/NFOEC 2009, San Diego, USA, March 2009, paper OTHQ5.
- [31] X. Liu, S. Chandrasekhar, "High Spectral-Efficiency Mixed 10G/40G/100G Transmission", in Proc. AOE 2008, OSA Technical Digest (CD) (Optical Society of America, 2008), paper SuA2.
- [32] T. J. Xia, G. Wellbrock, D. Peterson, W. Lee, M. Pollock, B. Basch, D. Chen, M. Freiburger, M. Alfiad, H. de Waardt, M. Kuschnerov, B. Lankl, T. Wuth, E.D. Schmidt, B. Spinnler, C.J. Weiske, E. de Man, C. Xie, D. van den Borne, M. Finkenzeller, S. Spaelter, R. Derksen, M. Rehman, J. Behel, J. Stachowiak, M. Chbat, "Multi-rate (111-Gb/s, 2x43-Gb/s, and 8x10.7-Gb/s) transmission at 50 GHz channel spacing over 1040-km field- deployed fiber", in Proc. ECOC 2008, Brussels, Belgium, September 2008.
- [33] A. Nag, M. Tornatore, B. Mukherjee, "Optical Network Design With Mixed Line Rates and Multiple Modulation Formats", J. Lightwave Technol. 28, 466- (2010).
- [34] H. Masuda, E. Yamazaki, A. Sano, T. Yoshimatsu, T. Kobayashi, E. Yoshida, Y. Miyamoto, S. Matsuoka, Y. Takatori, M. Mizoguchi, K. Okada, K. Hagimoto, T. Yamada, and S. Kamei, "13.5-Tb/s (135 x 111-Gb/s/ch) No-Guard-Interval Coherent OFDM Transmission over 6,248 km Using SNR Maximized Second-Order DRA in the Extended L-Band", in Proc. OFC/NFOEC 2009, San Diego, USA, March 2009, paper PDPB.

# Chapter 2

## 2. Dynamic Impairment-Aware Single Line-Rate Networks

Dynamic Impairment-Aware Single Line-Rate networks refer to networks that employ reconfigurable switching equipment, carry a fixed single line-rate and use information originating from the physical layer to introduce an increased level of “intelligence” to the networking layer. This feature applies to processes that take place either during the network planning or operation phase. In what follows the topics of network planning and operation are introduced in the framework of such networks. Next, the main benefits of the DICONET architecture are discussed by presenting the key features of this multiplane solution that enable the vision of dynamic and impairment-aware networking.

### 2.1. Network Planning and Operation

In a core WDM network the traffic that travels from node to node is carried over a set of optical channels effectively dividing the bandwidth of the fiber medium into a number of non-overlapping wavelengths. Given a connection demand between two optical nodes, a *lightpath* is established between the destination and the source node forming a (semi)-permanent circuit. A lightpath is essentially an optical signal running on a specific wavelength travelling possibly via multiple fiber links until it reaches the destination node. To serve a connection demand, a lightpath is realized by determining the sequence of nodes and allocating to it one of the available optical channels. The traffic matrix (or demand set) that is active in a wavelength-routed network is served by an equal number of lightpaths, as depicted in Figure 2-1. An OXC serves either as a switching element when it is an intermediate node or as an add/drop element when it is the source/destination node respectively. All links carry equal numbers of wavelengths and typically consist of one fiber per direction; link  $A \rightarrow B$  is different than  $B \rightarrow A$ .

The selection of the route and the wavelength is an optimization problem known in the literature as *Routing and Wavelength Assignment (RWA)*. RWA is indeed an important process for the efficient operation of a WDM network. Given a network topology and a number of available wavelengths per link, an RWA algorithm returns an optimal solution when it manages to accommodate the connection demands with minimum rejection (blocking). Blocking may occur due to lack of resources or other performance metric. The valuable resource here is the available wavelengths. In the case where the allocated wavelength of a lightpath remains the same along the traversed links of the path it is said to satisfy the *wavelength continuity* constraint (see Figure 2-1). If the optical switching nodes (OXCs) are equipped with wavelength conversion capabilities then the problem is relaxed to typical routing in a circuit-switched network where the only constraint is the number of channels per link. RWA was introduced more than a decade ago and numerous works have proposed different solutions to address it as summarized in [1].

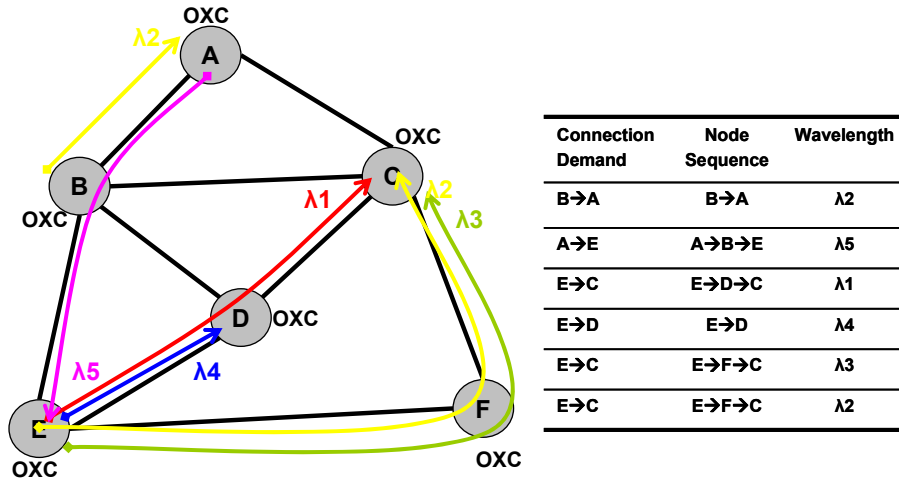


Figure 2-1: Lightpaths established in a typical WDM network.

Most of these works though assume that the optical fiber is a non-impairing transmission medium and therefore all RWA solutions are feasible. In reality as the optical signal propagates inside the fiber it experiences certain physical effects that attenuate and distort the optical pulses, limiting the reach. Therefore a selected lightpath that does not yield acceptable physical-layer performance is not really a valid solution. In the end this lightpath would not be established as it would fail to be correctly detected at the receiver point because of the high bit-error ratio (BER). Hence to overcome the limitations imposed by the *physical layer impairments (PLIs)* QoT is introduced in the RWA process as an additional constraint. To achieve this, typically the impact of the dominant PLIs is mapped to a single figure of merit (e.g. Q-factor) that determines the QoT of a lightpath, which in turn is considered in the routing and wavelength allocation decision. The term commonly used in the literature to describe the RWA process that always takes into account the PLIs that degrade the quality of the signal is *Impairment Aware RWA (IA-RWA)*. IA-RWA has received great attention by the research community as evident in [2] and [3].

IA-RWA is a resource optimization process that employs a cross-layer technique to minimize the resources and improve the overall network performance. During the *planning* phase of a core WDM network and given an initial traffic matrix IA-RWA algorithms are used to route all the predetermined connection demands and essentially to dimension the network. IA-RWA applies, nonetheless, also during the *operation* phase of a reconfigurable core network where the demands arrive and depart in a dynamic fashion.

Figure 2-2 illustrates abstractly the two phases of a core WDM network, that is the planning and the operational phase. During the planning phase it is assumed that the topology is in place meaning that the operator is aware of the characteristics of the network such as distances, node connectivity, link design, amplifier spans. Then for a set of connection demands that are know in advance of the actual operation of the network, IA-RWA algorithms compute the paths and allocate the optical channels considering the impact of the PLIs. These IA-RWA algorithms, usually referred to as *Offline*, assume that the input traffic is static and optimize the RWA process for the entire set of the lightpaths. In the case where the WDM network is also equipped with regenerators the appropriate offline IA-RWA is used that also minimizes their use. Since this phase is indeed “offline” it gives the operator the opportunity to revisit their infrastructure needs, as the objective here is to maximize the traffic that is served for a given number of wavelengths or minimize the

necessary wavelengths (resources) for a given initial traffic matrix. All in all the offline case of IA-RWA is a global design and optimization problem and as it takes place before the operation of the network the processing time is not an important constraint.

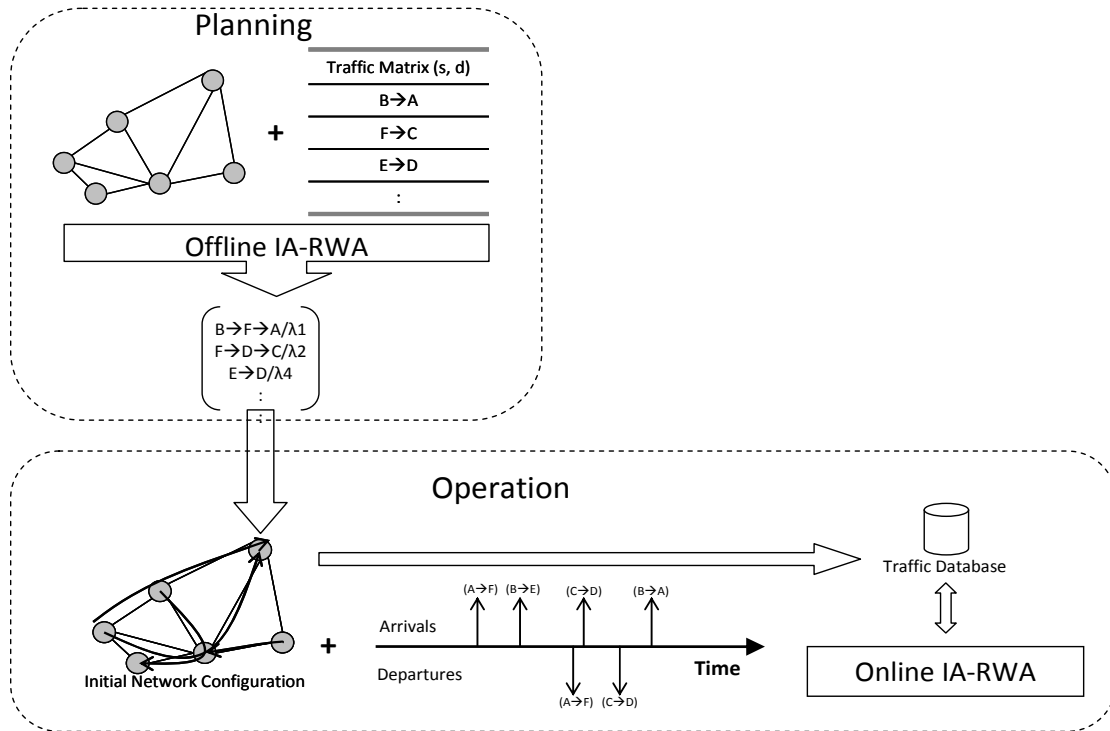


**Figure 2-2:** Planning and Operational Phases of a WDM core network. In the planning phase the traffic is considered static and the routing is handled by an Offline IA-RWA algorithm, whereas in the operational phase demands arrive and depart at random time instants. Specially designed Online (Dynamic) IA-RWA algorithms compute the route and wavelength of each demand on a one-by-one basis as they arrive.

Following the planning phase the initial configuration of the network is set having established all the pre-determined lightpaths. During the operational phase though, additional demands request connection at random time instances. These connection demands are served as soon as they arrive and in a sequential way. This type of lightpath provisioning is known as *Online (or Dynamic)* and considers the case where during the network operation demands arrive at any point in time without a-priori knowledge. In a dynamic traffic scenario demands get established upon their arrival, remain established for a finite time period and get released at random points in time. In a core network with reconfigurable optical nodes, dynamic traffic gets served on-the-fly and remotely. The Online (dynamic) IA-RWA, as opposed to the offline case, computes a lightpath on a one-by-one basis taking into account the traffic that is already established in the network but also the current physical-layer parameters. The objective here is to minimize over time the blocking ratio with the resources that are available at each moment. In a dynamic core network existing lightpaths should not get disrupted by the connections established or torn down over time, unless a physical failure occurs. In that case restoration mechanisms take over and again online IA-RWA is required to compute new routes and channels for the connections that failed.

## 2.2. Dynamic Impairment-Aware Architecture

In the framework of the EU DICONET project a comprehensive solution was proposed to tackle issues in the planning or offline phase as well as the operation or online phase of an optical core network. The planning phase includes processes that are directly linked to the network capital. To this end, *resource optimization* is required to minimize the capital and operational cost associated with the various network components, i.e. transponders, monitors and regenerators. In the DICONET approach this challenge is addressed by dedicated resource optimization modules that minimize and efficiently allocate the available resources (i.e. monitor and regenerator placement, offline Impairment-Aware Routing and Wavelength Assignment – IA-RWA), exploiting the maximum transparent optical reach.

During operation, employing the dynamic and impairment-aware solution implies a situation where the network is *fully aware of the physical status* of its components and the QoT of the established connections. Optimum decision making is therefore achieved also during operation, utilizing intelligent online IA-RWA algorithms that serve the dynamic traffic. In addition, *dynamism and high performance end-to-end connectivity* strengthen the online operation as the lightpath provisioning is achieved in *low setup times*. Apart from the fast connection establishment the DICONET solution is capable of rapidly localizing potential physical failures and restoring the affected traffic, rendering the network intelligent and robust. Besides, operators always seek for *Quality of Service (QoS)* as it is an important revenue-generating attribute.

As a whole, DICONET is designed to work *independent of the scale* of the network topology as its tools are applicable to both core networks where regeneration of the optical signal is not necessary (transparent) and networks of bigger scale, where some strategically selected regeneration sites are required (translucent). Furthermore recognizing the importance of the *use of standardized protocols*, Generalized Multi-Protocol Label Switching (GMPLS) is adopted in the DICONET approach to control the transport plane. Indeed the control plane entities that run the optical transport employ the full GMPLS protocol suite, yet properly enhanced to support the PLIs. In what follows the main building blocks that induce these benefits are presented.

## 2.3. Network Planning and Operation Tool

The key innovation of DICONET is the design and development of NPOT that integrates in a common platform cross-layer algorithms that make use of physical-layer assessments, serving the network during planning and operation [4]. Following the development and testing of the various cross-layer techniques, the most suitable of each task was selected and all together were combined to act as the building blocks of NPOT. The most important of those are illustrated in the graphical representation in Figure 2-3. The planning mode of NPOT consists of the Optical Monitor Placement, the Regenerator Placement and the offline IA-RWA modules, supporting the network manager before the actual network operation. In the operation mode the tool includes the online IA-RWA and the Failure Localization modules. The global network information, including the physical layer, the topology and the traffic parameters, populate two data repositories that are kept as external databases (Physical Parameters Database (PPD) and Traffic Engineering Database (TED)). All the input data are introduced to the two databases in a simple XML format.

In the core of the NPOT is situated a QoT estimator which is elaborated in detail in Chapter 3. The various components of the tool consult the QoT estimator to make physical-layer aware decisions. The RWA process, whether online or offline, uses the QoT estimator

either as a quality metric during the routing and wavelength assignment process or after the routing and wavelength assignment has taken place to evaluate and validate the computed solution. In turn the regenerator and monitor placement algorithms invoke the QoT estimator in order to find the optimum location for these components. The QoT estimator utilizes the updated information stored in the databases to estimate in a single figure-of-merit (i.e. Q-factor) the quality of the signal travelling on a lightpath. It is noteworthy that the modular design of NPOT allows any of its building blocks to be upgraded or replaced by other algorithms in a seamless way.

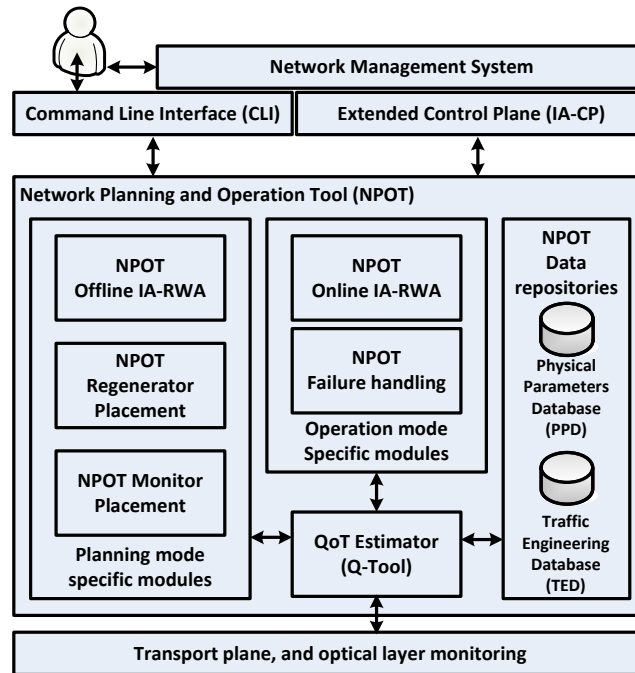


Figure 2-3: Anatomy of DICONET Network Planning and Operation Tool

## 2.4. Cross-Layer Optimization Modules

Throughout the project the consortium dedicated significant effort to develop and study offline IA-RWA algorithms for transparent and translucent networks [5], [6]. Considering PLIs in offline RWA has a certain particularity, as it involves the joint assignment of routes and channels to the connections requests, and interference among the selected lightpaths is inevitable once the solution has been found. Extensive comparative simulations for transparent topologies were performed using the various offline IA-RWA algorithms under realistic network and traffic parameters, exploiting a common QoT estimator tool developed within the project [4]. The experiments showed the applicability of these algorithms to real scale experiments, as they demonstrated good performance characteristics and implementation complexity and relatively low execution times. Indicatively, two of the developed impairment-aware algorithms are compared here with a standard k-shortest path RWA algorithm without physical-layer constraints in an effort to highlight the added value of the impairment awareness. Figure 2-4 (a) includes the blocking ratio of the three offline RWA algorithms with respect to the number of available wavelengths. The two IA-RWA algorithms use Linear Programming techniques and account for the interference among lightpaths in their formulation. The first algorithm (IA-RWA 1) takes the physical-



layer indirectly into account by limiting the impairment-generating sources. The second algorithm (IA-RWA 2) uses noise variance-related parameters to directly account for the most important physical impairments [7]. The experiment used as reference topology the generic national backbone network of Deutsche Telekom (DT) and assumed a realistic traffic matrix corresponding to the yearly traffic of 2009 (2.8 Tb/s) (see Appendix A: Network Topologies). The simulations of each algorithm were executed on a PC with Intel Core2 Duo at 3.0GHz and 4 GB RAM. Evidently the plain RWA cannot compete with the IA-RWA methods and yields very high blocking for the entire range of available channels.

In addition offline RWA algorithms constrained by the PLIs were also proposed for translucent networks, where regenerators are necessary in certain nodes to serve the traffic demands. Assuming a static traffic scenario yet with regenerators placed sparsely at certain a-priori known locations, the solution consists of the routes and assigned wavelengths and includes the decision of whether a connection will be served with or without the use of regenerators. In the former case also the sequence of regenerators is returned [6].

Before the RWA process, operators that employ the DICONET solution have additional cross-layer optimization tools at their disposal to support the planning phase. Regenerator and monitor placement refer to the modules developed to make optimized decisions on the number and location of the regenerating and monitoring equipment required in the network, by considering again the physical-layer performance [8]. This task has been specially focused on the regenerator placement techniques as those components imply significant capital and operational expenditures. Minimizing the particularly power-consuming opto-electronic interfaces of regenerators leads to the invaluable optimization of the total energy consumption of the network.

During network operation, a new demand is served constrained by the traffic and physical-layer characteristics present at the time of the arrival. The objective here is to assign routes and wavelengths to these dynamic demands taking PLIs into account, so as to satisfy their QoT requirements without disrupting the QoT of the already established connections. The time needed for making a connection assignment decision should be short, so that the connection's establishment delay is also acceptably short. Similar to the offline case a number of online IA-RWA algorithms were developed and simulation experiments were set up to assess their performance under identical conditions and utilizing the same QoT estimator. Indicatively Figure 2-4 (b) illustrates the capabilities of two multi-cost algorithms against a simple shortest-path-based that does not consider the QoT. In multi-cost routing, a vector of cost parameters is assigned to each link, from which the cost vectors of the paths are calculated. The first algorithm (Online IA-RWA 1) utilizes cost vectors consisting of impairment-generating source parameters, so as to be generic and applicable to different physical settings. These parameters are combined into a scalar cost that indirectly evaluates the quality of candidate lightpaths. The second algorithm (Online IA-RWA 2) uses specific physical-layer models to define noise variance-related cost parameters, so as to directly calculate the Q-factor of candidate lightpaths [9]. The comparison scenario assumed the DT reference topology and a dynamic input traffic. Connection requests (each requiring bandwidth equal to 10Gbps) are generated according to a Poisson process with rate  $\lambda=1$  (requests/time unit). The source and destination of a connection are uniformly chosen among the nodes of the network. The duration of a connection is given by an exponential random variable with average  $1/\mu$  (time units). Thus,  $\lambda/\mu$  gives the total network load in Erlangs. In each experiment 2000 connection requests are generated. Figure 2-4 (b) demonstrates two different performance metrics, blocking probability and execution time. Upon arrival of a traffic demand, fast response is essential

together with accurate QoT-aware routing decisions. Moreover effort was made to develop IA-RWA algorithms for translucent networks. In this context specially designed algorithms were also developed to jointly address the route, lightpath and regenerator selection problem, attempting to minimize the usage of the available regenerators [10].

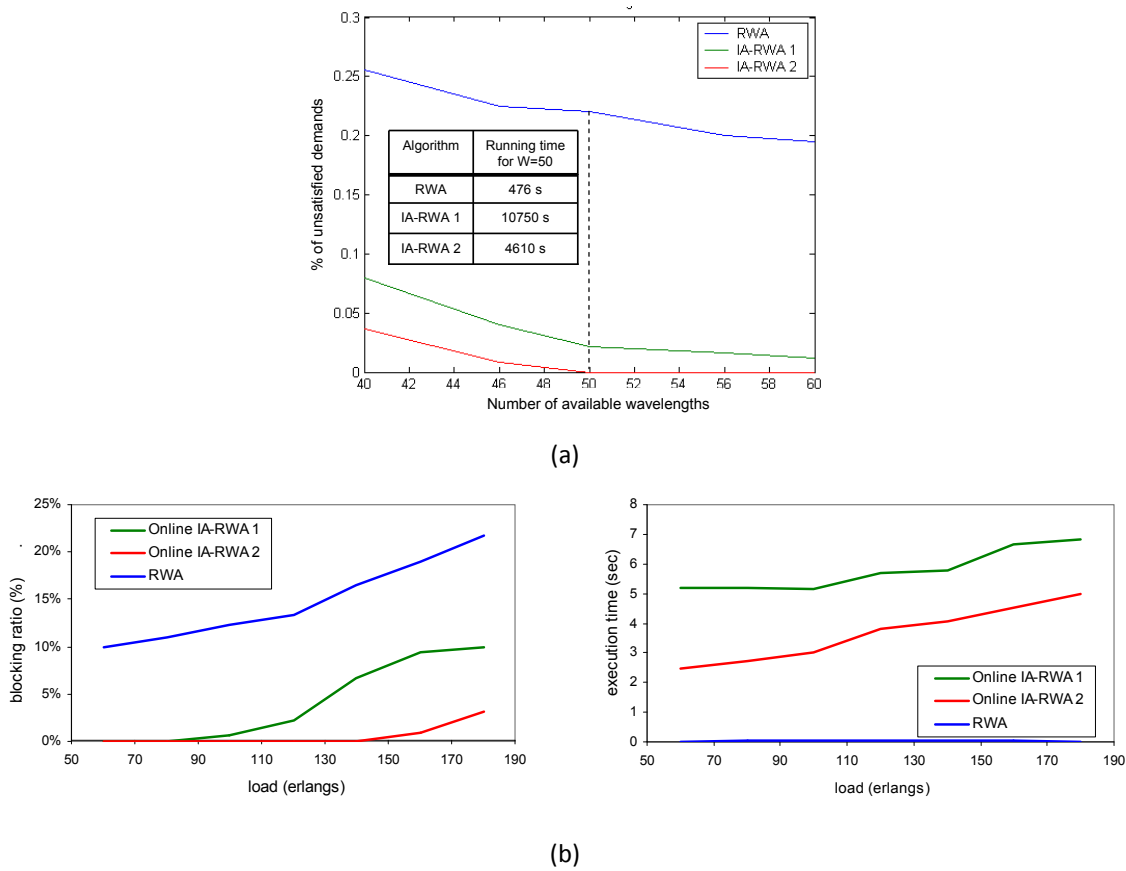


**Figure 2-4:** (a) Offline IA-RWA Blocking Ratio and running times as a function of the available wavelengths  $W$  (b) Online IA-RWA - Blocking ratio and average execution time per connection in seconds presented as a function of the network load, for a fixed number of wavelengths ( $W=20$ ).

Another important building block of the overall networking solution is responsible for monitoring the network for failures and locating the exact link that needs to be recovered. Upon a failure, following the fault localization process, the network utilizes its reaction mechanisms and restores all affected traffic. The result is a robust and reliable core network with guaranteed QoS. In the framework of the project, localization techniques for failures that cause a complete interruption of a connection (e.g. fiber cut) or merely a QoT degradation were developed and studied [11]. These techniques are fed with monitoring data from supervising devices (such as BER, power, or OSNR monitors) spread throughout the network which feed the restoration mechanisms.

## 2.5. Control Plane

The dynamic and impairment-aware networking relies heavily on a control plane enhanced with features that together with NPOT essentially enable the realization of this vision.

Recently, the adoption of the GMPLS framework developed by the IETF seems to prevail as the winning solution for the efficient control of an optical network. One of the main applications of GMPLS in the context of optical networks is the dynamic establishment and tear-down of lightpaths. DICONET utilizes the GMPLS protocol set but is not limited to its standard capabilities. One of the key tasks of the project concerned the extension of the GMPLS protocols to carry physical-layer information [4]. Whenever a change in the physical-layer status occurs it needs to be communicated to all responsible entities that need to take actions. The availability of this up-to-date information is essential so as to accurately evaluate the effect of PLIs and decide the feasibility of a lightpath in the optical domain.

Various control plane architectures were evaluated for implementation in the dynamic and impairment-aware network, including centralized and distributed solutions. The centralized approach implies a central point of control accessible by all network entities and aware of the complete network topology, resource availability and physical-layer information. In the distributed case all network entities are involved in the control plane signalling and routing processes but are deprived of global data knowledge. Three distributed architectures were considered; a signalling-based approach where the signalling component (i.e. Resource Reservation Protocol with Traffic Engineering extensions - RSVP-TE) is extended to consider the PLI information, a routing-based approach where the routing component is extended (i.e. Open Shortest Path First with Traffic Engineering extensions - OSPF-TE) but also a hybrid one that overcomes the limitations of the other two by extending both the routing and signalling protocols. The distributed approaches along with a centralized architecture that employs a Path Computation Element-based (PCE-based) method underwent a qualitative comparison to explore the performance and applicability of the four options using performance and engineering metrics (Figure 2-5).

Two control plane schemes were eventually selected to implement and test for the purposes of the project. The two schemes differ with respect to the role of the NPOT in the overall multi-plane architecture; one is hereafter referred to as the centralized (PCE-based) and the other as hybrid/distributed. In the former the NPOT is an engine common to all Optical Communication Controllers (OCCs). The set of the OCCs essentially realize the control plane and each of them runs the full GMPLS protocol suite, i.e. RSVP-TE, OSPF-TE and Link Management Protocol (LMP). Apart from extending the OSPF-TE to disseminate the PLI information, the novelty of this approach lies in the PCE which in collaboration with the NPOT forms the so-called Enhanced PCE (E-PCE) that deals with all the path computation and provision related actions. *Path Computation Reply* message of the standard Path Computation Element Protocol (PCEP) is extended and two novel messages, namely the *Path Allocation Result* and the *Path Tear-down Result* are defined to match the requirements of the PCE-based approach [12]. The standard RSVP-TE is deployed to establish, maintain, and tear down connections.

In the latter architecture all the network nodes run their own instance of the NPOT and extended versions of OSPF-TE and RSVP-TE. OSPF-TE is extended to disseminate wavelength availability information, while RSVP-TE carries the PLIs information for the QoT feasibility check. Due to the distributed nature of this implementation, upon receiving a new connection request from the Network Management System (NMS) the lightpath computation and the QoT estimation processes take place in the local NPOTs of the source and destination nodes. Prior to final integration and validation of the DICONET concept, emulation experiments were conducted to explore the capabilities of both selected control plane architectures under dynamic conditions and traffic load.

Following the development of the different pieces, all were eventually integrated in a multi-plane test-bed spanning from the transport to the management plane. Both the centralized and the distributed architectures were implemented in the 14-node experimental test-bed bearing 1 or 14 NPOTs respectively. These activities are elaborated in section 3.6 of the next chapter.

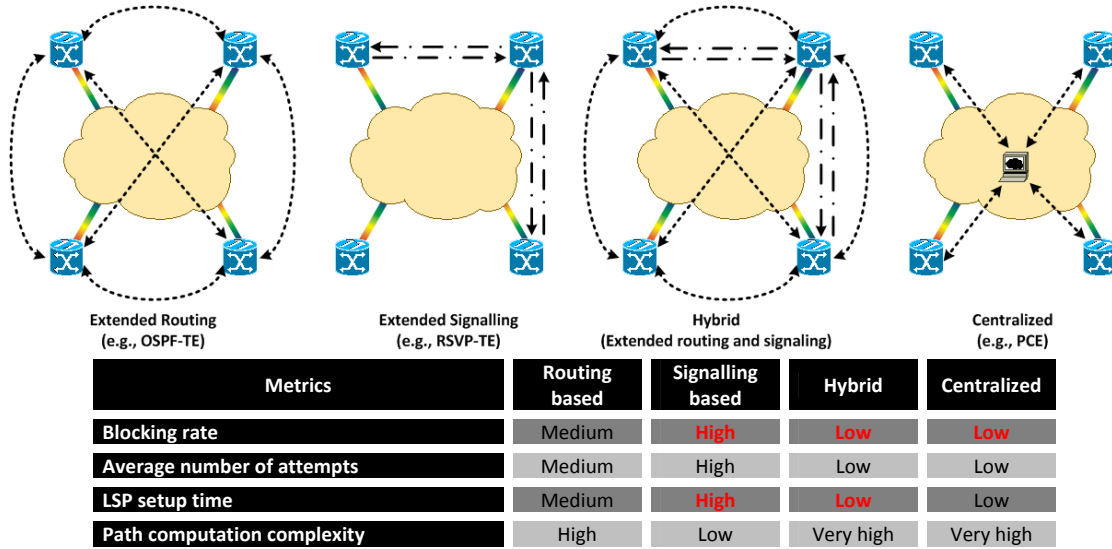


Figure 2-5: Qualitative assessment of the various control plane options

## 2.6. Chapter Summary

Dynamic optical networking allows operators to effectively maximize the capacity of their physical infrastructure and cope with the rapid growth rates of the Internet traffic. The European DICONET project proposed and developed a comprehensive solution that utilizes the dynamicity as well as the valuable physical-layer information of a reconfigurable WDM core network to provide a smooth transition from the quasi-static networking of today to an intelligent reconfigurable and physical impairment-aware architecture. This chapter first introduces the topics of network planning and operation in the context of a dynamic core optical network. Then, it reviews the benefits of implementing the DICONET solution and presents some of the major achievements of the project that support both the planning and operation phase of a core optical network. In what follows the physical layer awareness aspect of the DICONET approach is presented in detail as this has been one of the major contributions of the research work conducted in the course of this PhD.

## 2.7. References

- [1] H. Zang, J.P. Jue, and B. Mukherjee, "A Review of Routing and Wavelength Assignment Approaches for Wavelength-Routed Optical WDM Networks," *Optical Network Magazine*, pp. 47-59, Jan. 2000.
- [2] S. Azodolmolky, M. Klinkowski, E. Marín Tordera, D. Careglio, J. Solé-Pareta, and I. Tomkos, "A Survey on Physical Layer Impairments Aware Routing and Wavelength Assignment Algorithms in Optical Networks," *Computer Networks (Elsevier)*, vol. 53, no. 7, pp. 926-944, May 2009.

- [3] C.V Saradhi and S. Subramaniam, "Physical layer impairment aware routing (PLIAR) in WDM optical networks: issues and challenges," *Communications Surveys & Tutorials*, IEEE, vol.11, no.4, pp.109 -130, Fourth Quarter 2009.
- [4] Siamak Azodolmolky, Jordi Perelló, **Marianna Angelou**, Fernando Agraz, Luis Velasco , Salvatore Spadaro, Yvan Pointurier , Antonio Francescon, Chava Vijaya Saradhi, Panagiotis Kokkinos, Emmanouel Varvarigos , Sawsan Al Zahr, Maurice Gagnaire, Matthias Gunkel, Dimitrios Klondis, and Ioannis Tomkos, "Experimental Demonstration of an Impairment Aware Network Planning and Operation Tool for Transparent/Translucent Optical Networks", *IEEE/OSA Journal of Lightwave Technology*, vol.29, no.4, pp.439-448, Feb.15, 2011.
- [5] Siamak Azodolmolky, Yvan Pointurier, **Marianna Angelou**, Josep Solé-Pareta, and Ioannis Tomkos, "An Offline Impairment Aware RWA Algorithm with Dedicated Path Protection Consideration," *OFC/NFOEC 2009, OWI1*, San Diego, California, USA, 22-26 March 2009.
- [6] K. Manousakis, K. Christodoulopoulos, E. Kamitsas, I. Tomkos, and E. A. Varvarigos, "Offline impairment-aware routing and wavelength assignment algorithms in translucent WDM optical networks," *J. Lightw. Technol.*, vol. 27, no. 12, pp. 1866-1877, Jun. 2009.
- [7] K. Christodoulopoulos, K. Manousakis, E. Varvarigos, "Offline Routing and Wavelength Assignment in Transparent WDM Networks", *IEEE/ACM Transactions on Networking*, vol. 18, no. 5, October 2010.
- [8] M. Youssef, S. A. Zahr, and M. Gagnaire, "Cross optimization for RWA and regenerator placement in translucent WDM networks," in *Proc. IFIP ONDM*, Feb. 2010, pp. 1–6.
- [9] K. Christodoulopoulos, P. Kokkinos, E. Varvarigos, "Indirect and Direct Multicost Algorithms for Online Impairment-Aware RWA", *IEEE/ACM Transactions on Networking*, IEEE Early Access 2011.
- [10] K. Manousakis, P. Kokkinos, K. Christodoulopoulos, and E. Varvarigos "Joint Online Routing, Wavelength Assignment and Regenerator Allocation in Translucent Optical Networks," *Journal of Lightwave Technology*, vol.28, no.8, pp.1152-1163, April 15, 2010.
- [11] E. A. Doumith, S. Al Zahr, M. Gagnaire, "Monitoring-Tree: An Innovative Technique for Failure Localization in WDM Translucent Networks" in *Proc. GLOBECOM 2010*, vol., no., pp.1-6, 6-10 Dec. 2010.
- [12] S. Spadaro, J. Perelló, F. Agraz, S. Azodolmolky, **M. Angelou**, Y. Qin, R. Nejabati, D. Simeonidou, P. Kokkinos, E. Varvarigos, Y. Ye, and I. Tomkos, "Experimental demonstration of an enhanced impairment-aware path computation element", in *Proc. OFC/NFOEC 2011*, paper OMW5.

# Chapter 3

## 3. Physical-Layer Awareness in Dynamic Single Line-Rate Networks

In an all-optical network it is essential to consider the degradation effects that affect the transmission due to potentially very long transparent paths and high WDM channel count. Indeed it is essential to account the impact of the physical layer impairments on the QoT and use this information to take sophisticated decisions to optimize the network operation in terms of resources. For instance an IA-RWA algorithm requires fast yet accurate assessment of the physical degradation, particularly when it has to be performed “on the fly” (Online IA-RWA). This chapter intends to introduce the topic of physical-layer awareness and describe a physical layer performance evaluator, called “Q-tool” which was developed for the estimation of the signal quality of multichannel 10 (On-Off Keying) OOK Gb/s systems. In this context the key design issues of the Q-tool will be presented and the physical models implemented will be identified. In addition its applications on various modules of an impairment-enabled optical network are discussed. The chapter concludes with an experimental evaluation of routing algorithms fed by the Q-tool in a GMPLS-based control plane that was extended to carry physical layer information.

### 3.1. The Q-Tool

The Q-tool was developed to cover the need for an efficient module that would evaluate the impact of the physical layer impairments on the signal quality and feed this information to the modules useful for both the planning and operation phases of an optical network that is Monitor Placement, Regenerator Placement, Offline IA-RWA and Online IA-RWA. In the framework of the development of the tool effort was made to identify the dominant impairments, implement the physical layer models and integrate them into a single figure of merit, the Q-factor.

The input of the tool is abstractly divided into two parts: the physical topology and a set of lightpaths. The physical topology is essentially the entire set of physical parameters that characterize the network topology in the most complete way possible. The second part of the input consists of a set of computed paths (routes) along with their corresponding assigned wavelengths. This input is typically the solution of the RWA process that served a given traffic matrix. The tool then uses the introduced physical layer information to evaluate all the physical layer impairments and their combined effect and return the Q-factor of each lightpath. The computed Q-factor of each lightpath is merely a metric that characterizes its QoT as acceptable, or not-acceptable, weak or strong. The invoking modules may then use this knowledge accordingly. A case in point is the RWA module where in the case that a lightpath fails to achieve the minimum level of acceptable quality it has to take over again and calculate an alternative route.

The Q-tool was designed in a way that makes it inherently unaware of the physical topology, rendering it a black box that may assess the QoT of any set of lightpaths that may be established in a given network. The Q-tool receives the lightpaths (or even a single lightpath) from the calling function and returns its Q value. Figure 3-1 depicts the main building blocks of Q-tool. Before the actual core function of Q-tool, lies a layer that adapts the physical topology information to input suitable for Q-tool. The Q-tool function subsequently calls the processes that evaluate the impact of the impairments individually and in the end combines all respective results to the Q-factor. Each process receives the necessary input and feeds the result to Q-factor. These processes account for the physical layer impairments that were identified as dominant for 10Gb/s OOK WDM systems.

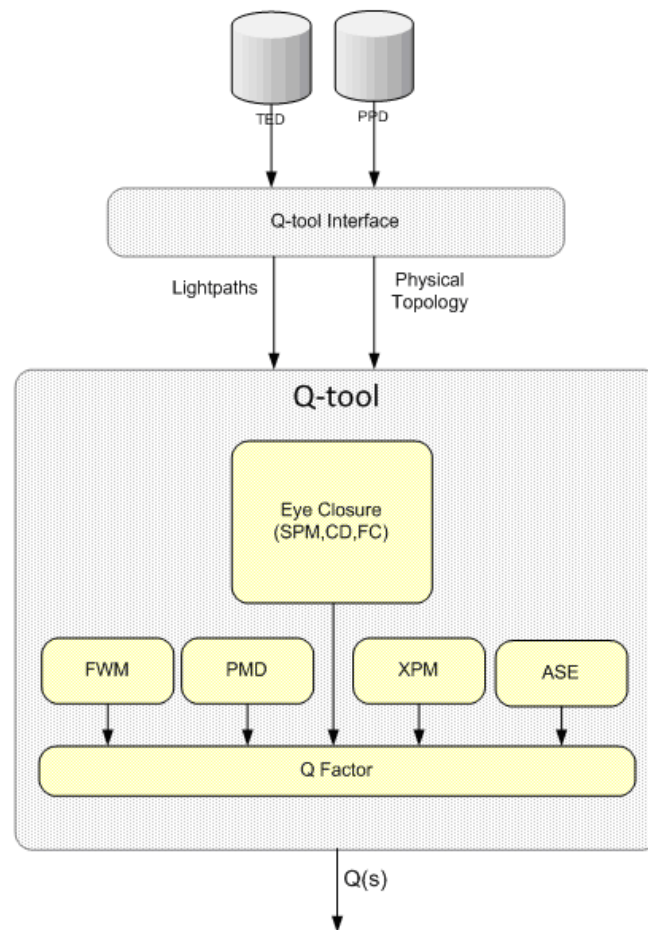


Figure 3-1: The Q-tool building blocks and flow.

### 3.2. Physical-layer Modelling in 10Gb/s OOK systems

In the framework of the design and the development of the Q-tool as a performance evaluator, the following impairments were considered:

- Chromatic Dispersion (CD)
- Filter Concatenation (FC)
- Self Phase Modulation (SPM)

These deterministic impairments impose distortions that affect the eye opening (see Figure 3-2) and are modelled using numerical single channel simulations.

Next follow the random effects:

- Amplifier Spontaneous Emission Noise (ASE)
- Polarization Mode Dispersion (PMD)
- Cross Phase Modulation (XPM)
- Four Wave Mixing (FWM)

These introduce degradations at the amplitude levels (see Figure 3-2) and are considered using analytical Q-factor modelling.

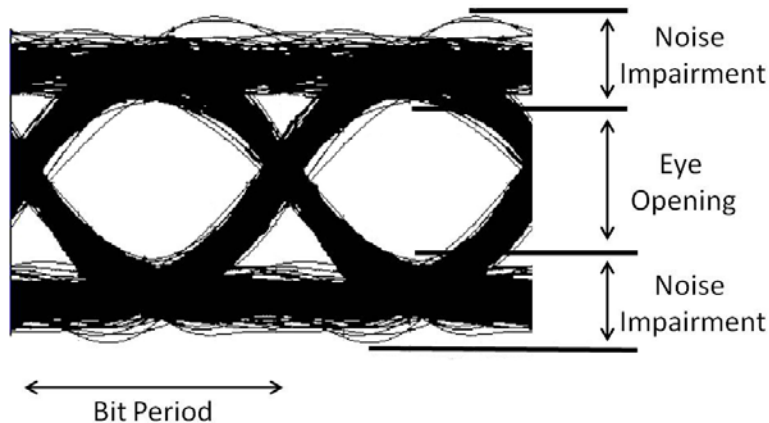


Figure 3-2: The distorted eye diagram.

### Chromatic Dispersion (CD)

Chromatic Dispersion or Group Velocity Dispersion (GVD) is the phenomenon that causes different wavelengths of light to travel at different speed. This speed variation results to broadening of the optical pulses as they propagate through the fibre. The pulses then overlap, leading to Inter-Symbol Interference (ISI) and higher bit error ratio. In general, the chromatic-dispersion limits the maximum transmission distance by decreasing it rapidly in inverse proportion to the square of the bit rate.

Chromatic dispersion occurs due to two reasons: the dependence of the optical fibre's index on the optical wavelength and the waveguide dispersion where the power distribution of a mode between the core and the cladding of the fibre is a function of the wavelength. In a purely linear system (transmission fibre), it is possible to completely cancel the effects of CD through the utilization of dispersion compensation modules. There are, however, two practical limitations to this solution. First, it is not always possible to compensate exactly for the dispersion occurring in transmission fibres. Dispersion Compensation modules come at predefined lengths while transmission fibre can be as long as the distance to be covered. Hence, transmission lines exhibit some amount of residual, uncompensated dispersion which causes ISI. Second, and more importantly, there is an inherent interdependence between chromatic dispersion and the nonlinear effects (see below), which again contributes ISI. Although such effects can be mitigated through optimization of the dispersion map, they can nonetheless never be fully annihilated and ISI has to be accounted for in a QoT estimator.

### Filter Concatenation (FC)

In an optical network, the light wave signal passes through a number of concatenated components, such as WDM multiplexers (MUXs), demultiplexers (DEMUXs) and noise



limiting optical bandpass filters, all of which can serve as optical filters. The concatenation of optical filters makes the system susceptible to filter passband misalignments arising from device imperfections, temperature variations and aging.

The effects of filter concatenation are generally not a concern in a point-to-point optical system, as a given signal passes through, at most, two filters (a multiplexer and a demultiplexer). However, in a transparent optical network, a signal may be de-multiplexed and re-multiplexed at many optical cross-connects or optical add-drop elements throughout its path before it is finally received. Thus, the signal experiences the concatenation of the entire set of filters in its path.

The filters have transmission functions that could be fitted using a Butterworth-like filter transfer function. In particular, many filters have characteristics that are well approximated by third-order Butterworth filter transfer functions. The equation describing a complex third-order Butterworth filter is given as (1):

$$H(f) = \frac{1}{\prod_{k=1}^3 \left[ \frac{if}{f_{3dB}} - \exp\left(\frac{i\pi}{2} \left(1 + \frac{2k-1}{3}\right)\right) \right]} \quad (1)$$

where  $i = \sqrt{-1}$ ,  $f$  is the frequency assumed to be centred around 0,  $f_{3dB}$  is the half bandwidth of the filter at the -3dB power transmission level.

The effective spectral transfer function of the cascaded filter set is the multiplication of each of the individual filters, which can, therefore, be much narrower in spectral width than a single filter. Spectral narrowing of the effective transfer function can be further exacerbated by any misalignments in centre frequency of the individual filters traversed by the signal. If the transmission laser is offset from the centre of the passband of the effective filter transfer function, then part of the signal spectrum may be attenuated out of proportion to the rest of the spectrum as the signal gets too close to one of the sidewalls of the filter transfer function. This, in turn, can lead to a time-domain distortion and a distortion-induced eye-closure penalty in addition to simple excess signal loss. Thus, the overall FC degradation is taken into consideration by estimating the eye closure penalty that introduces at the receiver node. In practice, filter concatenation is taken into account at the same time as SPM, which is described next.

### Self Phase Modulation (SPM)

Self Phase Modulation arises because the refractive index of the fibre has an intensity-dependent component. This nonlinear refractive index causes an induced phase shift that is proportional to the intensity of the pulse. Thus different parts of the pulse undergo different phase shifts, which give rise to chirping of the pulses. Pulse chirping in turn enhances the pulse-broadening effects of chromatic dispersion. This chirping effect is proportional to the transmitted signal power so that SPM effects are more pronounced in systems using high transmitted powers. The SPM-induced chirp affects the pulse-broadening effects of chromatic dispersion and thus is important to consider for high-bit-rate systems that already have significant chromatic dispersion limitations. For systems operating at 10 Gb/s and above, or for lower-bit-rate systems that use high transmitted powers, SPM can significantly increase the pulse-broadening effects of chromatic dispersion.

The combined effects of SPM and chromatic dispersion are difficult to estimate analytically, and here we resort to solving the Non Linear Schrödinger Equation (NLSE) numerically. This is done as follows; an input signal is generated based on the transmitter

characteristics; then the signal is propagated through the spans of fibres along the lightpath, with optical filtering occurring each time the signal traverses a node. At the end of the transmission line the signal is passed through a receiver and the following quantities are extracted: the eye opening, the average power  $P_0$  of the “0” samples, and the average power  $P_1$  of the “1” samples. The distortion induced eye closure is in essence the metric that quantifies the combined effects of SPM and CD. Since this effect has a deterministic nature in the absence of noise and in the effort to capture accurately the impact of SPM-CD, it is estimated utilizing a worst-case method based in [1] where  $eye = I_{1,min} - I_{0,max}$ , where  $I_{1,min}$  and  $I_{0,max}$  are the minimum the maximum detected current of marks and spaces respectively. These are retrieved from within a moving time window that comprises of the sample points that are centred on, and include, the optimum eye-opening position.

### Amplifier Spontaneous Emission Noise (ASE)

The advent of optical amplifiers capable of simultaneously amplifying multiple signal wavelengths that occupy an appreciable range of the optical spectrum was a key technological advance that ushered in the WDM revolution. Optical amplifiers are used at the end of each fibre span to boost the power of the WDM signal channels to compensate for fibre attenuation in the span. Yet, ASE noise is always present when optical amplification takes place and can be classified among the most severe impairments in terms of reach and capacity. Each amplifier contributes ASE noise that acts cumulatively throughout the amplifier chain. This accumulated ASE gives rise to signal-spontaneous beat noise at the receiver, which is the fundamental noise limit in an optically amplified transmission system.

The accumulated ASE power for a cascade of  $N$  amplifiers is estimated with the well-known formula that follows [2]:

$$P_{ASE} = 2h\nu B_o n_{sp} N(G-1) \quad (2)$$

where  $P_{ASE}$  is the power in an optical bandwidth  $B_o$ ,  $h$  is Planck’s constant,  $\nu$  is the optical frequency,  $n_{sp}$  is the spontaneous emission factor, and  $G$  is the optical amplifier gain. The spontaneous emission factor  $n_{sp}$  is determined by the inversion of the amplifiers Er ions. The contribution of each amplifier’s ASE to the accumulated ASE is characterized by the amplifier’s noise figure (NF), which at high gain can be approximated by  $N_F \approx 2n_{sp}$ . The coefficient 2 in the formula of the accumulated ASE power accounts for the two orthogonal polarizations, one parallel to the signal polarization and one orthogonal to it. The ASE noise variance at the end of the chain is described by [13]:

$$\sigma_{ASE,i}^2 = 4R_\lambda^2 P_{i,avg} (N, \lambda) \frac{P_{ASE}(N, \lambda)}{2} B_e / B_o \quad (3)$$

where  $P_{i,avg}$  is the average power of the spaces if  $i = 0$  or the average power of the marks if  $i = 1$ ,  $R_\lambda$  is the responsivity of the receiver, and  $B_e$  the electrical bandwidth of the receiver. The average power of the signal takes into account the finite extinction ratio that is introduced into Q-tool as a physical parameter of the transmitters, rendering  $P_{0,avg} \neq 0$ . It is noteworthy that only half of  $P_{ASE}$  is considered here since only the noise power whose

polarization is parallel to the signal polarization affects the signal-spontaneous beating. The ASE noise variance is used to calculate the Q factor degradation due to ASE.

### Polarization Mode Dispersion (PMD)

When light travels down a single mode fibre toward the receiver, it has two polarization modes that follow the path of two axes. When the core of the fibre that bounds the light is asymmetrical, the light travelling along one polarization axis moves slower or faster than the light polarized along the other axis and thus the two polarization modes arrive at different times at the receiver. This difference in arrival time is described by the differential group delay (DGD). The average separation can be calculated from the PMD coefficient of the fibre.

This effect can spread the pulse enough to make it overlap with other pulses or change its own shape enough to make it undetectable at the receiver. DGD is the fundamental measure of PMD. If DGD is severe, the receiver at some distance  $L$  cannot accurately decode the optical pulse, and bit errors can result. The penalty on Q factor induced by the PMD is modelled using [3]:

$$Q_{penPMD} = 10.2B^2D_{PMD}L \text{ in dB}, \quad (4)$$

where  $D_{PMD}$  is the fibre dispersion parameter,  $L$  is the length of the transmission fibre and  $B$  is the signal bit rate. Here  $Q_{penPMD}$  is the penalty to be deducted from the Q factor (expressed in dB) that does not incorporate the PMD effects.

### Cross Phase Modulation (XPM)

In WDM systems, the intensity-dependent nonlinear effects are enhanced since the combined signal from all the channels can be quite intense, even when individual channels are operated at moderate powers. Thus the intensity-dependent phase shift, and consequent chirping, induced by SPM alone is enhanced because of the intensities of the signals in the other channels. This effect is referred to as cross-phase modulation. If the fields have the same intensity, in the case of a WDM system with two channels, the effect of XPM appears to be twice as severe as that of SPM.

In practice, the effect of XPM in WDM systems operating over standard single-mode fibre can be significantly reduced by increasing the wavelength spacing between the individual channels. Because of fibre chromatic dispersion, the propagation constants of these channels then become sufficiently different so that the pulses corresponding to individual channels walk-away from each other, rapidly. This happens as long as there is a small amount of chromatic dispersion (1-2 ps/nm-Km) in the fibre, which is generally true except close to the zero-dispersion wavelength of the fibre. On account of this pulse walk-off phenomenon, the pulses, which were initially temporally coincident, cease to be so after propagating for some distance and cannot further interact. However, the spectrum broadened due to XPM will induce more significant distortion of temporal shape of the pulse when large dispersion is present, which makes the effect of dispersion on XPM complicated.

We investigate the impact of XPM on the performance of a single link considering the Cartaxo analytical model [4], properly modified to match the specific link architecture. The XPM induced intensity modulation (IM) frequency response is described by:

$$H_{XPMk}^{IM}(\omega) = \frac{P_{XPM,ik}(\omega)}{P_k(\omega)} = 2P_i(0)g_i^{net}(L_T) \exp[-j\omega \sum_{l=1}^N \frac{L^{(l)}}{u_{gi}^{(l)}}] \sum_{l=1}^N \gamma_i^l \exp \left[ j\omega \sum_{l=1}^N d_{ik}^{(n)} L^{(n)} \right] \cdot \prod_{n=1}^{l-1} e^{-a^{(n)} L^{(n)}} g_k^{(n)} \left\{ \begin{array}{l} \frac{1}{(a_{ik}^{(l)})^2 + (b_i^{(l)} + q_k^{(l)})^2} [a_{ik}^{(l)} \sin(B_i^{(l-1)} - Q_k^{(l)}) - (b_i^{(l)} + q_k^{(l)}) \cos(B_i^{(l-1)} - Q_k^{(l)})] \\ [a_{ik}^{(l)} \sin(Q_k^{(l+1)} - B_i^{(l)}) + (b_i^{(l)} + q_k^{(l)}) \cdot \cos(Q_k^{(l-1)} - B_i^{(l)})] \cdot e^{-a_{ik}^{(n)} L^{(l)}} \\ + \frac{1}{(a_{ik}^{(l)})^2 + (b_i^{(l)} - q_k^{(l)})^2} [a_{ik}^{(l)} \sin(B_i^{(l-1)} + Q_k^{(l)}) - (b_i^{(l)} - q_k^{(l)}) \cos(B_i^{(l-1)} + Q_k^{(l)})] \\ + [-a_{ik}^{(l)} \sin(Q_k^{(l+1)} + B_i^{(l)}) + (b_i^{(l)} - q_k^{(l)}) \cos(Q_k^{(l+1)} + B_i^{(l)})] e^{-a_{ik}^{(n)} L^{(l)}} \end{array} \right\} \quad (5)$$

for multi-segment fibre links ,where  $i$  stands for the probe signal and  $k$  for the pump,  $P_{XPM,ik}(\omega)$  represents the XPM-induced IM originated by pump channel  $k$  ,  $P_k(\omega)$  the pump channel,  $P_i(0)$  the power of channel  $i$  at the fibre input,  $g_i^{net}(L_T)$  the net power gain for the  $i$  channel from the transmitter up to the receiver,  $L_T$  the total system length,  $N$  the total number of spans,  $\gamma^{(l)}$  the nonlinear coefficient for the  $l$  segment,  $d_{ik}^{(l)}$  is the walk-off parameter between channels  $i$  and  $k$  in the  $l^{th}$  segment (given by  $d_{ik}^{(l)} = (u_{gi}^{(l-1)} - u_{gk}^{(l-1)})$ ),  $a^l$  the attenuation coefficient of the  $l^{th}$  segment,  $D_i^{(l)}$  is the dispersion parameter of the  $l^{th}$  segment of channel  $i$  and

$$a_{ik}^{(l)} = a^{(l)} - j\omega d_{ik}^{(l)} \quad (6)$$

$$b_i^{(l)} = \omega^2 D_i^l \lambda_i^2 / (4\pi c) \quad (7)$$

$$q_k^{(l)} = \omega^2 D_k^l \lambda_k^2 / (4\pi c) \quad (8)$$

$$B_i^{(l)} = \omega^2 \lambda_i^2 \sum_{n=l+1}^N L^{(n)} D_i^{(n)} / (4\pi c) \quad (9)$$

$$Q_k^{(l)} = \omega^2 \lambda_k^2 \sum_{n=1}^{l-1} L^{(n)} D_k^{(n)} / (4\pi c) \quad (10)$$

Using the above equations we can obtain an analytic expression for the XPM noise-like variance given by [5][5]:

$$\sigma_{XPM}^2 = \bar{P}(0)^2 \sum_{k=1, k \neq i}^N \frac{1}{2\pi} \int_{-\infty}^{\infty} |H_{XPM,ik}^{IM}(\omega, L)|^2 \cdot |H_{opt.filter}(\omega)|^2 \cdot PSD_k(\omega) d\omega \quad (11)$$

where  $\bar{P}(0)$  is the average channel power,  $H_{XPM,ik}(\omega)$  the transfer function due to XPM as described above,  $H_{opt.filter}(\omega)$  the transfer function of the optical filter at the receiver and  $PSD_k(\omega)$  is the power spectral density of channel  $k$  . The estimated variance will then account for the contribution of XPM in the Q factor equation.

#### Four Wave Mixing (FWM)

The four-wave mixing nonlinear interaction in an optical fibre is originated from a weak dependence of the fibre refractive index on the intensity of the optical wave propagating

along the fibre. In this interaction, an optical wave of frequency  $f_{ijk}$  is generated through mixing three waves of frequencies  $f_i, f_j, f_k$  that obey the relationship  $f_{ijk} = f_i + f_j - f_k$  which is required by the energy conservation condition. Strict phase matching requires  $\Delta\beta_{ijk} = \beta_i + \beta_j - \beta_k - \beta_{ijk} = 0$ , where  $\beta_n$  ( $n = i, j, k$  and  $ijk$ ) is the propagation constant of optical waves with frequency  $f_n$  ( $n = i, j, k$  and  $ijk$ ). Due to dispersion in single-mode fibre, the exact phase matching condition is difficult to satisfy, but approximate phase matching may be obtained in a low-dispersion fibre over significant length of fibre.

In a real multi-wavelength system the actual total FWM power is very sensitive to fibre dispersion, wavelength channel spacing and amplifier spacing. A very small change of the above three parameters can result in significant variation in the total FWM power. Decreasing the channel spacing increases the four-wave mixing effect, and so does decreasing the chromatic dispersion. This FWM power will appear as noise or crosstalk to the wavelength channel located at frequency  $f_n$ . An interesting point to note is that the total FWM power does not always increase with increasing number of fibre segments. This is because FWM waves generated in each fibre segment may cancel each other if they are out of phase at the end of the transmission link.

For the assessment of the FWM effect an expression is derived based on the analysis of [6] and [7]. The signal power of a single FWM product at the end of a link, properly modified to fit the link architecture, can be expressed as:

$$P_{pqr} = \frac{1024\pi^6}{n_0^4 \lambda^2 c^2} (d\chi)^2 \frac{P_p P_q P_r}{A_{eff}^2} \exp\left[\sum_{m=1}^M (-2A^{(m)})\right] \times \left[ \sum_{m=1}^M \left[ \prod_{k=1}^{m-1} \sqrt{G^{3(k)}} \times \exp\left[\sum_{k=1}^{m-1} (-2A^{(k)} + i\Delta\psi^{(k)})\right] \prod_{k=m}^{M-1} (\sqrt{G^{(k)}}) \times \frac{1 - \exp[(-\alpha_i + i\Delta\beta_i)L^{(m)}]}{\alpha_i - i\Delta\beta_i} \right] \right]^{(12)}$$

where  $n_0$  is the refractive index,  $d$  is the degeneracy factor ( $d=3$  for  $f_p = f_q \neq f_r$ ,  $d=6$  for  $f_p \neq f_q \neq f_r$ ),  $P_i$  is the launched signal power per channel (equal power per channel assumed, and also same polarization assumed),  $\chi$  is the third-order nonlinear susceptibility and  $A_{eff}$  the effective area of the specific fibre segment,  $L$  is the length of a fibre segment and  $\alpha$  is its corresponding attenuation,  $G$  is the gain of the amplifiers,  $M$  is the number of spans in the link,  $A^{(m)}$  ( $A^{(m)} = \alpha_i L_i^{(m)}$ ) is the attenuation in span  $m$ , and  $\Delta\beta_i$  is the phase mismatch which is related to signal frequency differences and chromatic dispersion  $D_i$  and may be expressed as:

$$\Delta\beta_i = \frac{2\pi\lambda^2}{c} |f_i - f_k| |f_j - f_k| \left\{ D_i + \frac{dD_i}{d\lambda} \left( \frac{\lambda^2}{2c} \right) (|f_i - f_k| + |f_j - f_k|) \right\}, \quad (13)$$

where  $\partial D_i / \partial \lambda$  is the dispersion slope.  $\Delta\psi^{(m)}$  ( $\Delta\psi^{(m)} = \Delta\beta_i L_i^{(m)}$ ) is the accumulated phase mismatch. In a multi channel transmission system an analytical expression for the noise-variance due to FWM is derived:

$$\sigma_{FWM}^2 = 2K^2P_s \left\{ \frac{1}{8} \sum_I P_{pqr} + \frac{1}{4} \sum_{II} P_{pqs} + \frac{1}{4} \sum_{III} P_{ppr} \right\} \quad (14)$$

where  $P_s$  is the peak power of the selected signal light,  $P_{pqr}$  is the power of is the FWM light generated from a channel combination of  $p$ -,  $q$ - and  $r$ th channels that satisfy  $p+q-r=s$ ,  $K=ne/hf$ ,  $n$  is the quantum efficiency of the detector,  $e$  is the electron charge,  $h$  is Planck's constant, and  $f$  is the light frequency. The channel combinations are classified into three categories. One is a case where all channels, including the selected channel, are different ( $p \neq q \neq r \neq s$ ). The second one is when  $p$ -,  $q$ -, and  $r$ th channels are different but the  $r$ th channel is identical to the selected channel ( $p \neq q \neq r = s$ ). The last one refers to the case where  $p$ - and  $q$ th channels are identical ( $p = q \neq r$ ). We express the above classification as follows:

$$\sum_{pqr} = \sum_{p \neq q \neq r \neq s} + \sum_{p \neq q \neq r = s} + \sum_{p = q \neq r} = \sum_I + \sum_{II} + \sum_{III} \quad (15)$$

where summations I, II, and III denote summations for  $p \neq q \neq r \neq s$ ,  $p \neq q \neq r = s$ , and  $p = q \neq r$ , respectively. It is noteworthy at this point that the experimental validation of the last two models that refer to XPM and FWM have been validated with re-circulating loop experiments and demonstrated in [5].

#### Q-factor

The overall performance of the signal quality is reflected in the Q-factor, which combines the impact of all impairments mentioned above:

$$Q = 20 \log \left( \frac{I_{1,\min} - I_{0,\max}}{\sigma_{0,ASE} + \sqrt{\sigma_{1,ASE}^2 + \sigma_{XPM}^2 + \sigma_{FWM}^2}} \right) - Q_{penPMD} \quad (16)$$

The nominator of the formula refers to the difference of the minimum detected current at the level of "1" and the maximum at the "0" level which defines the distortion induced by FC, SPM and CD on the signal. The summand in the denominator of the Q formula includes the variances of all the noise impairments that add up to the total signal power variance.  $\sigma_{0,ASE}^2$  and  $\sigma_{1,ASE}^2$  refer to the variance of the detected spaces and marks due to ASE noise. XPM and FWM are assumed only to add noise at the level of "1"s and therefore the non-linear induced degradation is expressed by  $\sigma_{XPM}^2$  and  $\sigma_{FWM}^2$ . Finally, since the Q-factor is in fact a figure of merit the PMD-induced penalty is subtracted from the total estimated Q-factor. In a nutshell through Q-factor the Q-tool offers fast assessment of the QoT of a signal given a specific traffic matrix and physical topology and based on analytical estimations and numerical simulations.

To illustrate the function of Q-tool the DTNet (See A.1 Deutsche Telekom's Backbone Network) network topology in the simulation studies is utilized. This network has 14 nodes and 23 bidirectional links, with an average node degree of 3.29. The line rate in this network is assumed to be 10 Gb/s. A heterogeneous network topology is assumed in which the node and link architectures have different impact and contributions on physical layer impairments.

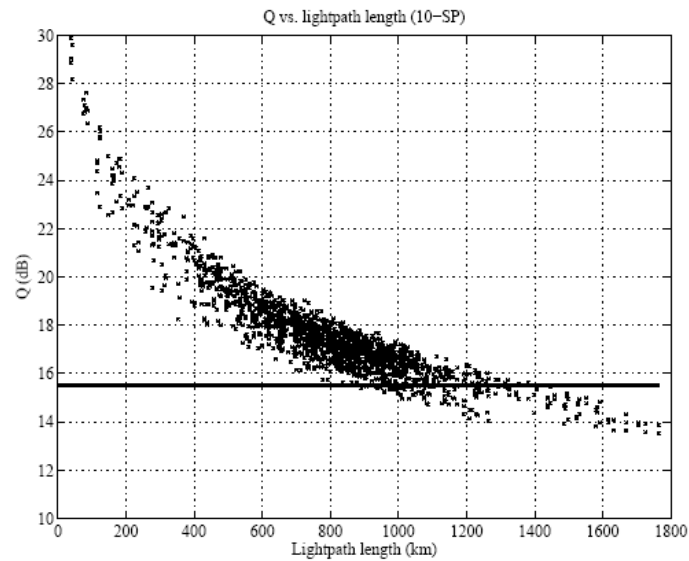


**Figure 3-3:** Q-factor value vs. lightpath length ( $Q_{\text{Threshold}}=15.5$  dB).

The input power to the links is -4 dBm and 3 dBm per channel for Dispersion Compensation Fibre (DCF) and Standard Single Mode Fibre (SSMF) fibres respectively. It is also assumed that pre-dispersion compensation of -400 ps/nm is considered in the links. The SSMF amplifier span length in each link was set at 100 km, followed by a DCF segment that under-compensates the dispersion of the preceding SSMF of a value of 30 ps/nm/km. At the end of each link the accumulated dispersion is fully compensated. It was assumed that the SSMF fibres have a dispersion parameter of 17 ps/nm/km and attenuation of 0.25 dB/km. The DCF segments have a dispersion parameter of  $D = 80$  ps/nm/km and an attenuation of 0.5 dB/km. The PMD coefficient for all fibre segments is set to  $0.1 \text{ ps}/\sqrt{\text{km}}$ . The channel spacing was set to 50 GHz. The noise figures that were utilized in simulation studies had a mean value of 6 dB with a variation of 1 dB. The threshold value for computing the impact on Q-factor (i.e.,  $Q_{\text{threshold}}$ ) is 15.5 dB (corresponding to  $\text{BER}=10^9$  without FEC). In Figure 3-3 the Q-factor value of the 10 shortest paths between all possible pairs of the nodes in the network is depicted.

### 3.3. QoT development approach

Q-tool provides an efficient way to estimate the signal performance via an all-optical path while having global knowledge of the network topology and traffic. As aforementioned, the Q-tool models the identified as dominant physical impairments in a WDM system and evaluates the system performance in terms of the Q factor. The extent to which these effects degrade the QoT of the system depends on the operating and topological features of the optical network. Combining a different set of values for parameters ranging from the distance to the intrinsic characteristics of the network components and from the bit rate to the power budget, the resulting Q factor seeks to evaluate the system's QoT. Naturally, the overall optical path Q factor in a multi-channel system is calculated in Q-tool taken into consideration all the critical effects from the presence of the other simultaneously transmitted paths. This denotes that in a dynamic network environment, a single change in the optical paths (i.e. a new request for optical path establishment) will not only require the performance evaluation of the newly appearing lightpath in the presence of other active

channels but also the performance “re-evaluation” (i.e. recalculation) of all the existing paths, in order to determine the impact of the new one on them. Evidently, the implementation of Q-tool in a fully scaled network (e.g. the DT network in Germany detailed in Appendix A.1 Deutsche Telekom’s Backbone Network) sets demanding requirements in terms of computational and processing power requirements. Therefore the selection of the Q-tool performance evaluation model was done in order to achieve fast processing for dynamic variations and also acceptable accuracy.

In the absence of impairment monitors, the Q-tool partially uses fast analytical models in combination with single-channel numerical modelling that provide relatively fast performance estimation at a certain level of accuracy. Before proceeding with the discussion of the individual Q-tool parts it is important to note that an alternative way to implement a QoT-estimation tool would be to use the complete numerical modelling of a WDM system. This approach would be based on the Split-Step Fourier (SSF) method that is commonly used to solve the Non-linear Schrödinger Equation (NLSE) which regulates the propagation of the optical signal through the non-linear medium. However, the complete numerical approach, although it is widely used in link performance evaluation models and even professional simulation tools (e.g. VPI TransmissionMaker®), it is computationally very complex and particularly time-consuming and therefore does not agree with the dynamically varying and fast processing requirements of a network in operation.

In a nutshell the SSF method treats the linear and non-linear part of the equation separately by breaking the solution in very small steps. The non-linear part is solved in the time domain while the linear in the frequency domain. Therefore, at every step the method has to switch between the domains using Fast Fourier Transforms (FFT). However, the efficiency and the speed of the SSF method depend highly on the size of the step and the number of the FFTs. Clearly, the smaller the size of the step is, the greater the number of the required FFTs. It has been shown though, that most of the computational time is consumed when evaluating the FFTs. Especially when it comes to a multi-channel transmission, the numerical simulations become extremely time-consuming ([9]). This happens because in order to correctly capture the effect of XPM and FWM the step size has to be very small ([10]). Hence, a fully numerical approach is not suitable for the “on-line” operation of a dynamic network. If there is need for QoT evaluation to serve the Online IA-RWA, it is vital to be able to perform it “on-the-fly”. In order to tackle such limitations the Q-tool provides fast QoT assessment considering both linear and non-linear impairments in a method that combines numerical simulations and analytical approximations.

The selection of the Q-tool approach is a balance between processing speed and accuracy. According to the adopted approach the Q-tool estimates the Q-factor of a given optical path in a two-step approach. First, single channel numerical simulations are performed to account for the deterministic distortions and second all the noise terms are calculated and added to the total Q value. The purpose for this selection was to have a combination of an accurate numerical method that applies only on a per channel basis, having therefore minimum effect in the processing time consumption, with a fast analytical estimation method that incorporates all additional distortions in the form of added noise. The following paragraphs discuss in detail the characteristics of the sub-models that constitute the Q-tool model and evaluate their use in terms of speed and accuracy.

### **SPM-CD and filtering effects**

The Q-tool resorts first to the detailed numerical SSF method in order to quantify the impact of the SPM-CD and the filtering effects on the signal quality. In this context every optical



signal is treated as if there is only single-channel propagation, thus accounting only for SPM, CD and FC. This approach achieves accurate computation of the state of the optical signal at the receiver-end without considering the presence of neighbouring channels that would impose a prohibitive time penalty in the process. Thus, contrary to various similar works ([8], [11], [12]) that rely solely on analytical or semi-analytical models to estimate the QoT, Q-tool introduces a balance between speed and accuracy by simulating numerically the single-channel signal propagation. In these works the impairments were considered in the framework of the RWA problem or a regenerator placement algorithm.

#### **EDFA-induced noise**

Identifying in the EDFA-induced noise one of the fundamental degrading factors of OSNR along an optical path, the accurate estimation of noise power has its own significance. The analytical model utilized in Q-tool to estimate the power of the ASE noise of a cascade of inline amplifiers is similarly utilized in ([13], [14], [15]) to assess the accumulation of this effect and its impact on the lightpath performance. The Gaussian distribution of the ASE-signal beating noise facilitates the incorporation of its contribution to the Q-factor by considering the noise variances that are superimposed on the levels of marks and spaces.

#### **XPM, FWM**

Furthermore, Q-tool treats XPM and FWM as random noise that affects the QoT just as ASE noise, imposing fluctuations that typically occur at the mark level. As was shown in [16] this can be considered as a good approximation particularly at the regime of relatively high Q and at the same order of magnitude as ASE noise. In the same work ([16]) the XPM-induced distortion is estimated using the frequency response of XPM-induced intensity modulation from a modulated pump channel to a CW probe channel ([4] “Cartaxo model”), as in Q-tool. In [5] the “Cartaxo model” was compared with numerical simulations and other analytical models and proved to give a good approximation for the Q-factor. The authors also demonstrated a comparison between a simplified (faster) version of the same model and loop experiments illustrating its accuracy and also observed a Gaussian distribution of the XPM both from Split-Step Fourier numerical simulations and experimental measurements. To further support what is argued here, the validity of the pump-probe approach followed by the “Cartaxo model” was also investigated in [17] through experiments that measured the Q degradation due to XPM and the measurements were found to be in good agreement with the analytical results.

In a similar manner it was shown ([16]) that FWM is well approximated with a Gaussian distribution. Assuming a random behaviour is particularly applicable in FWM due to the fact that many independent channels contribute to the total FWM power. The work in [16] utilizes the model reported in [7] and is extended for a multi-span system, same as it is implemented in the Q-tool. The work in [18] illustrates the behaviour of the noise variance of the specific FWM model with respect to the channel wavelength of a WDM system as well as the contribution of FWM to the overall Q estimation. It is noteworthy that in [19] the authors verified the analytical model with experimental results obtained with a recirculating loop setup with respect to a variable number of spans in a transmission link. The same analytical model was also compared to results taken from numerical simulations which showed a very good match.

### **PMD**

Q-tool also accounts for PMD, by considering a Q penalty associated to it that is subtracted from the overall Q value. To estimate the PMD induced Q penalty the approach used by [3] was adopted in Q-tool. This form which was first reported in [20] and corrected for the experimental results of [21], is accounting only for the first order PMD using an analytical approach. To calculate the PMD-induced penalty two different methods have been generally followed ([22]). One of them relies on a sophisticated statistical modelling method that approximates the all-order PMD, while the other considers only the first-order PMD using an analytical or numerical approach. Nevertheless, despite that the analytical model is restricted to the first-order PMD a comparison for a 10 Gb/s NRZ signal in [22] demonstrated that its penalty was in good agreement with the penalty obtained with the statistical modelling. The authors compared the statistical approach with the analytical for various mean DGD values and demonstrated excellent matching conditions between the two. In fact NRZ signals are primarily dominated by the first-order PMD rendering the choice for the analytical approach valid for the framework of the DICONET NPOT. However, it is noted that in a higher-bit-rate system this approach could not be applied, since a format that is more robust to PMD (such as RZ) should be considered.

In view of the overall complexity of a WDM system, the method that the Q-tool employs to estimate the impact of transmission impairments on the lightpath quality aims at a compromise between speed and accuracy in the manner described above.

## **3.4. Physical-Layer Awareness in Network Planning and Operation**

The QoT estimator plays a fundamental role in the cross-layer optimization from the data plane up. No matter what is the metric, i.e. BER, Optical Signal-to-Noise Ratio (OSNR) or Q-factor, it determines the feasibility of the optical paths. Figure 3-4 depicts the anatomy of the network planning and operation tool that was developed for the purposes of the EU DICONET project (see section 2.3). It utilizes the QoT estimator presented in this chapter which is situated in the core of the overall tool. It is noteworthy here that the various components of the tool consult the QoT estimator to make educated decisions. As mentioned already the RWA process, whether online or offline, uses the QoT estimator either as a quality metric during the routing and wavelength assignment process or after the routing and wavelength assignment has taken place to validate the computed RWA solution. In turn the regenerator and monitor placement algorithms invoke the QoT estimator in order to find the optimum location for these components. For instance regenerators should only be placed to sites (nodes) where regeneration is actually required and lightpaths tend to bear a weak signal.

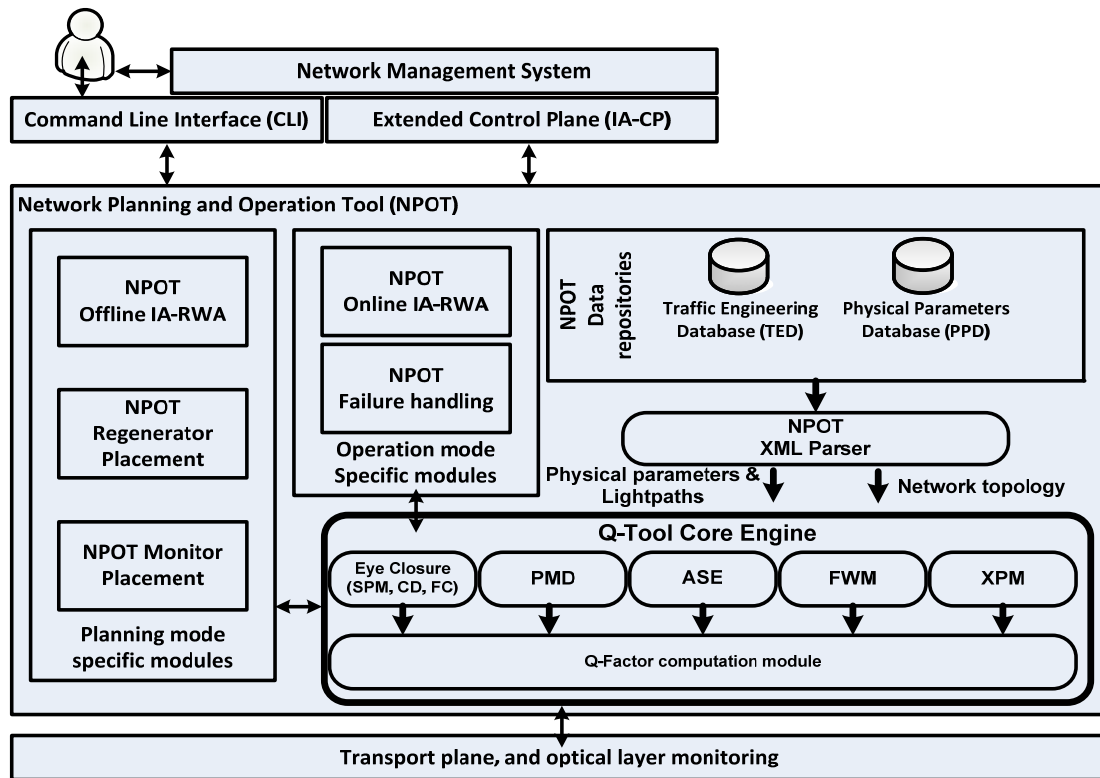


Figure 3-4: A Network Planning and Operation Tool with the Q-Tool.

Then the cooperation of the QoT estimator with the control plane renders the latter “Impairment-Aware”. Figure 3-5 a) depicts a distributed integration scheme where the GMPLS protocols have been extended and are capable of collecting and disseminating real-time information from the physical layer. These data are then fed to the QoT estimator so as to always have an up to date knowledge of the physical parameters of the network. The control plane in this scheme is in fact responsible of routing and establishing lightpaths yet verifies its decisions with the QoT estimator. Figure 3-5 b) shows a centralized integration scheme that utilizes the QoT estimator for the lightpath restoration process. Upon a physical failure and after its location has been spotted the control plane notifies accordingly the network planning and operation tool about the “failed” element. New wavelengths and routes are then computed for the disrupted traffic avoiding the physical elements that have stopped functioning properly.

Hence, although the applications of the estimator are plenty, what is crucial for the validity of its operation concerns the physical impairment models as discussed in sections 3.2 and 3.3). Impairments caused by the propagation of the signal in the non-ideal transmission medium, accumulate and degrade the signal quality along its journey. Nonetheless, the QoT estimation is highly dependent on the parameters and the characteristics of the system for which it works.

Figure 3-4 and Figure 3-5 are introduced here only to highlight the role of the QoT estimator in the overall architecture and the cross-layer optimization process in general and for this reason the details of the elements and the interfaces included in these figures are omitted. The complete architecture of the NPOT and the control plane schemes has been reported in [23].

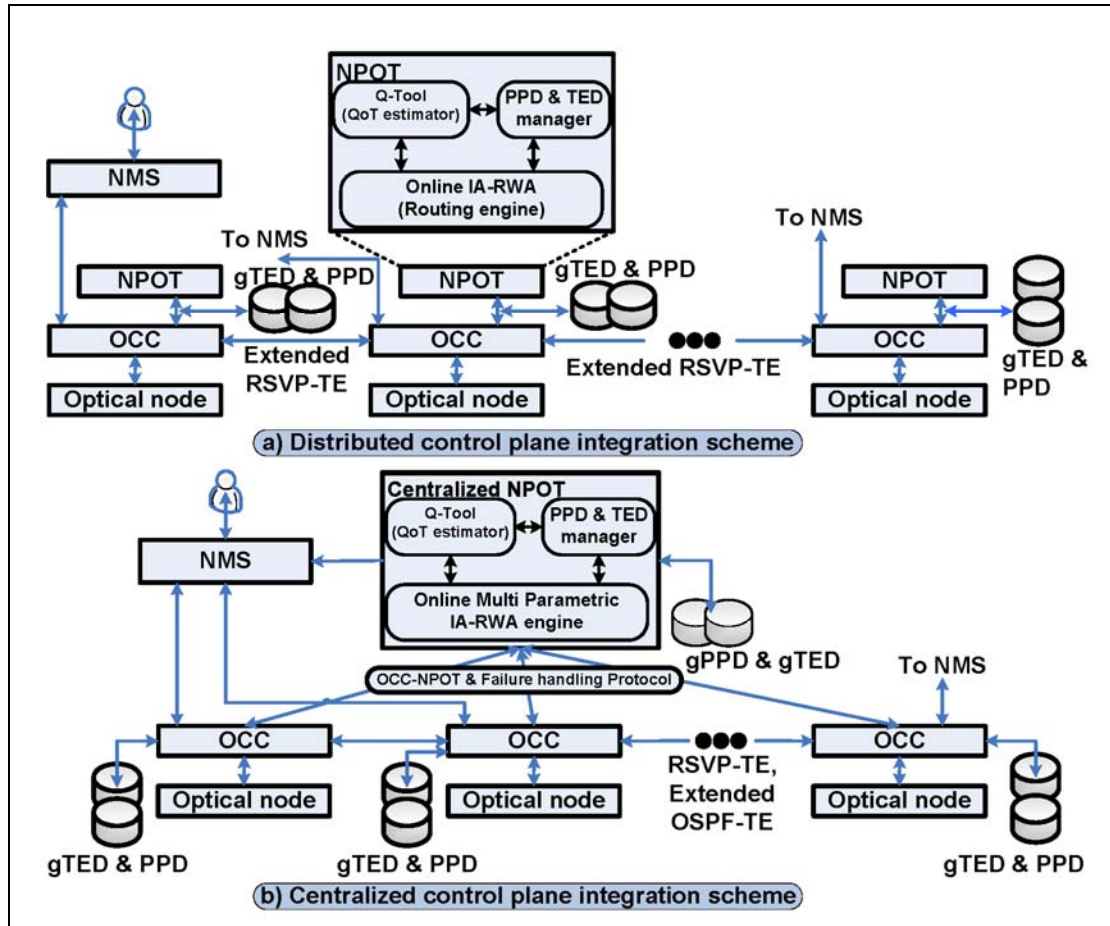


Figure 3-5: Distributed and Centralized Control Plane Integration Schemes.

### 3.5. Monitor Placement

A cross-layer module that utilizes physical layer information to optimize the network planning phase reported in [27] has been also developed in the course of this PhD. A special monitor placement scheme was designed that takes into account partial monitoring information coming from the physical layer to decide the optimum number and locations of the optical monitoring devices. This work is presented in the following chapter (Chapter 4).

### 3.6. Experimental Evaluation of IA-RWA Processes using the Q-Tool

The Q-tool was utilized to experimentally evaluate the performance of IA-RWA algorithms in terms of the blocking ratio and lightpath setup time they can achieve in an operational scenario. The suitability and performance of two particular IA-RWA algorithms was tested in a 14-node experimental test-bed that employed a centralized control-plane architecture under the same network and traffic conditions.

The centralized scheme that integrates the routing engine in a unified extended GMPLS control plane is depicted in Figure 3-5 b). The online IA-RWA engine that resides at the core of this scheme is responsible for the route computation and the wavelength assignment for

every new connection demand that arrives, always utilizing the available physical-layer information. Evidently the performance of the integrated solution relies highly on the performance of the QoT-aware routing engine. Although the IA-RWA algorithms are typically tested individually as a standalone module, it is the goal of this work to demonstrate their importance as part of an operational network platform, not only in terms of the blocking ratio but also in terms of the connection setup time. To achieve this, the 14-node experimental test-bed of DICONET was utilized to evaluate in turn two different IA-RWA algorithms under the same conditions. The results shown here demonstrate a trade-off between the setup time and the blocking ratio of the two employed IA-RWA algorithms.

An important building block in the integrated test-bed (detailed in section 2.3) is a custom Network Planning and Operation Tool (NPOT), which at operation mode encompasses all the modules necessary for the dynamic connection provisioning, i.e. the routing engine, the QoT estimator and a database manager. The QoT estimator (i.e. the Q-tool) is responsible for the signal quality assessment by utilizing the global Physical Parameters and Traffic Engineering Databases (gPPD and gTED). The two databases essentially carry all the real-time information that is required for the computations of the IA-RWA and the QoT estimator, including the network topology, the physical-layer status and the wavelength availability.

As depicted in Figure 3-6 the lightpath computation process is performed by a single NPOT that communicates with all the optical nodes of the network thus providing a centralized point of control. The control plane is composed of a set of 14 Optical Connection Controllers (OCCs) each corresponding to a network node. The OCCs employ the full GMPLS protocol suite, including standard RSVP-TE and extended OSPF-TE [23]. The two protocols are responsible for the lightpath establishment and the proper update of the global and local databases. Each OCC node controls the respective Optical Cross Connect (OXC) emulator through the Connection Controller Interface (CCI) (Figure 3-6). The set of OXC emulators form the emulated transport plane.

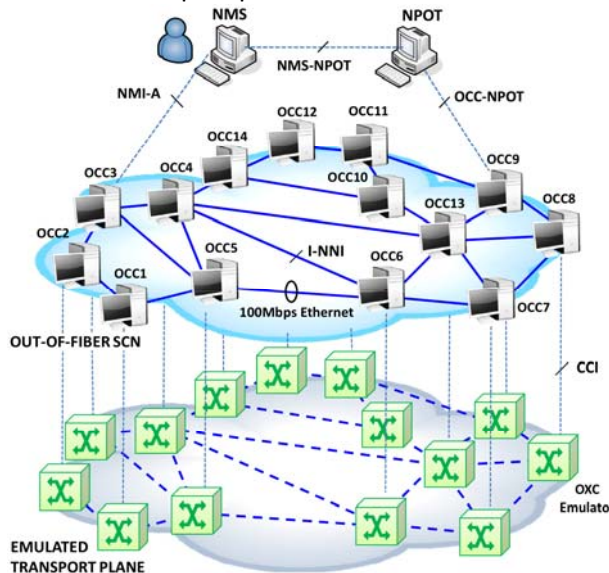
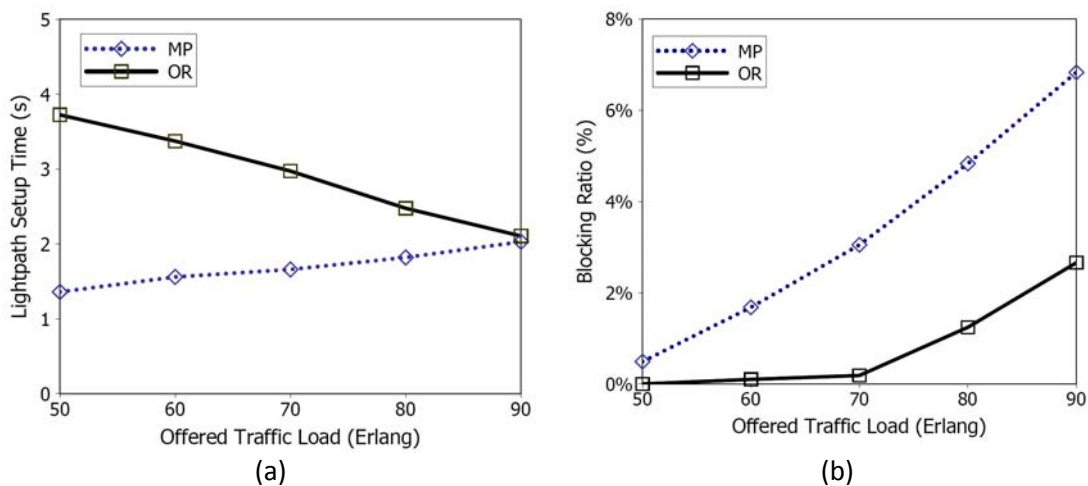


Figure 3-6: The experimental test-bed.

Upon the arrival of a new demand, the source node OCC is notified by the Network Management System (NMS) to initialize the lightpath request process. In turn, the request is forwarded to the online IA-RWA engine, through the OCC-NPOT interface. The IA-RWA engine accesses the databases to get an update of the available resources and consults the

QoT estimator to make an impairment-aware decision. In [23] the centralized scheme used as routing engine the Multi-Parametric IA-RWA algorithm (MP) [24]. Important rationale for the initial selection of this algorithm was the need for an engine that can respond fast to a given connection demand. Typically the bottleneck in the path computation is located in the QoT estimation. Indeed the QoT estimator utilized here (Q-Tool), as discussed in section 3.3, estimates the joint impact of the dominant physical layer impairments (PLIs) in a method that combines analytical models and numerical simulations. Given the computational intensity of the QoT estimator the MP algorithm was designed so as to avoid the Q-Tool invocations whenever possible. It utilizes a multi-cost routing approach that includes impairment generating sources to indirectly account for the physical layer degradations. In this way it efficiently allocates the network resources while keeping the execution times low. The performance of the MP algorithm in terms of the blocking ratio depends highly on the weights assigned to the various impairment generating sources. The exact values of these weights are selected during a training period.

Herein the MP algorithm is compared to an IA-RWA engine whose primary goal is to return optimum lightpaths in terms of QoT. The algorithm in question refers to an IA-RWA heuristic named Rahyab and presented in [25]. The algorithm that was initially designed for planning and featured also path-protection capabilities, was properly adapted for online operation (further denoted as OR). Given a connection request, OR, constrained by the wavelength continuity and the channel availability, searches among all possible lightpaths (for  $k$ -shortest paths) to find the one that yields the best QoT both for the new connection but also for the already established ones. Essentially it decomposes the network topology into  $W$  planes, where  $W$  is the number of channels per link, and computes  $k$  shortest paths for each of the planes. Consider for instance that  $W$  is equal to 10,  $k$  is equal to 3 ( $k$  is an input parameter of OR) and all 3 computed shortest paths are available end-to-end in all planes. Then OR forms a pool of 30 candidate lightpaths and invokes the QoT estimator for each of them separately to assess them in the presence of the established lightpaths. The optimization benefit of this algorithm comes with a cost in execution time as it requires the consecutive execution of the QoT estimator several times for each connection request.



**Figure 3-7:** (a) OR yields longer connection setup times that tend to improve for more loaded traffic scenarios, (b) MP leads to higher blocking ratios than OR that makes optimal impairment-aware decisions.

## Results

Thanks to the modular design of the centralized NPOT, the MP QoT-aware engine was replaced in the test-bed with the OR engine in order to evaluate and compare OR to the MP algorithm. The 14-node experimental test-bed represented the same topology as the nation-wide backbone network of Deutsche Telekom (DT) (Appendix A.1 Deutsche Telekom's Backbone Network). The DT topology consists of 46 unidirectional links and it was assumed that each link is able to carry 10 optical channels. The offered traffic was generated by uniformly distributed connection requests to all network nodes following a Poisson process. The load was determined by assuming connection holding times (HTs) exponentially distributed with mean 600s and by decreasing the connection inter-arrival times (load=HT/IAT). The resulting load ranged from 50-90 Erlangs with a step of 10. Both algorithms used the Q-tool QoT estimator.

Recognizing the importance of setup time in the online dynamic connection provisioning process, we measured the time it takes for a connection to get served and established at each of the aforementioned scenarios. In particular Figure 3-7 (a) shows the setup time averaged over the 10K connections for both algorithms and includes the delay of the IA-RWA routing and QoT estimations as well as the signalling that takes place by the control plane, following the successful lightpath computation. In case of unacceptable QoT or lack of resources a demand gets blocked. For reasons of completeness we also computed the resulting blocking ratio of the two algorithms (Figure 3-7 (b)).

As shown in Figure 3-7 (b), OR outperforms MP in all traffic scenarios, yielding a blocking ratio lower than 3% for 90 Erlangs. Apparently, OR takes full advantage of the QoT information and manages to make optimal impairment-aware decisions. Nonetheless its benefit is counterbalanced by its performance in terms of time. Figure 3-7 (a) shows that OR requires more than twice the time of MP to serve and establish a lightpath for traffic load of 50 Erlangs. MP makes faster decisions that in the case of the lower traffic assumed (50 Erlang) is also coupled by low blocking ratio that may be further improved with better selection of the weights of the impairment-generating sources. As the load increases though, OR demonstrates improved setup times, almost reaching the setup time of MP for 90 Erlangs. As mentioned before, OR selects a lightpath among the set of all possible lightpaths, on the grounds of QoT. As the load increases more network resources are occupied, leading to less possible candidate lightpaths and therefore less QoT estimations. As a consequence the execution time shortens resulting in improved setup delays.

## 3.7. Chapter Summary

This chapter summarizes the work performed on the introduction of physical-layer awareness in dynamic single line-rate networks. The main outcome of this work has been the design and development of a physical-layer performance estimating tool responsible for fast and accurate QoT assessments in single line-rate WDM networks employing 10 Gb/s OOK systems. In the impairment-modelling process the physical effects that impose the most severe degradations were identified including CD, FC, PMD, ASE, SPM, XPM and FWM. The development approach that was followed combined analytical models and numerical simulations and the outcome of both was combined in a single figure of merit, the Q-factor formula. The Q-tool was developed so as to serve with the invaluable physical-layer awareness the various modules of a dynamic single line-rate network both at the planning and operation phases. It finds multiple applications in offline RWA, monitor placement,

regenerator placement, online RWA, failure handling and interacts with the control plane so as to enable the vision of the multi-plane impairment-aware core network.

In addition this work demonstrated the significance of the physical-layer awareness and the role of Q-tool in the online routing strategy in a control plane experimental configuration. Focusing on the performance of the IA-RWA algorithms inside an operational network, two such algorithms were compared, namely MP and OR, in a 14-node experimental test-bed using a centralized impairment-enabled control plane, under the same network and traffic conditions. On the whole the results indicated that the IA-RWA algorithms make optimum impairment-aware decisions at the expense of higher lightpath setup time. In terms of the lightpath setup time MP performed in general better in the considered scenarios. On the other hand, OR demonstrated lower blocking ratios and higher setup times that tend to improve as the traffic load increases. Indeed for the scenario with the highest traffic load considered (i.e. 90 Erlangs), OR seems to be a suitable choice as it prevents unnecessary blocked connections keeping setup times comparable to MP.

### 3.8. References

- [1] J.D. Downie, I. Tomkos, N. Antoniadis, and A. Boskovic, "Effects of Filter Concatenation for Directly Modulated Transmission Lasers at 2.5 and 10 Gb/s", *Journal of Lightwave Technology*, Vol. 20, No. 2, February 2002.
- [2] G. P. Agrawal, "Fibre-Optic Communication Systems", Third Edition, Wiley-interscience, 2002.
- [3] C.D. Cantrell, "Transparent optical metropolitan-area networks," *LEOS 2003, 16th Annual Meeting*, Vol: 2, pp. 608-609.
- [4] V.T. Cartaxo, "Cross-Phase Modulation in Intensity Modulation-Direct Detection WDM Systems with Multiple Optical Amplifiers and Dispersion Compensators", *Journal of Lightwave Technology*, 17, 178-190 (1999).
- [5] S. Pachnicke, J. Reichert, S. Spalter, and E. Voges, "Fast analytical assessment of the Signal Quality in Transparent Optical Networks", *J. of Lightwave Technology*, Vol. 24, No.2, Feb. 2006.
- [6] W. Zeiler, F. Di Pasquale, P. Bayvel, and J.E. Midwinter, "Modelling of four-wave mixing and gain peaking in amplified WDM optical communication systems and networks," *Journal of Lightwave Technology*, vol. 14, no. 9, pp. 1933-1996, Sep. 1996.
- [7] K. Inoue, K. Nakanishi, K. Oda, "Crosstalk and Power Penalty Due to Fibre Four-Wave Mixing in Multichannels Transmissions", *J. of Lightwave Technology*, Vol. 12, no. 8 pp.1423-1.
- [8] S. Pachnicke, J. Reichert, S. Spalter, and E. Voges, "Fast analytical assessment of the Signal Quality in Transparent Optical Networks", *J. of Lightwave Technology*, Vol. 24, No.2, Feb. 2006.
- [9] Oleg V. Sinkin, Ronald Holzlöhner, John Zweck, and Curtis R. Menyuk, "Optimization of the Split-Step Fourier Method in Modeling Optical-Fiber Communications Systems," *J. Lightwave Technol.* 21, 61- (2003)
- [10] J. Leibrich; W. Rosenkranz, "Efficient numerical simulation of multichannel WDM transmission systems limited by XPM," *IEEE Photon. Technol. Lett.*, Vol. 15, Iss. 3, pp.395-397, March 2003.
- [11] S. Pachnicke, T. Paschenda, and P. Krummrich "Assessment of a constraint-based routing algorithm for translucent 10 Gbits/s DWDM networks considering fibre nonlinearities", *Journal of Optical Networking*, Vol. 7, No. 4, April 2008.
- [12] R. Cardillo, V. Curri, and M. Mellia, "Considering Transmission Impairments in Configuring Wavelength Routed Optical Networks", in *Proceedings of OFC/NFOEC 2006*, paper OFG6.
- [13] B. Ramamurthy, D. Datta, H. Feng, J.P. Heritage, and B. Mukherjee "Impact of Transmission Impairments on the Teletraffic Performance of Wavelength-Routed Optical Networks" *J. of Lightwave Technol.*, vol. 17, no 10, October 1999.
- [14] Yong Ouyang, Qingji Zeng, and Wei Wei, "Dynamic lightpath provisioning with signal quality guarantees in survivable translucent optical networks," *Opt. Express* 13, 10457-10468 (2005).
- [15] R. Cardillo, V. Curri, M. Mellia, "Considering transmission impairments in wavelength routed networks," in *Proceedings of ONDM 2005*, pp. 421- 429, Milan, Italy, Feb. 2005.



- [16]Mingchia Wu and Winston I. Way, "Fiber Nonlinearity Limitations in Ultra-Dense WDM Systems," J. Lightwave Technol. 22, 1483- (2004).
- [17]H. Thiele, R. I. Killey, and P. Bayvel, "Simple technique to determine cross-phase modulation induced penalties in WDM transmission," in Optical Fiber Communication Conference, OSA Technical Digest Series (Optical Society of America, 2000), paper ThM2.
- [18]S. Ten, K. Ennsner, J. Grochocinski, S. Burtsev and V. da Silva, "Comparison of four-wave mixing and cross-phase modulation penalties in dense WDM systems", in Proc. Optical Fiber Communication Conf. and Int. Conf. Integrated Optics and Optical Fiber Communication (OFC/IOOC), vol. 3, San Diego, CA, Feb. 21-26 1999, pp. 43-45.
- [19]S. Pachnicke, E. De Man, S. Spalter, and E. Voges, "Impact of the in-line dispersion compensation map on four-wave mixing (FWM)-impaired optical networks," IEEE Photon. Technol. Lett., 17, 235-237, Jan. 2005.
- [20]C. D. Poole, R. W. Tkach, A. R. Chraplyvy, and D. A. Fishman, "Fading in Lightwave Systems Due to Polarization-Mode Dispersion", IEEE Photon. Technol. Lett., 3, 68-70 (1991).
- [21]H. Taga, M. Suzuki and Y. Namihira, "Polarisation Mode Dispersion Tolerance of 10 Gbit/s NRZ and RZ Optical Signals", Electronics Letters 34, 2098-2100 (1998).
- [22]Y. R. Zhou, A. Lord, S. Santoni, D. Setti, T. Fischer, G. Lehmann, H. Bulow, H. Haunstein, and A. Schinabeck, "PMD Rules for Physical Constraint-Based Routing in All Optical Networks," in Proceeding of OFC 2006, paper JThB17.
- [23]S. Azodolmolky, J. Perelló, **M. Angelou**, F. Agraz, L. Velasco , S. Spadaro, Y. Pointurier, A. Francescon, C. Vijaya Saradhi, P. Kokkinos, E. Varvarigos , S. Al Zahr, M. Gagnaire, M. Gunkel, D. Klondis, and I. Tomkos, "Experimental Demonstration of an Impairment Aware Network Planning and Operation Tool for Transparent/Translucent Optical Networks," J. Lightwave Technol. 29, 439-448 (2011).
- [24]P. Kokkinos, K. Christodoulopoulos K. Manousakis, E.A. Varvarigos, "Multi-Parametric Online RWA Based on Impairment Generating Sources," Proc. of IEEE GLOBECOM 2009.
- [25]Siamak Azodolmolky Yvan Pointurier, **Marianna Angelou**, Josep Solé Pareta, and Ioannis Tomkos, "An Offline Impairment Aware RWA Algorithm with Dedicated Path Protection Consideration", in Proceedings of OFC/NFOEC 2009, paper OW11.

# Chapter 4

## 4. Optimized Monitor Placement for Accurate QoT Assessment in Core Optical Networks

In view of the rapid growth of Internet traffic, optical performance monitoring (OPM) is essential to manage effectively high-capacity, wavelength-routed optical mesh networks [1]. In such networks, degradations, which can be static or dynamic, are induced by physical-layer effects and accumulate along the lightpaths (a lightpath is the combination of a route and a wavelength) that transport the data, and potentially affect the performance of the network's physical layer performance, measured for instance through the quality of transmission (QoT) of the carried signals. It is therefore important for operators to use OPM in order to monitor their network at the physical layer and ensure that the network behaves as planned. In the past, techniques were proposed to monitor optical networks using partial information only, thereby decreasing the number of physical devices required to monitor the network [2]; however, the problem of placing these devices was not addressed. In this work, a monitor placement technique is proposed where monitor locations are chosen in order to maximize the accuracy of the monitoring scheme in the absence of full monitoring information in the network.

The applications of the estimation of signals' QoT based on (preferably) real-time measurements include lightpath provisioning, impairment mitigation, failure localization and maintenance. The continuous supervision of a network that can be dynamically reconfigured enables the concept of impairment-aware routing and wavelength assignment where online connection demands can be routed based on educated QoT-constrained decisions [3]. In addition, optical monitors allow network operators to utilize the real-time feedback for dynamic mitigation of the impairments in order to meet the service level agreements established with their customers. Monitoring information can be further utilized for precise failure isolation that leads to fast and successful re-routing of the affected traffic [4] but also for fast troubleshooting of the physical failures. In this work, the topic of OPM is considered as the mechanism to assess the quality of the optical signal for any relevant application, such as those described above.

Monitoring is hence an important field in optical networking; for this reason various monitoring techniques, driven by the establishment of a high-capacity optical transport that can be dynamically reconfigured, have been proposed during the last decade [5]-[8]. In the following, *performance* monitoring (where several physical layer impairments are combined in a single metric such as Bit Error Ratio, BER) is assimilated to the terminology of *impairment* monitoring, where dedicated hardware equipment employs advanced monitoring techniques to measure individual physical layer impairments or performance metrics such as residual Chromatic Dispersion (CD) [9]-[11], Polarization Mode Dispersion (PMD) [12], [13] or Optical Signal-to-Noise Ratio (OSNR) [14]-[16]. The proposed algorithms apply to both performance and impairment monitoring.

A monitoring scheme generally consists in two phases. In a first phase, during network planning, locations where monitoring devices are to be placed are chosen, using a *monitor placement algorithm*. This is the topic of this work. Then, in a second phase, during network operation, the data from those monitors is collected in order to assess the performance of the network through some estimation framework. This second phase is out of the scope of this work, which assumes that such an estimation framework is given. Specifically, the “network kriging” framework is used to perform the monitoring step itself [17]. The network kriging framework enables the estimation of the end-to-end metrics for all established lightpaths, given that only a subset of those are monitored, under some assumptions which are discussed further in this chapter.

Placing an impairment monitor at the end of an optical lightpath feeds the network management system with an end-to-end real-time measurement of the monitored impairment. However placing a physical monitoring device at the receiver end of every link in the network is costly. Although network operators have to deploy optical monitors to ensure uninterrupted network operation, they also seek for cost-effective deployment strategies that can maximize the benefit of their investment. As mentioned above, many works have dealt with impairment and performance monitoring, however, few studied the optimal *placement* of the monitoring equipment in view of QoT monitoring.

In fact, all monitor placement techniques focused on a single application: failure localization [18]-[22], where the smallest set (preferably reduced to a single network element) of possible locations of a failure needs to be determined using the minimum amount of monitoring equipment. This chapter presents a placement algorithm that is more generic; it applies to QoT metrics which are continuous, while protection-oriented placement algorithms that target minimization problems are restricted to cases where metrics are integers or binary (a component has either failed or not failed). One notable exception is [17] where a placement algorithm is proposed in the context of IP network monitoring. That algorithm is compared further with the proposed algorithm.

The placement technique proposed herein and referred to as Pseudo-Monitoring (PM), exploits the feedback received by only a small set of monitors that allows, nonetheless, estimating accurately the corresponding end-to-end metric of the lightpaths that are not monitored.

The performance of the placement algorithm is evaluated for network topologies of various scales and is compared to other placement methods. In addition, extensive simulations were performed to investigate the proximity of the PM solutions to the optimum. The algorithm was tested under static and incremental traffic conditions.

The chapter is organized as follows: the network model, notations and problem statement are given in section 4.1. The proposed PM placement algorithm, along with a simpler heuristic and the QR placement algorithm from [17] are described in 4.2. Section 4.3 discusses the optimization capability of the proposed algorithm and presents the results from the application of all the considered placement methods in core networks of small (e.g. nation-wide) and large (e.g. pan-European) scales; it focuses on the static case where a demand traffic is given. Section 4.4 tackles the dynamic case, where the network traffic increases. Finally section 4.5 concludes this chapter.

## 4.1. Modelling and Problem Formulation

### Notations

When planning a network it is critical to allocate the available resources in a cost-effective manner. Therefore in the context of monitor deployment, the goal is to be able to monitor

the entire network with a limited number of devices. As shown in [2], there exists a trade-off between the number of deployed monitors and the overall monitoring accuracy achieved in the network. However in [2] the problem of optimal monitor placement, that is, selecting the locations for a given number of monitors such that the network monitoring accuracy is maximized, was not tackled. This is the problem tackled in this work, and we introduce the formalism to solve it in this section.

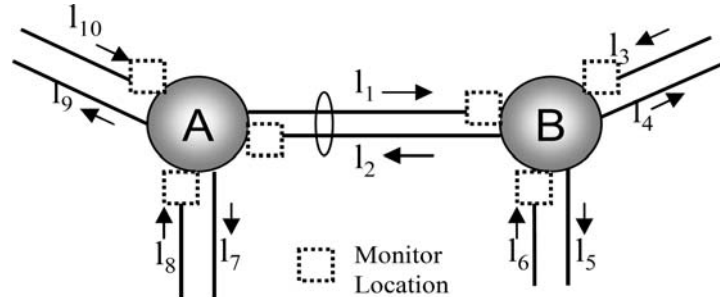


**Figure 4-1:** Two nodes with nodal degree of 3 are connected with a pair of unidirectional links. Monitors may be placed at the drop points of the nodes, yielding 6 possible monitor locations.

The monitor placement technique that we propose here applies to mesh WDM networks without wavelength conversion, however adaptation of the technique to networks with wavelength converters is straightforward as will be seen in section 4.3. Consider a network graph  $G(V,E)$  with a set of nodes  $V$  (e.g., optical crossconnects or OXC) and a set of unidirectional links  $E$ .

To measure the end-to-end performance metric or impairment (e.g., OSNR, CD or PMD) of a lightpath, a dedicated monitoring device has to be placed at the receiver end of that lightpath. It is assumed here that a monitor can only be placed at the drop ports of a node or, in other words, at the termination point (drop port) of a link, as shown in Figure 4-1. Each of these monitors collects measurements for all the channels that are dropped at this link. Consequently there are  $|E|$  potential monitor locations; every node can be equipped with at most a number of monitoring devices equal to the node degree.

Assume that  $L$  lightpaths are established in the network.  $R \in \{0,1\}^{L \times |E|}$  denotes the routing matrix corresponding to those lightpaths, where  $R(i,j)=1$  if lightpath  $i$  uses link  $j$  and  $R(i,j)=0$  otherwise. Denote by  $y \in \mathbb{R}^L$  an end-to-end metric related to the QoT of a lightpath that accumulates linearly along a lightpath. Examples of metrics that behave in this fashion are given in subsection “Modeling of the physical layer” below. Column-vector  $y$  contains the end-to-end metric for each established lightpath. Some of those lightpaths are monitored, and the others are not monitored.

Without loss of generality, the rows of  $R$  and the elements of  $y$  are reordered so as  $R = \begin{bmatrix} R_{mon}^T & R_{nmon}^T \end{bmatrix}^T$  and  $y = \begin{bmatrix} y_{mon}^T & y_{nmon}^T \end{bmatrix}^T$ , where  $R_{mon}$  and  $R_{nmon}$  describe the lightpaths that are monitored and not monitored, respectively, and  $y_{mon}$  and  $y_{nmon}$  contain the metrics for the lightpaths that are monitored and not monitored, respectively.

### Estimation Framework

Having partial information about a link-additive impairment from monitors located throughout a network it is possible to use a linear estimator to derive the impact of the impairment even for the lightpaths that are not monitored (Figure 4-2). This work utilizes

the so called “Network Kriging” (NK) [17] estimation framework that essentially leverages the correlation between lightpaths that share links. In the NK framework the network traffic is abstracted through the routing matrix  $R$ . The accuracy of the estimates is assessed through the  $\ell_2$  norm: the network kriging estimator is the linear estimator that maximizes monitoring accuracy, i.e., it returns the vector  $\hat{y}_{nmon}$  with minimum  $\ell_2$  norm, given the routing matrix  $R = [R_{mon}^T, R_{nmon}^T]^T$  and the monitored data  $y_{mon}$ . The closed form for this estimate is [17]:

$$\hat{y}_{nmon} = R_{nmon} R_{mon} (R_{nmon} R_{mon}^T)^+ y_{mon} \quad (1)$$

where  $(\cdot)^+$  denotes a matrix pseudo-inverse such as the Moore-Penrose inverse.

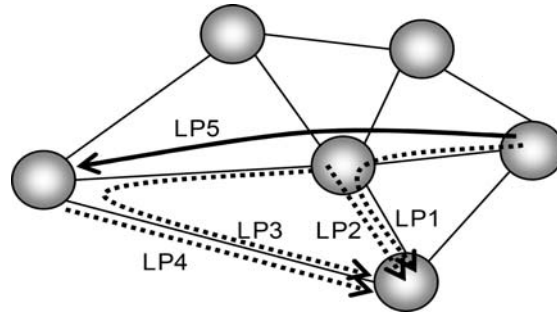


**Figure 4-2:** It is possible to use monitoring measurements collected from a subset of all the network lightpaths (LP1, LP2, LP3, LP4) to estimate accurately the corresponding end-to-end metric (e.g. OSNR) of a lightpath that is not monitored (LP5) using the “network kriging” estimation framework [2], [17], [23]. Placing monitoring devices at the termination points of LP1, LP2, LP3 and LP4 would allow the operator to also estimate the QoT of LP5 using only partial network information.

### Problem formulation

Assume that we are given only  $m \leq |E|$  monitors to install in a network, where lightpaths are routed according to  $R$ . Then it is not possible to monitor every lightpath in the network and the QoT of non-monitored lightpath must be estimated with the estimation framework described in the previous subsection (Estimation Framework). Let  $\mathcal{E}_m$  be the set of all subsets of  $E$  of size  $m$  ( $\forall F \in \mathcal{E}_m : F \subset E$  and  $|F| = m$ ).  $\mathcal{E}_m$  represents the set of all possible monitor placements (placement of  $m$  monitors). Each monitor placement (a set of  $m$  locations) determines exactly  $R_{mon}, R_{nmon}, y_{mon}$  and  $y_{nmon}$ , and hence  $\hat{y}_{nmon}$ .

In other words, the mapping  $f$  such that  $\hat{y}_{nmon} = f(F)$  where  $F \in \mathcal{E}_m$  is well-defined.

The network monitoring accuracy is defined as the  $\ell_2$  norm of the difference between the actual values of the QoT metrics of interest and the estimated QoT metrics, normalized by the  $\ell_2$  norm of the actual values of the QoT metrics of interest. Hence, if we monitor some metric with actual values  $y$  given a routing matrix  $R$ , monitor placement  $M$ , and unmonitored locations  $P$ , and if we let  $\hat{y} = [y_{mon}^T, y_{nmon}^T]^T$  (note that  $y_{mon}$  and  $\hat{y}_{nmon}$  are functions of  $R, M$  and  $P$ ), then the accuracy of the monitoring scheme is  $rRMSE(R, M, P) = \|y - \hat{y}\| / \|y\|$ , where  $\|\cdot\|$  denotes the  $\ell_2$  norm. Note that the accuracy  $rRMSE(R, M, P)$  is effectively the

relative root mean square error of the QoT metric of interest. Hence the problem of monitor placement is: find the optimal placement  $F^* \in \mathcal{E}_m$  such that

$$F^* = \arg \min_{\mathcal{E}_m} \frac{\|y - \hat{y}\|}{\|y\|} \quad (2)$$

An exhaustive search to find  $F^*$  is very computationally expensive since  $|\mathcal{E}_m| = \binom{|E|}{m}$ ,

and heuristics are needed to solve (2). Before presenting heuristic algorithms that solve (2), more details on the physical layer model are given in what follows.

### Modeling of the physical layer

In this study a mesh network topology is considered to be traversed by a number of pre-planned transparent lightpaths. Cascades of EDFAs between spans of transmission and dispersion compensating fiber segments form typical WDM links. The physical layer impairments that are considered here are link-additive over a path, meaning that the end-to-end parameter that corresponds to the entire lightpath can be computed by adding the link-level parameters of the impairment in question. In addition it is assumed that there are hardware devices that can effectively measure each of these impairments; the optimized placement of these devices is the goal of this work. Examples of parameters that measure those impairments are i) OSNR, ii) PMD, iii) residual CD and iv) nonlinear phase [24]. Using a combination of those 4 impairments, it is possible to compute the signal's BER in intensity-modulated (non-coherent) systems [25]. More details on the link-additivity property of those parameters can be found in [23].

For the remainder of the chapter a generic impairment that accumulates additively is considered, yet in the scenarios simulated in sections 4.3 and 4.4 OSNR monitoring has been assumed as the targeted application.

## 4.2. Monitor Placement Algorithms

Hereafter 3 heuristics that solve problem (2) are described. The first algorithm (proposed in this work) is called "Pseudo-Monitoring" (PM) and greedily removes monitors (starting from a situation where each link is equipped with a monitor) to iteratively minimize the estimation error for the lightpaths that are not equipped with monitors. The second algorithm (also developed for the purposes of this work), called "Busy Link" (BL), is a simplification of the first heuristic, which is used to demonstrate that the complications of the PM algorithm are indeed needed to achieve good performance. The third algorithm, called QR, was proposed in [17].

### The pseudo-monitoring (PM) heuristic

The algorithm (Table 4-1) is a greedy heuristic that starts by assuming that all monitoring locations are equipped and sequentially removes the monitors that contribute the least with their measurements to the estimation process (NK). The algorithm relies on the notion of "busy link": the "busyness" of a link is the number of connections that are terminated at this link. The busier a link, the more connections can be monitored by this link, and hence the more information a monitor located at this link can gather about the network. Note that it is not only the amount of information about the network that we can collect which matters, but also how the information collected by several monitors can be correlated.

Hence, it is not always a good strategy to select the busiest links as monitor locations, as will be shown in section 4.3. Given this, the proposed PM algorithm consists of 3 phases.

**Table 4-1:** Pseudo-Monitoring (PM) monitor placement algorithm

<b>Input:</b> graph $G$ , links $E$ , lightpaths $R$ , desired number of monitors $m$ , accuracy threshold $\epsilon$
<b>Output:</b> $M \subset E$ : hardware monitor locations, $PM \subset E$ : pseudo-monitor locations.
1) Using $E$ and $R$ : let $B$ be the sorted list of links in ascending busyness. 2) $M = B$ ; $PM = \{\}$ ; $c=0$ ; 3) <b>for</b> $j \in B$ (from least to most busy link) 4) $M' = M \setminus \{j\}$ ; $PM' = B \cup \{M'\}$ ; 5) $c = rRMSE(R, M', PM')$ ; 6) <b>if</b> $c \leq \epsilon$ ; $M = M'$ ; $PM = PM'$ ; <b>end if</b> 7) <b>if</b> $ M  = m$ ; <b>return</b> ; <b>end if</b> 8) <b>end for</b> 9) <b>for</b> $j \in M$ 10) $cost(j) = rRMSE(R, M \setminus \{j\}, B \cup \{M'\})$ ; 11) <b>end for</b> 12) Rank $cost(.)$ in descending order to place monitors on the $ M  - m$ locations with lowest $cost$ .

In a first phase (Table 4-1, line 1), or “pre-processing phase”, the links are sorted by ascending busyness. All links are fitted with monitors (line 2).

Then, in a second phase (lines 3-8), the list of links is scanned (line 3) and, for each link in the list, we tentatively remove the monitor installed at this link (line 4): an end-to-end metric for any lightpath terminated at this link would need to be estimated rather than monitored. The impact of removing the monitor from this location on the monitoring accuracy is evaluated as follows. The overall network monitoring accuracy metric  $rRMSE(R, M, P)$  is defined as in section 4.2 (Problem Formulation) for the network defined by the routing matrix  $R$ , monitor locations  $M$  and un-monitored locations  $P$ .

At network planning time, physical measurements of a number of metrics such as OSNR are not available, as real deployment of monitors would be required to obtain that data. Instead, realizing that the NK estimator can be used on any link-additive metric, lightpaths and link physical lengths (the total length of a lightpath is the sum of the lengths of the links of this lightpath) are used to compute the  $rRMSE(R, M, P)$  figure of merit. If this metric is smaller than a predefined accuracy threshold  $\epsilon$  then it is possible to replace the physical monitor with an estimate, and the selected location is removed for good from the list (line 6). The process repeats until only  $m$  monitors are left, or when there is no more links to assess (line 7).

It is possible that, after examining all links, the algorithm has not been able to remove enough locations from the list and that  $|M| > m$  locations are retained. In this case, the third phase starts in order to remove the extra  $|M| - m$  monitors. In this phase (lines 9-12), for each remaining possible link/monitor location, the rRMSE metric is evaluated assuming that the considered link is not fitted with a monitor (lines 9-11). This list of rRMSE is ordered in descending order and links corresponding to the  $|M| - m$  highest rRMSE metrics are selected as additional monitor locations (line 12).

Note that any link-additive metric can be used in the planning phase to determine monitor placement, since the network kriging estimator relies on the link-additivity property. The performance of the estimator during the operation phase depends on the

monitor placement and hence on the metric used during planning. Link length is a suitable metric because many impairments grow (although not necessarily proportionally) with transmission distance, and hence link length gives a good indication of the intensity of the impairments sustained by a signal propagated within a link. It is possible to use other metrics than link length in the planning phase, however, the problem of choosing and comparing the choices for such a metric is outside the scope of this work; in addition, in section 4.3 it is discussed that the chosen metric yields relatively small estimation errors, such that the quest for another metric to be used in the planning phase may not yield substantial benefits.

#### The Busy Link (BL) heuristic

The busy-link heuristic is a much simplified version of the PM heuristic, which essentially consists solely of the first phase of PM. Links are sorted by ascending busyness, and the  $m$  busiest links are fitted with monitors. As indicated above the rationale for this is that busiest links tend to collect more information about the network.

#### The QR heuristic

The monitor placement problem was also tackled by the authors in [17] using an algebraic method based on QR decompositions of routing matrices (further referred to as the QR method). In [17] the authors argue that the selection of routes within  $R$  to minimize estimation errors amounts to the so-called “subset selection problem (finding the set of the rows of  $G$  such that the space spanned by those rows matches as closely as possible the space spanned by all rows of  $R$ ), which is NP-complete. A good heuristic to solve this problem consists of using a QR factorization of  $R$  with column pivoting to select the first  $m$  left singular vectors of  $R$ . The reader is referred to [17] for further details about this heuristic.

## 4.3. Numerical Results

### Performance Evaluation

To test the monitor placement methods, the algorithms are applied to three different meshed topologies (see Appendix A: Network Topologies and Table 4-2) using traffic matrices of varying load. A traffic load of 1 corresponds to the establishment of  $|V|/(|V|-1)$  lightpaths in a topology with  $V$  nodes.

The placement algorithms are evaluated using OSNR as the monitored metric. Note that OSNR is indeed link-additive through its inverse since  $OSNR_{TOT} = \left( \sum \frac{1}{OSNR_i} \right)^{-1}$  where

$OSNR_{TOT}$  is the OSNR for a lightpath and  $OSNR_i$  is the OSNR for the  $i_{th}$  hop of that lightpath; hence the estimation and placement frameworks described above apply to OSNR monitoring. To evaluate OSNR, the chain of optical amplifiers that the signal traverses along a lightpath is considered to compute the end-to-end OSNR due to the Amplified Spontaneous Emission (ASE) noise [26]. The amplifier spans are assumed to be 80 km long and the noise figure of the amplifiers is set at 6 dB. The  $\epsilon$  threshold used by the PM algorithm is set to  $10^{-9}$ .

For a given load, every traffic matrix is served by an equivalent number of lightpaths computed by a  $k$ -shortest path Routing and Wavelength Assignment (RWA) process assuming 80 wavelengths available per fiber in a single-rate WDM transmission system. For the Deutsche Telekom (DT) topology (detailed in A.1 ) that consists of 14 nodes and 46



unidirectional links, a traffic matrix of load 1 corresponds to 182 traffic demands. The demands are drawn randomly uniformly among all possible (source, destination) pairs of nodes.

**Table 4-2:** Network Topologies Specifications

Topology Name	Deutsche Telekom (DT)	Polish Telecom (TP)	GEANT2
Number of unidirectional links	46	48	104
No. of Nodes	14	14	34
Node degree	3.29 (min. 2, max. 6)	3.42 (min. 2, max. 9)	3.18 (min. 2, max.5)

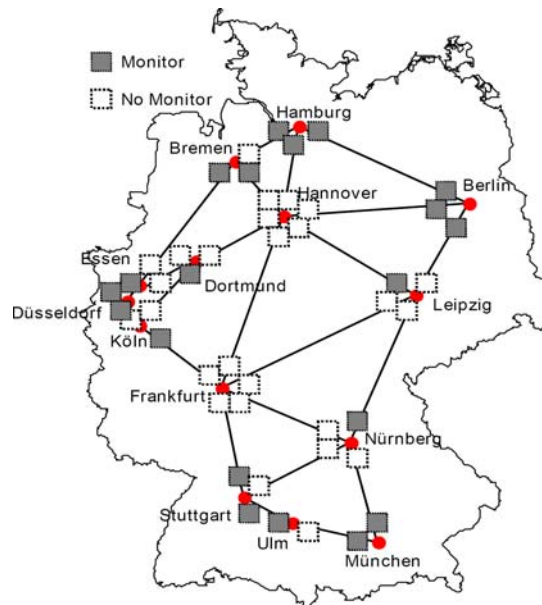


**Figure 4-3:** The Deutsche Telekom backbone network is shown with 20 monitored locations resulting from the PM placement.

Figure 4-3 illustrates the monitor placement solution returned by the PM algorithm for a certain set of lightpaths traversing the DT topology, where  $m=20$  links out of the possible 46 locations are equipped with monitors. Using a random traffic generator, 50 different traffic matrices all corresponding to load equal to 2 are fed as input to PM, QR and Busy Link monitor placement algorithms for the same topology (DT). The three algorithms along with a random placement method are tested for a range of available monitors from 5 to 35 (Figure 4-4). To compare their performance the mean rRMSE of all 50 traffic matrices are reported, along with error bars corresponding to one standard deviation around the mean relative RMSE. Particularly for the random placement each of the 50 traffic matrices 50 random solutions were generated (i.e. mean rRMSE from a total of 2500 solutions) for each case of available monitors; the lower the rRMSE the more powerful the placement solution. PM outperforms the other techniques for the entire range of available monitors as its solutions yield the highest estimation accuracy (lowest mean rRMSE). Indeed it is observed that 15 locations out of the total 46 are only required to be equipped if the target OSNR estimation accuracy is 1%.

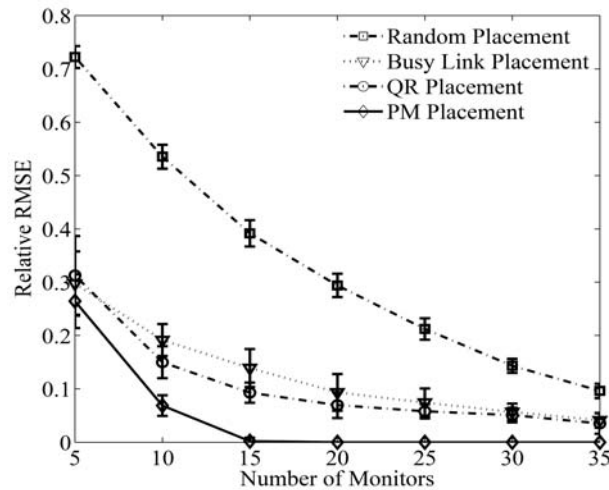


**Figure 4-4:** Comparison of the placement techniques for the Deutsche Telekom (DT) network. The averaged relative root mean square error was computed for all placements methods applied in the DT backbone network for traffic load equal to 2, i.e. 2 connections on average per pair of nodes. With the PM heuristic, 15 monitors out of the possible 46 locations are enough to yield an estimation error for OSNR below 1%.

Estimation as done by the kriging framework is facilitated when the energy of the unobserved lightpaths, when projected onto the subspace spanned by the observed lightpaths, is small [2]. Indeed such small energy means that the observed lightpaths capture most of the information regarding the unobserved lightpaths. In Figure 4-5, the average fraction of the energy (“energy ratio”) of the unobserved lightpaths that lies in the space spanned by the observed lightpaths for each placement algorithm and for the DT topology with a load of 2 is depicted. This fraction increases with the number of monitors (and hence of observed lightpaths, and of the captured information about the unobserved lightpaths) for the proposed PM placement algorithm. The energy ratio is significantly larger for PM than for the other considered algorithms. The energy ratio decrease that is observed for the busy link and the QR algorithms for 20 to 25 (QR) or 40 (busy link) monitors may seem counter-intuitive, but can be explained like this: although with a large number of monitors few lightpaths are unobserved, little is known about them through the observed lightpaths. This is to be contrasted with PM, which gradually collects information about all lightpaths as more monitors are deployed.

#### Gap to Optimality

Having compared PM with the other methods, extensive simulations (i.e., an exhaustive search across the full solution space) are run to investigate how close PM is from the optimum placement solution. For a given topology the total number of possible placement solutions is calculated by  $|\mathcal{E}_m| = \binom{|E|}{m}$ , where  $E$  is the set of unidirectional links and  $m$  the

number of monitors to be deployed. Consider for instance the DT topology  $|E|=46$  and  $m=5$  available monitors; the total possible solutions sum up to 1370754. The number becomes prohibitively large for  $m>5$ . Hence this effort is inevitably constrained by the required processing time and is limited to the optimum solutions for  $m=1,2,\dots,5$ . Obviously an operator would not install only 1 or even 5 monitors in their network as this would not allow accurate performance estimations; this range was merely selected to demonstrate the performance of PM compared to the optimum when possible.

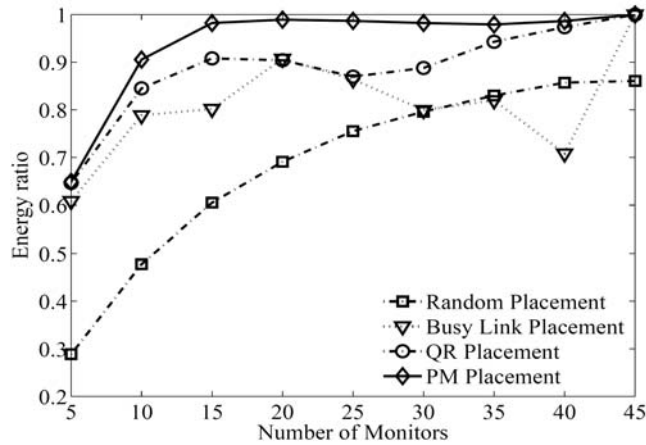


**Figure 4-5:** Fraction of the energy (“energy ratio”) of the unobserved lightpaths that lies in the space spanned by the observed lightpaths for the DT Topology with a load of 2. The energy ratio is higher when more information about the unobserved lightpaths through the observation of other lightpaths with the deployed monitors.

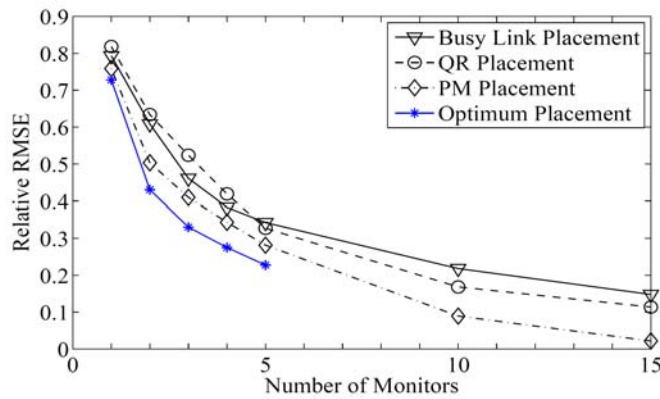


**Figure 4-6:** Comparison of optimum solutions against the solutions retrieved by the 3 heuristics for the DT topology; the resulting error is the average of 50 randomly generated traffic matrices of load equal to 1.

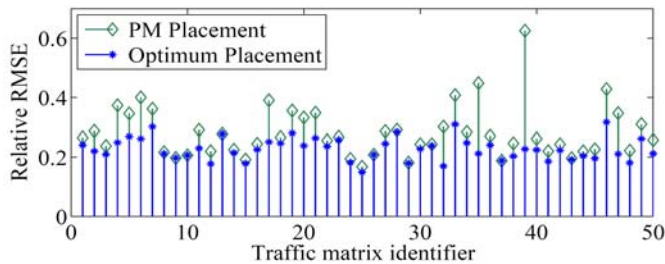


**Figure 4-7:** PM and optimum relative RMSE error results for each of the 50 traffic matrices, when 5 monitored locations are assumed.

All the possible placement solutions for  $m=1,2,\dots,5$  were enumerated and evaluated using the NK estimation framework for a set of 50 different traffic matrices of load equal to 1. The optimum solution, i.e. the one with the lowest relative error, was retrieved and compared to the corresponding solutions of PM, QR and Busy Link as depicted in Figure 4-6. Taking into account the sequential nature of the heuristic and noticing the rapid decrease of the relative error of the PM solutions with the increasing number of monitors in the various

network topologies, we observe that  $m=5$  monitors (over  $|E|=46$  locations in total) is a small number for PM to display its capabilities. Nonetheless based on the simulation results, the PM algorithm approaches the optimum solution within 5% (in terms of relative RMSE gap) for the case of 5 monitors.

Figure 4-7 depicts the raw RMSE for both the optimum and the PM algorithm for every considered input traffic matrix for  $m=5$ ; except for a small number of traffic matrices, the gap between PM and the optimal solution is fairly uniform across all the tested traffic matrices.

### Scalability of the monitor placement methods with network size

The optimized monitor placement is subjected to another meshed topology of the same scale as DT, yet with different connectivity characteristics. The goal of this experiment is to investigate the locations the proposed monitor placement selects in a commercial topology that is not evenly meshed, i.e., a topology where nodal degree is highly spread. It is expected that a topology with nodes that are not well-connected would require more monitored locations to achieve acceptable accuracy.

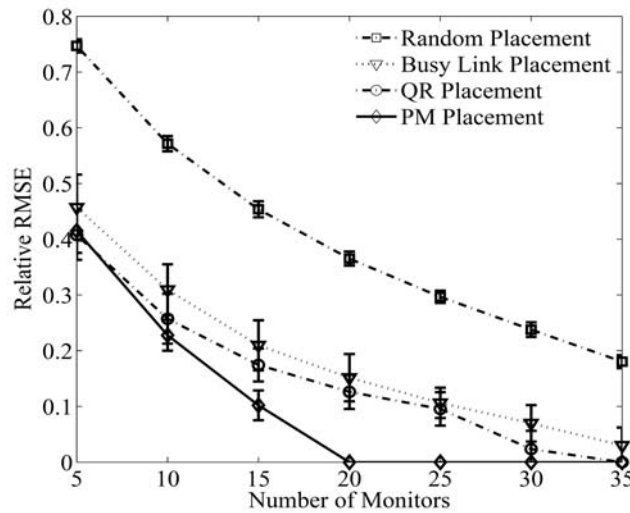


**Figure 4-8:** Averaged relative RMSE of all placements methods applied on the Polish Telecom topology. The traffic load is equal to 2.

The selected topology is the Polish Telecom backbone network (further denoted as TP) that consists of 14 nodes and 48 unidirectional links. TP topology (presented in Appendix A: Network Topologies) unlike the DT topology, has one highly connected node (Warsaw; degree 9) and several nodes with degree 2. As with the DT topology, PM, QR, Busy Link and the random selection of locations are evaluated through the relative RMSE with respect to the variable number of monitors. The results are averaged over 50 different randomly generated traffic matrices of load equal to 2, corresponding to 364 lightpaths. As shown in Figure 4-8, PM demonstrates a relatively high estimation error for low number of monitors (errors higher than with the DT topology), that, nevertheless, improves fast with additional monitored locations. With  $m=20$  monitors out of a possible  $|E|=48$  locations the accuracy is better than 1% with PM while it is still above 10% with the other techniques. The other algorithms require more than 30 monitors to achieve the same level (1%) of accuracy.

Focusing on the PM and QR techniques, the experiments for the TP topology are extended for traffic scenarios with load from 1 up to 3 in order to investigate the dependence of the monitor placement techniques on the induced traffic load. As illustrated

in Figure 4-9, PM experiences the same sharp decrease of the relative error at every monitor addition step that converges to <1% for  $m \geq 20$  monitors regardless of the traffic load. What is more, the estimation accuracy of PM and QR (the two techniques that perform best in terms of accuracy) are not affected by the increasing traffic (Figure 4-9 and Figure 4-10).

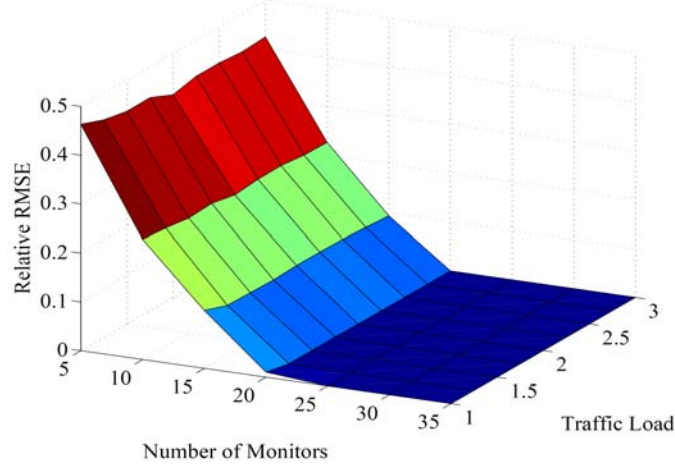


**Figure 4-9:** Relative RMSE for the PM monitor placement method with respect to the number of available monitors and increasing traffic load in the TP topology. PM is not affected by the traffic load and achieves estimation error below 1% for  $m = 20$  deployed monitors.

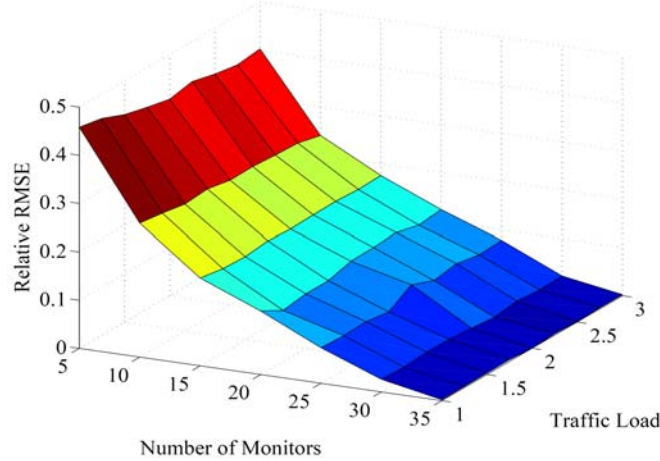


**Figure 4-10:** Relative RMSE for the QR monitor placement method with respect to the number of available monitors and increasing traffic load in the TP topology.

Having universal supervision of the network status with limited amount of physical resources becomes particularly important when considering large scale networks that may span a continent. Therefore, in addition to the standard nation-wide topologies, the optimization capability of the placement techniques is also tested in a topology of larger scale, i.e. GEANT2 (see Appendix A: Network Topologies). GEANT2 is by nature a translucent network, meaning that at least sparse regeneration of the optical signal may be required to ensure transmission with acceptable QoT. In this experiment no regeneration is assumed. The goal of this exercise is to focus on the scalability of the algorithms; besides the monitor placement techniques employed in this work do not depend on the physical lengths of the links. Note though that in the presence of regenerators the PM and QR algorithms could be adapted in the following simple fashion: consider a regenerator placed at an intermediate node of a lightpath. In the routing matrix  $R$  this lightpath is replaced by two lightpaths one being the segment of the original lightpath from the source node to the regenerator

location and the second from the regenerator to the termination point. In this way this lightpath contributes with physical information both from the regenerated and the non-regenerated parts.

In the GEANT2 topology, 34 nodes are interconnected with 104 unidirectional links. The same transmission and link design parameters as in the smaller topologies are used. Again 50 different traffic matrices are generated randomly for traffic load of 0.5 and 1, corresponding to 561 and 1122 lightpaths, respectively. The solutions retrieved by the algorithms are evaluated through their estimation accuracy (relative RMSE). As depicted in Figure 4-11 and Figure 4-12, PM performs significantly better than the other techniques for both traffic scenarios, demonstrating the same sharp decrease in estimation error, reaching a relative error of less than 1% for as few as 25 monitors (for load equal to 1) out of total 104 possible locations.

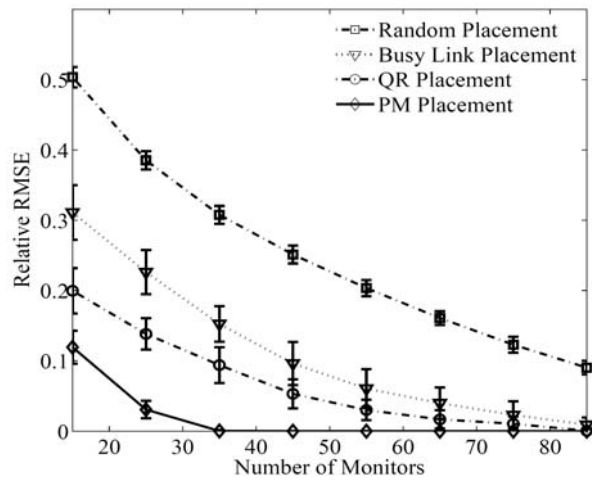


Figure 4-11: Averaged relative root mean square error of all placements methods applied on the GEANT2 topology (load 0.5).

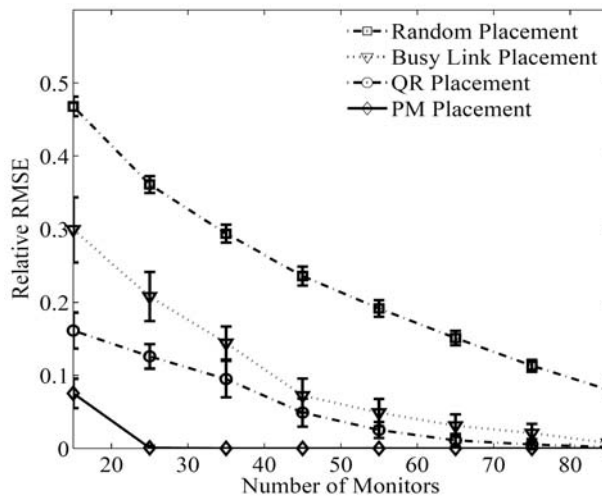
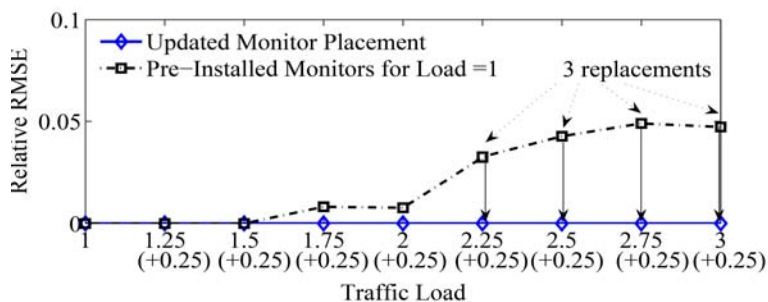


Figure 4-12: Averaged relative root mean square error of all placements methods applied on the GEANT2 topology (load 1). PM achieves estimation error below 1% for  $m = 25$  monitored locations out of 104 available.

## 4.4. Monitor Placement in the presence of Dynamic Traffic

So far the performance of the proposed monitor placement algorithm (PM) when a static set of lightpaths is established in the network, has been described in depth. In a dynamic optical network, the varying traffic can potentially affect the estimation accuracy of the deployed monitors, since lightpaths' terminations may vary while the monitor locations are de facto fixed at network planning time for the hardware monitors. Consider a set of deployed monitors for a given pre-planned set of lightpaths. As traffic varies with time new connections are getting established or existing are being torn down. Under such conditions the estimation accuracy of the monitoring technique may improve provided that more lightpaths terminate at monitored locations and that the monitored lightpaths provide the NK framework with enough information to estimate the un-monitored ones. The opposite effect would occur if the fraction of the traffic that is monitored becomes decorrelated with the un-monitored traffic.

In this context several scenarios with incremental traffic are examined. The investigation of a scenario with only incremental traffic was triggered by the constant and rapid increase of the IP traffic. It is assumed that a set of lightpaths corresponding to traffic load equal to 1 are established in the DT backbone network. The PM algorithm is used to compute the locations for  $m=20$  monitors that are assumed fixed. We select 20 monitors as this is a sufficient number of monitors to accurately (error is below 1%, as mentioned in section 4.3) supervise the global network traffic for load up to 3. To the initial set of lightpaths (of total load 1) randomly generated “chunks” of traffic are added, each corresponding to a load of 0.25 (i.e. approximately 46 new lightpaths per chunk of added traffic). The additional traffic was set to 0.25 because a smaller set would not allow observing significant modifications in the estimation accuracy. Indeed several similar scenarios (for different permutations of initial and additional traffic) were examined and it was observed that as more lightpaths are added, the estimation error increases, yet not beyond 5% as shown in Figure 4-13 (dotted curve with square marks).



**Figure 4-13:** Example of monitor placement in the presence of varying incremental traffic. 20 fixed equipped locations computed by the PM algorithm for a traffic matrix of load 1 is studied as “chunks” of traffic are added to the already established lightpaths. Without installing additional monitors the estimation error becomes larger than 1% for a traffic load larger than 2. It was observed by inspection that only 3 (out of 20 possible) monitors displacements are sufficient to decrease the estimation error back to less than 1%.

Furthermore, the PM algorithm was used to compute the optimized monitor locations in every increasing step, as if the monitors were *not* fixed. As depicted in Figure 4-13 the solutions (plain curve, solitaire marks) are compared to the pre-deployed one; it was

observed by detailed comparison of the placement results that only 3 mutual replacements of monitors (i.e. removal of a monitor from a certain location and placement to another) would allow the estimation error to become approximately 0 again. In this example, when the traffic load becomes higher than 2, an operator may deem that the estimation accuracy is not acceptable. In such case, moving (not adding) only 3 monitors to new locations is sufficient to accurately estimate again the QoT of all the traffic.

## 4.5. Chapter Summary

This work leverages the correlation of the QoT of channels traversing a mesh topology and proposes a monitor placement framework that first decides the placement of the monitoring devices to few strategically selected locations during the network planning phase and enables the universal supervision of all the established connections during network operation. The proposed heuristic (PM) outperformed other monitor placement methods in terms of monitoring accuracy or, equivalently, the number of monitors needed to achieve the same level of monitoring accuracy. It was indeed shown that through the efficient placement of monitors using the PM heuristic, only a fraction of the possible locations in a mesh topology need to be equipped; in the considered topologies only 1/4 or 1/3 of the possible monitor locations actually required a physical monitoring device in order to compute the QoT of all established lightpaths within a few percents; the un-monitored lightpaths have their QoT estimated, rather than directly measured. It was also argued that the proposed technique scales well with the network size, as topologies ranging from less than 50 to more than 100 links were investigated, for various static loads.

In addition, although the problem of monitoring placement is inherently a planning issue where monitors are physical devices that cannot be moved around easily during network operation, it was also hinted that the proposed placement technique is compatible with operation scenarios where the load of the network is incremental, i.e., lightpaths are added. In this case, the monitoring accuracy is little impaired by the changes in the network load, and if an operator needs to maintain a very high monitoring accuracy even after a load increase, only a few monitors would need to be displaced, thereby reducing network OPEX compared with a situation where the monitoring scheme would change completely due to a change in the load.

## 4.6. References

- [1] D. C. Kilper, R. Bach, D. J. Blumenthal, D. Einstein, T. Landolsi, L. Ostar, M. Preiss, and A. E. Willner, "Optical performance monitoring," *J. Lightw. Technol.*, vol. 22, no. 1, pp. 294–304, Jan. 2004.
- [2] Y. Pointurier, M. Coates, and M. Rabbat, "Cross-layer monitoring in transparent optical networks," *IEEE/OSA Journal of Optical Communications and Networking*, vol. 3, pp. 189–198, Mar. 2011.
- [3] S. Azodolmolky, M. Klinkowski, E. M. Tordera, D. Careglio, J. Solé-Pareta, and I. Tomkos, "A survey on physical layer impairments aware routing and wavelength assignment algorithms in optical networks," *Elsevier Computer Networks*, vol. 53, no. 7, pp. 926–944, May 2009.
- [4] C. Mas, I. Tomkos, and O. K. Tonguz, "Failure location algorithm for transparent optical networks," *IEEE J. Sel. Areas Commun.*, vol. 23, no. 1, pp. 1508–1519, Jan. 2005.
- [5] M. Petersson, H. Sunnerud, M. Karlsson, and B.-E. Olsson, "Performance monitoring in optical networks using Stokes parameters," *IEEE Photon. Technol. Lett.*, vol. 16, no. 2, pp. 686–688, Feb. 2004.



- [6] L. Meflah, B. Thomsen, J. E. Mitchell, P. Bayvel, G. Lehmann, S. Santori, and B. Bollezn, "Advanced optical performance monitoring for dynamically reconfigurable networks," in Proc. Networks and Optical Communication (NOC), 2005.
- [7] Y. K. Liz'e, J.-Y. Yang, L. C. Christen, X. Wu, S. Nuccio, T. Wu, A. E. Willner, R. Kashyap, and F. S'eguine, "Simultaneous and independent monitoring of OSNR, chromatic and polarization mode dispersion for NRZ-OOK, DPSK and duobinary," in Proc. OFC, 2007, paper OThN2.
- [8] S. L. Woodward, "Monitors to ensure the performance of photonic networks," in Proc. OFC, 2007, paper OMM1.
- [9] Y. Ku, C. Chan, and L. Chan, "Monitors to ensure the performance of photonic networks," in Proc. OFC, 2006, paper OFN2.
- [10] X. Yi, F. Buchali, W. Chen, and W. Shieh, "Chromatic dispersion monitoring in electronic dispersion equalizers using tapped delay lines," *Optics Express*, vol. 15, no. 2, pp. 312–315, Jan. 2007.
- [11] F. N. Khan, A. P. T. Lau, C. Lu, and P. K. A. Wai, "Chromatic dispersion monitoring for multiple modulation formats and data rates using sideband optical filtering and asynchronous amplitude sampling technique," *Optics Express*, vol. 19, no. 2, pp. 1007–1015, Jan. 2011.
- [12] G.-W. Lu, M.-H. Cheung, L.-K. Chen, and C.-K. Chan, "Simultaneous PMD and OSNR monitoring by enhanced RF spectral dip analysis assisted with a local large-DGD element," *IEEE Photon. Technol. Lett.*, vol. 17, no. 12, pp. 2790–2792, Nov. 2005.
- [13] J. Yang, C. Yu, L. Cheng, Z. Li, C. Lu, A. P. T. Lau, H.-Y. Tam, and P. K. A. Wai, "CD-insensitive PMD monitoring based on RF power measurement," *Optics Express*, vol. 19, no. 2, pp. 1354–1359, Jan. 2011.
- [14] J. H. Lee, D. K. Jung, C. H. Kim, and Y. C. Chung, "OSNR monitoring technique using polarization-nulling method," *IEEE Photon. Technol. Lett.*, vol. 13, no. 1, pp. 88–90, Jan. 2001.
- [15] L. Baker-Meflah, B. Thomsen, J. Mitchell, and P. Bayvel, "Simultaneous chromatic dispersion, polarization-mode-dispersion and OSNR monitoring at 40Gbit/s," *Optics Express*, vol. 19, no. 20, pp. 15 999–16 004, Sep. 2008.
- [16] J. Schröder, O. Brasier, T. D. Vo, M. A. F. Roelens, S. Frisken, and B. J. Eggleton, "Simultaneous multi-channel OSNR monitoring with a wavelength selective switch," *Optics Express*, vol. 18, no. 21, pp. 22 299–22 304, Oct. 2010.
- [17] D. B. Chua, E. D. Kolaczyk, and M. Crovella, "Network kriging," *IEEE J. Sel. Areas Commun.*, vol. 24, no. 12, pp. 2263–2272, Dec. 2006.
- [18] S. Stanić, S. Subramaniam, H. Choi, G. Sahin, and H.-A. Choi, "On monitoring transparent optical networks," in Proc. ICPPW, 2002.
- [19] Y. G. Wen, V. Chan, and L. Z. Zheng, "Efficient fault diagnosis algorithms for all-optical WDM networks with probabilistic link failures," *J. Lightw. Technol.*, vol. 23, no. 10, pp. 3358–3371, Oct. 2005.
- [20] P. Nayek, S. Pal, B. Choudhury, A. Mukherjee, D. Saha, and M. Nasipuri, "Optimal monitor placement scheme for single fault detection in optical network," in Proc. ICTON, 2005.
- [21] C. Mas Machuca and M. Kiese, "Optimal placement of monitoring equipment in transparent optical networks," in Proc. 6th International Workshop on Design and Reliable Communication Networks (DRCN), 2007.
- [22] A. Ferguson, B. O'Sullivan, and D. Kilper, "Transparent path length optimized optical monitor placement in transparent mesh networks," in Proc. OFC, 2008, paper OThI3.
- [23] N. Sambo, Y. Pointurier, F. Cugini, L. Valcarenghi, P. Castoldi, and I. Tomkos, "Lightpath establishment assisted by offline qot estimation in transparent optical networks," *IEEE/OSA Journal of Optical Communications and Networking*, vol. 2, no. 11, pp. 928–937, Nov. 2010.
- [24] J.-C. Antona, S. Bigo, and J.-P. Faure, "Nonlinear cumulated phase as a criterion to assess performance of terrestrial WDM systems," in Proc. OFC, 2002, paper WX5.
- [25] F. Cugini, N. Sambo, N. Andriolli, A. Giorgetti, L. Valcarenghi, P. Castoldi, E. Le Rouzic, and J. Poirrier, "Enhancing GMPLS signaling protocol for encompassing quality of transmission (QoT) in all-optical networks," *J. Lightw. Technol.*, vol. 26, no. 19, pp. 3318–3328, Oct. 2008.
- [26] G. Agrawal, *Fiber-Optic Communication Systems*, 3rd ed. John Wiley & Sons Inc., 2002.

- [27] **M. Angelou**, Y. Pointurier, S. Azodolmolky, D. Careglio, S. Spadaro, and I. Tomkos, "A novel monitor placement algorithm for accurate performance monitoring in optical networks," in Proc. OFC, 2011, paper JWA53.



# Chapter 5

## 5. Resource Optimization in Dynamic Single Line-Rate Networks

When traffic in telecom networks was voice-centric, designing and planning the network was not a complicated task. Novel capacity-demanding applications though, led to an unprecedented growth of data-dominated traffic with dynamic usage patterns. In this context, telecom operators seek for a cost-effective core optical network that satisfies the new traffic conditions. During network design, operators need to employ methods that minimise the total cost of ownership and the network-related operational expenses while ensuring scalability, dynamicity and adaptation to future demands. Given that network operators have a limited budget available when planning or upgrading a network it is of utmost importance to make investments that will not require adding racks of equipment at every traffic increase.

A telecom network, regardless of its size, entails two classes of expenditures for the operators: capital expenditures (CapEx) that include the cost of all the components that comprise the network and the operational expenditures (OpEx) that correspond to the costs stemming from the power consumption of the network, housing, labour and maintenance. A typical optical core network that spans over several hundreds or thousands of kilometres utilizes at the bottom of its multilayer structure a WDM transport plane that is responsible for the signal transmission and switching from the source node to the destination. Herein the cost analysis focuses on the expenses related to the WDM layer.

From an economic point of view, in an optical core network that spans over several thousands of kilometres it is essential to have the signal travel optically [1], [2] avoiding the optical-electronic-optical (O/E/O) conversions. The cost savings of a transparent network design over an opaque network may be up to 50% [1]. The Operational Expenditures (OpEx) savings in the all-optical core networks mostly due to the minimised power needs of photonics [2], along with the Capital Expenditures (CapEx) savings stemming from the elimination of the costly optoelectronic interfaces, render transparency highly correlated with the deployment of an economically viable network. Nonetheless error free detection of the optical signal can be achieved for a finite distance, as the physical-layer impairments accumulate degrading the quality of transmission (QoT) [3], [4]. In this context fully transparent networks need to make maximum use of the optical reach as this ends up to lower blocking rates and more efficient utilization of resources.

Further to the introduction of photonic switches that effectively enabled transparency, reconfigurable optical switching components are rapidly adopted due to their inherent ability to support the dynamic traffic evolution in a flexible and most importantly economic manner [4]. Reconfigurable optical networks present a clear business case since the operators do not have to over-provision their network with equipment meant to serve future variations in traffic. In such context the tools that were developed to serve DICONET (optimization algorithms and physical performance estimator) were utilized to explore the

potential cost savings in a commercial single line-rate core network. The goal of this work was to study the resource minimization achieved by an impairment-aware (IA) networking solution under the flexibility constraints of different node architectures and showed that the IA solution achieves better resource optimization compared to an Impairment Unaware (IUA) solution without QoT considerations.

## 5.1. Node Architectures

A significant portion of a network's cost of ownership is allocated to the nodes that mesh the network and whose role is to cross-connect or add/drop the traffic that reaches the nodes. In view of these cost considerations it is vital for the operators to make educated decisions in terms of the architectures and their corresponding features in order to ensure a viable and long-term investment. While all reconfigurable nodes that cross-connect traffic in the optical domain offer more or less the same functionality for the transit traffic, they primarily differ in how the traffic local to the node is treated. Therefore, the different types OXCs are categorized mainly based on the features/flexibility of the add/drop ports. Before listing the types of node architectures it is useful to introduce a few definitions that refer to the add/drop ports of the nodes.

### Colored - Colorless ports

Currently optical networks are evolving to support colorless add/drop ports which, unlike colored add/drop ports, do not have a permanently assigned wavelength but rather are adaptive with respect to which wavelength channel will be added/dropped. Colorless ports are attractive as generally fewer total add/drop ports are needed resulting in simpler operation and possibly more compact physical interfaces. Considering tunable transponders (TSP), colorless ports allow the wavelength to be selected and provisioned remotely (lower OpEx by simplifying deployment and enabling remote and rapid selection of a channel's wavelength). Colorless ports are generally created by replacing a fixed wavelength demultiplexing element (for example an arrayed waveguide grating (AWG) component) with a wavelength selective switch (WSS). A WSS can steer each optical channel present on its input port toward one of its output ports. In this basic node architecture, a colorless add/drop port is still dedicated to a single transmission fiber giving reason for some network blocking. This can be overcome by the next port category.

### Directed - Directionless ports

If a node is equipped with directed add/drop ports, a channel on a specific transmission fiber entering the node can be dropped only by a de-multiplexing element connected to this transmission fiber. In the same way, a locally added channel leaves the node on a pre-defined transmission fiber depending on the selected add port. As this architecture is comparably inflexible, architectures with directionless ports have been proposed which allow fully flexible transmission fiber selection for add/drop. The network operator is able to select provision and alter a signal pair's route at truly any point within network. Thus in an OXC with directionless add/drop ports not only transit traffic is switched from/to arbitrary transmission fibers, local traffic can be switched flexibly, too. Typically this directionless port property is realized by re-dedicating a transmission fiber port to a local port. It should be noted that for this implementation a particular wavelength can still be added/dropped to only one transmission fiber port. The use of this wavelength does not allow (blocks) adding/dropping the same wavelength to another fiber port.

### **Contentionless ports**

In optimum IARWA computation it is assumed that multiple demands are assigned to identical wavelengths but different transmission fiber pairs. Without any special measures for achieving wavelength blocking-free (i.e. contentionless) ports, a reconfigurable OXC provides only a single add/drop port for each wavelength. In this case – while the wavelength capacity is available on the transmission fibers – wavelength blocking may occur on the lightpath within the OXC itself. Typically the contentionless port property is realized by a spatial switch matrix. In contrast to a WSS, this type of switch cross-connects input ports irrespective of the specific wavelength.

The node architectures described in what follows, focus on the degree of flexibility they introduce and are considered in close correlation with the implications they impose to the network dimensioning and consequently to the cost evolution. R-OXC 1 is defined here as the reconfigurable OXC that carries the highest degree of flexibility and imposes no constraints to the problem of RWA, as it corresponds to a node that is colorless, directionless and contentionless. Considering R-OXC 1 as the reference architecture, a set of nodes that carry different combinations of the aforementioned features is presented. They are presented starting from the less flexible node to underline the architectural evolution towards the most flexible one. R-OXC 1 is not commercially available and difficult to implement with WSS components and therefore not described in the following. In the analysis presented following this section, only the architectures that are available in current networks were selected so as to study real-life scenarios. The node architectures are presented here merely to provide better comprehension of the performed analysis; more details on their implementation can be found in [5], [6].

### **Colored and Directed Node Architecture (R-OXC6)**

The colored transparent architecture is a WSS-based all-optical cross-connect with a broadcast-and-select architecture. In this node structure fixed and direction-specific transponders are used. As a consequence each transponder is connected via a wavelength multiplexer/de-multiplexer (e.g. AWG) to a fixed port of the node. If a particular wavelength is not equipped in the terminal for a port, it cannot be used for add/drop at that particular port. The advantage is that there is no need for extra WSS equipment in the add/drop terminals.

### **Colored and directionless node architecture (R-OXC 5)**

To avoid having separate multiplexers/demultiplexers for each network interface and to be able to share the add/drop ports between the network interfaces, one nodal degree of the OXC is used as a common add/drop port. Channels from a pool of (different) wavelengths can be switched towards any network port connected to the OXC. The drawback of this architecture is that only those wavelengths equipped in the channel pool can be used for traffic connections, and every wavelength can only be used to terminate a single network interface.

### **Colorless and directed node architecture (R-OXC 4)**

Here, the transponders have a tunable wavelength. The dropped channels from a network port are distributed to the corresponding wavelength transponders via a 1xN WSS. In the add direction, all wavelengths are combined and sent to the corresponding network interface. This allows the reduction of the number of equipped transponders while still maintaining routing flexibility.

**Colorless, directionless, partly non-blocking architecture (R-OXC 2&3)**

Here “degrees” of the OXC are used to add and drop channels. However the transponder cards used feature tunable wavelengths such that each channel card can be tuned to any wavelength of the WDM spectrum. Each channel can be connected to any network port, but, as before, each wavelength can be connected to only one network port. To partly overcome this wavelength blocking, additional degrees of the OXC can be used as flexible add/drop ports. With increasing number of “add/drop degrees” the blocking probability decreases until the number of add/drop degrees equals the number of network interfaces. With the reduction of blocking probability comes, however, an increase in required equipment. From the perspective of a pre-provisioning policy this type of architecture may still suffer from the 1-by-1 relation between an add/drop degree and the single usage of a wavelength.

Table 5-1 summarizes the node architectures described above as a function of the flexibility they incur.

**Table 5-1:** Types of R-OXCs

<b>Node Type</b>	<b>Directionless</b>	<b>Colorless</b>	<b>Contentionless</b>	<b>Remarks</b>
R-OXC 1	Yes	Yes	Yes	No architectural limitations
R-OXC 2	Yes	Yes	Partly	High flexibility
R-OXC 3	Yes	Yes	No	Relatively high flexibility
R-OXC 4	No	Yes	No	Medium flexibility, comparably expensive
R-OXC 5	No	Yes	No	Simple extension of R-OXC6
R-OXC 6	No	No	No	Limited flexibility, only flexible transit but static add/drop

## 5.2. Methodology

In the techno-economic analysis the network is dimensioned with a given traffic matrix as input. In this study different planning strategies were compared, namely the IA versus the IUA strategies. The output of a RWA algorithm is abstractly a list of routes and their assigned wavelengths corresponding to each of the demands. This output is processed to the number of drops per link in every node. The highest wavelength number is also necessary to know which type of WDM system is needed. The solutions provided by the RWA modules take also into account the impact of the various node architectures as these may possibly constrain the process given the available add/drop terminals. The assumptions and the details about the calculation method of the cost metrics are given in section 5.3. Figure 5-1 illustrates the various blocks and the flow of the entire analysis considered in this study.

### The Role of RWA

The efficient allocation of the available network resources has been discussed thoroughly so far, yet it has been seen from the perspective of optimizing the performance of the network. The minimisation of the blocking rate is achieved by utilising the physical layer knowledge in conjunction with the disposable resources (i.e. optical channels). However, herein the role of RWA is discussed under the perspective of network design. The solutions of different RWA methods may result into different needs in network equipment (e.g. transponders or regenerators), and eventually different operational costs. Of particular interest is the cost-effectiveness of the IA-RWA algorithms as these make more efficient use of the network

resources as opposed to simple RWA that ignore the Quality of Transmission (QoT). The RWA approach discussed hereafter is meant to assist the reader to comprehend how the solution of an RWA is mapped to the capital and operational expenses.

In the effort to assess the impairment-aware network planning, the IA-RWA algorithm developed and reported in [7] was utilized. Nonetheless this algorithm was developed assuming unidirectional traffic. The term unidirectional traffic signifies that each traffic demand from node “s” to node “d” is served independently of the traffic demand from node “d” to node “s”, rendering the traffic non-symmetrical. However in commercial networks, operators always assume that the traffic is symmetrical or otherwise noted as bidirectional and do the planning accordingly. In this case every demand in the traffic matrix has its “mirror” and both of them are assigned the same optical channel and the same route but in opposite directions. Identifying the need to capture the real-life implications this analysis focuses on planning for bidirectional traffic. In order to account for this type of traffic the offline IA-RWA [7] was properly adjusted to support it.

In the utilized IA-RWA algorithm lightpaths are established in a pre-defined sequence. The order in which the demands are considered plays an important role in the performance of the proposed algorithm. Hence, the main building block in the algorithm is a demand pre-processing ordering module. A-priori, the distance  $L(s, d)$  between source node  $s$  and destination node  $d$  of all the demands is computed using a shortest path algorithm. Then, the demands are ordered with respect to distance in decreasing order. The rationale behind this is that it is generally more difficult to accommodate demands with large resource requirements; hence we seek to accommodate resource-consuming requests first, which could easily be blocked by further, less resource-consuming requests. Longer hop paths may in general cross more imperfect components accumulating physical layer impairments and may interfere with more active lightpaths that produce excessive cross talk (multi-channel effects), which will increase the chances of blocking if the pre-processed demands follow a different sequence.

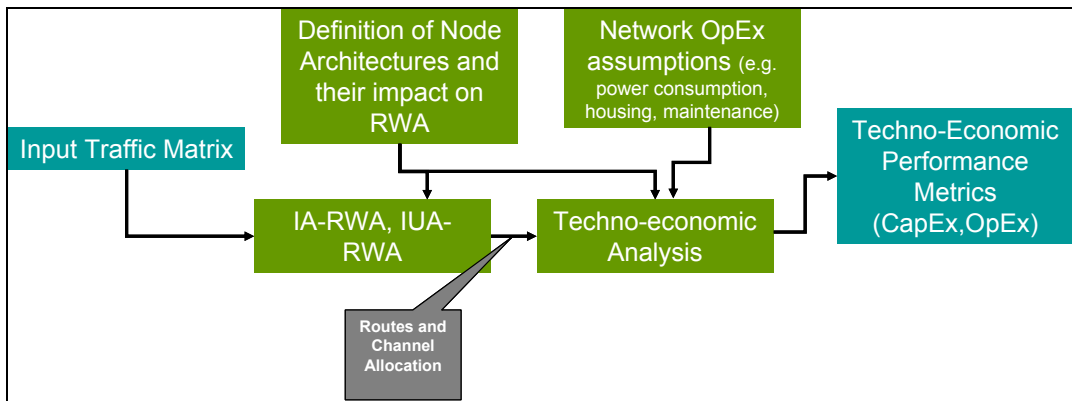


Figure 5-1: The flow of the techno-economic analysis process

The flow of the algorithm is depicted in Figure 5-2 . For each demand, in turn, a layered network graph (LNG) is constructed as follows. The network topology for a given WDM optical network is defined by  $G(V,E,W)$  where  $V$  is the set of nodes in the network,  $E$  is the set of bidirectional links, and  $W$  is the set of wavelengths. A layered network graph  $LNG(V;E)$  is a directed graph constructed from  $G$ . Each node  $i \in N$  in  $G$  is replicated  $|W|$  times in the LNG. These nodes are denoted by  $v_i(1), \dots, v_i(|W|)$ . If  $L_{i,j} \in L$  connects node  $i$  to node  $j$ , then vertices  $v_i(w)$  and  $v_j(w)$  are connected by two edges  $e_{i,j}(w)$  and  $e_{j,i}(w)$  for all  $w \in W$ .



A diverse routing engine then constructs a set of diverse routes in each wavelength layer of the LNG graph. After constructing the pool of candidate paths, we exploit the physical layer performance evaluator Q-tool (see Chapter 3) to compute the margin of each candidate route (with respect to the minimum allowed Q factor  $Q_{\text{threshold}}$ ) on the currently established lightpaths. The margin is computed by subtracting  $Q_{\text{threshold}}$  from the Q factors of all active lightpaths (including the candidate path) and finding the minimum value, as expressed in equation (1)), where  $Q$  is a vector that includes the Q factors of all lightpaths established in the network so far, without differentiating between primary and backup lightpaths:

$$Q_{\text{Margin}} = \min(Q - Q_{\text{Threshold}}) \tag{1}$$

The next step is to select a lightpath from the candidate lightpath list; the candidate lightpath with highest non-negative  $Q_{\text{Margin}}$  is selected. If this lightpath is found then the lightpath will be established and the network topology graph will be updated to reflect the wavelength and route allocation. If a proper lightpath is not found, then the demand is blocked. The algorithm was properly adjusted to account both for bidirectional and unidirectional traffic. In the bidirectional case discussed here the algorithm processes a demand and assigns the same channel and route (in opposite direction) to its “mirror” one.

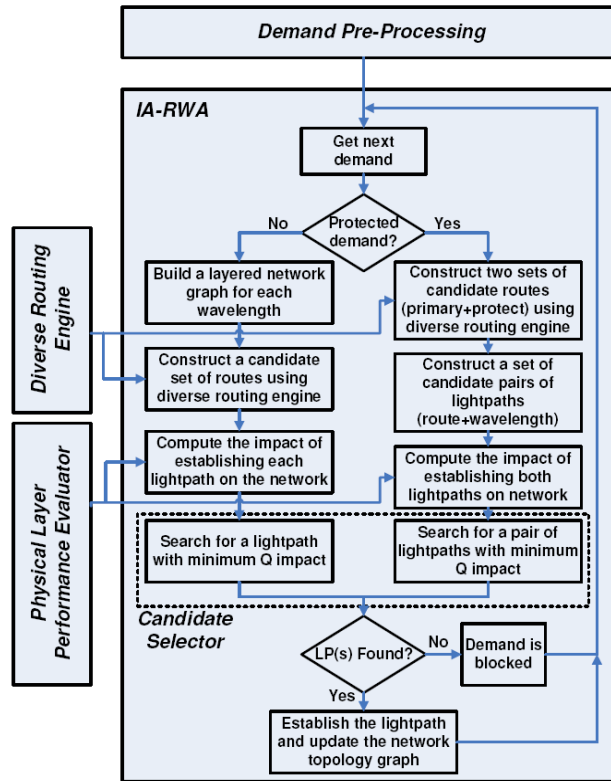


Figure 5-2: Flow chart of offline Rahyab algorithm

The IUA-RWA algorithm that is employed stems from the IA-RWA algorithm described above yet without the physical layer consideration and the pre-processing phase. The IUA method similarly to the IA one decomposes the network to the LNG(V;E) but only one shortest path is considered, yielding a smaller pool of candidate paths. The routes and wavelengths are then assigned, but only constrained by the available channels and the

wavelength continuity constraint. The routes assigned correspond to the shortest path and wavelength selected is the first available (index wise). In case there are no channels available along the shortest path then the second shortest path is assigned. After the end of the RWA process, the output of the algorithm is fed to the same QoT estimator (Q-tool) to check which of the lightpaths are feasible and which would be blocked because of unacceptable QoT.

### Assumptions and Input

The input traffic that was used in this case corresponds to traffic loads of [0.8-1.1] with a step of 0.1. The traffic matrix corresponding to load 1, assumes one bidirectional demand between its pair of nodes. In order to generate the matrices with lower load, demands from the load-1 matrix were removed randomly until reaching the 10% decrease in number of 10G demands. In the same way the matrix of load 1.1 was generated from the load-1 one and randomly adding connection demands until reaching load 1.1.

The reference topology considered here is the 14-node DT backbone network (Appendix A.1 Deutsche Telekom's Backbone Network). To quantify the planning solutions of the two RWA approaches it was assumed that the network is equipped with 80-channel line systems. As soon as the 80-channel system is exhausted in terms of resources or blocking occurs due to QoT not allowing the entire input traffic matrix to be served, an extra line has to be installed to support the blocked traffic. In other words the RWA algorithms are run assuming 80 wavelengths available. If for any reason a set of the demands does not get served, then a second parallel line system is assumed and the routes and channels of the blocked demands are re-computed.

## 5.3. Cost Modelling

### Network Capital Expenses

The cost model used in the analysis is based on [5] and is updated through a survey of the most recent list prices published by component manufacturers and system vendors. Table 5-2 summarizes the relative capital cost assumptions made for the components comprising the node architectures. As discussed in 5.1, the cost of the different node architectures depends on their physical implementation. An important subpart of all architectures is the network interface ( $NI$ ) whose cost ( $C_{NI}$ ) is the sum of the cost of the WSS ( $C_{WSS}$ ), the necessary splitter ports ( $C_{splitter}$ ) and the fixed cost for the casing ( $C_{case\_NI}$ ). Typically the RWA algorithms found in the literature assume a node design without architectural limitations. Here these limitations are considered in order to investigate the implications they impose to the network dimensioning.

**Table 5-2:** Component CapEx

Equipment	Relative cost	Power consumption [W]	Mean Time Between Failures
Long reach 10G TSP	1	30	250,000
EDFA, double stage	1.33	25	500,000
EDFA, single stage	1	15	500,000
1x4 WSS (80 channels)	2.35	30	300,000
1x8 WSS	4.7	40	300,000
1x20 WSS	7.05	50	300,000
1x40 WSS	10.58	60	150,000
Splitter	0.05	-	-

Combiner	0.13	-	-
AWG	0.7	-	-
Casing node	2.5	-	-
Casing NI	1-4	2-8	-
Casing AWG	0.5	-	-

In particular 4 different types are included in the analysis; R-OXC6, R-OXC4 and R-OXC2 & R-OXC3. Having only one add-drop terminal at a node leads to a potential blocking in case the RWA algorithm decides to add or drop at that node more than one connections running on the same wavelength. Here R-OXC2 assumes add-drop terminals equal to the node degree while R-OXC3 assumes only one add-drop terminal. Important rationale for the selection of these four architectures was the need to study the impact of the reconfigurable nodes that may be commercially employed today. The models for the capital cost of the four considered architectures are as follows:

$$C_{R-OXC6} = N \cdot (C_{NI} + C_{AWG} + 2 \cdot C_{EDFA2}) + C_{case\_node} \quad (2)$$

$$C_{R-OXC4} = N \cdot (C_{NI} + 2 \cdot C_{EDFA2}) + C_{case\_node} + \sum_1^N C_{a/d} \quad (3)$$

$$C_{R-OXC_{2|3}} = N \cdot (C_{NI} + 2 \cdot C_{EDFA2}) + R \cdot (C_{a/d_1} + C_{a/d_2} + 2 \cdot C_{EDFA1}) + C_{case\_node} \quad (4)$$

### Network Related Operational Expenses

Then the network-related OpEx refer to yearly recurring costs closely related to the total infrastructure cost. Regarding power consumption, the inputs are the power of a WSS, the fixed power per network interface and the fixed power per add/drop terminal. In the total power consumption, the power of the transponders and the EDFAs are included and a reference price of 0.1€ for 1KW is assumed [8]. In the rent cost of the floor space the general maintenance of the racks is also included. This results in a higher cost per square meter than the actual renting cost. We consider here a cost of 50€ per square meter per month [9]. Finally with respect to repair costs, if the mean time between failures (see equation 5) and the number of active components are known, then we can calculate the number of failures in the whole network. In the cost per failure we include the mean repair cost and the cost of the equipment. All used input values related to maintenance, power consumption and housing of the equipment are shown in Table 5-3.

$$MTBF = \frac{T}{R}, T = \text{total time}, R = \text{number of failures} \quad (5)$$

Table 5-3: Network-related OpEx

Network OpEx input	Relative cost
Floorspace (Cost per square meter per year)	0.27
Power Consumption (Cost per kW per year)	0.79
Repair cost per WSS failure	0.2
Repair cost per Transponder failure	0.1
Repair cost EDFA double/single stage	0.1

## 5.4. Results

### CapEx

Following the techno-economic evaluation of the two planning approaches, the results collected in terms of CapEx with respect to the traffic load for R-OXC6 are depicted in Figure 5-3. Focusing at first on load 0.8 of the scenarios studied, the two methods yield the same capital cost as both can serve the traffic with the 80 channels available. As the load is increasing towards load 1.1 the IA respective cost does not increase dramatically as it can still serve all of the demands with no blocking. Indeed the IA relative cost rises slightly due to the number of transponders, related to the increased number of demands.

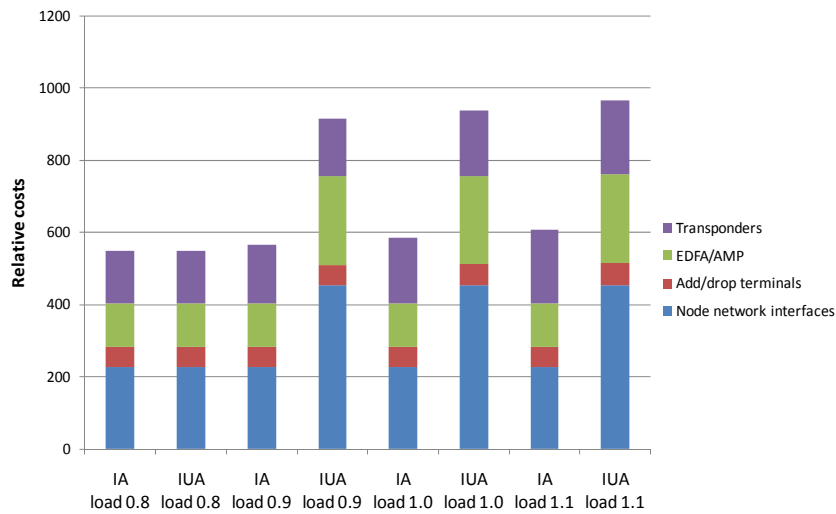


Figure 5-3: Total CapEx of IA vs. IUA with R-OXC6

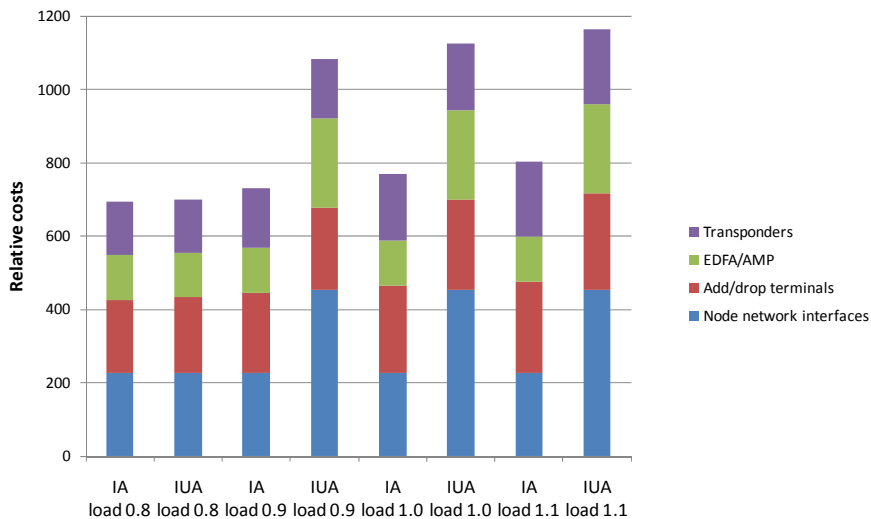


Figure 5-4: Total CapEx of IA vs. IUA with R-OXC4

Nonetheless, the IUA algorithm for loads higher than 0.8, experiences physical blocking that leads to a significant increase in capital. To resolve this, the analysis assumes an extra line system that results in a cost increase of around 60% at all cases (except 0.8) compared

to the IA counterpart. Evidently, the excessive computed cost stems from the need of the IUA of two times more EDFAs and network interfaces in the node because of the extra line system. The two planning methods were also assessed assuming another type of node, namely R-OXC-4. The results with respect to load are illustrated in Figure 5-4, where the same trend can be identified. The overall higher computed cost when compared to R-OXC-6 is due to the higher cost required for the add/drop terminals.

**Impact of Node Architecture**

As discussed above, the cost implications of four different node architectures were also studied when provisioning a network with bidirectional traffic. Figure 5-5 illustrates the computed relative costs for the four nodes for load 0.8. As load 0.8 is small enough for the IUA to serve the traffic without the need of extra equipment, there is no cost difference with the IA solution. On the contrary there is a significant difference between the two schemes (IA vs IUA) for load 1.1 (see Figure 5-6) due to the respective difference in CapEx requirements. Nevertheless, for both traffic matrices the cost corresponding to a specific node architecture, is driven primarily by the number of the add/drop terminals and secondly by the network interfaces. As a consequence, regardless of the traffic load the most flexible node, i.e. R-OXC2 is also the most costly.

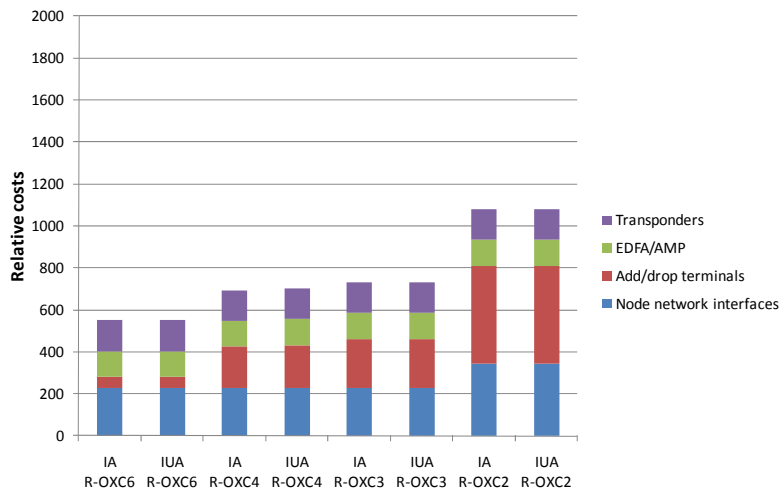


**Figure 5-5:** Cost difference between the different node architectures with load 0.8

R-OXC4 is more costly than R-OXC6 due to the extra WSS components in the add/drop terminals. To implement a directionless node (like in R-OXC3) we need an extra network interface components per add/drop terminal. R-OXC3 contains only one common add/drop terminal, with this implementation each wavelength can only be dropped once at that node. R-OXC2 solves this problem by adding extra add/drop terminals, here the number of add/drop terminals is equal to the node degree. The difference between R-OXC3 and R-OXC4 is little because with R-OXC4 there are more spare colorless ports per fiber input and in case of R-OXC3 we can use all the colorless ports to connect to all fiber pairs. If we do not modify the RWA, R-OXC3 will cause extra blocking due to the add/drop terminal. For load 0.8 we calculated a blocking of 32 demands. In case of load 1.1 there are 52 blockings. If we make the RWA aware of this constraint these blockings can be avoided. We confirmed this for load 0.8.

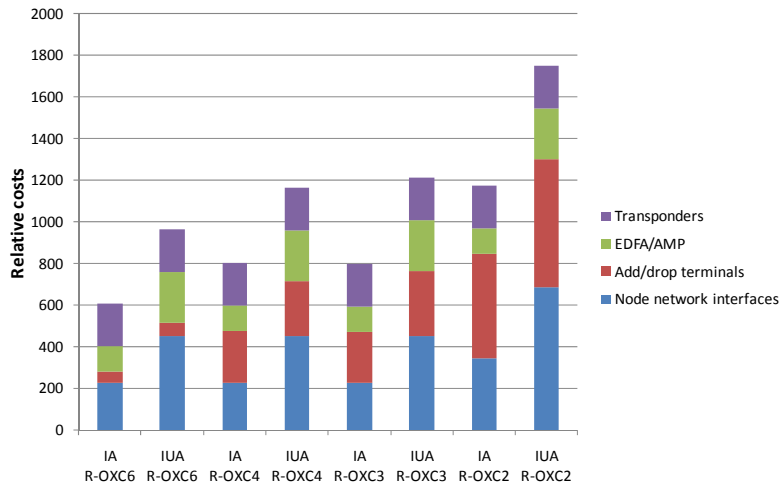


Figure 5-6: Cost difference between the different node architectures with load 1.1

**Network related OPEX**

In Figure 5-7, the network related OpEx of IA versus IUA in case of R-OXC 6 is illustrated. The OpEx in the IA case increases a little with the increased number of demands from load 0.8 to load 1.1. The operational expenses related to the transponders, such as the necessary repair costs and the power they need to run, are responsible for a slight OpEx raise with respect to the traffic. Similar to the CapEx calculated above, the sharp increase in the IUA case for loads higher than 0.8 depends on the extra equipment assumed which in turn leads to higher OpEx. In particular the housing cost doubles as there is a need for two times more floor space. In the same way all operational activities related to the node and line equipment require twice the same cost. On the contrary the power needs and maintenance of the transponders is effectively the same when compared between IA and IUA for a given load, as the number of transponders remains the same for the two cases.

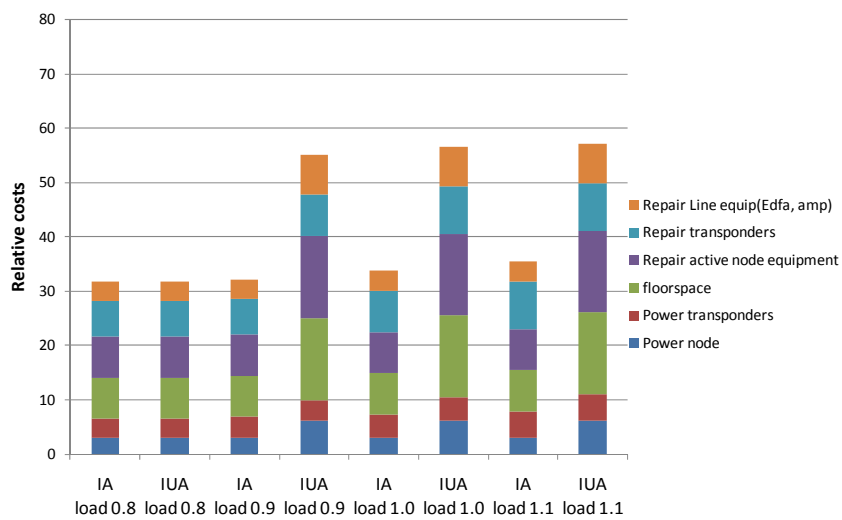


Figure 5-7: Network related OpEx of IA vs. IUA with R-OXC6.

Figure 5-8 then depicts the computed OpEx for the four different node architectures considered in the analysis. Overall the cost to repair the active node equipment accounts for the major part of the OpEx. Nonetheless, the OpEx follows the same trend as the corresponding CapEx when considering the impact of the architecture and R-OXC6 incurs the lowest OpEx requirement.

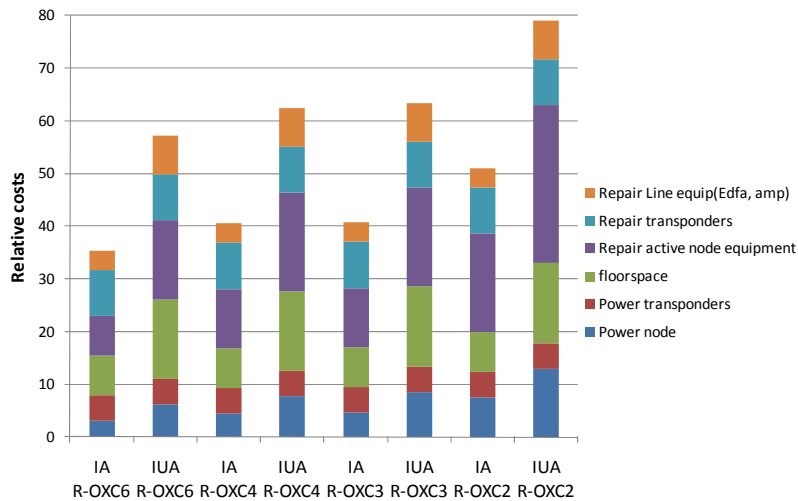


Figure 5-8: Network related OpEx of IA vs. IUA for the different node architectures with load 1.1

## 5.5. Chapter Summary

In the framework of dynamic single line-rate networks a techno-economic analysis was conducted to explore the cost implications stemming from resource optimization. IA-RWA and IUA-RWA algorithms were used to compare their planning solutions for a nation-wide backbone network in terms of CapEx and OpEx. A given traffic matrix with a specific annual increasing evolution was fed to the algorithms. Evidently the solutions of the IA-RWA algorithm illustrated that it may serve the input demand without any requirement for a second parallel line system, as opposed to the IUA-RWA method. The latter does not consider the QoT in the lightpath computation and therefore the routing and channel allocation is not optimised leading to physical-layer blocking. The IA solution outweighs the IUA one in CapEx and OpEx and the respective difference is directly proportional to the extra line system that would be required to serve without any blocking the given traffic. The IUA solution calls for a capital investment sooner than the IA one as the traffic increases. For the same scenario four different reconfigurable nodes were considered in order to quantify the relative CapEx required. A colourless, directionless but partly contentionless architecture (R-OXC3) appears to be a good choice for the specific scenario, as it is a node with a relatively high degree of flexibility and a moderate cost. Although R-OXC 3 is more inexpensive, it is anticipated that in the presence of an increased traffic volume the more flexible nodes (R-OXC2) would perform better in terms of blocking, possibly compensating for the higher CapEx.

This chapter concludes the research conducted in the framework of this PhD on core networks that carry a single line-rate. In the chapters that follow the research work focuses

on next generation core networks and solutions that bring about ultra high bit-rates yet with an increased level of flexibility on the utilization of resources.

## 5.6. References

- [1] M. Gunkel, R. Leppla, M. Wade, A. Lord, D.A. Schupke, G. Lehmann, C. Fürst, S. Bodamer, B. Bollenz, H. Haunstein, H. Nakajima, J. Martensson, "A Cost Model for the WDM Layer", in Proceedings of Photonics in Switching 2006.
- [2] A. Lord, C. Engineer, "OPEX savings of all-optical core networks", in Proceedings of ECOC 2009.
- [3] R. Cardillo, V. Curri, M. Mellia, "Considering Transmission Impairments in Wavelength Routed Networks", in Proceedings of OFC/NFOEC 2006, paper OFG6.
- [4] M. Ruffini, D. Kilper, D. O'Mahony, and L. Doyle, "Cost Study of Dynamically Transparent Networks", in Proceedings of OFC/NFOEC 2008, paper OMG2.
- [5] R. Huelsermann, M. Gunkel, C. Meusburger, D.A. Schupke, "Cost modeling and evaluation of capital expenditures in optical multilayer networks", OSA J. of Optical Networking, vol. 7, no. 9, 2008.
- [6] M. De Groote, K. Manousakis, P. Kokkinos, D. Colle, M. Pickavet, K. Christodoulopoulos, E. Varvarigos, P. Demeester, "Cost comparison of different Translucent Optical Network Architectures", in Proceedings of CTTE 2010.
- [7] Siamak Azodolmolky Yvan Pointurier, **Marianna Angelou**, Josep Sol'e Pareta, and Ioannis Tomkos, "An Offline Impairment Aware RWA Algorithm with Dedicated Path Protection Consideration", in Proceedings of OFC/NFOEC 2009, paper OW11.
- [8] Energy price statistics, Eurostat, [http://epp.eurostat.ec.europa.eu/statistics\\_explained/index.php/Energy\\_price\\_statistics](http://epp.eurostat.ec.europa.eu/statistics_explained/index.php/Energy_price_statistics).
- [9] Breda in perspective, DTZ Wadelhoff Research, [www.dtz.nl](http://www.dtz.nl)





# Chapter 6

## 6. Flexible Optical Networks

There is a growing awareness that the physical capacity of the optical fiber is rapidly approaching its maximum limit [1]. Indeed the capacity of the optical links has grown exponentially for the last 30 years. This growth has been enabled by important technological advancements, including, among others, the introduction of WDM, erbium-doped-fiber amplifiers and dispersion compensation. Considering that IP traffic is being reported to double every two years it is foreseen that demand will exceed supply in the near future.

Given the forecasted capacity crunch, the research community has focused on seeking solutions that make the most out of the scarce network resources and allow accommodating the ever-increasing traffic demand. In such context, *flexible optical networking* has been introduced as a way to offer efficient utilization of the available optical resources [2]. “Flexible”, “elastic”, “tunable”, “gridless” or “adaptive” are few examples of the terms used in literature to describe solutions that migrate from the fixed WDM single line rate (SLR) systems to systems with improved and heterogeneous transmission characteristics [3].

Nowadays 40-Gb/s and 100-Gb/s optical transport systems are a commercial reality. However current networks rely mostly on legacy on-off-keying (OOK) 10-Gb/s channels spaced on a fixed 50-GHz grid. Prior to the introduction of flexible optical networking, a mixed solution where 40-Gb/s and 100-Gb/s channels would co-exist with the 10-Gb/s ones has been extensively studied to upgrade the capacity of the existing systems. The *mixed line-rate* (MLR) solution allows the higher-rate channels to run in the same system while still capitalizing on the legacy infrastructure. It consists of a mixed transport system that utilizes the conventional fixed spectrum grid. As illustrated in Figure 6-1, it resembles a standard WDM system where optical connections occupy spectrum in predetermined center frequencies and slots taking advantage of the existing network components. MLR networks employ a migration scenario that allows operators to use higher-rate technologies to serve the traffic that increases with time.

Researchers have thoroughly studied the transition from low to higher bit rates, focusing on the physical implementation and requirements. Initially the feasibility of hybrid 10-40 Gb/s channels was demonstrated using OOK formats and standard 50-GHz and 100-GHz channel spacings [4], [5]. More recently differential quadrature phase-shift keying (DQPSK) has emerged as an attractive modulation format for the 40-Gb/s channels in the hybrid scheme, as it offers higher spectral efficiency and tolerance to polarization-mode dispersion. As the 40-Gb/s phase-modulated signals are prone to the interference stemming from the OOK channels, the authors in [6] developed a model to account for the nonlinear phase noise induced by cross-phase modulation (XPM). Indeed in such a configuration XPM is the dominant non-linear source that depends on the employed channel plan and dispersion map [7].

To enable the advent of the next generation 100G Ethernet (100GE) transport systems, new high data-rate transmission technologies have been also studied. Instead of using

multiple low-rate channels (e.g. at 10 Gb/s) to carry the 100GE channels, an approach that offers 100Gb/s on a single wavelength has been adopted. Nonetheless, a 100-Gb/s-per-channel rate poses certain limitations on the system performance related with the transceiver bandwidth and the CD and PMD tolerance. The emerging digital coherent detection technology has allowed the implementation of 100Gb/s transmission systems where CD and PMD are digitally compensated [8], [9]. Following this advancement, multi-rate 10G/40G/100G systems were proposed to upgrade existing networks without traffic interruption or major infrastructure changes [10], [11]. The feasibility of this mixed configuration has been experimentally demonstrated using either incoherent detection with polarization multiplexed differential quadrature phase-shift keying (POLMUX-DQPSK) [12], [13] or coherent detection with polarization multiplexed quadrature phase-shift keying (POLMUX-QPSK) [13] for the 100-Gb/s channels. The authors in [14] have studied the impact of XPM stemming from the OOK channels on the DQPSK and coherent QPSK channels and proposed analytical expressions to estimate the associated penalty.

From a networking point of view, the physical limitations of the MLR networking paradigm have been addressed by incorporating QoT constraints in the lightpath provisioning process [15]. A PCE-based scheme is proposed in [16] to provide QoT-aware routing and wavelength assignment. The authors in [17] have proposed analytical models to quantify the effect of XPM on the phase-modulated channels and showed improved blocking ratio by incorporating those in a GMPLS-controlled MLR network.

Cost-effective solutions have also been proposed to design an MLR with minimum resources [18], [19]. MLR networks achieve better resource optimization than a SLR network as they can fully exploit the versatility of the offered capacities and their associated transmission reach [19], [20]. In a similar context [21] studied the problem of cost-efficient routing when considering MLR as the underlay physical infrastructure for Carrier Ethernet and showed the impact of the transmission reach of the MLR channels on the overall network's cost.

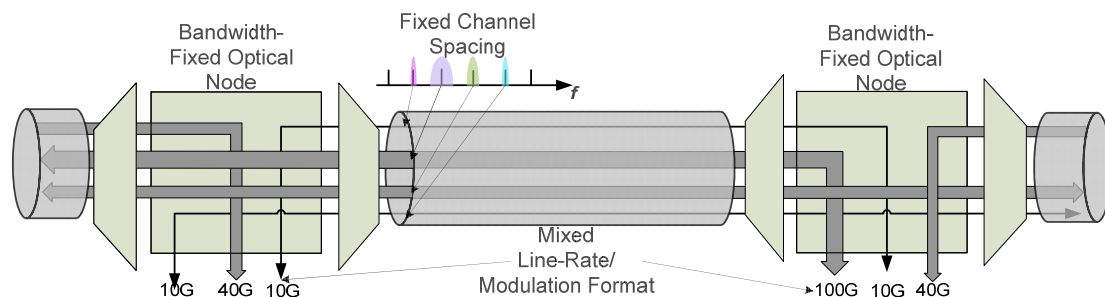


**Figure 6-1:** Fixed Optical Network with mixed line rates of 10Gb/s, 40Gb/s and 100 Gb/s – optical connections fit in fixed spectrum slots and get switched at specific center frequencies and optical bandwidths utilizing a standard DWDM system

However as discussed above, in order to deliver the various line-rates, MLR networks require a different technology, i.e. a different type of transponder for each of the supported rates (e.g. OOK for 10Gb/s, DQPSK for 40Gb/s and coherent POLMUX-QPSK). Instead, the recent technological advancements, have offered the possibility of a multi-rate network that uses an “adaptive” type of transponder. In essence this concept (i.e. flexible networking) assumes a single type of technology that adapts to the requested traffic rather than a rate-specific type of configuration such as the one employed by MLR. Adaptability is one of the principal characteristics of the emerging flexible networking paradigm. The benefits of such

a solution with respect to the achieved resource savings compared to SLR and MLR have been previously investigated in [22]-[26]. In addition Chapter 7 discusses in detail the resource optimization gained as a result of a study that compares the various networking solutions.

What is more, the rigid and large granularity of WDM on the wavelength level, leads to severe spectrum wastage. In view of this limitation, flexible optical networking promises to offer elasticity and adaptation by allocating just the spectral resources that are required for the given traffic demand [2], [27]. The concept of adaptation, however, is not new to the area of digital communications. Wireless networks as well as digital subscriber lines have effectively utilized such features to introduce higher spectral efficiency. Regardless of the employed technology, flexible optical networks (as depicted in Figure 6-2) enjoy a multiple degree of freedom where fiber is treated as a continuous field of shared resources. Therein, an optical end-to-end connection is characterized by flexible (a) spectral width, (b) line-rate and (c) modulation format, as opposed to the conventional WDM network where optical connections fit in fixed spectrum slots at specific center frequencies.

In contrast to a conventional network where optical connections fit in fixed spectrum slots at specific center frequencies, the flexible network architecture consists of components that enable the transport of data-streams in a spectrum-efficient and elastic manner. Key enabling technologies are the flexible optical nodes, transmitters and receivers; *spectrum-flexible* optical cross-connects (OXC) and reconfigurable optical add-drop multiplexers interconnect optical links whose ends are populated with rate/modulation format *flexible* transponders. To implement the spectrum-flexible OXC a wavelength selective switch (WSS) that can route signals with a variable spectral width and center frequency to any of the output ports is required. Bandwidth-flexible WSSs that are capable of switching variable spectral bands are commercially available today. On the other hand, transponders that can adapt on-demand the offered line rate and modulation format can be realized with the use of novel technologies such as optical orthogonal frequency division multiplexing (OFDM). More details on the relevant novel technologies are given in 6.4.

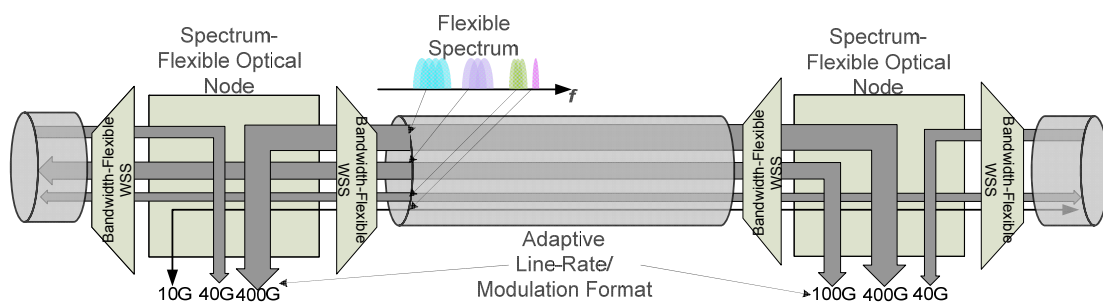


**Figure 6-2:** Flexible optical network concept – optical connections have flexible bandwidth and adaptive line-rate and modulation format; optical nodes are also bandwidth agnostic.

In summary flexible optical networking offers elimination of the poorly-filled wavelengths stemming from the fixed spectrum grid and adaptive sub-wavelength and super-wavelength services to the traffic demands. In what follows, this chapter reviews technologies and concepts proposed for the future core optical networks to cope with the high-capacity requirements and realize the concept of flexible optical networking; advanced modulation formats with coherent detection, software-defined optical transmission,

bandwidth-flexible network components and multi-carrier transmission certainly usher a new era in optical communications.

## 6.1. Advanced Modulation Formats

The evolution of capacity growth in communication systems has been defined mainly by the introduction of WDM, optical amplifiers and advancements in laser and filtering technologies. Once though, optical amplifiers approached their maximum capacity, growth started slowing down [1]. From that point on, capacity growth relied on methods that would increase spectral efficiency and thus advanced modulation formats have been adopted so as to increase the transmitted data rate.



Figure 6-3: Constellations that use only the real part of the field and carry 1 bit per symbol.

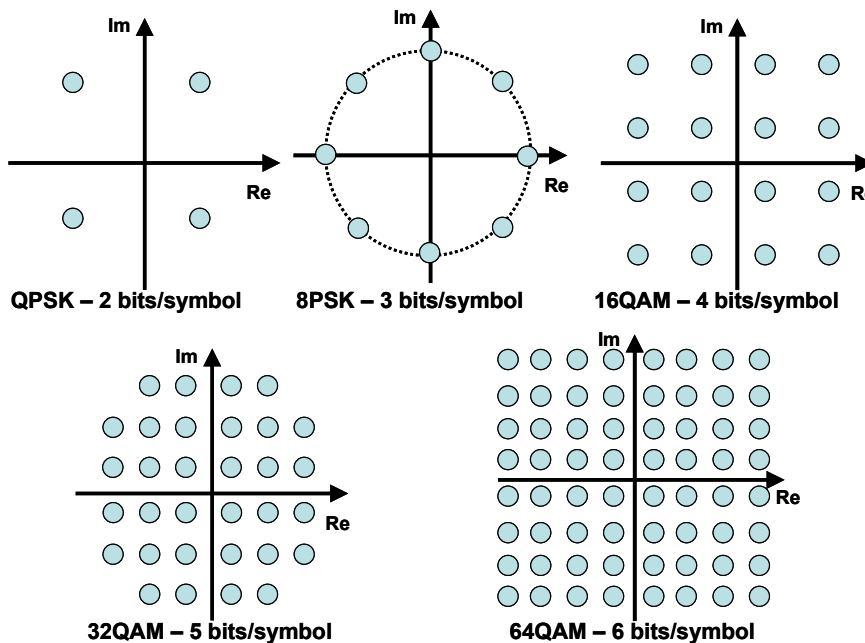




Figure 6-4: Constellations that use both quadratures of the field and carry multiple bits per symbol.

In typical optical communication systems, a symbol pulse is represented using an on-off-keying format where only the real part of the field is utilized. In such formats (see Figure 6-3) the symbol rate coincides with the bit rate as there are only two symbols populating those constellations. To achieve higher spectral efficiency via the chosen modulation format one has to employ a format that uses both the real and imaginary part of the field. In this case a symbol carries a higher number of bits that depends on the total number of

constellation symbols  $M$ . Hence, in a constellation each symbol represents  $\log_2 M$  bits. Figure 6-4 illustrates constellations that use both quadratures and are characterized by a higher modulation level  $M$ . Comparing two modulation formats that have different modulation level, the one with the higher level  $M$  delivers a higher data rate at the same symbol rate or equivalently delivers the same data rate  $B$  with reduced symbol rate  $B/\log_2 M$ .

Such advanced modulation formats are considered in the technologies to be adopted in the next generation core either in a single or multiple-carrier scheme due to the increased spectral efficiency they introduce. Nonetheless, constellations with large  $M$  are limited by the fact that the constellation points need to be placed closer together and therefore have higher requirements in signal-to-noise ratio (SNR) to achieve a certain bit error ratio (BER). As a consequence, the maximum transmission reach of each modulation format depends on the size of the symbol set leading to a trade-off between modulation level and distance. A signal modulated with 16-QAM carries twice as many bits per symbol as with QPSK and therefore requires half the bandwidth to deliver the same bit rate (Table 6-1). Nevertheless the SNR penalty of 16-QAM compared to QPSK, may render 16-QAM insufficient for a lightpath of certain distance. Distance-adaptive spectrum allocation has been proposed in [27] to take advantage of this feature in order to dynamically assign only the necessary spectral resources to a lightpath of certain characteristics, i.e. distance, required capacity, number of hops.

**Table 6-1:** Parameters in single-carrier modulation with variable bit and subcarrier [27]

Modulation Format	QPSK	16QAM
		
Symbol Rate (Hz)	$B/2$	$B/4$
Number of Carriers	1	1
Bits per Symbol	2	4
Bit Rate (b/s)	$B$	$B$

In addition to the single-carrier based modulation formats, multi-carrier based schemes (reviewed in section 6.4) gain ground on the implementation of the future flexible optical networks. Multi-carrier formats reduce substantially the symbol rate so as to achieve a given data rate. As shown in Table 6-1, an OFDM-based signal with multiple subcarriers modulated with QPSK reduce the symbol rate even more at  $B/2n$  where  $B$  is the required data rate and  $n$  the number of subcarriers. The equivalent symbol rate with 16QAM goes down to  $B/4n$ .

What is more, polarization multiplexing is used to increase spectral efficiency further [28]. Polarization is another physical attribute of the optical field that can be used to transport information. Polarization division multiplexing (PDM) allows two different signals to be transmitted at the same wavelength but in two orthogonal polarizations, thus doubling the total data rate.

**Table 6-2:** Parameters in multi-carrier modulation with variable bit and subcarrier [27].

Modulation Format	OFDM-QPSK	OFDM-16QAM
Symbol Rate (Hz)	$B/2n$	$B/4n$
Number of Carriers	$n$	$n/2$
Bits per Symbol	2	4
Bit Rate (b/s)	$B$	$B$

## 6.2. Fixed and Flexible Spectrum Grid

So far traditional WDM networks relied on the ITU-T grid and the spacings defined therein. Nevertheless its coarse granularity leads to poor spectrum utilization as discussed earlier. In the context of flexible optical networks the efficient management of spectrum is of paramount importance. In fact, to realize the vision of flexible optical networking it is necessary to migrate from the rigid ITU-T frequency grid to a flexible configuration that will maximize the total fiber capacity. What follows is an attempt to show how the changes that are expected in the next generation core optical networks are reflected in the frequency domain. Three cases are discussed, namely (i) *fixed-grid*, (ii) *flex-grid* and (iii) *gridless* (Figure 6-5). Prior to that, it is important to define here the notion of a *superchannel*. In literature the term superchannel is used to describe a signal that consists of multiple carriers that may originate from the same laser source [29] or individual laser sources [30], yet is perceived as a single entity. Regardless of the technology it is used to generate it, it is essentially a high bit rate channel that is transmitted and received as a continuous waveband signal formed by combining several low-rate subcarriers.

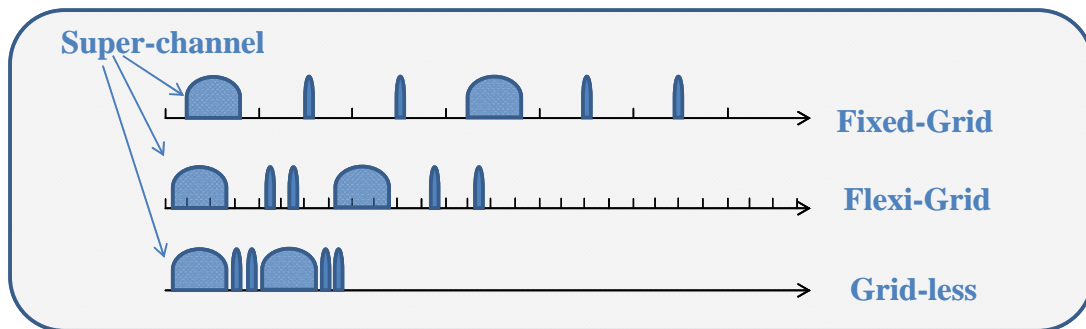


**Figure 6-5:** The cases of Fixed-Grid, Flexi-Grid and Grid-less.

In the fixed-grid case the standard ITU-T grid is employed. The grid is uniformly sliced with each channel assigned a slot of the same size and every lightpath is assigned a wavelength that coincides with the ITU-T grid wavelengths. In dense WDM networks, spacings vary between 200 GHz, 100 GHz, 50 GHz and 25 GHz. Regardless of the bandwidth required serving a given demand, each lightpath is allocated a fixed spectrum slot. As illustrated in Figure 6-5 a full-sized channel slot (e.g. 50GHz) is dedicated to the traffic demands although the occupied spectrum is smaller. In the presence of superchannels in a fixed-grid configuration their bandwidth would be inevitably limited by the size of the fixed slot.

In contrast gridless corresponds to the most flexible case, where a certain lightpath is arbitrarily assigned with a wavelength and a “chunk” of spectrum. Coherent detection techniques essentially allow this flexibility in the frequency of the carrier, since with appropriate tuning of a local oscillator at the receiver side signals can be demodulated at any wavelength. Any two channels in a gridless system may have their central carriers very close to each other as they do not have to conform to the ITU-T defined wavelengths. Channels occupy just the amount of spectrum they need and superchannels can be accommodated without bandwidth limitations. Comparing the fixed-grid and gridless cases as depicted in Figure 6-5, one can observe the spectrum savings that are achieved in the gridless case by the tight packing of channels in the frequency domain.

Nonetheless, most currently-available optical components cannot offer the tunability required to fully support the gridless paradigm. For instance, tunable lasers typically offer a resolution of 0.01 nm. Thus, a flex-grid spectrum is introduced as a compromise between the two extreme cases (i.e. fixed-grid and gridless). Rather than employing a fully flexible design, the flex-grid still follows a scheme with a discrete set of frequencies. However, it offers a finer granularity than a typical fixed-grid and most importantly it allows channels to span several mini-slots if needed (see Figure 6-5). Superchannels are spread in multiples of these mini-slots thus considerably improving the spectrum utilization compared to the fixed-grid case. Recent technology advancements based on liquid crystal on silicon (LCOS), have enabled the commercial introduction of WSS products that can dynamically select the center frequency of the mini-slots at 6.25 GHz resolution with 12.5 GHz wide mini-slots [31].

The networks that enjoy the flexibility of either a gridless or flex-grid scheme require, however, new processes for the routing of traffic demands. Special algorithms that compute routes and allocate the flexible spectrum (*Routing and Spectrum Allocation – RSA*) have been proposed to cope with the new constraints [32]. RSA processes need to respect (i) the *wavelength continuity* constraint that requires lightpaths to maintain their wavelength along their route, (ii) the *spectrum continuity* constraint that requires lightpaths to use the same spectrum band along their route and (iii) the *spectral conflict* constraint which describes the requirement for non-overlapping spectrum among channels on the same fiber. The authors in [33] have investigated the performance of a flex-grid multi-carrier scenario in terms of the blocking ratio and showed significant benefits when compared to an MLR network that uses a fixed grid spectrum allocation. The work of [34] confirmed the advantages of the flexible solutions (flex-grid and gridless) over the fixed grid with respect to the achieved blocking ratio. In addition the authors studied the conditions under which the flex-grid case can match the performance of the fully gridless case and showed that the flex-grid can perform equally to the gridless case under certain granularity.

Most of the works that deal with the flexible spectrum allocation focus on the offline problem that takes place during the network planning [33]-[36]. More recently researchers have attempted to solve the online problem where traffic is varying with time [37]-[40]. During network operation, connections are being torn-down and established dynamically. Due to this ongoing process the spectrum allocation deviates from the optimum one that took place during planning and the result is a fragmented spectrum of unused spectral bands. As a consequence, it becomes more difficult to find a contiguous spectrum window that will accommodate the new traffic demands, leading either to increased spectrum allocation or blocking of the traffic requests. This process resembles the memory utilization of computer hard disk drive, where periodic *defragmentation* is required to bring the hard disk to its optimal state. In a similar manner, operators need to periodically reconfigure their networks so as to optimize again the spectral resource utilization and minimize blocking.



However during the defragmentation process certain connections need to be disrupted before regaining a state of stability. In [38]-[40] heuristics are proposed to address the problem of defragmentation while trying to minimize the number of interrupted connections and the disruption time.

### 6.3. Single-carrier Solutions

Mixed line rate (MLR) networks were initially proposed for the core networks of the next generation, due to their ability to accommodate higher rate connections together with lower-rate ones. MLR systems, as discussed in the beginning of the chapter, constitute a single-carrier solution where a mixed set of data rates (typically 10G/40G/100G) co-exist in the standard DWDM infrastructure [10]-[11], [19].

Despite offering multiple rates in the same system, MLR requires a different type of transponder to deliver each of the offered rates. In contrast, multi-carrier solutions have been proposed to offer the required flexibility with a single adaptive type of transponder. Relevant technologies are reviewed in section 6.4. However there has been one solution that uses a single-carrier scheme yet delivers multiple line rates in an adaptive manner. It is based on format-versatile transmitters able to transmit data at 25 Gb/s, 50 Gb/s or 100 Gb/s [41].

POLMUX-QPSK seems to prevail as the winning solution for the 100 Gb/s channels [8], [9], [62]. Given this consideration the authors in [41] utilized a typical 28 Gbaud POLMUX-QPSK transmitter and proposed an adaptive version that can dynamically use the different phase states and polarizations to deliver multiple line rates. A typical POLMUX-QPSK transmitter consists of two quadrature modulators (nested Mach-Zender interferometers (MZI)) and a polarization beam splitter (PBS) that multiplexes the two outputs in the two polarizations. As depicted in Figure 6-6 a continuous wave laser source feeds a PBS that splits the light into two orthogonal polarizations. A splitter further divides light into two components of equal intensity which are then fed into two MZIs that act as phase modulators. A phase shifter follows after one of the two branches and the output of the two MZIs is combined again. In the end a polarization beam combiner (PBC) multiplexes the two polarization states to generate the POLMUX-QPSK signal. The MZIs in both polarizations are driven with four independent 28 Gb/s electrical signals which combined obtain a 112 Gb/s line rate. This allows for a 100 Gb/s net data rate and 12% overhead for forward error correction (FEC) and Ethernet framing.

The adaptive feature of the so-called PDM xPSK transmitter is based on the following idea. If the electrical signals are not independent the same transmitter as depicted in Figure 6-6 can be used to generate signals with lower data rate. By driving the in-phase and quadrature modulators with identical electrical signals in the same polarization (i.e.  $I_1=Q_1$  and  $I_2=Q_2$ ) generates a 50 Gb/s POLMUX-BPSK signal. In a similar manner if all driving signals are identical (i.e.  $I_1=Q_1=I_2=Q_2$ ) then a 25 Gb/s single polarization (SP) BPSK signal is generated.

At the receiver side, the optical signal is detected using coherent technology similar to that of a coherent POLMUX-QPSK transceiver. The received optical signal is split into to arbitrary orthogonal polarizations. Both are then mixed with a local oscillator in a 90° hybrid structure to get the in-phase and quadrature components. Photodiodes then detect the optical signals and ADCs are used to convert them to the digital domain. The authors in [41] foresee that a number of the DSP functions used for electronic compensation of the signal distortions, can be shared between the different modulation formats without significant additional complexity.

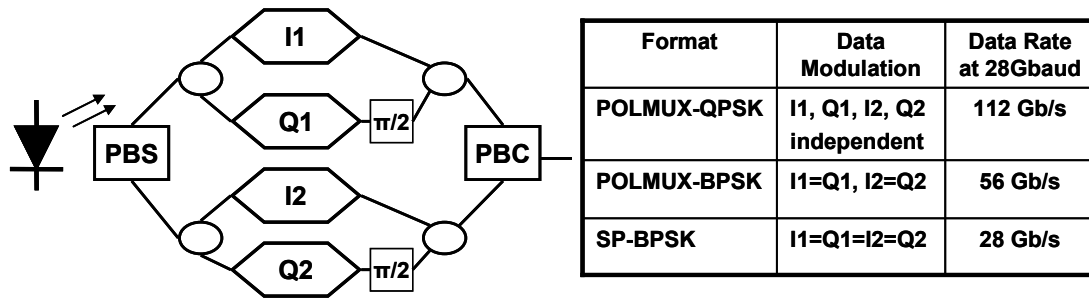


Figure 6-6: Single-carrier adaptive transmitter – Structure and characteristics of the PDM-xPSK transmitter [41].

In summary single-carrier approaches offer simplicity of implementation and the ability to capitalize on the existing infrastructure. Nevertheless they are generally characterized by poor spectral efficiency and scalability. It is expected that more advanced options such those introduced by the multi-carrier approaches will better cope with the challenges beyond 100 Gb/s.

### 6.4. Multi-carrier Solutions

Ultra high-speed channels at the terabit level that would satisfy future capacity needs could theoretically be transmitted over a single carrier modulated with formats of extremely large constellations such as PM-1024QAM. Nevertheless such formats would pose significant physical restrictions (e.g. intolerance to phase noise and non-linearities, fast digital-to-analog converters (DACs) at the transmitter, poor sensitivity, hardware bandwidth limitations) that would considerably limit the transmission reach. As an alternative solution, assembling a superchannel (as it was discussed in section 6.2) not only offers spectral efficiency it also allows the generation of very high bit-rate channels out of low-rate subcarriers. For instance, using 10 subcarriers of POLMUX-QPSK operating at 28 Gbaud allows the formation of a 1.12 Tb/s superchannel such as the one depicted in Figure 6-7. Besides, high bandwidth efficiency is achieved by utilizing very closely spaced subcarriers.

Multi-carrier transmission techniques have been proposed as a solution to the need for flexible and efficient use of the available spectrum as they essentially enable the formation of high bit-rate superchannels but also granularity at the subcarrier level. In what follows the most prominent optical multi-carrier techniques are reviewed namely OFDM and Nyquist-WDM (N-WDM).

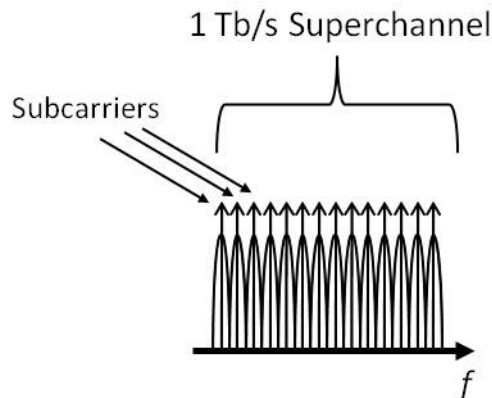
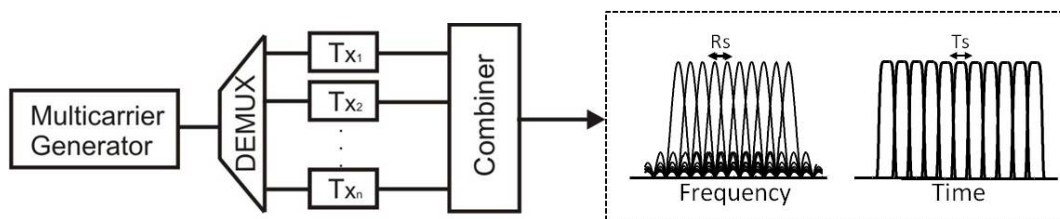


Figure 6-7: Example of a terabit superchannel made up of 10x100Gb/s subcarriers, generated with a multi-carrier transmission technique.

### Optical OFDM (CO-OFDM)

OFDM is a technology that has been widely used in almost all the major RF communication standards for almost 4 decades now [42]. Its application to optical communications is rather recent yet it has almost monopolized the attention of the research community in the recent years for its application in long-haul systems due to its intrinsic flexibility and scalability [43]-[45]. {Take this out}

The OFDM multi-carrier solution is based on the use of coherent optical carriers that are orthogonally multiplexed in the frequency (wavelength) domain. It is noted that the implementation of OFDM directly on multiple optical carriers is referred also as coherent OFDM (CO-OFDM) [46] to separate with the electronic version of OFDM which is generated with advanced digital signal processing (DSP) and applies in electrical carriers modulated then on one optical carrier [47], [48]. This scheme allows the maximum theoretical spectral efficiency to be achieved by placing the carrier at the minimum spectral distance equal to the aggregated baud rate of the modulated signal per carrier. As it is shown in Figure 6-8, the subchannel individual spectra have overlapping sidelobes, crossing exactly at the maxima or minima of the neighbouring spectral channels' sidelobes, thus cancelling out the intersymbol interference among the adjacent channels. The principle of the coherent and orthogonal carrier multiplexing in the frequency imposes the necessary condition for the penalty free demultiplexing of the carriers at the receiver end by coherently tuning the receiver to the required subchannel carrier while the other appear as uncorrelated noise.



**Figure 6-8:** Generic design of a Co-OFDM transmitter and signal output. Co-OFDM signals consist of sinc-shaped subcarriers in the frequency domain and rectangular pulses in the time domain.

For the generation of CO-OFDM signals, a single laser multicarrier generator is required in order to maintain a coherent phase and most importantly a stable spectral difference among the carriers [48]. The orthogonally spaced coherent carriers are then separated and modulated individually. The modulated carriers are combined again resulting in a multicarrier signal with orthogonally overlapping spectra among the carriers. The carrier separation and signal combination process requires increased accuracy among the different paths in order to maintain the orthogonality properties. This can be achieved only with the use of integrated transmitters incorporating arrays of modulators over fixed waveguide paths. However, the integration of a large number of modulators in one photonic integrated chip is still rather challenging [49]. Additionally, another critical issue for the realization of CO-OFDM systems stems from the separation and detection of the orthogonally multiplexed carriers. This can be performed with the combination of coherent detection and intensive DSP, mimicking the FFT process required [50]. However the real time implementation of DSP over a wide spectrum is limited in practise by the bandwidth of the available electronics. A more practical solution has been proposed in [51] which implements the FFT process directly in the optical domain allowing up to 8 CO-OFDM carriers to be separated and then processed individually. Finally, the extreme sensitivity of CO-OFDM in phase noise requires

also the use of optical carriers with ultra-low linewidth  $<0.5\text{MHz}$  [48] both for the subcarrier generator and the local oscillator at the coherent detector, in order to increase the performance of the orthogonal carriers at the receiver after detection.

### Nyquist WDM

Nyquist-WDM is a multi-carrier solution recently proposed and is based on the so-called “Nyquist principle” [52]. Terabit superchannels utilizing the N-WDM technique have been experimentally demonstrated [53], [54]. Shaping the sub-carrier spectrum so as to take a rectangular formation and approach the Nyquist-limit is an efficient way to improve spectral efficiency. According to the Nyquist principle, achieving a rectangular spectral shape with bandwidth equal to the symbol rate allows for inter-symbol interference-free transmission. As depicted in Figure 6-9 right, the rectangular spectra of N-WDM transform to sinc-like shaped optical pulses in the time domain demonstrating an interesting reverse correspondence to the equivalent CO-OFDM output signals.

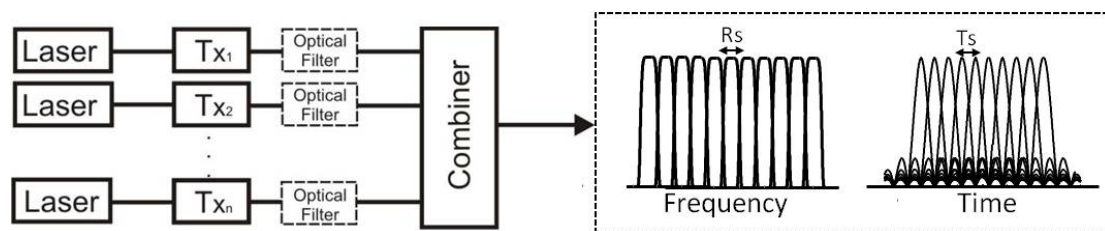


**Figure 6-9:** Generic design of a Nyquist-WDM transmitter and signal output. Nyquist-WDM superchannels consist of rectangular-shaped subcarriers in the frequency domain and sinc pulses in the time domain.

Nevertheless the ideal spectral shaping required for N-WDM is not trivial to be achieved. After modulating the individual subcarriers with the selected modulation format (e.g. 112 Gb/s POLMUX-QPSK) and before multiplexing them a special optical filter is required as shown in Figure 6-9 in order to obtain a quasi-rectangular frequency shape [55]. A 4<sup>th</sup>-order Super-Gaussian filter was used by the authors in [52] optimizing each time the 3dB bandwidth for the selected modulation format.

An alternative solution to band-limiting the modulated subcarriers with specific filters, involves driving electro-optical modulators with appropriate electrical signals that force the modulated carriers to take the desired rectangular shape. This technique requires DACs at the transmitter to generate the driving signals and can be considered as the “digital” N-WDM equivalent. “Digital” N-WDM was experimentally demonstrated in [56] where a channel spacing of  $1.05 \times$  (symbol rate) was achieved for a superchannel that consisted of 16 112 Gb/s POLMUX-QPSK subcarriers and was transmitted over 3,700 km. The receiver structure of a N-WDM superchannel does not vary depending on the selected modulation format and it includes a conventional coherent receiver for each of the received subcarriers with corresponding DSP at the end.

### Multi-band OFDM

A more practical alternative to the CO-OFDM approach that utilises the concept of OFDM while at the same time resembles the spectral characteristics of the N-WDM method is the multi-band OFDM (MB-OFDM) multicarrier scheme [57]. This scheme multiplexes RF generated OFDM channels over closely spaced coherent optical carriers resulting in increased spectral efficiency that mainly stems from the intrinsic efficiency of the electronic OFDM format. It is noted that the CO-OFDM solution considers coherent and orthogonal

carriers generated directly in the optical domain. The key advantage of this technique is that the spectrally efficient OFDM signal is restricted to spectral band that is able to be handled directly by advanced electronics and DSP modules, while the ultra-high super-channel capacity is achieved with the coherent multiplexing of multiple RF generated OFDM bands. Moreover, the RF OFDM signal per subchannel has an almost rectangular spectral shape, allowing the close spectral position of the multiple bands with minimum spectral overlapping as in the case of N-WDM [58].

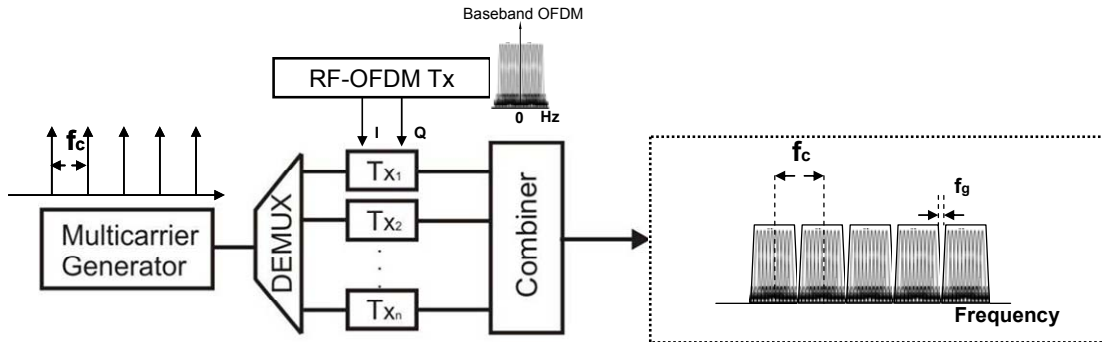


**Figure 6-10:** Generic design of a multi-band OFDM transmitter and signal output. Multi-band OFDM superchannels consist of RF generated OFDM channels with almost rectangular-shaped spectra separated by a small guard band.

The concept of a MB-OFDM transmitter is presented in Figure 6-10. A multicarrier generator provides a set of coherent optical carriers with spectral difference of  $f_c$  Hz. These carriers are demultiplexed and each one is modulated with a different RF-generated OFDM signal. The combined bands of OFDM subchannels have a small guard band,  $f_g$ , in order to avoid any interference between the adjacent OFDM subcarriers of neighbouring bands. This guard band is important as it affects the overall spectral efficiency, but studies shown that it can be kept to minimum typical value of around 2GHz [57]. The overall bandwidth of the OFDM channels must be equal or less than the difference of  $f_c$  and  $f_g$ .

MB-OFDM can be used as a practical solution to efficiently create subchannels with nearly rectangular spectra that can then be assembled into superchannels as it is shown in the combined spectrum at the right of Figure 6-10. Moreover at the lowest granularity level, each of the OFDM bands can be seen as a channel that includes a large number (tend to hundreds) of “electrical” subcarriers. Over the last year various transmission experiments have shown great potential. Up to 400 Gb/s [59] or 128 QAM [60] and transmission of a 1.12 Tb/s 32 QAM OFDM superchannel [61] have been demonstrated. The current state-of-the-art in the design of high performance OFDM transponders up to multi-100-Gbit/s data transport is mainly based on constellations that use QPSK and 8/16 QAM format for OFDM subcarrier modulation. However, for the transport of high information bit rates, over a limited spectral range, 2N-QAM (up to 256-QAM) formats have been reported.

It is noted that both MB-OFDM and CO-OFDM can in principle achieve the same maximum theoretical spectral efficiency (SE), which is also the same as that of N-WDM, introduced above. However the MB-OFDM and N-WDM approaches offer a much more practical solution both in terms of signal generation and detection as well as processing at the switching nodes at the optical subchannel level of the superchannel. Table 6-3 contains a brief comparison between N-WDM and MB-OFDM under the assumption that each subchannel uses full-rate serial transmission for N-WDM and that it uses a great number of electrical subcarriers for OFDM bands.

**Table 6-3:** Comparison between N-WDM and MB-OFDM

Parameters	N-WDM	MB-OFDM
Ultimate subchannel bandwidth	Equal to the symbol rate	Equal to the (aggregate) symbol rate
Ultimate subchannel spacing	Equal to the ultimate subchannel bandwidth	Equal to the ultimate subchannel bandwidth
Ultimate spectral efficiency	2M bit/sec/Hz (given a constellation with $2^M$ points and PM)	2M bit/sec/Hz (given a constellation with $2^M$ points and PM)
Factors preventing reaching the ultimate SE	Spectrum different than rectangular.	Side lobes et the edges of subchannel, cyclic prefix, training symbols
Sensitivity to phase noise	Mild: no problem with commercial SC tuneable lasers, at least up to 16QAM	High: due to the long symbol times, countermeasures must be adopted to combat it
Bit rate flexibility	Good: bit rate can be changed by either changing the symbol rate or (coarsely) by changing Tx format	Excellent: bit rate can be changed by either using fewer electrical subcarriers at the edges or (coarsely) by changing Tx format
Bit rate granularity	Data stream logical separation is done by framing and TDM	Ideally each electrical subcarrier could be an independent logical data stream
DSP computational effort	Ideally the same for the two cases In practice so far 20-30% larger effort for N-WDM is required	Ideally the same in the two cases. However, due to the block nature of OFDM, tracking of fast phenomena (such as polarization variation) can only occur at the block rate.
Non-linear transmissive performance	Same as for standard single carrier systems. 16-QAM and higher level modulation schemes have higher non-linear limitations.	Same as for N-WDM for non-dispersion compensated links. In case of dispersion compensation OFDM suffers from high peak-to-average power ratio (PAPR) leading to high non-linear limitations.

## 6.5. Software-Defined Optics

Looking back at the evolution of optical networks, one will observe software playing an increasing role in the various layers of the network. Depending on the application, software-defined processes promise improved performance features through better network control, optimized utilization of the available resources, easier and faster service delivery. On the whole software-based solutions empowered the network with an increased level of “intelligence” and agility. Although this has been generally true for the higher layers, the optical layer has failed to follow the same course.

More recently though the advances in electronics and signal processing, have boosted research even in the optical layer mainly focusing on the development of transponders (transmitter + receiver) that are able to adjust their operational parameters i.e. data rates and bandwidth according to demand. Programmable transponders and optical nodes will

provide just the flexibility required to plan and reconfigure a network in the new era of optical networking.

Progress in coding, modulation and signal processing in optics has been following a similar path with the evolution followed in wireless systems although with a certain difference in time. In fact the term *software-defined optics* (SDO) [63] has been adopted from radio where the concept of software-defined radio (SDR) [64], [65] is well established for more than a decade now and refers to devices where almost all waveform properties are defined in software. Looking closer to the evolution in radio systems, one may observe a continuous effort to increase spectral efficiency that started with the use of QPSK and saturated with the use of 512QAM and a spectral efficiency of 11Bits/s/Hz in the early part the previous decade. Following this advancement, research in radio switched focus to cost-effective and self-adaptive schemes that would cope with the limitations related with required SNR of the advanced modulation formats (as discussed in section 6.1) and would offer a higher degree of flexibility. Thus SDR was introduced to allow adaptation to the varying systems conditions in a cost-effective manner without physical interventions. Cost-effectiveness is achieved as the software-defined processes allow new features and capabilities to be added to existing systems without requiring new hardware.

Justified by the similar steps followed in optics in the recent past, it is fair to expect that evolution in optics will resemble that in radio and will not just focus on ever-growing spectral efficiency through advanced modulation formats and multicarrier schemes. Rather SDO is emerging already so as to bring flexibility and cost-efficiency in a similar manner as in SDR. SDR is defined as “Radio in which some or all of the physical layer functions are software defined”. Correspondingly, SDO can be described as a set of software-based solutions where some of the optical transmission operations are performed through modifiable software operating on *programmable* processing technologies (e.g. Field Programmable Gate Arrays (FPGA), Digital Signal Processors).

In [63] SDO refers to optical layer devices that are (i) intelligent and self-aware and (ii) programmable. To date enhancing the optical network with “intelligence” implied operations in the higher network layers. Indeed, higher layers were generally unaware of exactly how bits are transmitted. In contrast, the emergence of SDO facilitates cross-layer optimization processes that really take advantage of the advanced functionality of the physical layer. As a case in point, SDO enables operators to exploit the trade-off discussed in section 6.1, between capacity, transmission reach, and bandwidth using software-defined flexible transponders [27]. Essentially the same transponder within sufficient system margin may provide large capacity over short distances or lower capacity over longer distances. In addition software defined transponders are expected to find applications in resilience mechanisms [67]. Cost savings are expected by avoiding 100% resilience capacity. What is more, different types of traffic may be supported in protection scenarios by the flexible transponders, i.e. high-priority and low-priority traffic. Under failure conditions, transponders discard the low-priority and keep only the high priority traffic. In general the flexibility of the transponder and the fact that their properties can be defined in software allow savings in capital that stems from the minimized number of required optical interfaces.

To better illustrate the adaptation feature, example use-cases of a software-defined transponder are described next [68]:

- (i) An existing optical connection with certain bandwidth requirements (e.g. an available spectral band of specific size) requires higher capacity. The flexible transponder will be utilized to adjust the modulation level of the carriers and therefore the data rate in

order to accommodate the requested capacity while conforming to the specific bandwidth requirements.

- (ii) An existing optical connection with certain capacity requirements needs to be accommodated in a narrower spectral band (e.g. to serve more traffic). The flexible transponder will be utilized to increase the number of bits per symbol of the carriers reducing the symbol rate and occupying less spectrum, yet delivering the required data rate.
- (iii) Apart from reducing the symbol rate as in use-case (ii), an existing optical connection can adjust the optical bandwidth by varying the number of subcarriers accordingly. Provided that there is enough system margin the bandwidth can be reduced by using higher modulation level, keeping the same symbol rate and utilizing fewer subcarriers.

The authors in [69] demonstrated a software-defined multiformat transmitter that can change formats ranging from OOK to 16QAM at 30 Gbaud while in [70] they demonstrated a transmitter that achieves switching between 8 different formats within 5ns.

In addition to flexible transponders, technological advancements have allowed the introduction of software defined optical nodes that essentially enable the gridless functionality in the optical transport. Programmable WSSs based on LCOS switching elements [31], [71] where the bandwidth and the center frequency can be dynamically changed, are today a commercial reality triggering the cost-efficient implementation of flexible nodes.

## 6.6. Experimental Investigation of a Multi-carrier Spectrum-flexible System

The concept of a spectrum flexible heterogeneous superchannel has been studied experimentally with the purpose to investigate the extraction of the appropriate physical-layer performance parameters (for a given optical link) required for use in resource allocation mechanisms of future flexible networks [72]. This extensive experimental study has been performed in collaboration with the DTU Fotonik Department of Photonics Engineering Metro-Access and Short Range Systems under the EU funded Network of Excellence project EUROFOS and conducted at the DTU Fotonik laboratory.

More specifically the work explored the physical layer parameters for dynamic resource allocation in spectrum-flexible networking and investigated the performance requirements needed for coherent multicarrier signals with variable format to be established within the available spectral slots of a superchannel, defined by a spectral window of variable width. In order to study this concept, several networking scenarios have been proposed and investigated over an experimental configuration emulating a set of different traffic demands. These traffic demands were served by allocating various combinations of 14 Gbaud DP-16QAM and DP-QPSK signals within the available spectrum of a 15-subcarrier long superchannel.

In what follows first the overall networking concept and the extracted scenarios are presented, followed by the description of the utilized experimental set-up. Finally, the physical layer performance parameters are extracted and commented for their use in an adaptive resource allocation mechanism for flexible network connections.

### Concept and implemented scenarios

In flexible optical networking, the introduction of flexibility (in terms of bandwidth, bit rate and signal format) imposes complex requirements with respect to the spectrum and



capacity allocation over the network's links that stem from the fact that routing algorithms should now perform an exhaustive search through a large number of possible solutions. This particularly applies in the operational phase of a network where traffic is changing with time, leaving windows of spectrum of variable size unused [26]. Special routing algorithms are required to decide the route, the modulation format, the bandwidth and the location inside the available spectrum gaps for each incoming traffic demand. Moreover, interference from the neighbouring channels has to be taken into account and sufficient guard-bands ought to be considered.

The introduction of a multicarrier-based superchannel in flexible networking (as this was defined earlier in this chapter) provides two levels of data grooming in the optical domain, allowing every connection between a pair of nodes to be carried over bands of spectrum with variable width within a superchannel. The spectral width of the available bands depends on the number of the available subcarriers and the traffic demand that has already been allocated. During network operation the spectral occupancy changes dynamically with time leaving spectral gaps available for future demands. In the following paragraphs, this spectral window within the superchannel is referred to as band-of-interest (BOI). In a BOI a source node can request and allocate a part or the entire band to a certain traffic demand. Depending on the traffic requirements and the link length, the adequate wavelength allocation, modulation format and bit rate should be used.

The assignment of the appropriate subcarrier(s), the rate and signal format should be determined by an intelligent spectrum and resource allocation mechanism based on extrapolated knowledge derived or estimated from past events [73]. This is the main concept of a cognitive and empirical decision system that in principle builds up a knowledge database of the performance of all possible signal combinations that could be found within a multicarrier superchannel and over certain link lengths in a flexible network. Such a mechanism, requires initially a limited set of measured performance values for each link and then based on this set of measurements it can extract (actually estimate) the expected performance of similar signal combinations.

In order to define and evaluate this concept, a number of transmission scenarios for different BOIs' bandwidths, wavelength allocation schemes, and modulation formats were designed and implemented. These scenarios are illustrated in the 2nd column of Table 6-4. In the examined cases shown here, the superchannel was composed by two outer bands, each one with four DP-QPSK modulated CO-OFDM subcarriers (red dashed arrows), surrounding the central band, which was the BOI (shadowed area). In scenarios A-D two dual-polarization (DP) 16-QAM carriers occupy the BOI, surrounded by eight DP-QPSK channels. A variable bandwidth BOI was investigated of 98 GHz (scenarios A, B, G, H), 70 GHz (C, F) and 42 GHz (D, E). The BOI was filled with either DP-16QAM (A, B, C, D) or DP-QPSK (G, H, F, E) modulated carriers. Illustrative spectrum allocation schemes and number of subcarriers for each scenario are shown in Table 6-4. The measured performance of the aforementioned scenarios constitutes the input that allows the network to adjust its characteristics with respect to offered capacity, spectral efficiency or reach.

It is noted that for the experimental studies a fixed link length was considered as a reference link in all cases and the performance metric was the required OSNR level for a BER of  $1 \times 10^{-3}$ . The RSONR is essential in order to compare the various cases and identify the operational limits required by the networks' control plane, so that in turn to decide whether a traffic demand should be served or not over a given BOI and what is the optimum type of format that can be used for the specific link length to increase the spectral utilization.

**Experimental configuration**

The experimental setup used for the study of all the defined flexible spectrum allocation scenarios is shown in Figure 6-11. At the transmitter side, the system is equipped with two independent transmitters (Tx), one used for 112 Gb/s DP-16QAM and one for 56 Gb/s DP-QPSK signal generation. For the 16QAM signal generation, two independent tunable external cavity lasers (ECLs) with a 100 kHz linewidth are modulated with a QAM signal in an I/Q modulator driven by four streams of 14 Gb/s binary electrical waveforms resulting in two 56 Gb/s 16QAM signals. The detailed setup for the electrical part of the 16-QAM Tx follows the approach reported in [74]. Later these signals are polarization multiplexed resulting in two 112 Gb/s POLMUX-16QAM data streams. For the CO-OFDM POLMUX-QPSK signals first a comp generator has been implemented following the set-up proposed in [48], which is based on single sideband frequency shift effect multiplied in spectrum with the use of single fibre loop. The comp generator was used to create subcarriers (SCs) with 14GHz spacing from one tunable ECL laser with a 100 kHz linewidth. This scheme provided 15 stable and coherent subcarriers which defined the total length of the superchannel.

For the generation of the appropriate spectral window that defines the BOI, a waveshaper was introduced to adaptively reject the appropriate number of subcarriers around the center band of the superchannel. Next, the remaining subcarriers were amplified and modulated with a QPSK signal by an I/Q modulator driven with two 14 Gb/s decorrelated electrical data streams. This resulted in a spectrally adjustable (by the waveshaper) OFDM QPSK signal surrounding the BOI. At the output of the transmitter the two bands of OFDM QPSK signals and the 16QAM signals were combined through a 3-dB coupler. Variable attenuators were used at the outputs of the two transmitter arms in order to maintaining the same average power per channel for all channels launched in the system. Finally, the total signal was again amplified and polarization-division multiplexed to double the overall capacity. An example of the spectrum for the total signal referring to case A is shown as inset in Figure 6-11.

The aforementioned flexible transmitter set-up allowed any combination of 16-QAM and QPSK signals to be generated inside BOI with a variable spectral width. This was achieved by setting up properly the waveshaper profile and activating/deactivating the QPSK subcarriers within the BOI and/or the 16-QAM channels.

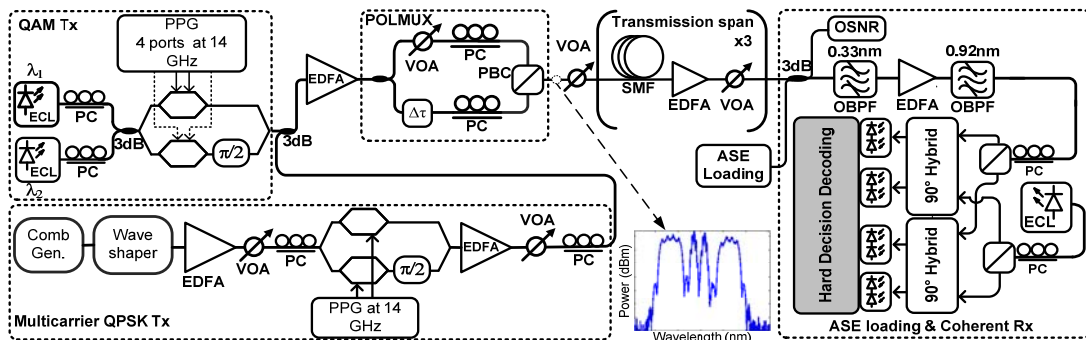


**Figure 6-11:** Experimental set-up for the study of spectrum allocation scenarios within a BOI of a superchannel.

At the output of the transmitter, the multicarrier signal under test was attenuated to an optimal power level and then launched into a 250 km transmission link. In the presented set of experiments the overall power was fixed at  $-2$  dBm per channel, which yields approximately to 8 dBm, 8.4 dBm and 9.1 dBm total input power to the fiber for, 10, 11 and

13 channels respectively. The transmission link was composed of three standard single mode fiber (SMF) spans of lengths 68 km, 80 km and 104.5 km, each followed by an EDFA and a variable optical attenuator (VOA). VOAs were used to keep the same input power level at the inputs of the consecutive spans of the link. ASE noise loading was performed after the last transmission span in order to vary the received OSNR and measure the required OSNR (ROSNR) level for a given bit error ratio (BER).

At the receiver side, a 0.33 nm 3-dB bandwidth band-pass filter (BPF) was used to filter out the central wavelength which was then preamplified and filtered again by a 0.92 nm 3-dB bandwidth BPF to remove out-of-band ASE noise. The signal was detected in a polarization- and phase-diversity coherent receiver. The local oscillator (LO) used was an ECL with 100 kHz 3 dB linewidth. The outputs of photodetectors were sampled using a real-time digital oscilloscope and stored for offline processing. The demodulated channel for scenarios A-D, is the one at the lower wavelength, whereas for scenarios E-H is the central one. For scenarios E-H the experimental setup is the same as in Figure 6-11, except the fact that the QAM Tx is disconnected and the Waveshaper is reconfigured to pass both the two outer bands and the BOI.

**Measured results and discussion**

The BER performance versus OSNR was examined for each of the flexible multicarrier traffic allocation scenarios presented above. Moreover, for each case we have calculated:

- a) the total aggregated traffic,
- b) the allocated traffic within the BOI,
- c) the spectral width of the available BOI (in multiples of the available SCs) and
- d) the achievable BOI spectral efficiency, defined as the ratio of the aggregated traffic within a BOI over the total spectral width of the available BOI.

All the above data together with the required OSNR (ROSNR) level for a BER of  $1 \times 10^{-3}$  being extracted for each of the 9 scenarios are summarized in Table 6-4. The table also contains the single carrier POLMUX-QPSK and POLMUX -16QAM measurements in both back-to-back and after transmission.

**Table 6-4:** Investigated scenarios and data obtained from the analysis of the results

Scenario	Spectrum allocation	BOI [GHz]	BOI capacity [Gb/s]	Total capacity [Gb/s]	Sp. Efficiency [b/s/Hz]	ROSNR for BER $10^{-3}$ [dB]
A		98	224	672	2.29	27.3
B		98	224	672	2.29	30.9
G		98	168	616	1.71	19.6
H		98	280	728	2.86	20.1
C		70	224	672	3.20	32.7
F		70	168	616	2.40	21
D		42	224	672	5.33	>35
E		42	168	616	4.00	22

From this study it is evident that a 98GHz (7 SC of 14GHz) BOI can be filled with up to 7 SCs with DP-QPSK data (case E) if ROSNR is above 24.9dBm. By reducing the number of allocated DP-QPSK SCs within the BOI to 5 and 3 (cases G and H) the ROSNR drops to 23.9dB and 19.6 dB respectively, at an expense though of reduced BOI spectral efficiency. It is important to note that safe conclusions on the ROSNR level can also be extracted for the cases of 2, 4 and 6 POLMUX-QPSK SCs, since these are expected to lie within the ROSNR levels of the measured cases.

Alternatively, the 98GHz BOI can be filled with two POLMUX-16QAM SCs (case A) at a ROSNR level of at least 27.3dB. In this case, POLMUX-16QAM SCs have been located 28GHz apart and at the centre of the BOI. Additional studies (case B) shown that if the two POLMUX-16QAM SC are located further apart to each other (by 56GHz), but closer to the neighboring channels of the BOI (by 28GHz) then the ROSNR increases to 30.9dB. This indicates that a traffic allocation mechanism should take into consideration not only the width of the BOI but also the spectral position of the channels within the BOI.

Considering a shorter BOI of 70GHz (5 SCs of 14GHz) being initially filled with 3 POLMUX-QPSK SCs (case F) a ROSNR level of 23.9dB is observed. This ROSNR level is similar to that of case H, denoting that the performance is mainly affected by the spectral distance of the allocated SCs from the neighboring channels of the BOI. The performance of the full POLMUX-QPSK SC allocation within the 70GHz BOI is defined again by case E (24.9dB ROSNR). The same BOI of 70GHz can also be filled with 2 POLMUX-16QAM SCs (case C) resulting in an increased ROSNR level of 32.7dB due to the close spectral proximity with the neighboring channels to the BOI.

Finally, it was observed that a short BOI of 42GHz is not possible to accommodate two POLMUX-16QAM channels (case D) since the close spectral proximity (14GHz) to the non-orthogonal adjustment channels leads to increased errors. On the other hand the allocation of three POLMUX-QPSK orthogonal channels is acceptable and refers to case E.

It is important to note that for cases F, G and H the measurements of the ROSNR refer to the middle channel of the allocated SCs within the BOI. Measurements on the other channels inside the BOI show a small only improvement in the ROSNR level that is up to 1dB for case G which has the largest spectral distance (42GHz) to the neighboring channels. For all other cases the ROSNR level of the SCs is very similar (<0.2dB of difference) and the worst value is reported in Table 6-4.

The 8 scenarios that have been evaluated for the specific link provide a set of the possible combinations for heterogeneous signal allocation (QPSK and 16QAM) within the available BOI. However, based on this set of measurements, some additional performance indications can be safely extracted for other scenarios that have not been evaluated. Therefore one may conclude that since performance is mainly affected by the spectral distance of the SC with the neighboring channels of the BOI, it is expected that:

- for the case of 70GHz BOI, the performance of 4 DP-QPSK subcarriers will be closer to that of 5 DP-QPSK subcarriers.
- for the case of 98GHz BOI, the performance of 6 DP-QPSK subcarriers will be closer to that of 7 DP-QPSK subcarriers.
- for the case of 42GHz BOI a single PD-16QAM channel allocated in the middle is expected to have the same performance as in case C.
- for the case of 98GHz BOI the allocation of three PD-16QAM channels with one subcarrier spectral distance is expected to have the same performance as in case C

These measurements and the extracted performance estimation criteria are essential for the identification of the system's physical layer parameters required in order to assign

(or not) specific capacity demands over given available BOIs on per link basis. Moreover, as it was mentioned in the overall concept, the identified ROSNR level from a limited number of spectrum filling scenarios can be used as initial values by a cognitive control algorithm to estimate the expected performance of many other cases, thus optimizing the processing complexity during the operational phase of a network.

## 6.7. Chapter Summary

This chapter summarizes the solutions proposed by the research community to implement the next generation core optical networks. It describes both the rate-specific solution of a mixed-line rate network and the flexible optical network that, regardless of the employed technology, has the ability to adapt to the traffic demands. Flexible optical networks are bandwidth agnostic and can allocate just the amount of network resources needed under certain traffic and networking conditions. The associated technologies and concepts that enable the vision of flexible optical networks are also presented, including the advanced modulation formats that offer higher spectral efficiency, the concept of a spectrum-flexible grid, software-defined optical transmission, single-carrier adaptive solutions and multi-carrier technologies.

In addition this chapter reports on the experimental investigation of a superchannel in the context of a flexible core network with heterogeneous capacity demands. For the first time the requirements of the physical layer parameters for a spectrum-flexible optical superchannel were experimentally investigated. The ROSNR levels for BER of  $1 \times 10^{-3}$  for a number of scenarios with variable BOIs being dynamically filled with DP-QPSK and DP-16-QAM with variable bit rates has been the main outcome of this effort. The importance of the result is that it can act as input for cognitive control algorithms to implement the new paradigm of flexible optical networks. Physical layer performance estimation in the new era of optical networks requires a somewhat different approach compared to the conventional single line-rate network. New challenges are imposed on analytical impairment modelling thus making the solution of combining experimental results with cognitive algorithms a rather attractive solution.

## 6.8. References

- [1] René-Jean Essiambre, Gerhard Kramer, Peter J. Winzer, Gerard J. Foschini, and Bernhard Goebel, "Capacity Limits of Optical Fiber Networks," *J. Lightwave Technol.* 28, 662-701 (2010).
- [2] M. Jinno, H. Takara, B. Kozicki, Y. Tsukishima, Y. Sone, S. Matsuoka, "Spectrum-efficient and scalable elastic optical path network: architecture, benefits, and enabling technologies," *IEEE Communications Magazine*, 47, 66-73 (2009).
- [3] C. Meusburger and D. Schupke, "Optimizing the Migration of Channels with Higher Bit-Rates," in *Proceedings of OFC 2009*, paper PDPD3.
- [4] T. Ito, K. Sekiya, and T. Ono, "Study of 10 G/40 G hybrid ultra longhaul transmission systems with reconfigurable OADMs for efficient wavelength usage," in *Proceedings of ECOC 2002*, paper 1.1.4.
- [5] K. Nakamura, H. Ooi, A. Miura, T. Katagiri, T. Naito, and G. Ishikawa, "10 G/40 G-hybrid sense-WDM systems with flexible OADM upgradability," in *Proceedings of ECOC 2003*, paper Tu3.6.6.
- [6] H. Griesser, J.-P. Elbers, "Influence of Cross-Phase Modulation Induced Nonlinear Phase Noise on DQPSK Signals from Neighbouring OOK Channels", in *Proceedings of ECOC 2005*.
- [7] S. Chandrasekhar, X. Liu, "Impact of Channel Plan and Dispersion Map on Hybrid DWDM Transmission of 42.7-Gb/s DQPSK and 10.7-Gb/s OOK on 50-GHz Grid", *IEEE Photonics Technology Letters*, 19, 1801-1803 (2007).

- [8] C. R. S. Fludger, T. Duthel, D. van den Borne, C. Schulien, E-D. Schmidt, T. Wuth, E. de Man, G. D. Khoe, and H. de Waardt, "10 x 111 Gbit/s, 50 GHz spaced, POLMUX-RZ-DQPSK transmission over 2375 km employing coherent equalisation," in Proceedings OFC 2007, paper PDP22.
- [9] G. G. Charlet, J. Renaudier, H. Mardoyan, P. Tran, O. Bertran Pardo, F. Verluise, M. Achouche, A. Boutin, F. Blache, J. -y. Dupuy, and S. Bigo, "Transmission of 16.4Tbit/s capacity over 2,550km using PDM QPSK modulation format and coherent receiver," in Proceedings of OFC 2008, paper PDP3.
- [10] T. Wuth, M. W. Chbat, and V. F. Kamalov, "Multi-Rate (100G/40G/10G) Transport over Deployed Optical Networks," in National Fiber Optic Engineers Conference, in Proceedings of OFC 2008, paper NTuB3.
- [11] X. Liu and S. Chandrasekhar, "High Spectral-Efficiency Mixed 10G/40G/100G Transmission," in Proceedings of AOE 2008, paper SuA2.
- [12] Alfiad, M.S.; Kuschnerov, M.; Wuth, T.; Xia, T.J.; Wellbrock, G.; Schmidt, E.-D.; van den Borne, D.; Spinnler, B.; Weiske, C.J.; de Man, E.; Napoli, A.; Finkenzeller, M.; Spaelter, S.; Rehman, M.; Behel, J.; Chbat, M.; Stachowiak, J.; Peterson, D.; Lee, W.; Pollock, M.; Basch, B.; Chen, D.; Freiberger, M.; Lankl, B.; de Waardt, H.; , "111-Gb/s Transmission Over 1040-km Field-Deployed Fiber With 10G/40G Neighbors," IEEE Photonics Technology Letters, 21, 615-617, (2009).
- [13] Xia, T.J.; Wellbrock, G.; Peterson, D.; Lee, W.; Pollock, M.; Basch, B.; Chen, D.; Freiberger, M.; Alfiad, M.; de Waardt, H.; Kuschnerov, M.; Lankl, B.; Wuth, T.; Schmidt, E.D.; Spinnler, B.; Weiske, C.J.; de Man, E.; Xie, C.; van den Borne, D.; Finkenzeller, M.; Spaelter, S.; Derksen, R.; Rehman, M.; Behel, J.; Stachowiak, J.; Chbat, M.; , "Multi-rate (111-Gb/s, 2x43-Gb/s, and 8x10.7-Gb/s) transmission at 50-GHz channel spacing over 1040-km field-deployed fiber," in Proceedings of ECOC 2008, paper Th.2.E.2.
- [14] A. Bononi, M. Bertolini, P. Serena, and G. Bellotti, "Cross-Phase Modulation Induced by OOK Channels on Higher-Rate DQPSK and Coherent QPSK Channels," J. Lightwave Technol. 27, 3974-3983 (2009).
- [15] N. Sambo, F. Cugini, M. Secondini, G. Bottari, F. Cavaliere, P. Iovanna, P. Castoldi, "10-40 Gbit/s Multi Bit-rate GMPLS-controlled Transparent Optical Networks in Presence of Cross-phase Modulation", in Proceedings of ECOC 2010, paper Th.10.F.4.
- [16] N. Sambo, F. Cugini, M. Secondini, P. Iovanna, G. Bottari, P. Castoldi, "Enforcing QoT via PCE in Multi Bit-Rate WSONs," IEEE Communications Letters, 15, 452-454, (April 2011).
- [17] N. Sambo, M. Secondini, F. Cugini, G. Bottari, P. Iovanna, F. Cavaliere, and P. Castoldi, "Modeling and Distributed Provisioning in 10-40-100-Gb/s Multirate Wavelength Switched Optical Networks," J. Lightwave Technol. 29, 1248-1257 (2011).
- [18] A. Nag, M. Tornatore, and B. Mukherjee, "Optical Network Design with Mixed Line Rates and Multiple Modulation Formats," in Proceedings of OFC 2009, paper PDP2.
- [19] Avishek Nag, Massimo Tornatore, and Biswanath Mukherjee, "Optical Network Design With Mixed Line Rates and Multiple Modulation Formats," J. Lightwave Technol. 28, 466-475 (2010).
- [20] A. Nag and M. Tornatore, "Transparent vs. Translucent Optical Network Design with Mixed Line Rates," in Optical Fiber Communication Conference, in Proceedings of OFC 2009, paper OWI7.
- [21] M. Batayneh, D.A. Schupke, M. Hoffmann, A. Kirstaedter, B. Mukherjee, "On Routing and Transmission-Range Determination of Multi-Bit-Rate Signals Over Mixed-Line-Rate WDM Optical Networks for Carrier Ethernet," IEEE/ACM Transactions on Networking, 19, 1304-1316 (2011).
- [22] O. Rival, A. Morea, J.-C. Antona, "Optical network planning with rate-tunable NRZ transponders," Optical Communication, 2009. ECOC '09. 35th European Conference on , vol., no., pp.1-2, 20-24 Sept. 2009
- [23] A. Klekamp, O. Rival, A. Morea, R. Dischler, and F. Buchali, "Transparent WDM Network with Bitrate Tunable Optical OFDM Transponders in Proceedings of OFC 2010, paper NTuB5.
- [24] A. Morea, O. Rival, "Advantages of Elasticity versus Fixed Data-rate Schemes for Restorable Optical Networks," in Proceedings of ECOC 2010, paper Th.10.F.5.
- [25] O. Rival and A. Morea, "Cost-efficiency of mixed 10-40-100Gb/s networks and elastic optical networks," in Proceedings of OFC 2011, paper OTu4.

- [26] **M. Angelou**, K.Christodoulopoulos, D. Klondis, A. Klekamp, F. Buchali, E. Varvarigos, I. Tomkos, "Spectrum, Cost and Energy Efficiency in Fixed-Grid and Flex-Grid Networks", in Proceeding of OFC 2012, paper NM3F.4.
- [27] M. Jinno, B. Kozicki, H. Takara, A. Watanabe, Y. Sone, T. Tanaka, and A. Hirano, "Distance-Adaptive Spectrum Resource Allocation in Spectrum-Sliced Elastic Optical Path Network", IEEE Communications Magazine, 48, 138-45 (2010).
- [28] P. J. Winzer, A. H. Gnauck, C. R. Doerr, M. Magarini, and L. L. Buhl, "Spectrally Efficient Long-Haul Optical Networking Using 112-Gb/s Polarization-Multiplexed 16-QAM," J. Lightwave Technol. 28, 547-556 (2010).
- [29] S. Chandrasekhar and X. Liu, "Terabit Superchannels for High Spectral Efficiency Transmission", in Proceedings of ECOC 2010, paper Tu.3.C.5.
- [30] A. Klekamp, R. Dischler, and F. Buchali, "Transmission Reach of Optical-OFDM Superchannels with 10-600 Gb/s for Transparent Bit-Rate Adaptive Networks," in Proceedings of ECOC 2011, paper Tu.3.K.2.
- [31] S. Frisken, G. Baxter, D. Abakoumov, H. Zhou, I. Clarke, and S. Poole, "Flexible and Grid-less Wavelength Selective Switch using LCOS Technology," in Proceedings of OFC 2011, paper OTuM3.
- [32] K. Christodoulopoulos, I. Tomkos, E. Varvarigos, "Elastic Bandwidth Allocation in Flexible OFDM-based Optical Networks," J. Lightwave Technol., 29, 1354-1366 (2011).
- [33] W. Zheng, Y. Jin, W. Sun, W. Guo, and W. Hu, "On the Spectrum-Efficiency of Bandwidth-Variable Optical OFDM Transport Networks," in Proceedings of OFC 2010, paper OWR5.
- [34] G. Shen and Q. Yang, "From Coarse Grid to Mini-Grid to Gridless: How Much can Gridless Help Contentionless?," in Proceedings of OFC 2011, paper OTuI3.
- [35] A. Bocoï, M. Schuster, F. Rambach, M. Kiese, C. Bunge, and B. Spinnler, "Reach-Dependent Capacity in Optical Networks Enabled by OFDM", in Proceedings of OFC 2009, paper OMQ4.
- [36] K. Christodoulopoulos, I. Tomkos, E. Varvarigos, "Spectrally/Bitrate Flexible Optical Network Planning", ECOC 2010.
- [37] K. Christodoulopoulos, I. Tomkos, and E. Varvarigos, "Dynamic Bandwidth Allocation in Flexible OFDM-based Networks," in Proceedings of OFC 2011, paper OTuI5.
- [38] A. N. Patel, P. N. Ji, J. P. Jue, and T. Wang, "Defragmentation of Transparent Flexible Optical WDM (FWDM) Networks," in Proceedings of OFC 2011, paper OTuI8.
- [39] T. Takagi, H. Hasegawa, K. Sato, Y. Sone, A. Hirano, and M. Jinno, "Disruption Minimized Spectrum Defragmentation in Elastic Optical Path Networks that Adopt Distance Adaptive Modulation," in Proceedings of ECOC 2011, paper Mo.2.K.3.
- [40] K. Wen, Y. Yin, D. J. Geisler, S. Chang, and S. J. B. Yoo, "Dynamic On-demand Lightpath Provisioning Using Spectral Defragmentation in Flexible Bandwidth Networks," in Proceedings of ECOC 2011, paper Mo.2.K.4.
- [41] O. Rival, G. Villares, and A. Morea, "Impact of Inter-Channel Nonlinearities on the Planning of 25–100 Gb/s Elastic Optical Networks," J. Lightwave Technol. 29, 1326-1334 (2011).
- [42] R. W. Chang, "Synthesis of band-limited orthogonal signals for multi-channel data transmission", Bell Syst. Tech. J., 45, 1775-1796 (1966).
- [43] W. Shieh and C. Athaudage, "Coherent optical orthogonal frequency division multiplexing," Electron. Lett., 42, 587-589 (2006).
- [44] A. J. Lowery, L. Du, and J. Armstrong, "Orthogonal frequency division multiplexing for adaptive dispersion compensation in long haul WDM systems," in Proceedings of OFC 2006, paper PDP 39.
- [45] I. B. Djordjevic and B. Vasic, "Orthogonal frequency division multiplexing for high-speed optical transmission," Opt. Exp., 14, 3767–3775 (2006).
- [46] Y. Ma, Q. Yang, Y. Tang, S. Chen, and W. Shieh, "1-Tb/s per channel coherent optical OFDM transmission with subwavelength bandwidth access," in Proceedings of OFC 2009, paper PDPC1.
- [47] R. Dischler and F. Buchali, "Transmission of 1.2 Tb/s continuous waveband PDM-OFDM-FDM signal with spectral efficiency of 3.3 bit/s/Hz over 400 km of SSMF," in Proceedings of OFC 2009, paper PDPC2.

- [48] S. Chandrasekhar, X. Liu, B. Zhu, D.W. Peckham, "Transmission of a 1.2-Tb/s 24-Carrier No-Guard-Interval Coherent OFDM Superchannel over 7200-km of Ultra-Large-Area Fiber", in Proceedings of ECOC 2009, paper PD2.6.
- [49] R. Nagarajan, M. Kato, J. Pleumeekers, P. Evans, S. Corzine, S. Hurtt, A. Dentai, S. Murthy, M. Missey, R. Muthiah, R.A. Salvatore, C. Joyner, R. Schneider, M. Ziari, F. Kish, D. Welch, "InP Photonic Integrated Circuits", IEEE Journal of Sel. Topics in Quantum Electronics, 16, 1113-1125 (2010).
- [50] X. Liu, S. Chandrasekhar, B. Zhu, and D. Peckham, "Efficient digital coherent detection of a 1.2-Tb/s 24-carrier no-guard-interval CO-OFDM signal by simultaneously detecting multiple carriers per sampling," in Proceedings of OFC 2010, paper OWO2.
- [51] D. Hillerkuss, M. Winter, M. Teschke, A. Marculescu, J. Li, G. Sigurdsson, K. Worms, S. Ben Ezra, N. Narkiss, W. Freude, and J. Leuthold, "Simple all-optical FFT scheme enabling Tbit/s real-time signal processing", OSA Optics Express Journal, Vol.18, No.9, pp.9324, April 2010.
- [52] G. Bosco, V. Curri, A. Carena, P. Poggiolini, F. Forghieri, "On the Performance of Nyquist-WDM Terabit Superchannels Based on PM-BPSK, PM-QPSK, PM-8QAM or PM-16QAM Subcarriers," J. Lightwave Technol., 29, 53-61 (2011).
- [53] G. Gavioli, E. Torrenco, G. Bosco, A. Carena, V. Curri, V. Miot, P. Poggiolini, M. Belmonte, F. Forghieri, C. Muzio, S. Piciaccia, A. Brinciotti, A. La Porta, C. Lezzi, S. Savory, and S. Abrate, "Investigation of the Impact of Ultra-Narrow Carrier Spacing on the Transmission of a 10-Carrier 1Tb/s Superchannel," in Proceedings of OFC 2010, paper OThD3.
- [54] J. Cai, Y. Cai, C. Davidson, D. Foursa, A. Lucero, O. Sinkin, W. Patterson, A. Pilipetskii, G. Mohs, and N. Bergano, "Transmission of 96x100G Pre-Filtered PDM-RZ-QPSK Channels with 300% Spectral Efficiency over 10,608km and 400% Spectral Efficiency over 4,368km," in Proceedings of OFC 2010, paper PDPB10.
- [55] G. Bosco, A. Carena, V. Curri, P. Poggiolini and F. Forghieri, "Performance limits of Nyquist-WDM and CO-OFDM in high-speed PM-QPSK systems", IEEE Photon. Technol. Lett., 22, 1129-1131 (2010).
- [56] R. Cigliutti, A. Nespola, D. Zeolla, G. Bosco, A. Carena, V. Curri, F. Forghieri, Yoshinori Yamamoto, Takashi Sasaki, P. Poggiolini, "Ultra-Long-Haul Transmission of 16x112 Gb/s Spectrally-Engineered DAC-Generated Nyquist-WDM PM-16QAM Channels with 1.05x(Symbol-Rate) Frequency Spacing," OFC 2012.
- [57] W. Shieh, H. Bao, and Y. Tang, "Coherent optical OFDM: theory and design," OSA Optics Express Journal, vol. 16, no. 2, pp. 841-859, 2008.
- [58] Qi Yang, N. Kaneda, Xiang Liu, S. Chandrasekhar, W. Shieh, Y.K. Chen, "Real-time coherent optical OFDM receiver at 2.5-GS/s for receiving a 54-Gb/s multi-band signal," Optical Fiber Communication (OFC) 2009, paper PDPC5, March 2009.
- [59] H. Takara, T. Goh, K. Shibahara, K. Yonenaga, S. Kawai, and M. Jinno, "Experimental Demonstration of 400 Gb/s Multi-flow, Multi-rate, Multi-reach Optical Transmitter for Efficient Elastic Spectral Routing," in 37th European Conference and Exposition on Optical Communications, OSA Technical Digest (CD) (Optical Society of America, 2011), paper Tu.5.A.4.
- [60] D. Qian, M. Huang, E. Ip, Y. Huang, Y. Shao, J. Hu, and T. Wang, "101.7-Tb/s (370x294-Gb/s) PDM-128QAM-OFDM Transmission over 3x55-km SSMF using Pilot-based Phase Noise Mitigation," in Optical Fiber Communication Conference, OSA Technical Digest (CD) (Optical Society of America, 2011), paper PDPB5.
- [61] X. Liu, S. Chandrasekhar, X. Chen, P. Winzer, Y. Pan, B. Zhu, T. Taunay, M. Fishteyn, M. Yan, J. M. Fini, E. Monberg, and F. Dimarcello, "1.12-Tb/s 32-QAM-OFDM Superchannel with 8.6-b/s/Hz Intrachannel Spectral Efficiency and Space-Division Multiplexing with 60-b/s/Hz Aggregate Spectral Efficiency," in 37th European Conference and Exposition on Optical Communications, OSA Technical Digest (CD) (Optical Society of America, 2011), paper Th.13.B.1.
- [62] D. van der Borne, V. Sleiffer, M.S. Alfiad, S.L. Jansen, T. Wuth, "POLMUX-QPSK modulation and coherent detection: the challenge of long-haul 100G transmission", ECOC'09, paper 3.4.1, 2009



- [63] G.N. Rouskas, R. Dutta, I. Baldine, "A new internet architecture to enable software defined optics and evolving optical switching models," in Proceedings of BROADNETS 2008, vol., no., pp.71-76, 8-11 Sept. 2008.
- [64] J. Mitola, "The software radio architecture. IEEE Communications Magazine", 33(5), 26-38, May 1995.
- [65] W. Tuttlebee (Ed.). Software Defined Radio. John Wiley, New York, 2002.
- [66] Wireless Innovation Forum, <http://www.wirelessinnovation.org/>
- [67] B. Teipen, K. Grobe, M. Eiselt, J.-P. Elbers "Adaptive Optical Transmission for Dynamic Optical Networks", in Proceedings of ICTON 2010, paper We.C1.2.
- [68] M. Eiselt, B. Teipen, K. Grobe, A. Autenrieth, J.-P. Elbers, "Programmable Modulation for High-Capacity Networks", in Proceedings of ECOC 2011, paper Tu.5.A.5.
- [69] D. Hillerkuss, R. Schmogrow, M. Hübner, M. Winter, B. Nebendahl, J. Becker, W. Freude, J. Leuthold "Software-Defined Multi-Format Transmitter with Real-Time Signal Processing for up to 160 Gbit/s", in Proceedings of SPPCom 2010, paper SPTuC4.
- [70] W. Freude, R. Schmogrow, B. Nebendahl, D. Hillerkuss, J. Meyer, M. Dreschmann, M. Huebner, J. Becker, C. Koos, J. Leuthold, "Software-Defined Optical Transmission", in Proceedings of ICTON 2011, paper Tu.D1.1.
- [71] G. Baxter, S. Frisken, D. Abakoumov, H. Zhou, I. Clarke, A. Bartos, and S. Poole, " Highly Programmable Wavelength Selective Switch Based on Liquid Crystal on Silicon Switching Elements," in Proceedings of OFC 2006, paper OTuF2.
- [72] Robert Borkowski, Fotini Karinou, **Marianna Angelou**, Valeria Arlunno, Darko Zibar, Dimitrios Klondis, Neil Guerrero Gonzalez, Antonio Caballero, Ioannis Tomkos, Idelfonso Tafur Monroy, "Experimental Demonstration of Mixed Formats and Bit Rates Signal Allocation for Spectrum-flexible Optical Networking", in proc. Optical Fibre Communications Conference, paper OW3A.7, Los Angeles CA, USA, March 2012.
- [73] I. Tafur Monroy, D. Zibar, N. Guerrero Gonzalez, R. Borkowski, "Cognitive heterogeneous reconfigurable optical networks (CHRON): Enabling technologies and techniques (Invited), In proc. ICTON 2011, paper Th.A1.2, 2011
- [74] P. J. Winzer, et. al, "Spectrally Efficient Long-Haul Optical Networking Using 112-Gb/s Polarization-Multiplexed 16-QAM," J. Lightwave Technol. 28, 547-556 (2010).

# Chapter 7

## 7. Resource Optimization in Mixed Line-Rate and Flexible Networks

In the pursuit of the technologies to be adopted by the next-generation core networks it is vital to be able to support channel rates beyond 100 Gb/s. Concurrent research efforts are focused on advanced transmission methods that achieve long reach and high spectral efficiencies either employing fixed-grid [1] or flex-grid [2] systems. Optical networks that rely on the ITU-T fixed grid need to accommodate all channels inside a fixed channel spacing, which may not be sufficient for the future 400 Gb/s channels or under-utilize the spectrum for the low-rate demands. On the other hand, flex-grid networks which are able to adapt the bandwidth utilization to the demands entail a significant capital investment over the existing infrastructure. Operators seeking to migrate to the next-generation core are likely to select the winning solution by taking into account the extra capital investment that it requires together with its performance. However, in addition to the capital cost of the future core network, power consumption is another parameter that becomes relevant, mainly due to the operational economic implications, considering the pace at which traffic is increasing annually. The goal of this chapter is to evaluate the new core networks from a cost, spectral and energy perspective and give a comprehensive view of the potential of each solution.

In the context of next generation core networks spectral efficiency is a key metric for the evaluation of a technological solution. Focusing on the importance of spectrum as a resource, novel algorithms for path and resource allocation in flex-grid networks are exploited herein. These algorithms solve the problem of Routing and Spectrum Allocation (RSA) [3], a process equivalent to the typical Routing and Wavelength Assignment (RWA) problem of traditional WDM networks. Overall, recent works [4] that studied the performance of flexible networks over the traditional single line-rate (SLR) architecture, showed superior performance that justifies the great attention received from the industry.

Nevertheless, to realize the level of flexibility of the multi-carrier solutions, new network and transmission elements need to be introduced in the optical transport, implying extra capital investment. Software-defined transponders [5] and bandwidth-flexible optical nodes [6] employing spectrum-flexible WSSs (SF-WSS) are the key enablers for the implementation of this architecture. The term spectrum-flexible (SF) is used here to signify networks that employ a flex-grid or even gridless solution that would require a SF type of equipment at the switching and source-destination nodes (transponders). So far though, few works have addressed this transition from an economic point of view and have studied only specific aspects. The authors in [1] focused their study on the comparison of a mixed-line-rate (MLR) network with a network employing a single, rate-adaptive transmitter that may offer 25/50/100Gbps, while [7] compared the CapEx of a 10/40Gbps network to a solution based on OFDM transponders. Section 7.1 presents a methodology to explore the conditions under which the vision of flexible networking makes a good business case. The proposed

methodology is used to investigate the requirements in capital of the flex-grid networks over the fixed-grid solutions in correlation with the gained spectrum optimization (sections 7.2 and 7.3).

Following the optimized resource allocation, all solutions are evaluated under the prism of energy efficiency (section 7.4). The energy efficiency that each solution incurs was estimated considering the power consumption needs of the associated networking elements. It is shown that a transition to a flex-grid network can overcome the added cost of the equipment due to the minimized spectrum. In addition solutions that offer finer bit-rate granularity and efficient spectrum allocation achieve low energy per bit as they use just the amount of network resources needed for certain input traffic.

## 7.1. Methodology

The key metric considered here is the “spectrum saving” which results from the optimized packing of connections in the frequency domain when the capabilities of OFDM technology are used, as opposed to traditional fixed-grid WDM networks. In this framework, it is expected that spectrum savings could be utilized for the provisioning of new traffic and/or revenue generating services. To translate the spectrum savings to a measurable entity, the cost of a “dark” 50GHz channel slot  $c_{wavelength}$  is introduced here. This definition of a 50GHz channel slot corresponds only to the cost of the link infrastructure (equipment/fiber) to support a 50GHz channel and excludes any cost associated with “lighting-up” this channel. The total cost of a system is abstracted considering three main cost contributions. The first is related to the cost of the transponders, the second is related to the cost of the node equipment and the third is related to the number of “dark” 50GHz channel slots that are utilized and are associated only with the link infrastructure cost. In the following this approach is used to model the cases of a 100 Gb/s SLR WDM network and that of a SF network:

$$Cost_{SLR} = n_{SLR-100G} c_{100G} + n_{WSS} c_{WSS} + n_{SLR-wavelengths} c_{wavelength} \quad (1)$$

$$Cost_{SF} = n_{SF} c_{SF} + n_{WSS} c_{SF-WSS} + n_{SF-slots-to-wavelengths} c_{wavelength} \quad (2)$$

In the above equations,  $n$  denotes the number of the elements that are considered and  $c$  the corresponding cost of each element.

To illustrate the value analysis methodology a comparison of the SLR and the SF network is performed using the following indicative cost values. We have assumed the cost of the 10 Gb/s transponder equal to  $c_{10G}=2K$  € and we set the targeted cost for the 100Gbps transmitter  $c_{100G}=6 \cdot c_{10G}$ . It was also assumed that the transmission distance of the 100Gbps transponder is equal to 800 Km. The SF transponder has two flexibility degrees: (a) the spectrum, in terms of the number of 12.5 GHz subcarriers that it uses, and (b) the modulation format of the subcarriers, as a function of the transmission distance. To have a fair comparison it was assumed that the SF transponder can utilize up to four subcarriers of 12.5 GHz each. The corresponding transmission distance limits of the SF transponder was set equal to that assumed for the 100Gbps WDM transponder, so that if all four subcarriers are utilized, the SF transponder can transmit 100 Gb/s to 800 Km. The achieved transmission distance varies with the selected modulation level assuming a decrease by half of the transmitted distance when the level doubles.

The SLR WDM networks utilize fixed grid wavelength selective switches (WSSs), assuming 50 GHz ITU-grid, with corresponding cost  $c_{WSS}$ , while the SF network needs to employ SF-WSS with corresponding cost  $c_{SF-WSS}$ . The basic switching capability of the SF-WSS

was assumed to be 12.5 GHz. We set the corresponding cost of a conventional fixed-grid WSS  $c_{WSS}=12$  K€, and the corresponding cost of the flexible SF-WSS to be variable and range between 0% and 100% over the cost of the conventional fixed-grid WSS.

In the analysis a range from 10K€ to 100K€ was considered reasonable for the cost of a “dark” 50GHz channel slot  $c_{wavelength}$ . In fact, the typical range of prices for leasing a dark-fiber infrastructure (which of course excludes also the cost of transponders and optical nodes) ranges from 1-3 € per meter for a long-term IRU (15-20 years). Considering that in a national scale network the average length of a light-path is several hundred of kilometers, one can easily deduce that the cost of leasing the corresponding dark fiber (with potential to carry 80 channels in 50GHz slots) is within a couple of million €. Therefore, the equivalent average link equipment/fiber related cost estimate for a 50GHz channel slot is within the range that it was assumed in the analysis. However, it should be emphasized here that the wholesale leasing price of a fully operational 50GHz channel slot (for either 10Gb/s or 40Gb/s channel speeds which are currently available by some operators) is significantly higher (since this market is unregulated and not many companies can offer such wavelength services) than the cost range of a "dark" 50GHz channel slot considered in the calculations. To be more precise, the price of a fully operational 50GHz channel slot (carrying 10Gb/s or 40Gb/s) ranges between 20K-60K € per month or 2M-6M € for a 20-year long-term leasing.

To examine the performance of the proposed networking solutions the nation-wide DT network consisting of 14 nodes and 46 directed links (see Appendix A: Network Topologies) was assumed. The realistic traffic matrix of the DT network for 2009, given in section A.1 , was scaled up to 10 times to obtain traffic ranging from 3.6 Tb/s up to 36 Tb/s, respectively. In addition, directionless, colorless, and contention-less nodes that require in total 92 WSS elements were assumed.

Figure 7-1 presents the utilization of spectrum and the savings in terms of 50 GHz slots of the SF network as opposed to the 100-Gb/s SLR system. These results were produced by applying the algorithm of [3], using the SF transponder and transmission distance assumptions that are considered in this preliminary study.

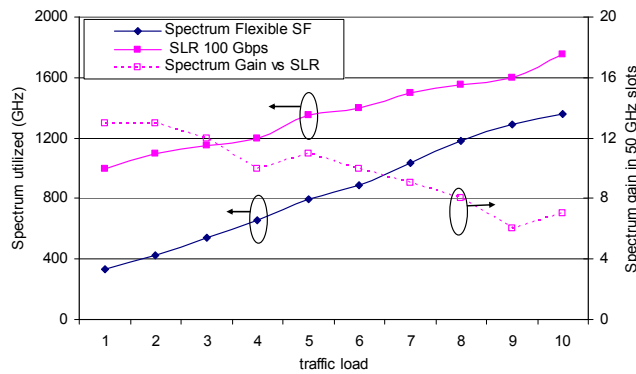


**Figure 7-1:** Spectrum utilization and spectrum gain (in 50GHz slots ) of the SF network as opposed to a SLR 100 Gb/s system for different traffic loads.

Figure 7-2 to 7-6 depict the main results of the current work. Figure 7-2 presents the percentage of the additional cost of the SF transponder over the cost of the 100 Gb/s transponder, in order to achieve SF total cost equal to that of the SLR network. The results for traffic loads equal to 1, 3, 5, 7 and 10 times the base traffic matrix of DT are shown here, assuming that the additional cost of the SF-WSS compared to the conventional 50GHz WSS is 50%. In Figure 7-2 for instance, one may observe that for load=5 and for a cost  $c_{wavelength}=50$ K€ for a 50GHz channel slot, SF networking is preferable over SLR if the SF

transponder costs 1.15 or less than that of the corresponding 100 Gb/s transponder. From Figure 7-2 and with the aforementioned assumptions it can be concluded that SF networking is preferable over SLR network when the additional cost that is tolerable for the flexible transponder ranges between 10% to 45%, for a 50GHz channel slot ranging from 10K€ to 100K€. Since, according to Figure 7-1, the spectrum savings (i.e. 50GHz slots) are more pronounced for low traffic loads, the slopes of the graphs decrease as the load increases. Thus, for high values of  $c_{wavelength}$ , the extra SF cost that can be tolerated for lower loads is higher than that for higher loads.

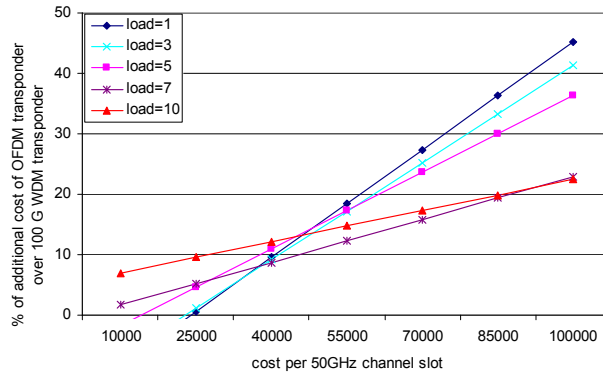


**Figure 7-2:** Percentage of additional cost of the SF transponder over the cost of the 100 Gb/s transponder as a function of the cost of the 50 GHz slot, for different traffic loads and 50% SF-WSS extra cost.

Figure 7-3, Figure 7-4 and Figure 7-5 illustrate the corresponding results for traffic 1, 5 and 10 times the base traffic matrix and different values for the extra cost of the SF-WSS over the cost of a conventional 50GHz WSS. The cost of the SF-WSS could be considered quite high at present, however it stands to reason that in the future the SF-WSS cost would decrease and be comparable to that of a conventional WSS element. The SF network becomes significantly more cost-efficient as the extra cost of the SF-WSS goes below 50% for all cases of traffic load. For example from Figure 7-4 it can be observed that when moving from 50% to 25% extra SF-WSS cost, we can tolerate to spend 10% more for the SF transponders.

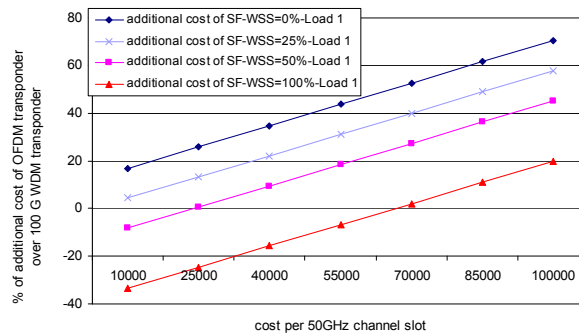


**Figure 7-3:** Percentage of additional cost of the SF transponder over the cost of the 100 Gb/s transponder as a function of the cost of the 50 GHz slot, for different SF-WSS extra cost percentages and for load=1.

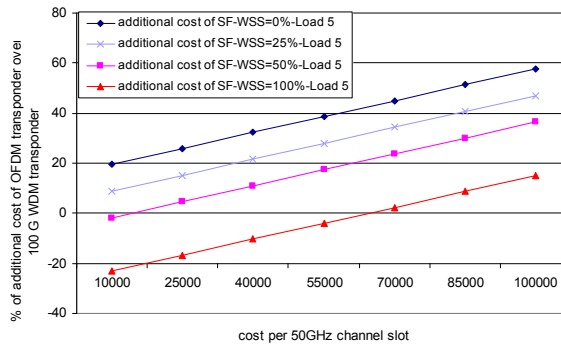


**Figure 7-4:** Percentage of additional cost of the SF transponder over the cost of the 100 Gb/s transponder as a function of the cost of the 50 GHz slot, for different SF-WSS extra cost percentages and for load=5.

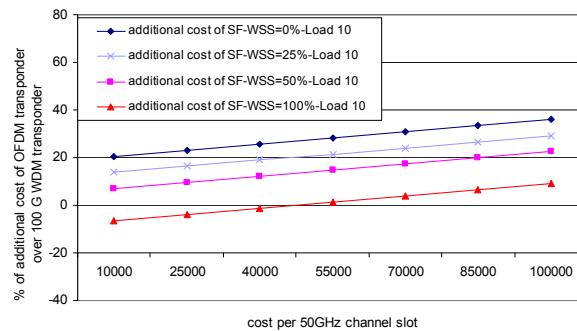


**Figure 7-5:** Percentage of additional cost of the SF transponder over the cost of the 100 Gb/s transponder as a function of the cost of the 50 GHz slot, for different SF-WSS extra cost percentages and for load=10.

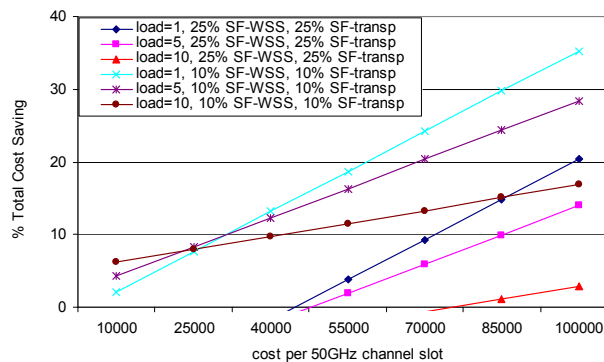


**Figure 7-6:** Percentage of total network cost saving as a function of the cost of the 50 GHz slot, for different SF-WSS and different SF-transponder values.

Having observed that the SF-WSS cost should be below 1.5 more than that of a conventional WSS, this value was fixed to 1.25 and 1.1 to examine the impact of the transponders' cost to the entire network cost. Figure 7-6 illustrates the percentage of the total network cost saving of the SF over the SLR network. From Figure 7-6 it is evident that the savings increase fast with the increasing cost of the 50 GHz slot. For 10% extra SF-WSS cost and for 10% extra SF-transponder cost the SF network achieves more than 10% saving for all examined loads. Depending on the channel slot cost, the extra equipment required to

implement an SF network should cost within 25% more than that of a 100G SLR network. Cost savings are gradually reduced as the traffic load increases and the saving in spectrum is also reduced, as shown in Figure 7-1. It is emphasized that the results in Figure 7-2 to 7-6 consider capital costs and do not account for any savings that may arise due to operational life-cycle cost savings associated with the capabilities of the flexible networks.

## 7.2. Spectrum Allocation in Fixed-Grid and Flex-Grid Networks

The previous section elaborated a methodology for the estimation of the value of flexible optical networking compared to standard single line-rate WDM solutions. In order to explore the proposed methodology it was tested on OFDM-based flexible optical networks under different conditions and assumptions. It was found that if the additional network elements that are required to support their operation (flexible transponders and WSSs) cost up to 20-25% over the cost of their counter-parts for a fixed SLR system, then the additional investment may be justified.

Following this preliminary attempt to study the cost implications of the next-generation flexible network, the analysis is extended to networking solutions that can deliver up to 400 Gb/s per channel in a fixed or flexible spectrum grid utilizing physical-layer aware algorithms to route and allocate the available spectrum [1], [8]. The methodology introduced in section 7.1 above, is used to investigate the requirements in capital of the flex-grid networks over the fixed-grid solutions in correlation with the gained spectrum optimization.

The study includes fixed WDM SLR networks that deliver either 40 Gb/s, 100 Gb/s or 400 Gb/s per channel and MLR [1] networks with data rates of 10Gb/s, 40 Gb/s, 100 Gb/s and 400 Gb/s. Regarding the flex-grid solutions, two multi-carrier solutions have been considered; one refers to the case where subcarriers are electrically (Orthogonal Frequency Division Multiplexing) OFDM modulated [9] offering ultra fine sub-wavelength granularity (denoted as E-OFDM) while the other refers to the case where a comb of frequency-locked subcarriers are conventionally modulated at the baud rate of the subcarrier spacing [10] (denoted as O-OFDM). Both multi-carrier solutions can adapt the transmitted bit-rate from 10Gb/s-400Gb/s by modulating subcarriers with the necessary modulation level that varies between BPSK, QPSK and n-QAM (n=16, 32, 64).

**Table 7-1:** Reach of fixed-grid signals

Line Rate	Transmission Reach
10 Gb/s	3200 km
40Gb/s	2300 km
100 Gb/s	2100 km
400Gb/s	790 km

Reach-adapting routing and resource allocation algorithms with realistic transmission reach data [9] developed for both flex-grid [3] and fixed-grid [8] networks are utilized to minimize the spectrum utilization and the number of transponders. In the fixed-grid cases a 50 GHz channel-spacing has been assumed. The transmission reach is set to 3200km, 2300km, 2100km and 790 km for the fixed-grid signals of 10Gb/s, 40 Gb/s, 100 Gb/s and 400 Gb/s respectively (Table 7-1). In E-OFDM, superchannels are assigned a variable bandwidth depending on the selected symbol rate and format and the reach-adaptive model presented in [9] is employed. O-OFDM superchannels are generated with a group of subcarriers spaced

at 12.5 GHz and the reach depends on the modulation level selected, i.e. 4000 km, 2500 km, 1200 km, 800 km and 400 km for 1, 2, 4, 5 or 6 bits per symbol respectively (Table 7-2).

**Table 7-2: Reach of O-OFDM channels**

Modulation format of subcarriers	Transmission Reach
BPSK	4000 km
QPSK	2500 km
16QAM	1200 km
32QAM	800 km
64QAM	400 km

To calculate the bandwidth utilized by the various solutions the Deutsche Telekom core network (14 nodes, 23 bidirectional links) and the realistic traffic matrix of the DT network for 2010 scaled up to 11 times to obtain traffic ranging from 3.6 Tb/s up to 39.6 Tb/s (see Appendix A: Network Topologies) has been utilized. Under the given assumptions, the flexible multi-carrier solutions offer the most efficient spectrum allocation as expected from the optimized packing of the connections in the frequency domain, with E-OFDM outperforming all (Figure 7-7). The performance of O-OFDM is constrained by the 12.5 GHz subcarrier spacing assumed here. It should be noted that in the 400 Gb/s SLR network, regenerators are required for the connections with longer paths than its maximum transmission reach.

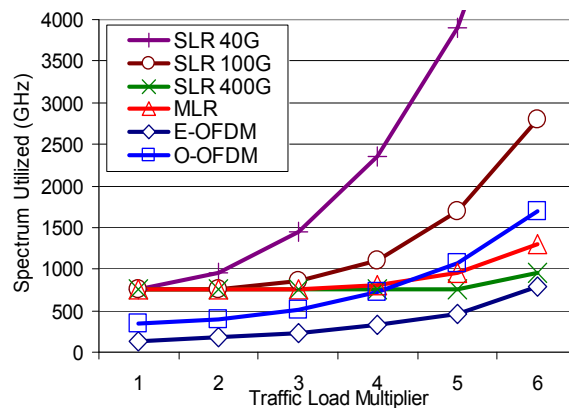


Figure 7-7: Spectrum utilization for all solutions and different traffic loads.

### 7.3. Cost Efficiency

Spectrum utilization is presented not only as a way to evaluate the networking solutions but also in the form of spectrum savings (considered here in 50GHz slots) that can be utilized for the provisioning of new traffic. Based on the methodology introduced in section 7.1 we model the total cost of a system considering three cost parameters; the cost of transponders, the cost of node equipment and the third is related to the number of “dark” 50GHz channel slots that are utilized and are associated only with the link infrastructure cost.

Among the fixed-grid networks the distinctive component that determines the capital requirements is the type of the transponders. Figure 7-8 illustrates the absolute number of transponders per networking solution. Figure 7-9 shows the relative transponder cost of all fixed-grid solutions; the relative cost values are set at 1/2.5/3.75/5.5 for the 10 Gb/s, 40



Gb/s, 100 Gb/s and 400 Gb/s transponders respectively [11]. For MLR systems, two variations of the planning algorithm are reported; the first one seeks to minimize the number of utilized wavelengths, and the second plans the network optimizing the transponder cost.

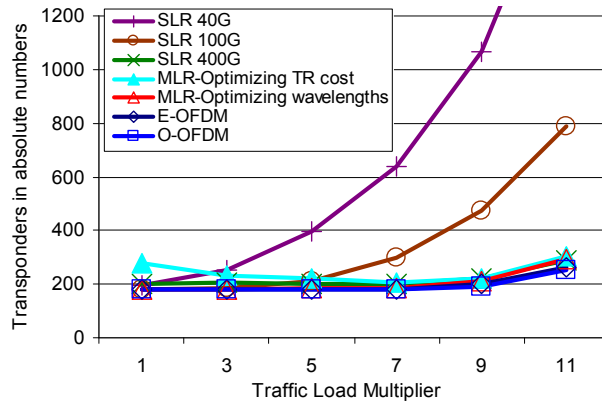


Figure 7-8: Required number of transponders for all solutions to serve the different traffic matrices (in absolute numbers).

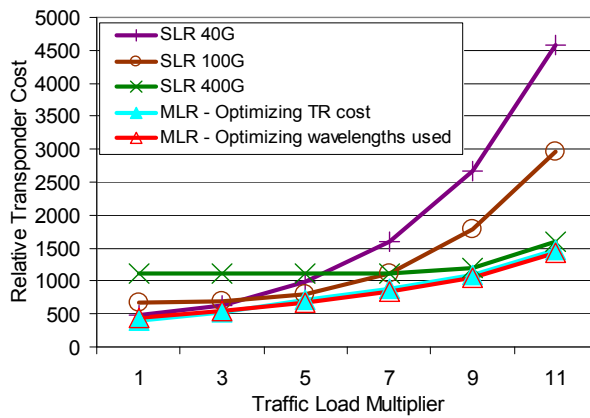


Figure 7-9: Relative transponder cost for the fixed-grid networking solutions

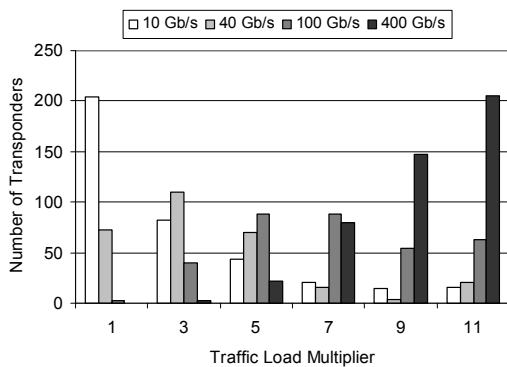


Figure 7-10: Number of allocated 10Gb/s, 40 Gb/s, 100 Gb/s, 400 Gb/s transponders for each traffic scenario for an MLR network with transponder cost optimization.

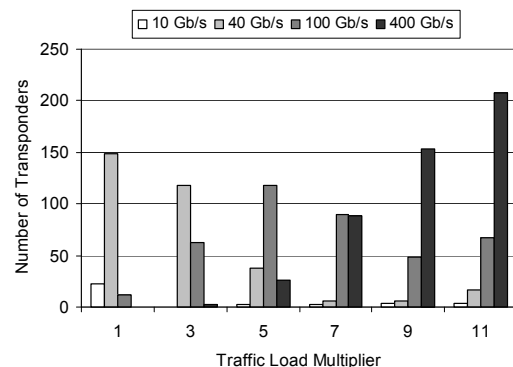
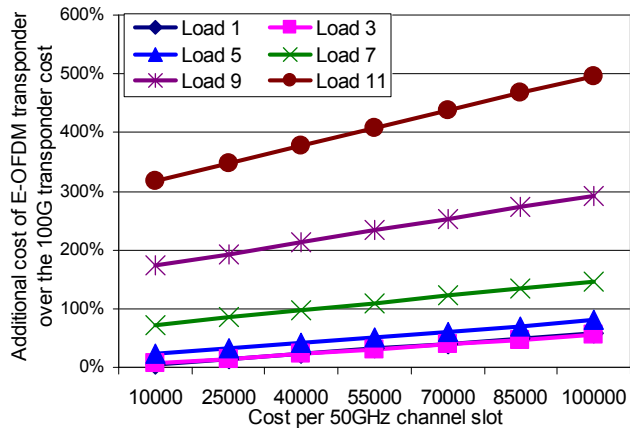


Figure 7-11: Number of allocated 10Gb/s, 40 Gb/s, 100 Gb/s, 400 Gb/s transponders for each traffic scenario for an MLR network with wavelength optimization.

In Figure 7-10 and Figure 7-11 the MLR transponder allocation is illustrated per type of transponder, i.e. number of 10Gb/s, 40 Gb/s, 100 Gb/s and 400Gb/s transponders required for each traffic scenario. MLR is the sole solution from the ones examined in this study that require a set of different types of transponder in order to offer variable line-rates. As shown in Figure 7-10 and Figure 7-11, the combination of the different types of transponders vary significantly for each traffic scenario with a tendency to move to higher rates as the traffic increases. In contrast, the multi-carrier and flex-grid solutions offer adaptive services employing a single type of transponder that allows operators to capitalize on the investment.



**Figure 7-12:** Allowable additional cost for E-OFDM transponder compared to SLR 100G from spectrum savings for different traffic loads.

However, reliable data for the cost of the flex-grid networks components i.e. the software-defined transponders and bandwidth-variable nodes, are currently not available. To overcome this, the extra cost of the E-OFDM and O-OFDM transponders over the cost of a 100 Gb/s transponder so as to achieve total network cost equal to that of the related SLR network is examined. The comparison was focused on the cost of the E-OFDM and O-OFDM transponders as those rely on electronics for DSP. We set the corresponding cost of a fixed-grid wavelength selective switch (WSS) at 12 K€ and the cost of the 100 Gb/s transponder at 12 K€. Directionless, colorless, and contention-less nodes were assumed that require 92 WSS elements for the pass-through traffic of the DT topology, which in the case of the flex-grid networks it is assumed to cost 1.25 times the conventional fixed-grid WSS. The resource allocation algorithms were utilized to calculate the required transponders and the spectrum savings for the different traffic matrices. Figure 7-12 presents the allowable additional cost for the E-OFDM transponder compared to the SLR 100 Gb/s transponder for different traffic loads. For a 50-GHz-channel cost that ranges from 10K€ to 100K€, an E-OFDM transponder may cost 3 to 5 times more when the traffic load is equal to 11 so as to achieve total network cost equal to that of the SLR network. For the lowest traffic scenario (load=1), where the spectrum savings of the flex-grid solution compared to the 100G SLR are less pronounced, the E-OFDM solution is preferable over the SLR network when the additional cost that is tolerable ranges between 6% to 50%.

In a similar manner, Figure 7-13 presents the results for the comparison between O-OFDM and 100G SLR. The O-OFDM transponder may cost approximately 2-3 times more for the highest traffic load scenario. The difference with the O-OFDM case is justified by its higher spectrum utilization as shown in Figure 7-7. From the operators' perspective, these

results indicate how the spectrum savings of the flex-grid networks can be used to mitigate the additional cost of the new spectrum flexible transponders.

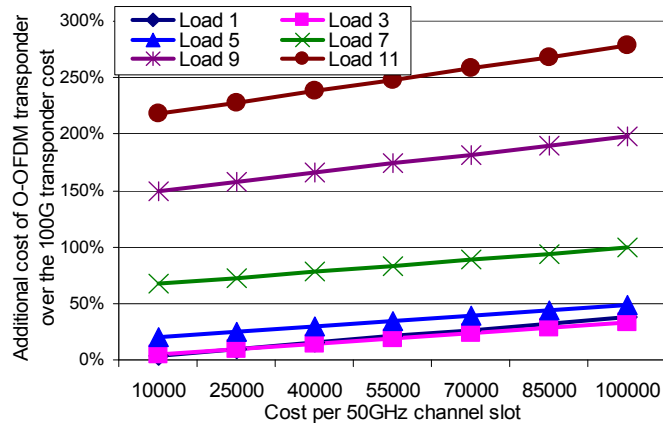


**Figure 7-13:** Allowable additional cost for O-OFDM transponder compared to SLR 100G from spectrum savings for different traffic loads.

## 7.4. Energy Efficiency

In addition to the capital cost of the future core network, power consumption is another parameter that becomes relevant in network planning, mainly due to the operational economic implications but also the growing ecological awareness, considering the pace at which traffic is increasing annually. Following the resource allocation of all solutions, the energy efficiency is estimated considering the power consumption needs of the associated networking elements.

Hence, the considered solutions were compared with respect to their power consumption. The transponders of the fixed-grid solutions were assumed to require 47W, 125W, 215W, and 330W for the 10 Gb/s, 40 Gb/s, 100 Gb/s and 400 Gb/s transponders [11]. In the flex-grid solutions, E-OFDM and O-OFDM have similar receiver architectures, yet they differ in the transmitter part. E-OFDM requires a DSP module and digital-to-analog/analog-to-digital converters (DACs/ADCs) at both the transmitter and receiver ends. In O-OFDM these are present only at the receiver part, similar to a typical coherent transponder. Nevertheless, as reported in [12] E-OFDM has the same DSP complexity as a coherent 40 Gb/s QPSK despite the fact that a DSP module is present at both ends, giving insight into the associated power consumption. In this study it was assumed that the E-OFDM transponder consumes power equal to that of a 100 Gb/s transponder for bit rates from 10-100 Gb/s and equal to a 400 Gb/s transponder for bit rates 100-400 Gb/s, to also indirectly account for the DACs. As opposed to this conservative assumption, a linear function may be proven more suitable as DSP has been reported to scale linearly with bit-rate. At the O-OFDM transmitter, the source laser is shared among the subcarriers that are modulated at low baud-rates. Therefore, it is assumed that the power consumption per subcarrier matches that of a 10 Gb/s transponder and the power per transponder is estimated on the basis of the number of allocated subcarriers. In addition to that 6 ADCs and one DSP module have been considered per transponder, assuming 4W power dissipation for each ADC and 100W for the DSP.

OXC and optical line amplifiers (OLAs) are considered to consume an equal amount of power for all cases. Bandwidth-variable WSSs are expected to require the same amount of

power to operate as the conventional WSSs. The power consumption of OXCs was set to 430W including control overhead, for the node degree of the DT topology. OLAs were set to 145W per direction of a double-stage EDFA, including control overhead. 120 OLAs were assumed for the entire DT topology. In addition a cooling factor equal to 2 has been assumed for all considered components.

**Table 7-3:** Power Consumption of Fixed-Grid Transponders

Fixed-grid Transponder	Power Consumption (W)
10 Gb/s	47W
40 Gb/s	125W
100 Gb/s	215W
400 Gb/s	330W

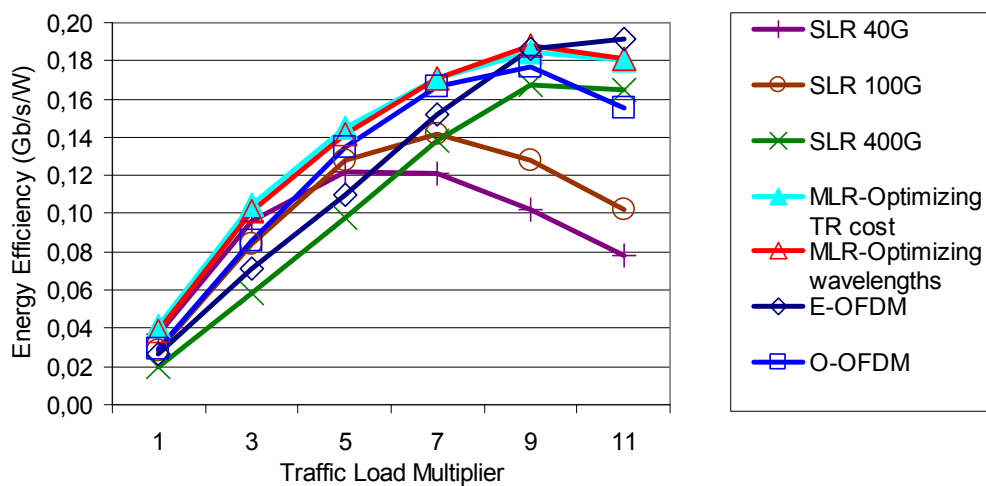


**Figure 7-14:** Energy Efficiency achieved for all solutions and different traffic loads.

The estimated energy efficiency (in Gb/s/W) for the various traffic loads is illustrated in Figure 7-14. 400G SLR appears to be the least efficient for traffic load up to 5 although it tends to improve for higher loads. The other SLR solutions achieve better efficiency that decreases for high loads justified by the great number of transponders as depicted in Figure 7-8. On the other hand the granularity of 10G/40G/100G/400G in MLR and of the low-rate subcarriers in O-OFDM, appears to be sufficient for the entire range of traffic loads optimizing the number and type of transponders and leading to low power consumption. Under the given power consumption assumptions, E-OFDM demonstrates lower energy efficiency for load up to 5. Moving up in traffic load, the transponders assumed run at higher bit rates leading to superior energy efficiency.

The MLR networks achieve such efficiency assuming that optimization of the type of the required transponders is performed independently for each traffic scenario. Indeed in each of the traffic scenarios different number of each type of transponder is required to be allocated in the various network sites, result of the resource optimization process that takes place for every traffic scenario. Such re-optimization leads to replacements of already acquired transponders and not just additions as the traffic increases and varies with time (see Figure 7-10 and Figure 7-11). In the context of cost efficiency the solutions that employ

a single type of transponder offer a clear benefit as they allow making use of the already invested capital, as discussed in section 7.3.

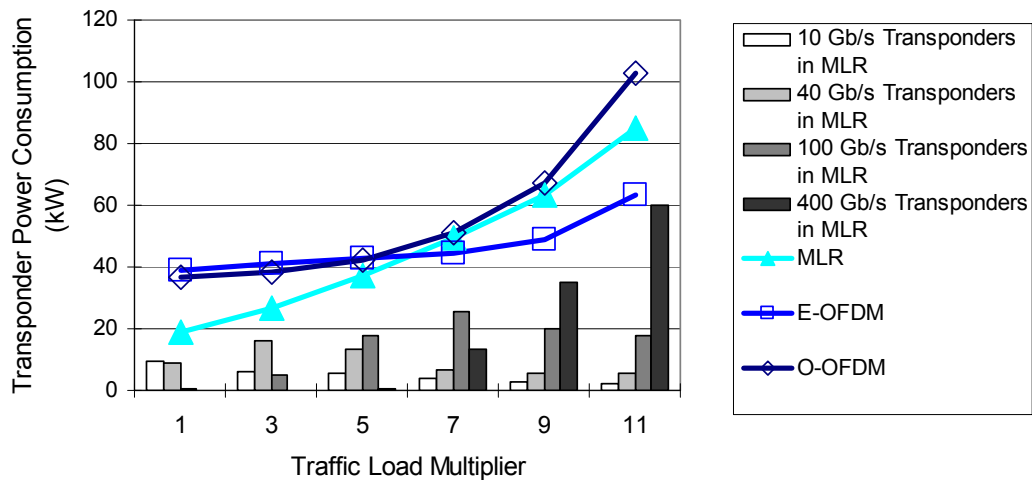


**Figure 7-15:** Power consumption of transponder in MLR, E-OFDM and O-OFDM solutions.

Let us assume, though, that such changes in the network planning and therefore in the network resources are affordable by the operator of the MLR network at every traffic increase. Focusing only on the transponders that essentially differentiate the various networking solutions in terms of their power needs, it is useful to examine how the different types of transponders affect the power consumption estimations. Figure 7-15 illustrates the power consumption of the required transponders of the MLR network in comparison with the two multi-carrier solutions. In the low traffic cases, where mostly 10-Gb/s and 40-Gb/s transponders are utilized the overall power consumption is kept low for MLR. Moving up in traffic load, low bit-rate transponders become obsolete and more high-bit-rate transponders are needed contributing to the fast power-consumption increase shown in Figure 7-15.

Although E-OFDM transponders have been assumed to consume power that is not proportional to the flexible line rates they offer, they achieve superior performance than MLR for load higher than 7. In those scenarios the innate flexibility of the E-OFDM solution allows a low number of required transponders to serve the given traffic, leading to lower power consumption compared to MLR. For the low-traffic scenarios where low bit-rates are required to serve the traffic, transponders are assumed to run at the power level of either a 100-Gb/s or 400-Gb/s-transponder even if they deliver lower aggregated capacity leading to relatively high power consumption. O-OFDM transponders exhibit power consumption similar to that of E-OFDM for load up to 5 justified by the low number of required transponders (see Figure 7-8) in combination with the fine exploitation of the offered granularity. In the higher-load scenarios O-OFDM is limited by the subcarrier spacing which leads to higher power consumption.

## 7.5. Chapter Summary

This chapter examines the resource optimization achieved in mixed line-rate and flexible networks under the prism of cost and energy efficiency. Section 7.1 introduces a methodology that leverages the resource optimization achieved in a multi-carrier network

to estimate the value of flexible networking in comparison to a single-line rate WDM solution. It is studied how spectrum savings can overcome the additional cost of software-defined transponders and bandwidth-flexible nodes. Specifications for the cost of the required flexible transponders and WSSs are extracted to indicate the range within which a transition to a flexible network would be viable.

Single and multi-carrier networks offering channel rates up to 400 Gb/s are then evaluated under realistic reach parameters. The methodology of Section 7.1 is applied to examine how the efficient spectrum utilization (section 7.2) and fine bit-rate granularity of flex-grid core optical networks may affect the requirements in capital and power compared to fixed-grid solutions. It is shown that the capability of the flex-grid networks to allocate efficiently the available spectrum counterbalances the additional capital expenditures that are required to migrate to a multi-carrier system (section 7.3). Finally, in terms of the overall network energy efficiency, flex-grid solutions achieve low energy per bit as they use just the amount of network resources needed for given input traffic (section 7.4).

## 7.6. References

- [1] A. Nag, M. Tornatore, B. Mukherjee, "Optical Network Design With Mixed Line Rates and Multiple Modulation Formats," *J. Lightwave Technol.* 28, 466-475 (2010).
- [2] M. Jinno, H. Takara, B. Kozicki, Y. Tsukishima, Y. Sone, S. Matsuoka, "Spectrum-efficient and scalable elastic optical path network: architecture, benefits, and enabling technologies," *IEEE Communications Magazine*, 47, 66-73 (2009).
- [3] K. Christodoulopoulos, I. Tomkos, E. Varvarigos, "Elastic Bandwidth Allocation in Flexible OFDM-based Optical Networks," *J. Lightwave Technol.*, 29, 1354-1366 (2011).
- [4] N. Ankitkumar, P.N. Ji, J.P. Jue, Ting Wang, "Survivable Transparent Flexible Optical WDM (FWDM) Networks," in *Proceedings of OFC 2011*, paper OTuI2.
- [5] Christoph Glingener, "Optical Networking Trends and Evolution," in *Proceedings of OFC 2011*, paper OThAA1.
- [6] S. Poole, S. Frisken, M. Roelens, C. Cameron, "Bandwidth-flexible ROADMs as Network Elements," in *Proceedings of OFC 2011*, paper OTuE1.
- [7] A. Bocoï, M. Schuster, F. Rambach, D.A. Schupke, C.-A. Bunge, B. Spinnler, "Cost Comparison of Networks Using Traditional 10&40 Gb/s Transponders versus OFDM Transponders," in *Proceedings of OFC 2008*, OThB4.
- [8] K. Christodoulopoulos, K. Manousakis, E. Varvarigos, "Reach Adapting Algorithms for Mixed Line Rate WDM Transport Networks" *J. Lightwave Technol.*, 29, 3350-3363 (2011).
- [9] A. Klekamp, R. Dischler, and F. Buchali, "Transmission Reach of Optical-OFDM Superchannels with 10-600 Gb/s for Transparent Bit-Rate Adaptive Networks," in *Proceedings of ECOC 2011*, paper Tu.3.K.2.
- [10] S. Chandrasekhar, X. Liu, B. Zhu, D.W. Peckham, "Transmission of a 1.2-Tb/s 24-Carrier No-Guard-Interval Coherent OFDM Superchannel over 7200-km of Ultra-Large-Area Fiber", in *Proceedings of ECOC 2009*, paper PD2.6.
- [11] A.N. Patel, P. Ji, J.P. Jue and Ting Wang, "First Shared Path Protection Scheme for Generalized Network Connectivity in Gridless Optical WDM Networks", in *Proceedings of ACP 2010*, PD6, 1-2, Dec. 2010.
- [12] S. J. Savory, "Digital Signal Processing Options in Long Haul Transmission", in *Proceedings of OFC 2008*, paper OTuO3.
- [13] I. Dedic, "56Gs/s ADC: Enabling 100GbE", in *Proceedings of OFC 2010*, paper OThT6.



# Chapter 8

## 8. Conclusions and Future Work

Core optical networks evolved to networks that span over thousands of kilometres of fiber, carry high-capacity traffic and switch connections all-optically. In this context, network planning and operation require processes that lead to a cost-effective core optical network that effectively serves the given traffic. Telecom operators seek to employ methods and technologies that minimise the total cost of ownership and the network-related operational expenses while ensuring scalability, robustness and adaptation to future demands. To achieve optimal resource utilization and network performance, cross-layer techniques have been introduced and identified by the research community as an efficient solution. Regardless of the underlay infrastructure (wireless/wireline) the notion of *cross-layer optimization* implies the utilization of knowledge coming from one communication layer by another communication layer to improve the performance of the network. The cross-layer optimization methods presented herein focus on the exploitation of information coming from the transport plane to serve either the network planning or the operation phase.

Optical networks followed a path that transformed them from opaque to translucent or transparent so as to satisfy the ever-growing demand for bandwidth, yet with improved economics. The dynamic traffic patterns that came along with the rapid traffic increase though, led to the fast adoption of reconfigurable networking equipment that allow the operators to adapt dynamically their network to the new conditions. To cope with these new challenges *dynamic impairment-aware networking* was proposed as a comprehensive solution that utilizes the dynamicity as well as the valuable physical-layer information of a reconfigurable WDM single-line rate network to provide a smooth transition from the quasi-static networking of today to an intelligent reconfigurable and physical impairment-aware architecture. In the core of the multiplane architecture the concept of *physical layer awareness* allows intelligent techniques to offer optimal planning, dynamic configuration and management of optical signal with acceptable QoT. Static and dynamic routing and wavelength assignment, performance and impairment monitoring, failure localization and handling work in conjunction with the control and management plane to offer resource optimization, robustness and dynamicity.

To introduce physical-layer awareness in dynamic single line-rate networks, a physical-layer performance estimating tool called Q-tool, has been designed and developed. Q-tool is responsible for fast and accurate QoT assessments in single line-rate WDM networks employing 10 Gb/s OOK systems. In the impairment-modelling process the physical effects that impose the most severe degradations were identified including CD, FC, PMD, ASE, SPM, XPM and FWM. The development approach that was followed combined analytical models and numerical simulations and the outcome of both was combined in a single figure of merit, the Q-factor formula. The Q-tool was developed so as to feed with QoT evaluations the various cross-layer modules of the network both for planning and operation purposes. It finds multiple applications in offline RWA, monitor placement, regenerator placement,



online RWA, failure handling and interacts with the control plane so as to enable the vision of the multi-plane impairment-aware core network.

The significance of the physical-layer awareness and the role of Q-tool in the online routing strategy have been experimentally investigated using an impairment-enabled control-plane testbed. Focusing on the performance of the IA-RWA algorithms inside an operational network, two such algorithms were compared, namely MP and OR, in a 14-node experimental test-bed using a centralized impairment-enabled control plane, under the same network and traffic conditions. On the whole the results indicated that the IA-RWA algorithms make optimum impairment-aware decisions at the expense of higher lightpath setup time. In terms of the lightpath setup time MP performed in general better in the considered scenarios. On the other hand, OR demonstrated lower blocking ratios and higher setup times that tend to improve as the traffic load increases.

A cross-layer module that utilizes physical layer information to optimize the planning phase of single line-rate network has been also developed. A special monitor placement scheme was designed that takes into account partial monitoring information coming from the physical layer to decide the optimum number and locations of the optical monitoring devices. This work leverages the correlation of the QoT of channels traversing a mesh topology and proposes a monitor placement framework that first decides the placement of the monitoring devices to few strategically selected locations during the network planning phase and enables the universal supervision of all the established connections during network operation. The proposed heuristic (PM) outperformed other monitor placement methods in terms of monitoring accuracy or, equivalently, the number of monitors needed to achieve the same level of monitoring accuracy. It was indeed shown that through the efficient placement of monitors using the PM heuristic, only a fraction of the possible locations in a mesh topology need to be equipped; in the considered topologies only 1/4 or 1/3 of the possible monitor locations actually required a physical monitoring device in order to compute the QoT of all established lightpaths within a few percents; the un-monitored lightpaths have their QoT estimated, rather than directly measured. It was also argued that the proposed technique scales well with the network size, as topologies ranging from less than 50 to more than 100 links were investigated, for various static loads.

In the framework of dynamic single line-rate networks a techno-economic analysis was also conducted to explore the cost implications stemming from resource optimization. IA-RWA and IUA-RWA algorithms along with the developed Q-tool were used to compare their planning solutions for a nation-wide backbone network in terms of CapEx and OpEx. A given traffic matrix with a specific annual increasing evolution was fed to the algorithms. Evidently the solutions of the IA-RWA algorithm illustrated that it may serve the input demand without any requirement for a second parallel line system, as opposed to the IUA-RWA method. The latter does not consider the QoT in the lightpath computation and therefore the routing and channel allocation is not optimised leading to physical-layer blocking. The IA solution outweighs the IUA one in CapEx and OpEx and the respective difference is directly proportional to the extra line system that would be required to serve without any blocking the given traffic. The IUA solution calls for a capital investment sooner than the IA one as the traffic increases. For the same scenario four different reconfigurable nodes were considered in order to quantify the relative CapEx required. A colourless, directionless but partly contentionless architecture (R-OXC3) appears to be a good choice for the specific scenario, as it is a node with a relatively high degree of flexibility and a moderate cost. Although R-OXC 3 is more inexpensive, it is anticipated that in the presence of an increased

traffic volume the more flexible nodes (R-OXC2) would perform better in terms of blocking, possibly compensating for the higher CapEx.

The cross-layer solutions discussed so far were proposed to cope with the challenges associated with core optical networks that deliver connections at a single line-rate, either 10 Gb/s or 40 Gb/s. Nevertheless, new challenges arise in the core networks of the next generation. Given the forecasted capacity crunch, the research community has focused on seeking solutions that make the most out of the scarce network resources and allow accommodating the ever-increasing traffic demand. In such context, *flexible optical networking* has been introduced as a way to offer efficient utilization of the available optical resources. Prior to the introduction of flexible optical networking, a mixed solution where 40-Gb/s and 100-Gb/s channels would co-exist with the 10-Gb/s ones has been extensively studied to upgrade the capacity of the existing systems. The *mixed line-rate* (MLR) solution allows the higher-rate channels to run in the same system while still capitalizing on the legacy infrastructure. It consists of a mixed transport system that utilizes the conventional fixed spectrum grid. However, the rigid and large granularity of WDM on the wavelength level, leads to severe spectrum wastage. In view of this limitation, flexible optical networking promises to offer elasticity and adaptation by allocating just the spectral resources that are required for the given traffic demand.

As opposed to the rate-specific and fixed-grid solution of an MLR network, flexible optical networks, regardless of the employed technology, are bandwidth agnostic and have the ability to deliver adaptive bit-rates. The associated technologies and concepts that enable the vision of flexible optical networks include advanced modulation formats that offer higher spectral efficiency, the concept of a spectrum-flexible grid, software-defined optical transmission, single-carrier adaptive solutions and multi-carrier technologies. Nevertheless the increased level of flexibility imposes complex requirements with respect to the spectrum and capacity allocation. During network operation traffic is changing with time, leaving windows of spectrum of variable size unused. Special routing algorithms are required to decide the route, the modulation format, the bandwidth and the location inside the available spectrum gaps for each incoming traffic demand. Moreover, interference from the neighbouring channels has to be taken into account and sufficient guard-bands ought to be considered.

In such context the requirements of the physical layer parameters for a spectrum-flexible optical *superchannel* were experimentally investigated. More specifically the work explored the physical layer parameters for dynamic resource allocation in spectrum-flexible networking and investigated the performance requirements needed for coherent multicarrier signals with variable format to be established within the available spectral slots of a superchannel, defined by a spectral window of variable width. In order to study this concept, several networking scenarios have been proposed and investigated over an experimental configuration emulating a set of different traffic demands. These traffic demands were served by allocating various combinations of 14 Gbaud POLMUX-16QAM and POLMUX-QPSK signals within the available spectrum of a 15-subcarrier long superchannel. The ROSNR levels for BER of  $1 \times 10^{-3}$  for a number of scenarios with variable spectrum bands being dynamically filled with POLMUX-QPSK and POLMUX-16-QAM has been the main outcome of this effort. The importance of the result is that it can act as input for cognitive control algorithms to implement the new paradigm of flexible optical networks. Physical layer performance estimation in the new era of optical networks requires a somewhat different approach compared to the conventional single line-rate network. New challenges

are imposed on analytical impairment modelling thus making the solution of combining experimental results with cognitive algorithms a rather attractive solution.

Finally effort was made to evaluate the new core networks from a cost, spectral and energy perspective and give a comprehensive view of the potential of each solution. The resource optimization achieved in MLR and flexible networks has been investigated under the prism of cost and energy efficiency. First a methodology was introduced to explore the conditions under which the vision of flexible networking makes a good business case. Single and multi-carrier networks offering channel rates up to 400 GB/s were evaluated under realistic reach parameters. The aforementioned methodology was applied to examine how the efficient spectrum utilization and fine bit-rate granularity of flex-grid core optical networks may affect the requirements in capital and power compared to fixed-grid solutions. It was shown that the capability of the flex-grid networks to allocate efficiently the available spectrum, counterbalances the additional capital expenditures that are required to migrate to a multi-carrier system. On the whole, in terms of the overall network energy efficiency, flex-grid solutions achieve low energy per bit as they use just the amount of network resources needed for given input traffic.

The key features of the new flexible networking paradigm along with the impressive results of the technological advancements justify the attention gained by the research community on those topics recently. Nonetheless the increased complexity of the new solutions gives rise to many interesting research challenges. Towards the completion of the research work conducted in the framework of this PhD a comprehensive study was performed to assess the new technologies in terms of the resource optimization they achieve. Nyquist-WDM has been omitted from this study; a similar study comparing Nyquist-WDM with Co-OFDM is a logical extension to this work as those two technologies achieve the same spectral efficiency. Given the need for sustainable and viable technologies, the two solutions should be evaluated with respect to the cost and energy efficiency they incur.

Regarding the other pillar of this PhD work, i.e. physical layer awareness, the complex nature of next generation networks imposes considerable implications in the estimation of signal degradation. As discussed in Chapter 3, analytical approximations have been used to model conventional single line-rate systems. Due to the limited flexibility of the old systems numerical simulations could also be used for more accurate assessments. Nevertheless dispersion-managed links rendered non-linearities an important limiting factor that led telecom operators to resort to specialized design rules. On the other hand flexible optical networks enjoy multiple degrees of freedom offering connections with adaptive spectrum, symbol rate and modulation format. The multiplicity of the possible scenarios causes physical layer awareness to be rather challenging particularly when considering online routing. Numerical simulations are thus no longer practical due to the excessive processing time they would require. The advent of the coherent technology though, offers a truly new circumstance; coherent systems not only operate over uncompensated links but they actually grant better performance than over dispersion-managed ones. The important aspect of this new condition concerns the signal modelling process as non-linear effects are easier to estimate using analytical formulas. In fact it appears that the non-linear noise is Gaussian-distributed and therefore easily accounted for in the performance estimation as extra-Gaussian noise. However the closed-form expressions proposed so far apply to the idealized case of transmission at the Nyquist limit. Therefore expressions that cover the more generic cases remain an open issue.

An alternative solution relies on a combination of analytical models with empirical design rules. Although this would appear challenging due to the extremely wide range of cases the flexible networking environment offers collaboration with cognitive algorithmic tools is expected to make it feasible. The first step of this proposal was discussed in Chapter 6. The experimental investigation that involved the performance assessment of a number of scenarios can act at the basis to build a knowledge base of initial measurements/rules to be used as input by the cognitive processes. Cognition has the ability to learn and act on current and past knowledge thus allowing frequent updates of the knowledge base. Hence, decision making on lightpath provisioning and resource allocation is continuously being optimized. As experimental data is inevitably limited analytical models can be used to fill in the “gaps”.



# Appendix A

## Appendix A: Network Topologies

### A.1 Deutsche Telekom's Backbone Network

The German national level reference network of Deutsche Telekom is shown in Figure A.1 together with the mapping of the Nodes ID to the city names. The characteristic parameters of this network are summarized next in Table A.1.

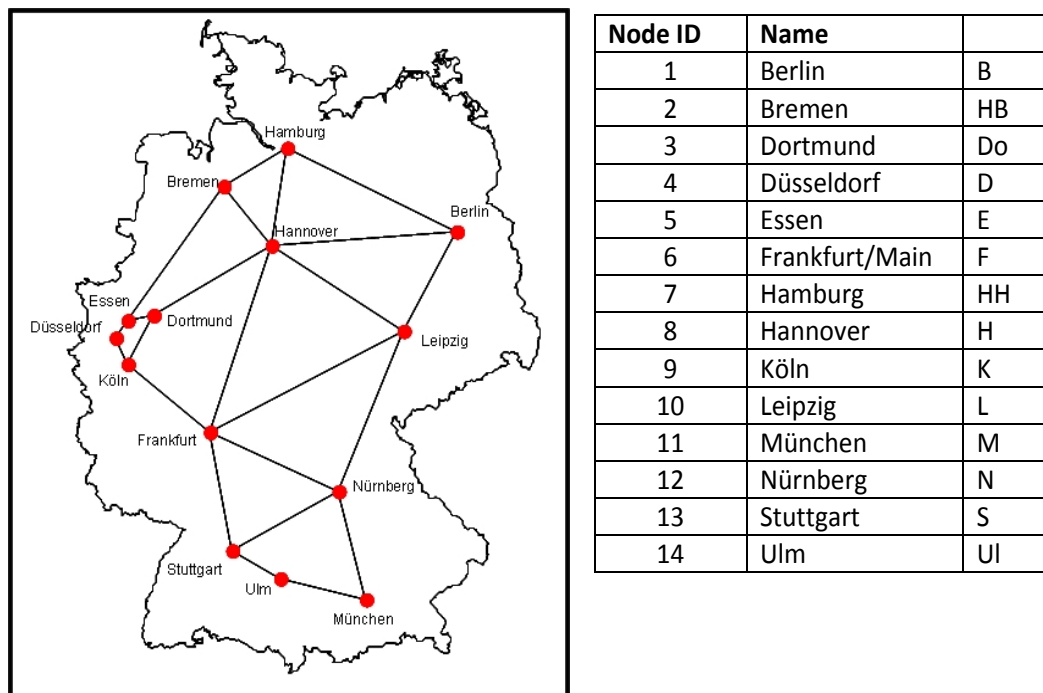


Figure A.1: DT Systems National Core Network and node ID table

Table A.1 Characteristic parameters of DT National Core Network

Parameter	Value
Number of Nodes:	14
Number of links:	23
Node degree:	3.29 (min. 2, max. 6)
Link length (km):	186 km (min. 37, max:353 km)
Span length (km):	25 km (Long Aggr.), (min.:0.21, max:65) 97 km (Short Aggr.), (min: 37, max.:149)
Number of Spans:	7.5 (Long Aggr.), (min: 1, max:17) 1.87 (Short Aggr.), (min: 1, max: 3)
Path length (km):	410 km (min.:37, max.:874)
Hop count:	2.35 (min:1, max:5)

Figure A.2 depicts the distributions of the links. This distribution is shown both in terms of frequency of the link lengths (km) in the network topology and also in term of percentage. More than 20% of the links (5 links) are in the range of 150 to 200 km in this network. Only three links are less than 50Km long in length and furthermore there is no link with a length more than 400 km.

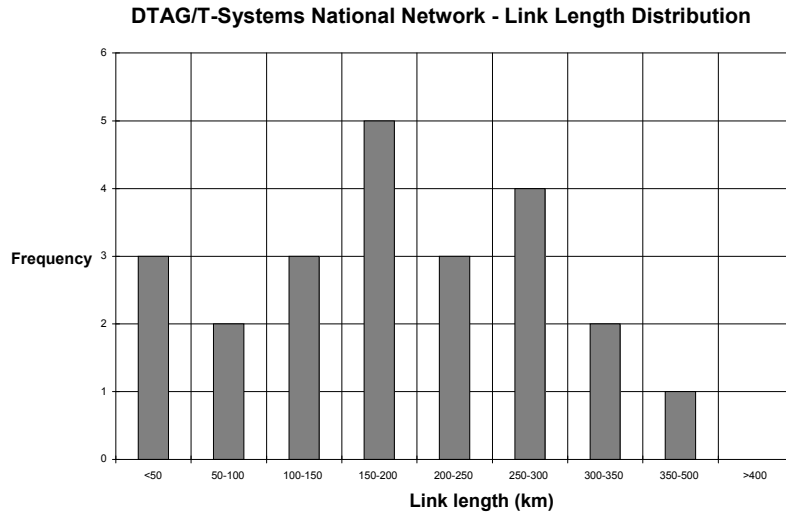


Figure A.2: Link lengths distribution (DT Network)

In Figure A.3 the cumulative distribution of the link length are shown. According to this graph more than 80% of the links, have lengths less than 300 km in this network. The next graph presents some statistics for the shortest path lengths in this network. In order to compute this statistics, an all-pair shortest path algorithm has been considered and computed this shortest path. The distribution is reported both in the form of frequency, percentage and also in the form of CDF. These characteristics are depicted in Figure A.4 and Figure A.5 respectively.

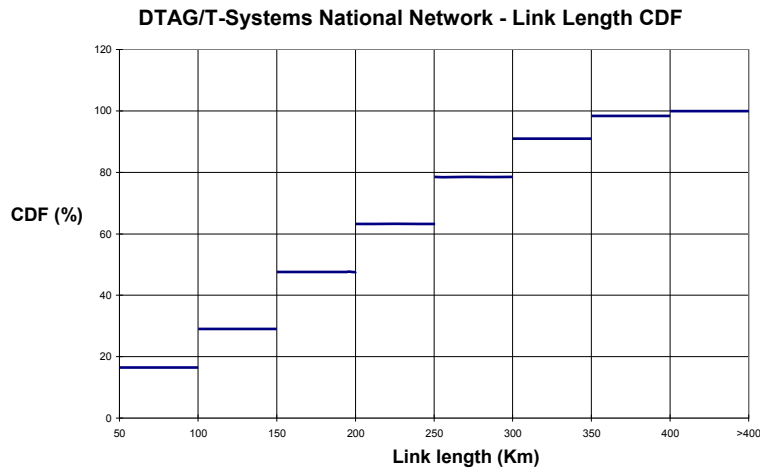


Figure A.3: CDF of link lengths (DT Network)

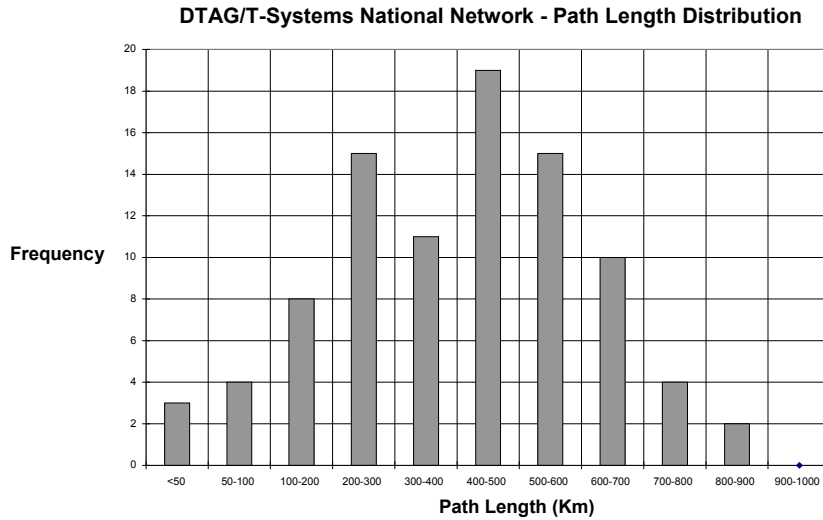


Figure A.4: Shortest path lengths distribution (DT Network)

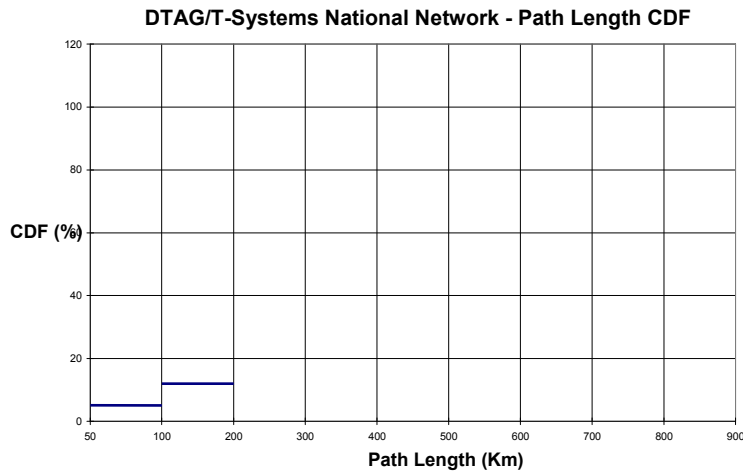


Figure A.5: CDF of shortest path lengths

From these two graphs useful information about the actual distances between all pairs in the network can be extracted. More specifically, it is observed that out of 91 possible paths  $[(n(n-1)/2)$ , where  $n=14$  is the number of nodes of the network] more than 60% of them (i.e. approximately 55 path) are less than 500 km in length. Furthermore all possible shortest paths are less than 900 km in this network topology.

The demand matrix for the Deutsche Telecom National network is presented in Table A.2. The calculation has been based on the distribution of the total (national level) generated traffic over backbone nodes considering the population density and the population growth. The overall traffic demand was summed to 2.8 Tbit/s.

Table A.2: The demand matrix for the Deutsche Telecom National network [Gb/s]

Node ID	1	2	3	4	5	6	7	8	9	10	11	12	13	14
1	0.00	8.98	12.35	13.64	9.74	32.70	19.34	21.04	14.59	33.68	15.40	12.32	23.74	11.07
2	8.98	0.00	5.76	6.23	4.51	14.19	9.92	10.56	6.59	12.59	6.43	5.13	10.15	4.69
3	12.35	5.76	0.00	12.27	10.90	21.94	11.38	13.34	12.17	17.73	9.33	7.50	15.10	6.88



Appendix A: Network Topologies

4	13.64	6.23	12.27	0.00	12.52	24.58	12.48	14.31	18.02	19.54	10.42	8.33	16.96	7.68
5	9.74	4.51	10.90	12.52	0.00	17.29	8.95	10.25	10.46	13.96	7.39	5.92	11.98	5.45
6	32.70	14.19	21.94	24.58	17.29	0.00	28.99	33.09	27.13	47.75	26.20	21.64	27.56	19.88
7	19.34	9.92	11.38	12.48	8.95	28.99	0.00	20.87	13.26	26.42	13.30	10.60	20.84	9.65
8	21.04	10.56	13.34	14.31	10.25	33.09	20.87	0.00	15.16	30.04	14.81	11.94	23.42	10.79
9	14.59	6.59	12.17	18.02	10.46	27.13	13.26	15.16	0.00	20.96	11.22	8.99	18.44	8.30
10	33.68	12.59	17.73	19.54	13.96	47.75	26.42	30.04	20.96	0.00	22.38	18.38	34.50	16.09
11	15.40	6.43	9.33	10.42	7.39	26.20	13.30	14.81	11.22	22.38	0.00	10.82	20.38	10.49
12	12.32	5.13	7.50	8.33	5.92	21.64	10.60	11.94	8.99	18.38	10.82	0.00	16.32	7.82
13	23.74	10.15	15.10	16.96	11.98	27.56	20.84	23.42	18.44	34.50	20.38	16.32	0.00	17.52
14	11.07	4.69	6.88	7.68	5.45	19.88	9.65	10.79	8.30	16.09	10.49	7.82	17.52	0.00

## A.2 Telekomunikacja Polska (TP SA) Network

The backbone network topology of the Telekomunikacja Polska national level reference network is illustrated in Figure A.6. Table A.3 shows the characteristic parameters of the TP network.

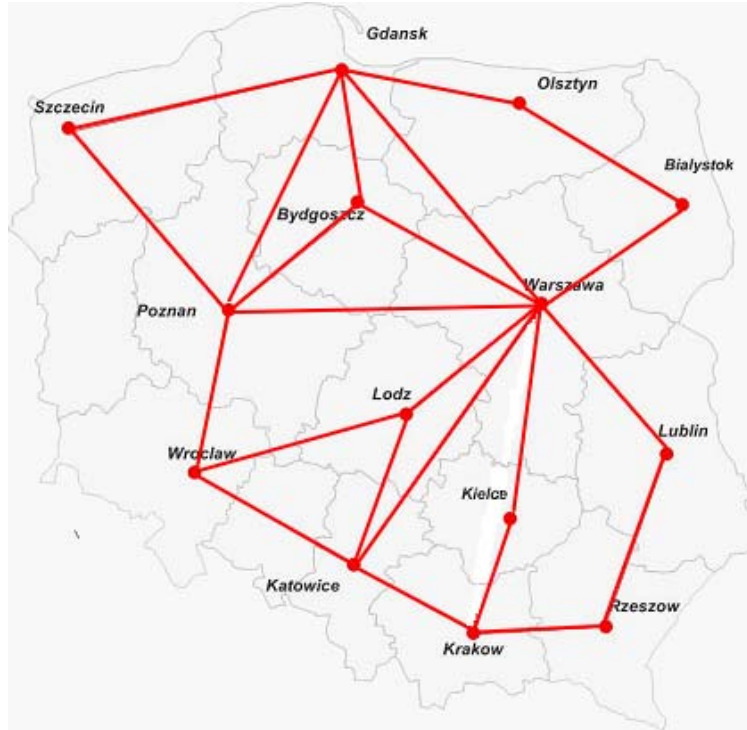


Figure A.6: TP SA National Core Networks

Table A.3: Characteristic parameters of TP SA National Core Network

Parameter	Value
Number of Nodes:	14
Number of links:	23
Node degree:	3.29 (min. 2, max. 8)
Link length (km):	237.2 km (min. 97 km, max:436 km)
Span length (km):	66 km (min. 34 km, max: 97 km)
Path length (km):	492 km (min.:97 km, max.:1021 km)

Figure A.7 depicts the distributions of the links. This distribution is shown both in terms of frequency of the link lengths (km) in the network topology and also in term of percentage. About 35% of the links (8 links) have lengths less than 200 km, and about 87 % of the links (20 links) have lengths less than 350 km in this network. Only two links are longer than 400 km, but all links fulfill physical requirements for 10 Gb signals.

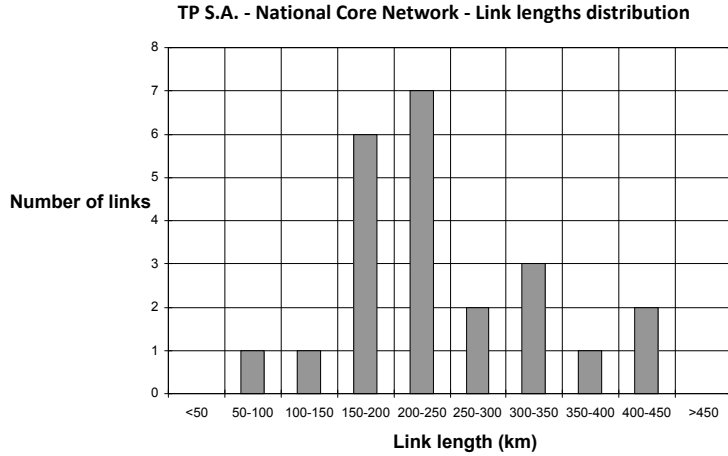


Figure A.7: Link lengths distribution (TP S.A. Network)

In Figure A.8 the cumulative distribution of the link length is shown. According to this graph more than 73% of the links, have lengths less than 300 km in this network.

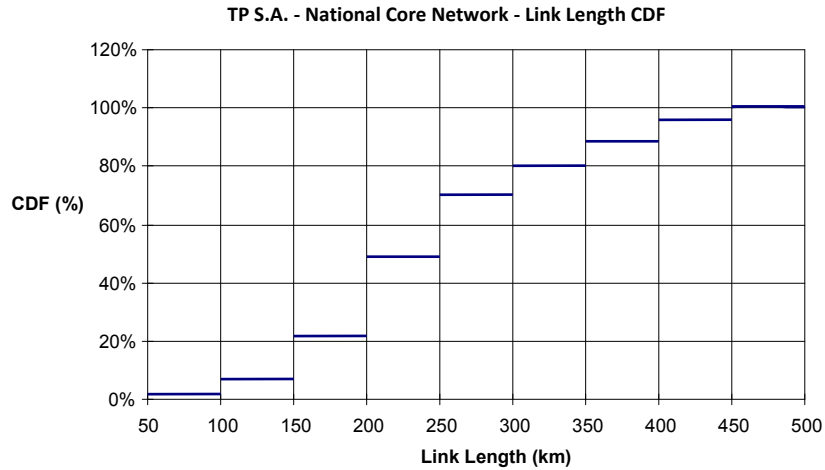


Figure A.8: CDF of link lengths (TP Network)

The graphs shown next, present some statistics for the shortest path lengths in this network. In order to compute this statistics, an all-pair shortest path algorithm has been considered and computed this shortest path. The distribution is reported both in the form of frequency, percentage and also in the form of CDF. These characteristics are depicted in Figure A.9 and Figure A.10 respectively.

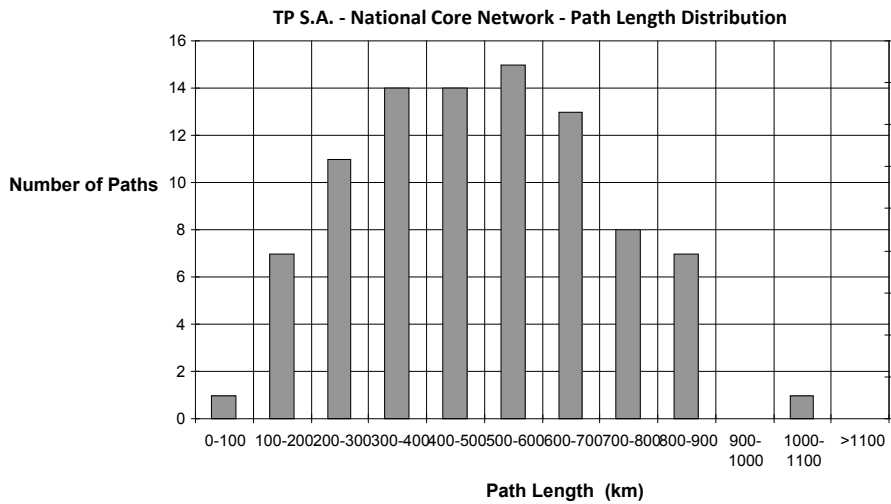


Figure A.9: Shortest path lengths distribution (TP S.A. Network)

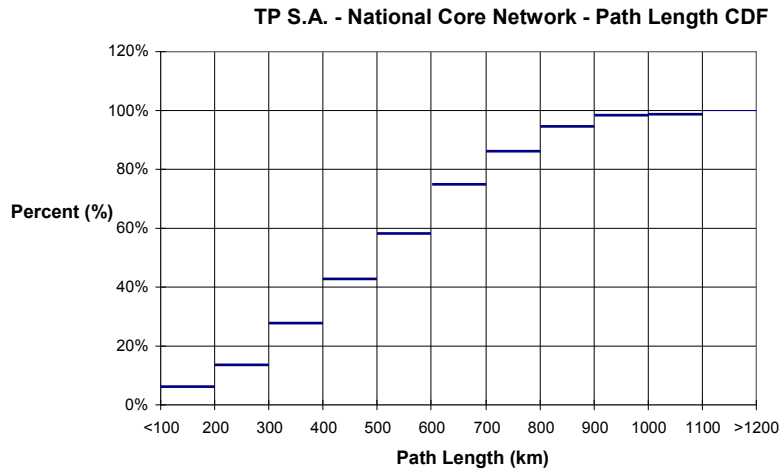


Figure A.10: CDF of shortest path lengths

From these two graphs we can extract many useful information about the actual distances between all pairs in the network that are needed later in order to determine the performance of the various modulation formats according to the path distances. More specifically, it is observed that out of 91 possible paths  $[(n(n-1)/2)]$ , where  $n=14$  is the number of nodes of the network] more than 82% of them are less than 700 km in length. Furthermore almost all possible shortest paths are less than 900 km in this network topology.

Table A.4 shows the traffic demand matrix for the TP S.A. network. The calculation has been based on the distribution of the total (national level) generated traffic over backbone nodes considering the population density and the population growth. The overall traffic demand was summed to 0.95 Tbit/s.

Table A.4: Traffic demand matrix for TP S.A. network [Mb/s]

	Białystok	Bydgoszcz	Gdańsk	Katowice	Kielce	Kraków	Lublin	Łódź	Olsztyn	Poznań	Rzeszów	Szczecin	Warszawa	Wrocław
Białystok		85	459	456	56	408	193	191	89	488	107	106	2555	249
Bydgoszcz	85		694	792	79	617	171	376	126	1390	162	152	2883	349

*Appendix A: Network Topologies*

Gdansk	459	694		5048	457	3088	1069	1549	2228	6382	722	861	1671 1	2025
Katowice	456	792	5048		653	8413	2242	2213	1040	9118	1058	730	2387 8	2893
Kielce	56	79	457	653		406	173	182	83	783	107	100	1846	229
Krakow	408	617	3088	8413	406		1394	1377	647	3671	856	765	1285 0	1799
Lublin	193	171	1069	2242	173	1394		623	270	2692	365	343	6190	787
Lodz	191	376	1549	2213	182	1377	623		289	2657	383	342	6636	804
Olsztyn	89	126	2228	1040	83	647	270	289		1248	175	159	1538	368
Poznan	488	1390	6382	9118	783	3671	2692	2657	1248		1653	2477	2866 8	3497
Rzeszow	107	162	722	1058	107	856	365	383	175	1653		210	3888	483
Szczecin	106	152	861	730	100	765	343	342	159	2477	210		3150	443
Warszawa	2555	2883	16711	23878	1846	12850	6190	6636	1538	28668	3888	3150		8382
Wroclaw	249	349	2025	2893	229	1799	787	804	368	3497	483	443	8382	

### A.3 Pan-European Topology based on the GÉANT2 Network

The Pan-European GÉANT2 reference network topology refers to a wide scale network and is a preferable selection for the emulation of large-scale network. Figure A.11 presents the topology of GÉANT2 network while Table A.5 provides information on characteristic parameters of the network.

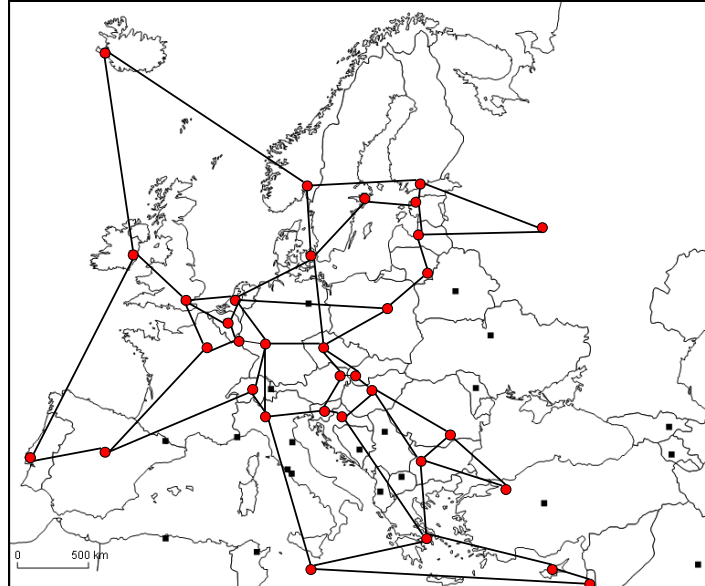


Figure A.11: GÉANT2 pan-EU reference network

Table A.5: Characteristics of GÉANT 2 Network

Parameter	Value
Number of Nodes:	34
Number of links:	52
Node degree:	3.18 (min.:2, Max:5)
Link length (km):	764 (min:67, Max:2361) km
Path length (km):	2397 (min: 67, Max:7575) km
Hop count:	4.12 (min.:1, Max.:11)

In Figure A.12, the distribution of links lengths in this network are compiled. The total numbers of links in this reference network are 52. More than 40% of these links have lengths less than 500 km. The cumulative distribution of the link lengths are also presented in Figure A.13. As shown in this figure 80% of the links have lengths less than 1300 km and except some few links the rest have lengths less than 2100 km, which is around the typical length of economical transparent optical reach.

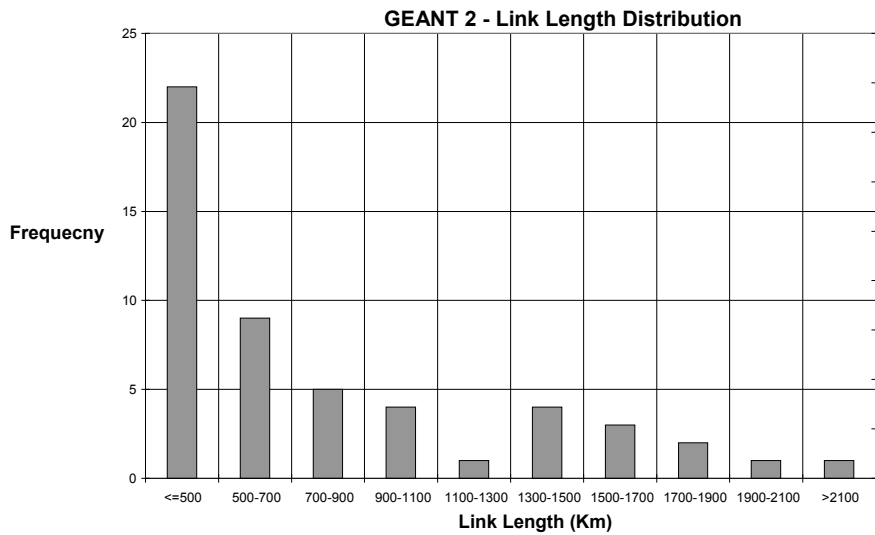


Figure A.12: Link lengths distribution (GEANT2)

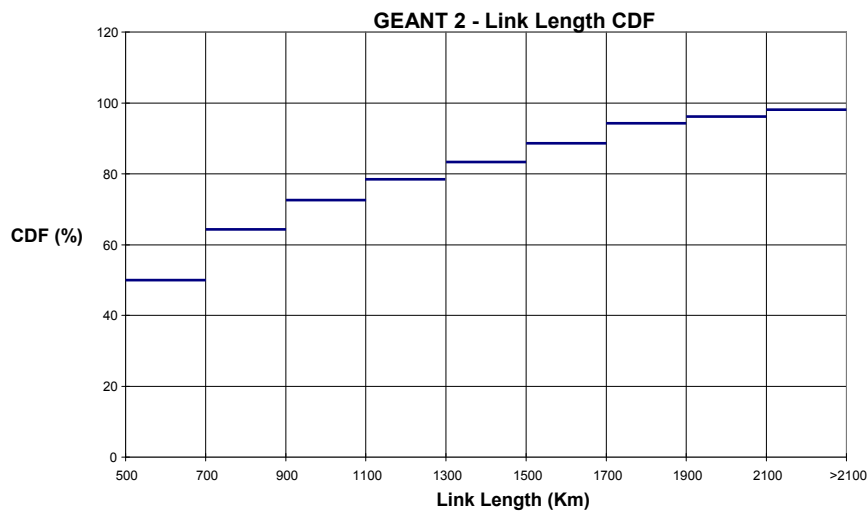


Figure A.13: CDF of link lengths (GEANT2)

The similar practice for GEANT 2 network has been performed as for the case of DT National Network, by computing all-pair shortest path. The results are presented in Figure and Figure A.14. The former is the distribution of path lengths in term of frequency and percentage, while the latter one depicts the cumulative distribution of the path lengths.

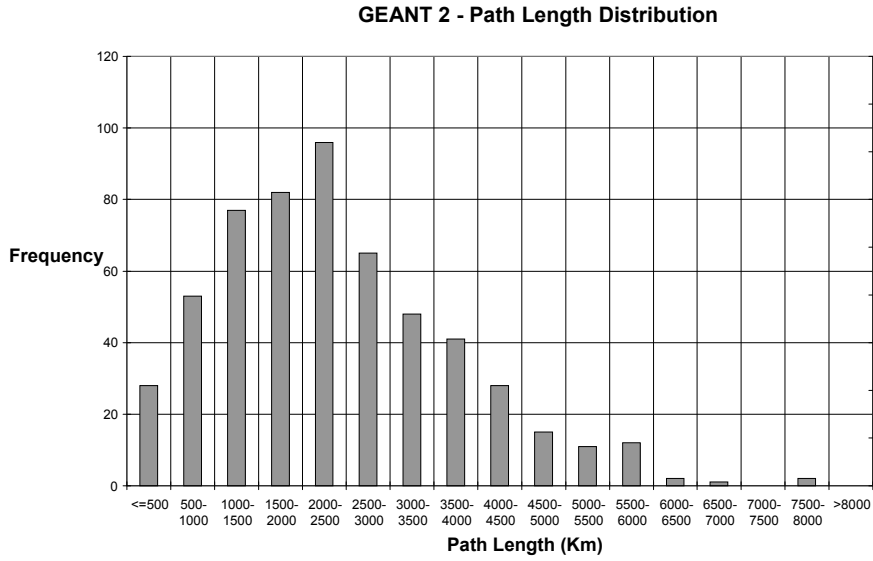


Figure A.14: Distribution of shortest path lengths (GEANT 2)

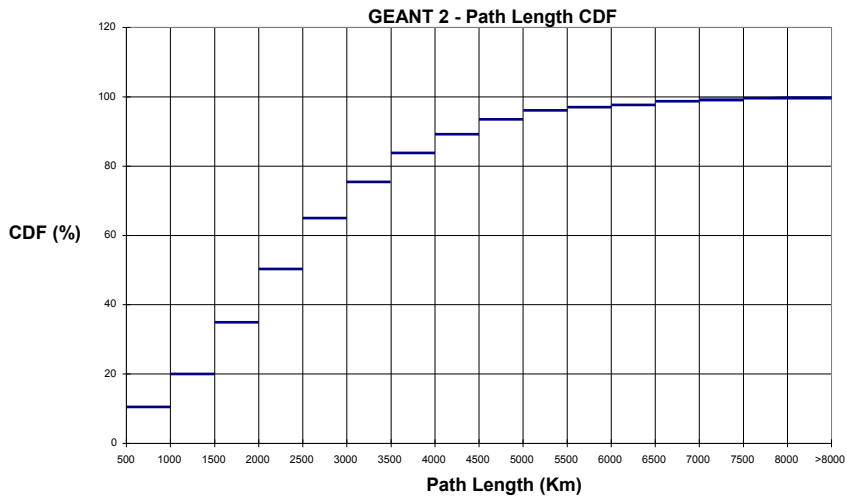


Figure A.15: CDF of the shortest path lengths (GEANT 2)

Based on these results the most frequent shortest paths have lengths in the range of 2000 to 3000 km. However the contribution of longer paths is also considerable. This is more pronounced in Figure A.15, in which 80% of the paths have lengths less than 3500 km.

Similar to the DT network, Table A.6 shows the traffic demand matrix for the GEANT2 network. In this table the traffic among the national backbone nodes is presented. Each of the national backbone nodes is denoted with the country's two letter reference name.



**Table A.6:** Total traffic between nodes of GÉANT2 network in Gbps

	AT	BE	BG	CH	CY	CZ	DE	DK	EE	ES	FI	FR	GR	HR	HU	IE	IL	IS	IT	LT	LU	LV	MT	NL	NO	PL	PT	RO	RU	SE	SL	SK	TR	UK						
AT		2	1	1		1	5	1		1	1	3	1	1	1	1	1		3																					
BE	1			1	3		1	9	2		2	1	12	1	1	1	1	1	5	1	1				8	1	1	1	1	2	2	1	1	1	1	16				
BG	1	1					1	2			1	1	1						1						1	1		1	1	1					2	2				
CH	1	3	1				1	10	1		1	1	5	1	1	1	1	1	7						2	1	1	1	1	2	1				1	1	6			
CY																																				1	1			
CZ	1	2	1	1			7	1		1	1	3	1	1	1	1	1		3					2	1	2	1	1	2	1					1	1	4			
DE	3	16	1	17		4		9	1	5	5	29	2	1	2	2	2	1	35	1	1		1	19	6	10	1	3	15	11	1	2	6	44						
DK	1	1					5			1	1	2	1						2					2	1	1	1	1	1	1						1	1	3		
EE																																					1	1		
ES	1	5	1	4			12	2			2	13	1	1	1	1	1	1	9	1	1	1		6	2	2	2	1	5	3	1	1	3	18						
FI	1	1					2	1			2	1							1					1	1	1	1	1	2	1							1	2		
FR	2	21	1	9		2	29	4	1	6	3		1	1	1	2	2	22	1	1	1		19	4	4	1	2	9	6	1	1	4	62							
GR	1	1	1	1			3	1		1	1	2		1	1	1	1	1	2					1	1	1	1	1	2	1						1	2	3		
HR	1	1					2			1	1	1							1					1	1	1	1	1	1	1							1	2		
HU	1	1	1	1			4	1		1	1	2	1	1					2					1	1	1	1	1	2	1	1	1	1	1	1	1	3			
IE	1	1					2	1		1	2	1							2					2	1	1	1	1	1	1							1	4		
IL	1	1	1	1			2			1	1	1	1	1					1					1	1	1	1	1	1	1							2	2		
IS																																						1	1	
IT	2	11	1	13		2	42	4	1	5	3	26	1	1	2	2	2			1	1	1		12	3	4	1	2	8	5	1	1	5	32						
LT																																						1	1	
LU																																							1	1
LV																																							1	1
MT																																							1	1
NL	1	8	1	2			11	2		2	1	11	1	1	1	1	1		6	1	1				2	2	1	1	3	3	1	1	2	20						
NO	1	1					3	1		1	1	2	1						1						1	1	1	1	1	1								1	3	
PL	1	4	1	3		2	17	2	1	2	2	7	1	1	1	1	1		6	1		1		5	2	1	1	2	7	3	1	1	3	10						
PT	1	1					2	1		2	1	3	1						2						2	1	1	1	1	1									1	4
RO	1	2	1	2			6	1		1	1	4	1	1	1	1	1		4	1				3	1	2	1	4	2	1	1	5	6							
RU	2	14	2	9	1	3	43	7	1	6	9	27	2	1	2	2	3	1	20	1	1	1	1	17	7	8	2	4	14	1	1	10	45							
SE	1	2	1	1			5	1		1	1	3	1	1	1	1	1		2	1	1			2	2	1	1	1	3								1	5		
SL	1	1																																					1	1
SK	1	1	1	1			3	1		1	2	1	1	1					2						1	1	1	1	1										1	2
TR	1	5	2	5	1	1	16	3	1	3	2	11	3	1	1	1	3	1	10	1	1	1		7	2	4	1	5	10	4	1	1	17							
UK	2	21	1	8		2	31	5	1	6	4	45	1	1	1	3	2	1	18	1	1	1		25	5	4	1	2	9	8	1	1	4							

tot ( 32 130 21 89 2 34 280 52 7 59 42 224 30 18 29 26 27 7 172 12 9 8 3 146 46 61 24 40 102 77 13 21 68 325

# Appendix B:

## Appendix B: List of Acronyms

### B.1 List of Acronyms

<b>ASE</b>	Amplifier Spontaneous Emission
<b>BER</b>	Bit Error Ratio
<b>BOI</b>	Band of Interest
<b>BPF</b>	Band Pass Filter
<b>BPSK</b>	Binary Phase Shift Keying
<b>CAPEX</b>	Capital Expenditure
<b>CD</b>	Chromatic Dispersion
<b>CO-OFDM</b>	Coherent Orthogonal Frequency Division Multiplexing
<b>DSP</b>	Digital Signal Processing
<b>DWDM</b>	Dense Wavelength Division Multiplexing
<b>ECL</b>	External Cavity Laser
<b>EDFA</b>	Erbium-Doped Fibre Amplifier
<b>FC</b>	Filter Concatenation
<b>FWM</b>	Four Wave Mixing
<b>GMPLS</b>	Generalized Multiprotocol Label Switching
<b>GVD</b>	Group Velocity Dispersion
<b>IA-RWA</b>	Impairment Aware Routing and Wavelength Assignment
<b>ILP</b>	Integer Linear Programming
<b>ISI</b>	Inter Symbol Interference
<b>IU-RWA</b>	Impairment Unaware Routing and Wavelength Assignment
<b>LO</b>	Local Oscillator
<b>LP</b>	Linear Programming
<b>MB-OFDM</b>	Multi-band Orthogonal Frequency Division Multiplexing
<b>MLR</b>	Mixed Line Rate
<b>N-WDM</b>	Nyquist Wavelength Division Multiplexing
<b>NMS</b>	Network Management System
<b>NPOT</b>	Network Planning and Operation Tool
<b>OADM</b>	Optical Add Drop Multiplexer
<b>OAM</b>	Operation, Administration, and Maintenance
<b>OEO</b>	Opto-Electro-Optical
<b>OFDM</b>	Orthogonal Frequency Division Multiplexing
<b>OPEX</b>	Operation Expenditure
<b>OPM</b>	Optical Performance Monitoring
<b>OSNR</b>	Optical Signal to Noise Ratio
<b>OSPF-TE</b>	Open Shortest Path First with Traffic Engineering
<b>OXC</b>	Optical Cross Connect

<b>PCE</b>	Path Computation Element
<b>PLI</b>	Physical Layer Impairments
<b>POLMUX</b>	Polarization Multiplexed
<b>PMD</b>	Polarization Mode Dispersion
<b>QAM</b>	Quadrature Amplitude Modulation
<b>QoT</b>	Quality of Transmission
<b>QPSK</b>	Quadrature Phase Shift Keying
<b>ROXC</b>	Reconfigurable Optical Cross Connect
<b>ROADM</b>	Reconfigurable Add Drop Multiplexer
<b>ROSNR</b>	Required OSNR
<b>RWA</b>	Routing and Wavelength Assignment
<b>SC</b>	Superchannel
<b>SLR</b>	Single Line Rate
<b>SMF</b>	Single Mode Fibre
<b>SPM</b>	Self Phase Modulation
<b>TED</b>	Traffic Engineering Database
<b>UNI</b>	User Network Interface
<b>VOA</b>	Variable Optical Attenuator
<b>WDM</b>	Wavelength Division Multiplexing
<b>WSS</b>	Wavelength Selective Switch
<b>XPM</b>	Cross Phase Modulation
<b>XT</b>	Crosstalk

# Appendix C:

## Appendix C: Contributions

### C.1 Journal Publications

- [1] **Marianna Angelou**, Yvan Pointurier, Davide Careglio, Salvatore Spadaro, Ioannis Tomkos, "Optimized Monitor Placement for Accurate QoT Assessment in Core Optical Networks," IEEE/OSA Journal of Optical Communications and Networking, IEEE/OSA J. Opt. Commun. Netw. 4, 15-24 (2012).
- [2] S. Azodolmolky, P. Kokkinos, **M. Angelou**, E. Varvarigos, I. Tomkos, "DICONET NPOT: An impairments aware Tool for Planning and Managing Dynamic Optical Networks," special issue of Journal of Network and Systems Management, vol. 19, 2011.
- [3] Siamak Azodolmolky, Yvan Pointurier, **Marianna Angelou**, Davide Careglio, Josep Solé-Pareta, and Ioannis Tomkos, "A Novel Impairment Aware RWA Algorithm With Consideration of QoT Estimation Inaccuracy," IEEE Journal of Optical Communications and Networking, vol. 3, pp. 290-299 (2011).
- [4] Siamak Azodolmolky, Jordi Perelló, **Marianna Angelou**, Fernando Agraz, Luis Velasco, Salvatore Spadaro, Yvan Pointurier, Antonio Francescon, Chava Vijaya Saradhi, Panagiotis Kokkinos, Emmanouel (Manos) Varvarigos, Sawsan Al Zahr, Maurice Gagnaire, Matthias Gunkel, Dimitrios Klonidis and Ioannis Tomkos, "Experimental Demonstration of an Impairment Aware Network Planning and Operation Tool for Transparent/Translucent Optical Networks," IEEE Journal of Lightwave Technology, vol. 29, no. 4, pp. 439-448 (2011).
- [5] Siamak Azodolmolky, Mirosław Klinkowski, Yvan Pointurier, **Marianna Angelou**, Davide Careglio, Josep Solé-Pareta, and Ioannis Tomkos, "A Novel Offline Physical Layer Impairments Aware RWA Algorithm With Dedicated Path Protection Consideration," IEEE Journal of Lightwave Technology, vol. 28, no. 20, pp. 3029-3040, October 2010.
- [6] Pablo Pavon-Mariño, Siamak Azodolmolky, Ramon Aparicio-Pardo, Belen Garcia-Manrubia, Yvan Pointurier, **Marianna Angelou**, Josep Solé Pareta, J. Garcia-Haro, Ioannis Tomkos, "Offline Impairment Aware RWA Algorithms for Cross-Layer Planning of Optical Networks," IEEE Journal of Lightwave Technologies vol. 27, no. 12, pp. 1763-1775, June 2009.
- [7] Konstantinos Christodouloupoulos, Konstantinos Manousakis, Emmanouel (Manos) Varvarigos-University of Patras, **Marianna Angelou**-Athens Information Technology "Considering Physical Layer Impairments in Offline RWA", IEEE Network Magazine, vol. 23, issue 3, pp. 26 - 33, May 2009.

## C.2 Conference Publications

- [1] **M. Angelou**, K. Christodouloupoulos, D. Klonidis, A. Klekamp, F. Buchali and I. Tomkos, "Spectrum, Cost and Energy Efficiency in Fixed-Grid and Flex-Grid Networks", OFC/NFOEC 2012, paper NM3F.4.
- [2] Robert Borkowski, Fotini Karinou, **Marianna Angelou**, Valeria Arlunno, Darko Zibar, Dimitrios Klonidis, Neil Guerrero Gonzalez, Antonio Caballero, Ioannis Tomkos, Idelfonso Tafur Monroy, "Experimental Demonstration of Mixed Formats and Bit Rates Signal Allocation for Spectrum-flexible Optical Networking", OFC/NFOEC 2012, paper OW3A.7.
- [3] Tamara Jiménez, Juan Carlos Aguado, Ignacio de Miguel, Ramón Durán, Natalia Fernandez, **Marianna Angelou**, David Sánchez, Noemi Merayo, Patricia Fernández, Neftis Atallah, Ruben Lorenzo, Ioannis Tomkos, Evaristo Abril, "A Cognitive System for Fast Quality of Transmission Estimation in Core Optical Networks", OFC/NFOEC 2012, paper OW3A.5.
- [4] Natalia Fernandez, Ramón Durán, Ignacio de Miguel, Juan Carlos Aguado, Tamara Jiménez, **Marianna Angelou**, David Sánchez, Patricia Fernández, Noemi Merayo, Neftis Atallah, Ruben Lorenzo, Ioannis Tomkos, Evaristo Abril, "Cognitive Genetic Algorithms to Design Impairment-Aware Virtual Topologies in Optical Networks, OFC/NFOEC 2012, paper OW3A.1.
- [5] Panagiotis Zakynthinos, **Marianna Angelou**, Dimitrios Klonidis, Ioannis Tomkos, "Performance Evaluation of Symmetrical 10 Gb/s WDM/TDM-PON with Respect to Different Downstream Signal Extinction Ratios", OFC/NFOEC 2012, paper JTh2A.66.
- [6] K. Christodouloupoulos, **M. Angelou**, D. Klonidis, P. Zakynthinos, E. Varvarigos and I. Tomkos, "Value Analysis Methodology for Flexible Optical Networks", ECOC 2011, Geneva, Switzerland, paper We.10.P1.89.
- [7] **M. Angelou**, F. Agraz, P. Kokkinos, Marianna Angelou, J. Perello, S. Azodolmolky, E. Varvarigos, S. Spadaro and I. Tomkos, "Experimental Comparison of Impairment-Aware RWA Algorithms in a GMPLS-controlled Dynamic Optical Network", Future Network and Mobile Summit 2011.
- [8] **Marianna Angelou**, Yvan Pointurier, Siamak Azodolmolky, Davide Careglio, Salvatore Spadaro and Ioannis Tomkos, "A Novel Monitor Placement Algorithm for Accurate Performance Monitoring in Optical Networks", OFC/NFOEC 2011, Los Angeles, USA, paper JWA53.
- [9] Dimitri Staessens, **Marianna Angelou**, Maarten De Groote, Siamak Azodolmolky, Dimitrios Klonidis, Sofie Verbrugge, Didier Colle, Mario Pickavet and Ioannis Tomkos, "Techno-economic Analysis of a Dynamic Impairment-Aware Optical Network", OFC/NFOEC 2011, Los Angeles, USA, paper JWA5.
- [8] Salvatore Spadaro, Jordi Perello, Fernando Agraz, Siamak Azodolmolky, **Marianna Angelou**, Yixuan Qin, Reza Nejabati, Dimitra Simeonidou, Panagiotis Kokkinos, Emmanuel Varvarigos, Yabin Ye and Ioannis Tomkos, "Experimental Demonstration of an Enhanced Impairment-Aware Path Computation Element", OFC/NFOEC 2011, Los Angeles, USA, paper OMW2.
- [9] Jordi Perello, Salvatore Spadaro, Fernando Agraz, **Marianna Angelou**, Siamak Azodolmolky, Yixuan Qin, Reza Nejabati, Dimitra Simeonidou, Panagiotis Kokkinos, Emmanuel Varvarigos, Sawsan Al Zahr, Maurice Gagnaire, and Ioannis Tomkos, "Experimental Evaluation of Centralized Failure Restoration in a Dynamic Impairment-Aware All-Optical Network", OFC/NFOEC 2011, Los Angeles, USA, paper OMW2.
- [10] Panagiotis Kokkinos, Siamak Azodolmolky, **Marianna Angelou**, Emmanouel (Manos) Varvarigos, and Ioannis Tomkos, "Performance Evaluation of an Impairment-Aware

- Lightpath Computation Engine," 36th European Conference and Exhibition on Optical Communication (ECOC) 2010, Torino, Italy, 19-23 September 2010.
- [11] Fernando Agraz, Jordi Perelló, **Marianna Angelou**, Siamak Azodolmolky, Luis Velasco, Salvatore Spadaro, Panagiotis Kokkinos, Emmanouel Varvarigos and Ioannis Tomkos, "Experimental Evaluation of Path Restoration for a Centralised Impairment-Aware GMPLS-Controlled All-Optical Network," 36th European Conference and Exhibition on Optical Communication (ECOC) 2010, Torino, Italy, 19-23 September 2010.
- [12] Ioannis Tomkos and **Marianna Angelou**, "New Challenges in Next-Generation Optical Network Planning", Invited at 12th International Conference on Transparent Optical Networks (ICTON) 2010, Munich, Germany, 27 June-1 July 2010.
- [13] F. Agraz, S. Azodolmolky, **M. Angelou**, J. Perelló, L. Velasco, S. Spadaro, A. Francescon, C. V. Saradhi, Y. Pointurier, P. Kokkinos, E. Varvarigos, M. Gunkel, and I. Tomkos, "Experimental Demonstration of Centralized and Distributed Impairment-Aware Control Plane Schemes for Dynamic Transparent Optical Networks," in National Fiber Optic Engineers Conference, OSA Technical Digest (CD) (Optical Society of America, 2010), paper PDPD5.
- [14] Siamak Azodolmolky, Yvan Pointurier, **Marianna Angelou**, Josep Solé-Pareta, and Ioannis Tomkos, "Routing and Wavelength Assignment for Transparent Optical Networks with QoT Estimation Inaccuracy," OFC/NFOEC 2010, OMM4, 21-25 March 2010, San Diego, California, USA.
- [15] Yixuan Qin, Yvan Pointurier, Eduard Escalona, Siamak Azodolmolky, **Marianna Angelou**, Ioannis Tomkos, Kostas Ramantas, Kyriakos Vlachos, Reza Nejabati and Dimitra Simeonidou, "Hardware Accelerated Impairment Aware Control Plane," OFC/NFOEC 2010, 21-25 March 2010, San Diego, California, USA.
- [16] Siamak Azodolmolky, Yvan Pointurier, Miroslaw Klinkowski, Eva Marin, Davide Careglio, Josep Solé-Pareta, **Marianna Angelou**, and Ioannis Tomkos, "On the Offline Physical Layer Impairment Aware RWA Algorithms in Transparent Optical Networks: State-of-the-Art and Beyond," 13th Conference on Optical Network Design and Modeling, (Invited paper), Braunschweig, Germany, Feb. 18-20, 2009.
- [17] Siamak Azodolmolky, Yvan Pointurier, **Marianna Angelou**, Josep Solé Pareta, and Ioannis Tomkos, "An Offline Impairment Aware RWA Algorithm with Dedicated Path Protection Consideration", Optical Fiber Communication Conference (OFC) 2009, San Diego, USA.
- [18] Demetris Monoyios, Kyriakos Vlachos, **Marianna Aggelou**, and Ioannis Tomkos, "On the use of Multi-Objective Optimization Algorithms for solving the Impairment Aware-RWA problem", IEEE International Conference on Communications (ICC) 2009.
- [19] K. Christodouloupoulos, K. Manousakis, E. A. Varvarigos - Computer Engineering and Informatics Department, University of Patras, Greece, and Research Academic Computer Technology Institute, **M. Angelou**, I. Tomkos - Athens Information Technology, Athens, Greece, "A Multi-cost Approach to Online Impairment-Aware RWA", IEEE International Conference on Communications (ICC) 2009.
- [20] Ioannis Tomkos, Siamak Azodolmolky, **Mariana Angelou**, Dimitris Klonidis, Yabin Ye, Chava Vijaya Saradhi, Elio Salvadori, Andrea Zanardi, "Impairment Aware Networking and Relevant Resiliency Issues in All-Optical Networks", Invited at European Conference on Optical Communications 2008.
- [21] Ioannis Tomkos, Siamak Azodolmolky, Dimitrios Klonidis, **Marianna Angelou**, Katerina Margariti, "Dynamic Impairment Aware Networking for Transparent Mesh

Optical Networks: Activities of EU project DICONET”, Invited at IEEE International Conference on Transparent Optical Networks 2008.

### C.3 Book Chapters

- [1] **Marianna Angelou**, Siamak Azodolmolky, Ioannis Tomkos, “Dynamic Impairment-Aware Routing and Wavelength Assignment”, Tentative Title “Cross-layer Design in Optical Networks”, Springer Science and Business Media, in press.
- [2] S. Azodolmolky, **M. Angelou**, I. Tomkos, T. Panayiotou, G. Ellinas, N. Antoniadis, “Impairment-Aware Optical Networking: A Survey,” Book chapter (WDM Systems and Networks), Springer Science and Business Media, 2011.

### C.4 Publications Under Review

- [1] **Marianna Angelou**, Siamak Azodolmolky, Ioannis Tomkos, Jordi Perelló, Salvatore Spadaro, Davide Careglio, Kostas Manousakis, Panagiotis Kokkinos, Emmanouel Varvarigos, Dimitri Staessens Didier Colle, Chava Vijaya Saradhi, Maurice Gagnaire, Yabin Ye, Under Review in IEEE Communications Magazine.
- [2] Robert Borkowski, Fotini Karinou, **Marianna Angelou**, Valeria Arlunno, Darko Zibar, Dimitrios Klonidis, Anton Dogadaev, Xiaodan Pang, Neil Guerrero Gonzalez, Antonio Caballero, Ioannis Tomkos, and Idelfonso Tafur Monroy, “Experimental study on OSNR requirements for spectrum-flexible optical networks”, Under Review in IEEE Photonics Technology Letters.

